



HAL
open science

RAFT polymerization of ethylene for the synthesis of polar-apolar olefin block copolymers

Cédric Bergerbit

► **To cite this version:**

Cédric Bergerbit. RAFT polymerization of ethylene for the synthesis of polar-apolar olefin block copolymers. Polymers. Université de Lyon, 2019. English. NNT : 2019LYSE1276 . tel-03018585

HAL Id: tel-03018585

<https://theses.hal.science/tel-03018585>

Submitted on 23 Nov 2020

HAL is a multi-disciplinary open access archive for the deposit and dissemination of scientific research documents, whether they are published or not. The documents may come from teaching and research institutions in France or abroad, or from public or private research centers.

L'archive ouverte pluridisciplinaire **HAL**, est destinée au dépôt et à la diffusion de documents scientifiques de niveau recherche, publiés ou non, émanant des établissements d'enseignement et de recherche français ou étrangers, des laboratoires publics ou privés.



N° d'ordre NNT : 2019LYSE1276

THESE de DOCTORAT DE L'UNIVERSITE DE LYON

opérée au sein de
l'Université Claude Bernard Lyon 1

Ecole Doctorale N° 206
Ecole Doctorale de Chimie de Lyon

Spécialité de doctorat : Chimie

Soutenue publiquement le 22/11/2019, par :

Cédric Bergerbit

RAFT polymerization of ethylene for the synthesis of polar-apolar olefin block copolymers

Devant le jury composé de :

HADDLETON David	Professeur, University of Warwick	Rapporteur
PASCUAL Sagrario	Maître de conférence, Université du Maine	Rapporteur
BEYOU Emmanuel	Professeur, Université de Lyon	Examinateur
RAPPO Maria	Docteur, Ingénieur R&D, Total	Examinatrice
D'AGOSTO Franck	Directeur de recherche, CNRS	Co-encadrant
LANSALOT Muriel	Directeur de recherche, CNRS	Co-encadrante
MONTEIL Vincent	Directeur de recherche, CNRS	Directeur de thèse

UNIVERSITE CLAUDE BERNARD - LYON 1

Président de l'Université

Président du Conseil Académique

Vice-président du Conseil d'Administration

Vice-président du Conseil Formation et Vie Universitaire

Vice-président de la Commission Recherche

Directeur Général des Services

M. le Professeur Frédéric FLEURY

M. le Professeur Hamda BEN HADID

M. le Professeur Didier REVEL

M. le Professeur Philippe CHEVALIER

M. Fabrice VALLÉE

M. Alain HELLEU

COMPOSANTES SANTE

Faculté de Médecine Lyon Est – Claude Bernard

Faculté de Médecine et de Maïeutique Lyon Sud – Charles Mérieux

Faculté d'Odontologie

Institut des Sciences Pharmaceutiques et Biologiques

Institut des Sciences et Techniques de la Réadaptation

Département de formation et Centre de Recherche en Biologie Humaine

Directeur : M. le Professeur J. ETIENNE

Directeur : Mme la Professeure C. BURILLON

Directeur : M. le Professeur D. BOURGEOIS

Directeur : Mme la Professeure C. VINCIGUERRA

Directeur : M. le Professeur Y. MATILLON

Directeur : Mme la Professeure A-M. SCHOTT

COMPOSANTES ET DEPARTEMENTS DE SCIENCES ET TECHNOLOGIE

Faculté des Sciences et Technologies

Département Biologie

Département Chimie Biochimie

Département GEP

Département Informatique

Département Mathématiques

Département Mécanique

Département Physique

UFR Sciences et Techniques des Activités Physiques et Sportives

Observatoire des Sciences de l'Univers de Lyon

Polytech Lyon

Ecole Supérieure de Chimie Physique Electronique

Institut Universitaire de Technologie de Lyon 1

Ecole Supérieure du Professorat et de l'Education

Institut de Science Financière et d'Assurances

Directeur : M. F. DE MARCHI

Directeur : M. le Professeur F. THEVENARD

Directeur : Mme C. FELIX

Directeur : M. Hassan HAMMOURI

Directeur : M. le Professeur S. AKKOUCHE

Directeur : M. le Professeur G. TOMANOV

Directeur : M. le Professeur H. BEN HADID

Directeur : M. le Professeur J-C PLENET

Directeur : M. Y. VANPOULLE

Directeur : M. B. GUIDERDONI

Directeur : M. le Professeur E. PERRIN

Directeur : M. G. PIGNAULT

Directeur : M. le Professeur C. VITON

Directeur : M. le Professeur A. MOUGNIOTTE

Directeur : M. N. LEBOISNE

Remerciements

Après un stage de M2 et une thèse, l'aventure au C2P2 s'achève. Ces trois années et demi passées au laboratoire m'ont permis de rencontrer des collègues formidables qui sont devenus des amis, tant au niveau humain que scientifique.

Tout d'abord, je souhaiterais remercier Tim McKenna pour m'avoir permis d'intégrer le C2P2, ainsi que l'Agence Nationale de la Recherche pour le financement de cette thèse. Je souhaite également remercier les membres du jury qui ont accepté d'évaluer mon travail de thèse : Sagrario Pascual, Maria Rappo, Dave Haddleton et Emmanuel Beyou. Je voudrais également accorder un remerciement spécial à Simon Harrisson et Mathias Destarac, avec qui j'ai eu le plaisir de pouvoir travailler pendant quelques mois et qui n'ont malheureusement pas pu être présent lors de la soutenance. J'ai vraiment apprécié travailler et échanger avec vous pendant mon séjour à Toulouse (et après !). Petit clin d'œil à une soirée de gala du GFP de folie ainsi qu'au sosie lyonnais de Mathias.

Je remercie très chaleureusement mes encadrants pendant ces trois années de thèse : Muriel, Franck et Vincent. Il y a eu des périodes difficiles, mais vos conseils et votre compréhension ont pour moi été un moteur essentiel pour mener cette thèse jusqu'au bout. Merci Muriel pour ta bonne humeur et ton peps, les discussions dans ton bureau qui doivent durer « juste 5 minutes » mais qui finalement durent 2 heures. C'est triste que la partie « émulsion » de la thèse ne soit intervenue qu'à la fin (et ait si peu marché !), j'espère que tu ne t'es pas trop sentie mise à l'écart pendant la partie organique 😊. Merci Franck pour ta rigueur sans faille et ton sens scientifique qui pousse toujours à aller un peu plus loin (parfois trop !? 😊). C'était vraiment agréable d'échanger avec toi pour faire avancer le schmilblick, et le running entre midi et deux était toujours un moment agréable (sauf le fractionné). Merci Vincent d'être toujours disponible et franc, de bonne humeur et de bon conseil. Ça n'a pas toujours été facile avec trois encadrants et heureusement que tu étais là avec une phrase en phase de devenir culte au labo « de toute façon c'est TA thèse ! ». Merci à tous les trois pour m'avoir fait confiance pendant ces trois ans.

Remerciement spécial pour Seb, Jean, Damien, Olivier Pierre-Yves qui m'ont bien aidé pendant cette thèse. Que ce soit pour le bon fonctionnement des réacteurs, des conseils en synthèse orga ou en matériaux ou bien des analyses, vous avez tous les quatre d'une grande pendant ces trois ans. Seb, la partie catalyse ne pourrait certainement pas tourner sans toi. Ça a toujours été un plaisir de régler les problèmes réacteurs ou bain d'huile avec toi, toujours dans la bonne humeur. Je remercie aussi tout particulièrement Nathalie. Tu es toujours là quand on a besoin de toi et tu fais toujours le maximum

pour nous aider, même si on te gonfle 😊. J'ai vraiment apprécié parler et rire avec toi, le labo a vraiment de la chance de t'avoir.

Je tiens à remercier plus globalement tous les membres du C2P2 qui participent au bon fonctionnement et à la bonne humeur très présente dans ce laboratoire. Je vais quand même citer quelques noms : Arne, pour ta bonne humeur et toute l'aide que tu m'as apporté au début de ma thèse. Florian, pour ta bonne humeur et toute l'aide que tu m'as apporté à la fin de ma thèse. Le groupe Douriya, Amel, Matthieu, James, Rémi, Paul, Florian pour des soirées inoubliables, du « juste un verre » qui se finit à 4 heures du mat'. Du nez qui saigne au babyfoot en passant par un certain bar « chelou », sombre, certes, mais jamais glauque. Clin d'œil au Soda Bar pour les intimes. Merci aux membres du club pas très fermé du bureau des intellos (Amel©) Priscilla, Mathieu, Arne et Astrid. Merci aussi à Amel, Priscilla, Rémi, Aurélien et Wassim pour les soirées jeux, où personne ne s'endort jamais. Merci aussi à Wilfried pour les blagues bien grasses et les fous rires, pas toujours au moment le plus opportun 😊.

Remerciement tout particulier à Astrid et aux (au moins) 1 184 cafés bus pendant nos thèses. Petite pensée pour les redbulls et vitamines qui ont aussi bien fait leur travail quand on en avait besoin. Ces trois ans n'auraient pas été les mêmes sans ma voisine de bureau. Merci pour toutes ces discussions et ta bonne humeur sans limite, agrémentée d'une touche de folie. Merci aussi pour avoir été là quand il y avait besoin. Pensée pour Bob Ross aussi.

Enorme remerciement aux petites poches : Alexi, Vico, Valou, Damien et Alain. Depuis 7 ans (!!!!!!!!!!!), toujours là pour boire des bières et rigoler, se faire une bonne bouffe ou quelques jeux, vous êtes de la bonne humeur à l'état pur les mecs, changez pas. On se souviendra des jeux divers et variés, de Twilight Imperium, de l'Elephant and Castle, de Monica (toutes mes condoléances), de l'Abreuvoir et du Bec de Jazz. On garde à l'esprit le #Vegas2020 à la fin de toutes nos thèses, prêts à lâcher les chiens ?

Remerciement tout particulier aux copains de l'IUT : Lucile, Jordan, Fred et Kéké. Ça m'a vraiment fait plaisir de vous voir pour ma soutenance et le pot. Merci à Lucile pour les bières au Ninkasi, véritable bouffée d'air frais et de bonne humeur au milieu de semaines pas toujours faciles. Un grand merci et un grand clin d'œil à Jordan, alias mon bichon. Depuis l'IUT, une coloc et CPE, même avec l'éloignement quand on se voit c'est comme si on s'était vu la veille. C'est toujours un immense plaisir de te voir et de discuter avec toi. A bientôt pour rebattre le record du plus grand nombre de parties de bowling à la suite. Je te souhaite tout le meilleur pour ta dernière année de thèse, tu vas tout déchirer.

Enfin, je souhaiterais remercier mes parents et mon frère. Vous êtes toujours de bons conseils et toujours là pour me soutenir, quand j'ai un problème je sais que je peux compter sur vous. Sans vous

j'aurai sûrement arrêter depuis bien longtemps et j'aurai peut-être finit chasseur-pêcheur. Merci aussi à Christine, Philippe et Alain pour tous les bons moments et les fous rires.

Pour finir, spéciale kassedédi à mes cheveux. Vous êtes là depuis ma naissance, je vous ai chéris et je vous ai aimé, parfois maltraités, parfois bichonnés, parfois oubliés. Vous étiez là au début de ma thèse, plus trop à la fin. Bientôt vous serez complètement partis, c'est triste. Vous allez beaucoup me manquer, ma vie ne sera plus la même sans vous. Peace.

Abstract

The synthesis of polar-apolar olefin block copolymers, combining a semi-crystalline polyethylene (PE) block and a polar block (poly(vinyl acetate) (PVAc), poly(methyl methacrylate) (PMMA), poly(ethylene oxide) (PEO)) was investigated by RAFT polymerization. A preliminary study on ethylene homopolymerization revealed parasite cross-termination reactions happening at the intermediate radical, resulting in the loss of chain-end fidelity when using aromatic xanthates as chain transfer agents (CTA) under relative mild conditions ($T = 70 - 80\text{ }^{\circ}\text{C}$, $P = 200\text{ bar}$). The extent of cross-termination was greatly reduced with aromatic dithiocarbamates, and for the first time, PE chains with a high livingness were obtained. These first results were used to equip polar macromolecular CTAs (PVAc, PMMA, PEO), with selected aromatic xanthates and dithiocarbamates, that were further used for block copolymerization with ethylene in a low-transferring organic solvent (dimethyl carbonate, DMC). A critical influence of the ethylene pressure was evidenced as block polymerization at 200 bar could not be achieved due to solubility issues in the resulting supercritical DMC/ethylene mixture. This was circumvented by performing the block copolymerization below the supercritical point of the mixture ($P < 100\text{ bar}$) and well-defined PVAc-*b*-PE, PMMA-*b*-PE and PEO-*b*-PE copolymers were eventually obtained. The block copolymers were found to feature self-assembly properties and worm-like morphologies were observed for PMMA-*b*-PE and PEO-*b*-PE synthesized in DMC, hinting at a plausible polymerization-induced self-assembly (PISA) mechanism. The successful switch from DMC to water for the synthesis of PEO-*b*-PE copolymers enabled the observation of various particle morphologies: spheres, vesicles and ellipsoidal particles, depending on the initial macro-CTA:initiator molar ratio.

Keywords

Polyethylene – RAFT – block copolymers – PISA – poly(vinyl acetate) – poly(methyl methacrylate) – poly(ethylene oxide)

Laboratoire C2P2 – Equipe LCPP
CNRS, Université Lyon 1, Université de Lyon
CPE Lyon, Bâtiment F, BP 2077
43, Bd. du 11 Novembre 1918
69616 Villeurbanne Cedex

Titre

Polymérisation RAFT de l'éthylène pour la synthèse de copolymères à blocs polaires-apolaires.

Résumé

La synthèse de copolymères à blocs, comprenant un bloc semi-cristallin de polyéthylène (PE) apolaire et un bloc polaire (poly(acétate de vinyle) (PVAc), poly(méthacrylate de méthyle) (PMMA), poly(oxide d'éthylène) (PEO)) a été étudiée par polymérisation RAFT. L'étude préliminaire de l'homopolymérisation de l'éthylène en conditions relativement douces ($T = 70 - 80\text{ °C}$, $P = 200\text{ bar}$) a révélé que l'utilisation d'agents de transfert de chaîne (CTA) de type xanthates aromatiques conduit à une perte de fonctionnalité des extrémités de chaînes au cours de la polymérisation, conséquence directe de réactions de terminaison se produisant sur le radical intermédiaire. L'utilisation de dithiocarbamates aromatiques a permis de s'affranchir de ce mécanisme parasite et pour la première fois des chaînes de PE présentant une fonctionnalité de bout de chaîne proche de 100% ont été obtenus. Des CTAs macromoléculaires polaires, obtenus avec les agents de transfert de chaînes identifiés au cours de l'étude préliminaire, ont ensuite été utilisés pour la synthèse de copolymères à blocs dans le carbonate de diméthyle (DMC), un solvant organique peu transférant. Le rôle clé de la thermodynamique du milieu de polymérisation (mélange DMC/éthylène supercritique à 200 bar) a alors été mis en évidence. En effet, les macro-ATCs sont insolubles dans un tel milieu, ce qui a conduit à la formation d'un mélange d'homopolymères. La diminution de la pression de polymérisation ($P < 100\text{ bar}$) a toutefois permis d'éviter ce phénomène et les copolymères PVAc-*b*-PE, PMMA-*b*-PE et PEO-*b*-PE attendus ont été obtenus. Des propriétés d'auto-assemblage ont été mises en évidence et des morphologies de type fibre ont été obtenues pour les copolymères PMMA-*b*-PE et PEO-*b*-PE synthétisés dans le DMC, permettant d'envisager un mécanisme de type auto-assemblage induit par la polymérisation (PISA). Le passage en milieu aqueux en utilisant le macro-CTA hydrosoluble PEO a permis l'observation de morphologies de type sphériques, vésicules ou encore ellipsoïdes selon le rapport molaire macro-CTA/amorceur utilisé.

Mots-clés

Polyéthylène – RAFT – copolymères à blocs – PISA – poly(acétate de vinyle) – poly(méthacrylate de méthyle) – poly(oxyde d'éthylène)

Laboratoire C2P2 – Equipe LCPP
CNRS, Université Lyon 1, Université de Lyon
CPE Lyon, Bâtiment F, BP 2077
43, Bd. du 11 Novembre 1918
69616 Villeurbanne Cedex

Table of contents

Table of contents	15
Résumé	21
Abbreviations	27
General introduction	31

Chapter I **State of the art**

I. General introduction on ethylene polymerization	39
I.1. A rapid overview on polyethylene (PE)	39
I.2. Synthesis of PE	41
I.2.1. Catalytic polymerization of ethylene	41
I.2.2. Radical polymerization of ethylene.....	41
I.3. Copolymerization of ethylene with polar monomers	51
I.3.1. Catalytic copolymerization	51
I.3.2. Radical copolymerization.....	52
I.4. Conclusion.....	53
II. Block copolymers synthesis based on a preformed PE segment obtained by catalytic polymerization	54
II.1. Foreword on reversible deactivation radical polymerization.....	54
II.2. Indirect block copolymer synthesis involving a PE block.....	58
II.2.1. Synthesis by anionic polymerization methods.....	59
II.2.2. Synthesis by radical polymerization methods.....	62
II.3. Block copolymer synthesis by successive coordination-insertion of ethylene and group transfer polymerization of the polar monomer.....	66
II.4. Synthesis of diblock copolymers by coupling two preformed blocks	68
II.5. Conclusion.....	69
III. Reversible-deactivation radical polymerization of ethylene	71
III.1. More activated monomers and less-activated monomers	71

III.2.	RDRP of ethylene <i>via</i> ITP	72
III.3.	RDRP of ethylene <i>via</i> TERP	73
III.4.	RDRP of ethylene <i>via</i> OMRP	74
III.5.	RDRP of ethylene <i>via</i> NMP.....	76
III.6.	RDRP of ethylene <i>via</i> RAFT polymerization	77
III.7.	Conclusion.....	80
IV.	Specificities of RAFT polymerization.....	81
IV.1.	RAFT polymerization.....	81
IV.1.1.	Choice of Z- and R- groups.....	83
IV.2.	Synthesis of block copolymers <i>via</i> RAFT polymerization	86
IV.2.1.	General guidelines for the successful synthesis of block copolymers by RAFT	86
IV.2.2.	Block copolymers between LAMs and MAMs <i>via</i> RAFT polymerization..	87
V.	Conclusion and positioning of this work.....	90
VI.	References	91

Chapter II

RAFT polymerization of ethylene

I.	Introduction	98
II.	Context of ethylene RAFT homopolymerization.....	99
II.1.	RAFT polymerization of ethylene with <i>O</i> -ethyl xanthate.....	99
II.2.	RAFT polymerization of ethylene with <i>O</i> -methyl xanthate	101
II.3.	Z-groups with aromatic substituents to suppress side-fragmentation.	101
II.3.1.	Xanthates with aromatic substituents	101
II.3.2.	<i>N,N</i> -dithiocarbamates with aromatic substituents.	104
III.	RAFT polymerization of ethylene with <i>O</i>-aryl xanthates	105
III.1.	RAFT homopolymerization of ethylene	105
III.1.1.	Polymerization at 70°C and 200 bar.....	105
III.1.2.	Polymerization at 80°C and 200 bar.....	110
III.1.3.	Rationalization of the emergence of free radical polymerization at a pressure of 200 bar in the presence of aromatic xanthates.	115
III.1.4.	Ethylene homopolymerization at 80°C and 80 bar.	116
III.1.5.	Origin of new side-products from cross-termination	119

III.2.	RAFT copolymerization of ethylene in the presence of vinyl acetate: Synthesis of EVA copolymers.....	122
III.3.	Conclusion on the use of xanthates for ethylene RAFT polymerization	122
IV.	RAFT polymerization of ethylene with <i>N</i>-aryl carbamates.....	125
IV.1.	Ethylene homopolymerization in the presence of 3,5-dimethyl-1H-pyrazole-1-carbodithioate (4).....	125
IV.2.	Ethylene homopolymerization in the presence of <i>N</i> -methylphenyl (3) and switchable <i>N</i> -methylpyridyl (5-7) dithiocarbamates	126
IV.2.1.	Kinetics of the polymerizations	126
IV.2.2.	Chain-ends analysis.....	128
V.	Conclusion	132
VI.	Experimental section	134
VII.	References	138

Chapter III

Synthesis of block copolymers based on ethylene and vinyl acetate

I.	Introduction.....	142
II.	Synthesis of PVAc macro-CTAs	144
III.	Synthesis of PVAc-<i>b</i>-PE copolymers.....	147
III.1.	Block copolymerizations at 200 bar	147
III.2.	Block copolymerizations at 80 bar	149
III.3.	Thermal properties of PVAc- <i>b</i> -PE copolymers.....	153
IV.	Conclusion	156
V.	Experimental section	157
VI.	References	159

Chapter IV

Synthesis of copolymers based on ethylene and methyl methacrylate

I. Introduction	162
II. Synthesis of PMMA-<i>b</i>-PE using a switchable dithiocarbamate... 165	
II.1. Synthesis of PMMA macro-CTA with 6-H ⁺	165
II.2. Chain extension of PMMA-6 with ethylene.....	167
II.3. Self-assembly of PMMA- <i>b</i> -PE copolymers in DMC.....	170
III. Synthesis of PMMA-<i>b</i>-PE by successive FRP and RAFT polymerization.....	173
III.1. Determination of the chain transfer constant.....	174
III.2. Synthesis of PMMA-T with TD	175
III.2.1. Chain-end analysis	176
III.2.2. Chain-extension with vinyl acetate	178
III.3. Chain extension of PMMA-T with ethylene.....	179
III.4. Self-assembly of PMMA- <i>b</i> -PE	184
IV. Conclusion.....	186
V. Experimental section	188
VI. References	190

Chapter V

Synthesis of copolymers based on a poly(ethylene oxide) macro-CTA

I. Introduction	194
I.1. RAFT-mediated emulsion polymerization	194
I.2. Emulsion polymerization of ethylene	195
I.3. Amphiphilic block copolymers with ethylene	196
II. Synthesis of PEO-<i>b</i>-PE copolymers in DMC.....	197
II.1. Polymerization of ethylene in the presence of PEO macro-CTAs.....	198
II.2. Chain-ends analysis.....	199

II.3. Self-assembly properties of PEO- <i>b</i> -PE	202
III. Synthesis of PEO-<i>b</i>-PE copolymers in water	205
III.1. Polymerization under RAFT conditions	205
III.1.1. Ethylene polymerization in water in presence of PEO macro-CTAs.....	205
III.1.2. Synthesis of PEO- <i>b</i> -EVA copolymers	207
III.2. Polymerization using lower amounts of macro-CTA	210
III.2.1. Synthesis of PEO- <i>b</i> -PE copolymers with PEO-NN	210
III.2.2. Synthesis of PEO- <i>b</i> -PE copolymers with PEO-N.....	211
IV. Conclusion	215
V. Experimental section	217
VI. References	220
General conclusion.....	223
Materials and Methods.....	229

Résumé

Les polymères, qu'ils soient synthétiques ou naturels, sont aujourd'hui omniprésents et font partie intégrante de notre mode de consommation. Parmi les polymères synthétiques, le polyéthylène (PE) est le plus utilisé et le plus produit dans le monde. Il doit son succès à ses faibles coûts de production, ses excellentes propriétés mécaniques et l'abondance du monomère à partir duquel il est produit : l'éthylène, issu en grande majorité de l'industrie pétrolière. Le PE peut être obtenu par polymérisation catalytique, par un mécanisme de coordination-insertion utilisant des complexes de métaux de transitions en conditions douces ($T < 65\text{ °C}$, $P < 30\text{ bar}$), ou par un procédé radicalaire en conditions très dures ($T > 200\text{ °C}$, $P > 1\ 000\text{ bar}$). Ces deux voies de production permettent d'obtenir des PE ayant différentes propriétés mécaniques et applications, allant de la production de sacs plastiques aux implants pour les hanches.

Composé d'un squelette exclusivement hydrocarboné, le PE est apolaire, ce qui lui confère une grande inertie chimique. Cela devient toutefois un inconvénient lorsqu'il s'agit de lui conférer des propriétés de surfaces et d'interfaces. La copolymérisation de l'éthylène avec des monomères polaires, et notamment la synthèse de copolymères à blocs, représente une solution intéressante à ce problème. Les procédés de production industriels du PE (catalytique et radicalaire) sont cependant incompatibles avec l'obtention de tels matériaux.

Dans ce contexte, les techniques de polymérisation radicalaire par désactivation réversible (RDRP en anglais), et notamment la polymérisation RAFT (transfert de chaîne par addition-fragmentation) sont aujourd'hui des procédés de choix pour la synthèse de copolymères à blocs. Il y a quelques années, le C2P2 a montré que le contrôle de la polymérisation radicalaire de l'éthylène est possible par RAFT, au moyen d'agents de contrôle de type xanthate. Cependant, une réaction parasite de fragmentation secondaire (*side-fragmentation*, SF), inhérente à la nature des agents de contrôle utilisés (*O*-alkyl xanthates), a été mise en évidence dans ces systèmes.

En s'appuyant sur ces résultats prometteurs, les travaux de thèse présentés ici ont pour objectif la synthèse de copolymères à blocs polaire-apolaire, basés sur l'éthylène, par le procédé RAFT. Pour cela, l'homopolymérisation RAFT de l'éthylène a d'abord été étudiée de manière approfondie. Des agents de contrôle possédant des substituants potentiellement défavorisant la SF ont donc été synthétisés et étudiés. L'utilisation de *O*-aryl xanthates a permis la suppression de la SF ainsi qu'un excellent contrôle des masses molaires aux faibles temps de polymérisation (dispersité de masse molaire, $\mathcal{D} < 1.3$). Cependant, de potentielles réactions de terminaison se produisant sur le radical intermédiaire (*cross termination*), conduisant à une perte de fonctionnalité des extrémités de chaînes, ainsi que des problèmes de ségrégation de phase en milieu supercritique ont été mis en évidence. L'utilisation de *N*-aryl dithiocarbamates s'est révélée plus prometteuse. En effet, ces agents de transfert permettent aussi de s'affranchir de la SF tout en conservant une fidélité des extrémités de chaînes de 100%. Aucune ségrégation de phase n'a

été observée, mais une consommation lente de l'agent de contrôle, dépendante de sa structure, a été mise en évidence.

Ces résultats ont ainsi permis d'identifier les agents de contrôle présentant les meilleurs compromis pour la synthèse de copolymères à blocs avec l'éthylène. Dans un premier temps, un xanthate a été utilisé pour la préparation de poly(acétate de vinyle) (PVAc), un dithiocarbamate pour celle de poly(méthacrylate de méthyle) (PMMA) et un poly(oxyde d'éthylène) (PEO) commercial a été fonctionnalisé avec différents dithiocarbamates. Dans le cadre d'une collaboration avec le Pr. Mathias Destarac et le Dr. Simon Harrison (Laboratoire des IMRCP, Université Toulouse III), des PMMA terminés par une extrémité dithiocarbamate ont été également obtenus par transfert irréversible. Dans un deuxième temps, ces macromolécules ont été utilisées comme macro-agents de contrôle (macro-CTA) dans le but de réaliser des extensions de chaînes en présence d'éthylène en milieux organique et aqueux pour l'obtention de copolymères à blocs.

C'est ainsi que des copolymères à blocs bien définis (distributions de masses molaires étroites) ont pu être obtenus : PVAc-*b*-PE, PMMA-*b*-PE, PEO-*b*-PE (**Figure 1**) dans le carbonate de diméthyle (DMC), un solvant connu pour activer la polymérisation radicalaire de l'éthylène tout en limitant les réactions de transfert au solvant. Ces résultats représentent les premiers exemples de synthèse de tels copolymères à blocs de façon contrôlée. Des difficultés de caractérisations et d'analyses des copolymères, notamment liées à leur caractère polaire-apolaire ont également été mises en évidence, rendant l'analyse des masses molaires par chromatographie d'exclusion stérique et RMN non triviale.

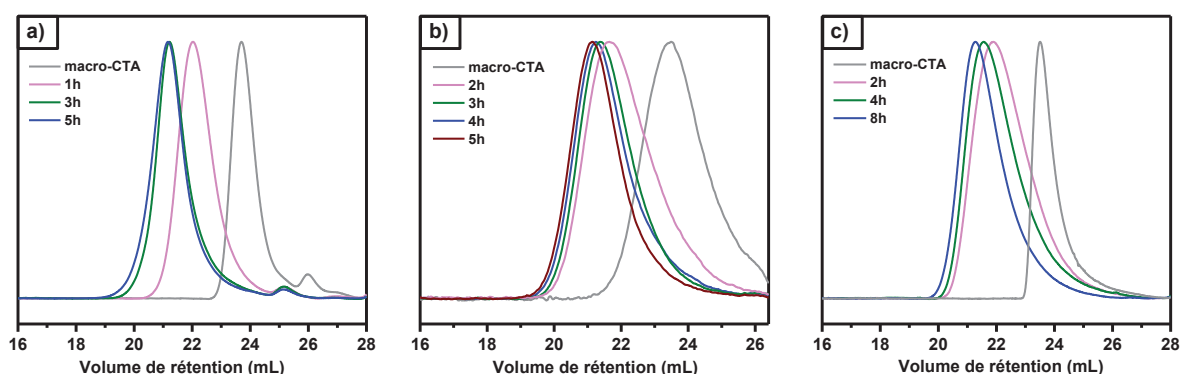


Figure 1. Extensions de chaînes avec l'éthylène à partir de différents macro-agents de contrôle pour la synthèse de copolymères à blocs : PVAc-*b*-PE (a), PMMA-*b*-PE (b) et PEO-*b*-PE (c).

Des propriétés d'auto-assemblage durant la synthèse des PMMA-*b*-PE et des PEO-*b*-PE ont été mises en évidence et des morphologies de type fibres ont été obtenues.

Les macro-CTAs de PEO ont ensuite été utilisés dans le cadre d'extensions de chaînes en milieu aqueux, et ont révélé un comportement très différent de celui observé dans le DMC. Une inhibition

complète de la polymérisation de l'éthylène a été observée pour des ratios molaires macro-CTA:amorceur de 3:1. Seuls des ratios plus faibles (0.06, 0.6 et 1) ont permis l'obtention de copolymères et des morphologies de type sphères, vésicules, ou encore ellipses ont été obtenues (Figure 2).

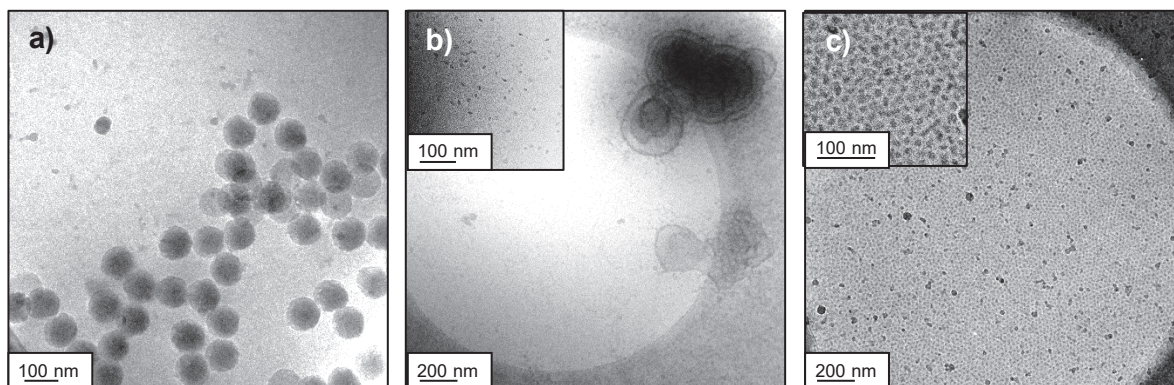


Figure 2. Images cryo-TEM des latex obtenus après extension de chaînes d'un macro-CTA de PEO à différents ratios macro-CTA:amorceur : 0.06 (a), 0.6 (b) et 1 (c).

En conclusion, les travaux décrits dans ce manuscrit regroupent les premiers exemples de polymérisation radicalaire contrôlée de l'éthylène par RAFT produisant des PE présentant un taux de fonctionnalité de 100% grâce à l'utilisation de dithiocarbamates aromatiques. Des copolymères à blocs polaires et apolaires ont été obtenus pour la première fois par addition séquentielle des monomères en utilisant la même chimie de polymérisation radicalaire pour les deux blocs. La synthèse de copolymères amphiphiles avec un bloc de PE semi-cristallin dans l'eau a également démontrée. Ces travaux ont montré que le choix de l'agent de contrôle est primordial pour la synthèse contrôlée des deux blocs.

Abbreviations

9-BBN	9-borabicyclo[3.3.1]nonane
AA	Acrylic acid
ADMET	Acyclic diene metathesis
AIBA	2,2'-azobis(2-amidinopropane) Dihydrochloride
AIBN	2,2'-azobis(2-methylpropionitrile)
AN	Acrylonitrile
APS	Ammonium persulfate
ATRP	Atom transfer radical polymerization
BIRP	Bismuth-mediated radical polymerization
CMRP	Cobalt-mediated radical polymerization
CTA	Chain transfer agent
CTAB	Cetyltrimethylammonium bromide
\bar{D}	Dispersity
DEC	Diethyl carbonate
DEPN	<i>N</i> -(2-methyl-2-propyl)- <i>N</i> -(1-diethylphosphono-2,2-dimethylpropyl)- <i>N</i> -oxy
DIPEA	<i>N,N</i> -diisopropylethylamine
DLS	Dynamic light scattering
DMAm	Dimethyl acrylamide
DMAP	4-dimethyl amino pyridine
DMC	Dimethyl carbonate
DMF	<i>N,N</i> -dimethylformamide
DMSO	<i>N,N</i> -dimethylsulfoxide
DP	Degree of polymerization
DSC	Differential scanning calorimetry
DT	Degenerative transfer
ESCP	Enhanced spin capturing polymerization
EVA	Poly(ethylene- <i>co</i> -vinyl acetate)
FRP	Free radical polymerization
GTP	Group transfer polymerization
HDPE	High density polyethylene
HT-SEC	High-temperature size exclusion chromatography
ITP	Iodine transfer polymerization
LALS	Left angle light scattering
LAM	Less activated monomer
LDPE	Low density polyethylene
LLDPE	Linear low density polyethylene
MA	Methyl acrylate
MALDI-TOF	Matrix-assisted laser desorption and ionization – time of flight
MAO	Methylaluminoxane
MMA	Methyl methacrylate
MMD	Molar mass distribution
M_n	Average molar mass by number
M_w	Molar mass distribution
<i>n</i> BuA	<i>n</i> -butyl acrylate
NIPAM	<i>N</i> -isopropylacrylamide
NMP	Nitroxide-mediated polymerization
NMR	Nuclear magnetic resonance
NVC	<i>N</i> -vinylcarbazole
NVP	<i>N</i> -vinylpyrrolidone
PCL	Poly(caprolactone)

PdI	Polydispersity
PE	Polyethylene
PEO	Poly(ethylene oxide)
PI-CDSA	Polymerization-induced crystallization-driven self-assembly
PISA	Polymerization induced self-assembly
PLA	Poly(lactic acid)
PMMA	Poly(methyl methacrylate)
p-MS	para-methylstyrene
PNVP	Poly(<i>N</i> -vinylpyrrolidone)
PS	Polystyrene
PVAc	Poly(vinyl acetate)
RAFT	Reversible addition fragmentation chain-transfer
RALS	Right angle light scattering
RDRP	Reversible deactivation radical polymerization
ROMP	Ring opening metathesis polymerization
ROP	Ring opening polymerization
<i>s</i> -BuLi	<i>s</i> -butyl lithium
S	Styrene
SBRP	Stibine-mediated radical polymerization
SDS	Sodium dodecyl sulfate
SEC	Size exclusion chromatography
SHOP	Shell higher olefin process
T_c	Temperature of crystallization
TEA	Triethylaluminum
TEM	Transmission electron microscopy
TEMPO	2,2,6,6-tetramethylpiperidinyl-1-oxy
TERP	tellurium-mediated radical polymerization
TfOH	Trifluoromethanesulfonic acid
TM	Transition metal
TMEDA	<i>N,N,N',N'</i> -tetramethylethylenediamine
T_g	Glass transition temperature
THF	Tetrahydrofuran
T_m	Melting temperature
UHMWPE	Ultra high molecular weight polyethylene
VAc	Vinyl acetate
VLDPE	Very low density polyethylene
Zav	Average diameter
ZN	Ziegler-Natta

General introduction

Polymers are ubiquitous in our everyday life and natural polymers (e.g. DNA, cellulose, starch) are essential to life on earth. Over the last century, we have learned to produce synthetic polymers that are otherwise non-naturally occurring, opening the ways to completely new applications and domains, from construction materials to heart replacement. Among synthetic polymers, polyolefins (POs) are the most industrially produced thanks to their simple and inexpensive building blocks, low production costs and extremely durable properties. The main strength of POs is also a disadvantage: their full-hydrocarbon backbone make them apolar, limiting their use in high-end applications demanding a certain degree of functionality and surface properties, such as electronics, medical applications or compatibility with other polymers. In particular, block copolymers incorporating polar and apolar olefins (polar OBCs) are very attractive materials. So far, polar OBCs have in great majority been obtained by a succession of different polymerization mechanisms with sometimes tedious post-modification steps. Obtaining polar OBCs by sequential monomer addition using the same polymerization mechanism is far more alluring.

Polyethylene (PE), obtained from ethylene, the simplest, cheapest and most available olefin (i.e vinyl monomer), is no exception to this. The industrial production of PE is dominated by catalytic coordination insertion polymerization techniques (Ziegler-Natta, Phillips or metallocene-based catalysis) but PE produced *via* free radical polymerization (FRP) still represents 24 % of the total production. These two polymerization techniques are not adapted for the synthesis of polar OBCs: catalytic coordination-insertion polymerization is intolerant towards polar olefins due to poisoning issues, and the conditions under which FRP of olefins is conducted (high pressures, high temperatures) do not allow the controlled growth of the polymer chains to access architected materials.

Reversible deactivation radical polymerization (RDRP) techniques are now established as mature and efficient processes for the synthesis of block copolymers. In particular, reversible addition-fragmentation chain transfer (RAFT) polymerization is one of the most versatile RDRP techniques and allows the block copolymerization of both activated and non-activated vinyl monomers. RAFT was recently used in our group to control for the first time the radical polymerization of ethylene using *O*-alkyl xanthates under relative mild conditions ($T \leq 80$ °C, $P \leq 200$ bar), paving the way to a myriad of new well-defined architectures, including block copolymers based on PE segments. Although controlled growth of PE chains was achieved, a detrimental side-fragmentation reaction, intrinsic to the nature of the chain transfer agent (CTA), led to the loss of chain-end fidelity and the accumulation of dead polymer chains, eventually posing issues for obtaining well-defined block copolymers.

Building on these results, this PhD project aims at improving the RAFT polymerization of ethylene by avoiding the side-fragmentation issues encountered with *O*-alkyl xanthates with the

ultimate goal of synthesizing block copolymers with ethylene and polar vinyl monomers by sequential monomer addition.

This manuscript is divided into five chapters:

Chapter I reviews the available methods used for ethylene homopolymerization and copolymerization with polar vinyl monomers. A special attention is paid to radical polymerization techniques and the methods developed to obtain polar OBCs with ethylene using different polymerization mechanisms. RDRP processes used for the controlled radical polymerization of ethylene is surveyed, with a more in-depth presentation of the RAFT process and its specificities for the synthesis of block copolymers.

RAFT homopolymerization of ethylene and CTAs investigated to circumvent side-fragmentation are described in **Chapter II**. Specificities, advantages and disadvantages of the use of *O*-aryl xanthates and *N*-aryl dithiocarbamates are highlighted. The statistical copolymerization of ethylene and vinyl acetate to produce well-defined ethylene-vinyl acetate (EVA) copolymers is also described.

The synthesis of block copolymers based on vinyl acetate and ethylene, two less activated monomers (LAMs) with similar reactivities, using *O*-aryl xanthates is discussed in **Chapter III**. This chapter highlights difficulties encountered with the characterization of polar-apolar block copolymers and the importance of the physical state of the polymerization medium to successfully produce block copolymers from a polar macro-CTA.

Two methods used to obtain block copolymers from methyl methacrylate and ethylene, two monomers with disparate reactivities (more activated vs. less activated monomer), are presented in **Chapter IV**. One method consists in the use of a switchable dithiocarbamate CTA, the other in combining successively irreversible transfer reactions and RAFT polymerization.

Eventually, **Chapter V** is dedicated to the synthesis of amphiphilic poly(ethylene oxide)-*block*-polyethylene copolymers in organic solvent and in water. Formation of the diblock copolymers *via* polymerization-induced self-assembly (PISA) was evidenced in some instances, leading to the synthesis of particle dispersions in water or organic solvent. The particle morphologies observed include spheres, worms, vesicles and ellipsoids.

Chapter I

State of the Art

I.	General introduction on ethylene polymerization.....	39
I.1.	A rapid overview on polyethylene (PE)	39
I.2.	Synthesis of PE	41
I.2.1.	Catalytic polymerization of ethylene	41
I.2.2.	Radical polymerization of ethylene	45
I.3.	Copolymerization of ethylene with polar monomers	51
I.3.1.	Catalytic copolymerization	51
I.3.2.	Radical copolymerization	52
I.4.	Conclusion.....	53
II.	Block copolymers synthesis based on a preformed PE segment obtained by catalytic polymerization	54
II.1.	Foreword on reversible deactivation radical polymerization	54
II.2.	Indirect block copolymer synthesis involving a PE block	58
II.2.1.	Synthesis by anionic polymerization methods	58
II.2.2.	Synthesis by radical polymerization methods	61
II.3.	Block copolymer synthesis by successive coordination-insertion of ethylene and group transfer polymerization of the polar monomer	65
II.4.	Synthesis of diblock copolymers by coupling two preformed blocks	67
II.5.	Conclusion.....	68
III.	Reversible-deactivation radical polymerization of ethylene	70
III.1.	More activated monomers and less-activated monomers	70
III.2.	RDRP of ethylene <i>via</i> ITP	71
III.3.	RDRP of ethylene <i>via</i> TERP	72
III.4.	RDRP of ethylene <i>via</i> OMRP	73
III.5.	RDRP of ethylene <i>via</i> NMP	75
III.6.	RDRP of ethylene <i>via</i> RAFT polymerization	76
III.7.	Conclusion.....	79
IV.	Specificities of RAFT polymerization	80
IV.1.	RAFT polymerization	80
IV.1.1.	Choice of Z- and R-groups.....	83
IV.2.	Synthesis of block copolymers <i>via</i> RAFT polymerization	85
IV.2.1.	General guidelines for successful synthesis of block copolymers by RAFT	85
IV.2.2.	Block copolymers between LAMs and MAMs <i>via</i> RAFT polymerization ..	86

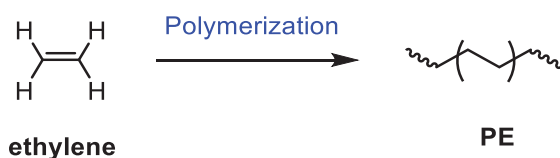
V. Conclusion and positioning of this work..... 90
VI. References 91

I. General introduction on ethylene polymerization

I.1. A rapid overview on polyethylene (PE)

Polyethylene (PE) is the most largely used and produced polymer in the world with a demand of 92 million metric tons in 2016^[1] and represents 38 % of all the polymers produced worldwide.

PE is the simplest polymer with a backbone consisting of only $-(\text{CH}_2-\text{CH}_2)-$ repeating units. It is produced by polymerization of ethylene ($\text{CH}_2=\text{CH}_2$) (**Scheme 1**), the simplest and cheapest vinyl monomer. Ethylene is produced by the petrochemical industry mainly by steam cracking of oil. To a lesser extent, ethylene can be produced from natural feedstock by dehydration of bioethanol.^[2] PE made using this bioethylene can be considered as a renewable resource. It is however worth mentioning that, as of today, ethylene produced by steam cracking is by far the cheapest way to get ethylene and polyethylene.



Scheme 1. General polymerization of ethylene

PE owns its industrial success to both its low production costs and interesting mechanical properties, primarily due to its crystallinity. The crystallinity of PE arises from the fact that the chains are mainly linear and non-hindered, so they can fold onto each other and create – within the polymer matrix – regions of high order that will bring rigidity to the material. The crystallinity of PE is directly impacted by its branching degree. The higher the branching degree, the lower the crystallinity. The most branched regions of the chains will not be able to crystallize and will be located in the amorphous region of the polymer matrix (a region of low to nonexistent order). In between those regions, some chains are partly trapped in polymer crystals, partly trapped in the amorphous region.

Using different methods of polymerization, which will be discussed later in this manuscript, PE properties can be adjusted by tuning its branching degree.

Rather than being designated and classified by its number-average molar mass (M_n), PE is usually classified by its density. The higher the crystallinity, the higher the density. Different degrees of crystallinity imply different mechanical strengths and different applications, ranging from food packaging for low density PE to bulletproof vests for ultra-high molecular weight PE.

Low Density Polyethylene (LDPE)

LDPE is historically the first PE ever produced on an industrial scale by Imperial Chemical Industries in 1937.^[3] It is produced by free radical polymerization (FRP) of ethylene under high pressure and high temperature (*vide infra*). The density of LDPE is comprised between 0.90 and 0.94 g cm⁻³. It contains a fair number of branches that hinder crystallization and result in a largely amorphous material. The branches consist mainly of ethyl and butyl ramifications, with some long chain branches that can themselves contain ramifications.^[4] Material properties of LDPE are interesting because of long ramifications, which are not found in other types of PE (see below), making LDPE less rigid while still retaining high chemical resistance. These long ramifications also render processing easier. Thus, LDPE still has a widespread use in the world today. Examples of material made from LDPE include plastic bottles, trash bags, tubing as well as laboratory equipment. Many of those materials are disposable. Throughout this manuscript, every PE synthesized can be considered as LDPE as it is made by a radical process.

Linear Low Density Polyethylene (LLDPE)

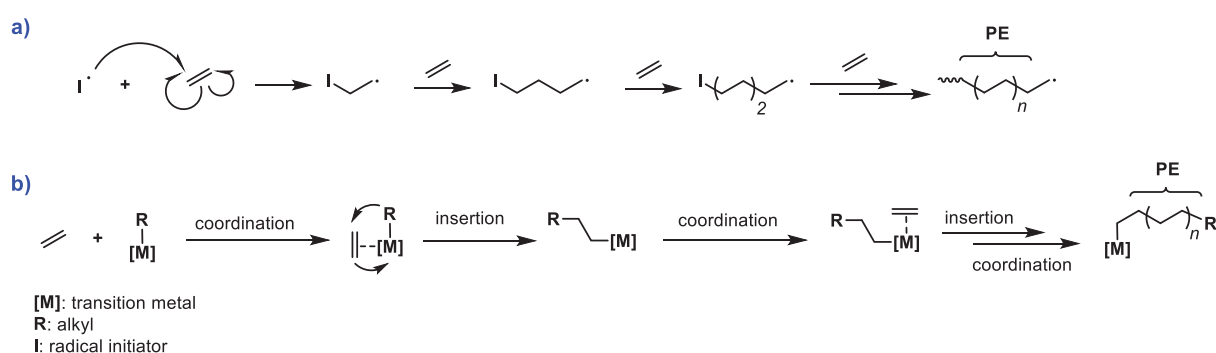
LLDPE is produced by catalytic copolymerization of ethylene with other α -olefins. By the very nature of its synthetic process, LLDPE contains short ramifications of a length that depends on the type of α -olefin used, separated by random intervals, typically between 25 and 100 carbon atoms. LLDPE can be seen as an intermediary product between LDPE and “true” linear polyethylene. The presence of short branches hinders crystallization, producing a material with a density in the range 0.90-0.94 g cm⁻³.^[4] A variant of LLDPE is very low density polyethylene (VLDPE). It contains more branching than LLDPE, lowering its density to the range 0.86-0.90 g cm⁻³.

High Density Polyethylene (HDPE)

HDPE is chemically the closest to pure linear polyethylene, with almost exclusively -(CH₂-CH₂)- repeating units in the polymer backbone. With very few branches to hinder its crystallinity, HDPE typically has a density in the range 0.94-0.97 g cm⁻³. It is made by a catalytic process and sometimes a very small amount of 1-alkene (α -olefin) is added in order to slightly reduce its crystallinity for better processability. HDPE can be produced with a high molar mass (up to several millions gram per mole), providing a material with unmatched mechanical properties for a thermoplastic. This material is then called ultra high molecular weight polyethylene (UHMWPE). Its toughness and impact strength are such that it can be used for medical applications for hip replacements, or even military applications with bulletproof vests.^[5]

I.2. Synthesis of PE

As aforementioned, PE is made industrially from ethylene either by a radical process (chain growth mechanism) or in the presence of a transition metal complex under catalytic conditions (coordination-insertion mechanism) depending on the type of PE and the properties desired. Radical polymerization of ethylene usually requires very harsh conditions (Temperature > 200 °C, Pressure > 1000 bar, **Scheme 2a**) whereas the use of catalytic amounts of transition metal [M] complexes requires much milder conditions (Temperature < 65 °C, Pressure < 30 bar) (**Scheme 2b**).^[4] It is also possible to polymerize ethylene *via* an anionic polymerization process called the “Aufbau” reaction^[6] but this process is only used to produce oligomers of ethylene.



Scheme 2. General mechanism of radical polymerization (a) and catalytic coordination-insertion polymerization of ethylene (b).

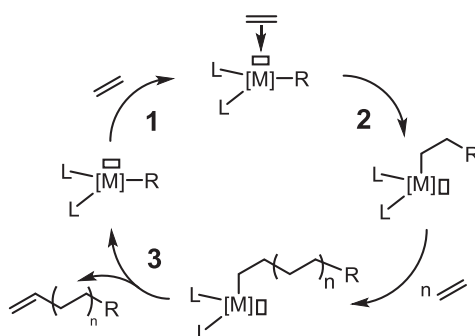
I.2.1. Catalytic polymerization of ethylene

In the early fifties, catalytic polymerization of ethylene, producing HDPE, was discovered almost simultaneously by the group of Hogan and Banks working for the Phillips Petroleum Company using chromium-based catalysts, known as Phillips catalysts,^[7] and by the group of Ziegler using titanium-based catalysts, known as Ziegler-Natta (ZN) catalysts.^[8] Further development of the catalysts allowed the copolymerization with other α -olefins, thus enabling the production of LLDPE. Those two catalysts, together with the metallocene^[9] and post-metallocene class catalysts, which were developed from the 1970's, represent the most used catalysts for the production of PE.

The conditions required for the catalytic polymerization of ethylene are mild and easy to implement in an academic laboratory. This has eased the extensive study of these systems and generated a vast literature on the subject. In this chapter, only the general principles of the catalytic polymerization of ethylene will be presented, along with the most important class of catalysts. The advantages and disadvantages of this technique for the copolymerization of ethylene with polar monomers will be discussed.

1.2.1.1. Generalities

The catalytic polymerization of ethylene proceeds *via* a coordination-insertion mechanism involving a transition metal [M] species possessing a [M]-R bond (R = H, alkyl) and an electronic vacancy which coordinates ethylene (**Scheme 3, 1**). Coordination of ethylene to the metal center will activate the C=C double bond and weaken the [M]-R bond, thus enabling the insertion of ethylene (**2**). Most catalysts do not possess the required [M]-R bond before the polymerization starts and must be activated with cocatalysts (aluminum alkyl for ZN catalysts, such as triethylaluminum (TEA), or methylaluminoxane (MAO) for group 4 metallocenes). The nature of the ligands (L) on the metal center [M] will greatly influence its reactivity, as well as its ability to make high molar mass chains.



Scheme 3. Simplified mechanism of catalytic coordination-insertion polymerization of ethylene. M = transition metal, R = alkyl/H, L = ligand.

After several monomer units are inserted, a transfer reaction will occur, such as β -H elimination, to release a polymer chain terminated by a vinyl function and regenerate the active [M] species (**3**), which is in turn able to insert ethylene and continue the catalytic cycle.

Transition metal catalysts can be either homogeneous or heterogeneous:

- **Homogeneous:** the catalyst is soluble in the polymerization medium and is usually a single-site catalyst.^[10] It means that every active site has the same environment, thus the same reactivity. Polymers made by such catalysts will tend to have low dispersities (\mathcal{D}) and contain only one molar mass population. For example, zirconium metallocene activated by MAO are homogenous catalysts.
- **Heterogeneous:** the catalyst is supported onto an inorganic framework, which makes it insoluble in the polymerization medium.^[11] These catalysts are called multi-site catalysts because active sites will have different environments and different reactivities. Each active site will produce its own chains and the resulting material will be a collection of all the macromolecules produced by the different active sites and will have a high dispersity value. The majority of industrial catalysts are heterogeneous, such as ZN (TiCl₄ supported on MgCl₂ and activated by TEA) or Phillips catalysts (chromium supported on silica, without cocatalyst).

Some catalyst specificities are directly linked to the nature of the transition metal used, which will be briefly discussed in the following paragraphs.

1.2.1.2. Group 4 to group 6 transition metals

Transition metals of group 4 (titanium, zirconium), 5 (vanadium) and 6 (chromium) are efficient for ethylene polymerization to produce HDPE of high molar mass with a high activity. They include both ZN and Phillips type catalysts, the most used catalysts in the industry. The main downside of those catalysts is that they are highly oxophilic, meaning that they will form stable chelate complexes with oxygen atoms. Indeed, the high affinity between the metal and the oxygen atom yields a very stable complex, and the vacancy on the metal is never freed, thus rendering the metal completely inactive for polymerization. This is why early transition metal catalysts are not effective in copolymerizing ethylene with polar monomers, which will form stable complexes with the metal, either before or after the insertion of the polar monomer if any (**Figure 1**). This is referred to as “catalyst poisoning” and has been dubbed the “polar monomer problem”.^[12]

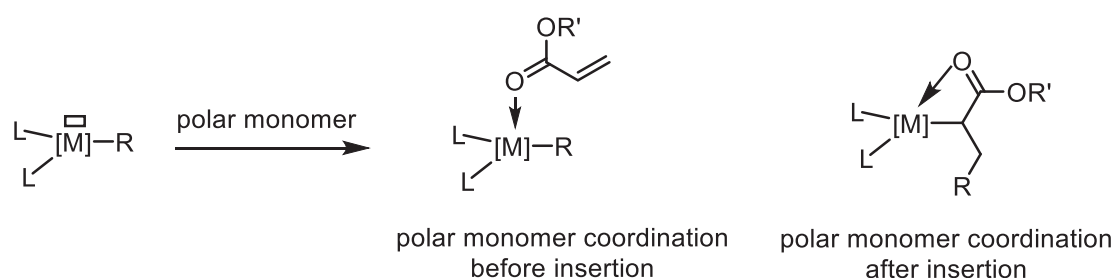


Figure 1. Catalyst poisoning by polar monomers.

Some groups have worked on means to counter this polar monomer problem, either by protecting^[13] or secluding^[14] the polar functions from the transition metal. However, the use of the less oxophilic late transition metals is a better alternative.^[15]

1.2.1.3. Group 8 and group 9 transition metals

Iron (group 8) and cobalt (group 9) post-metallocenes complexes with bis(imino)pyridine (**Figure 2**) ligands are fairly recent catalysts, developed in the late 1990's.^[16,17] Those complexes have the particularity of producing PE for which the molar mass depends on the steric hindrance of the ligand. The bulkier the ligand, the less favorable the elimination step and the higher the molar mass of the polymer chains. Iron and cobalt complexes have shown some tolerance to polar monomers, such as methyl methacrylate (MMA), methyl acrylate (MA) or styrene (S), but the copolymerization of ethylene with those monomers showed that only a mixture of homopolymers was obtained. On the other hand, monomers such as vinyl acetate (VAc) or acrylonitrile (AN) showed a complete deactivation of the catalyst.^[16,17]

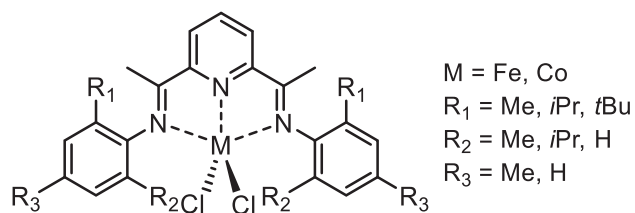


Figure 2. Cobalt and iron precatalyst complexes with bis(imino)pyridine ligands.

1.2.1.4. Group 10 transition metals

Traditionally, late transition metal catalysts were found to produce dimers or low molar mass oligomers due to chain termination *via* β -H elimination,^[18] which is taken advantage of in the Shell higher olefin process (SHOP). However, the use of large, bulky ligands allows the production of high molar mass PE.^[19]

Group 10 transition metals (nickel, palladium) can be sorted into four main categories: Brookhart type catalysts^[20] (diamine ligands), Grubbs type catalysts^[19] (phenoxyimine ligands), Keim type catalysts^[21] (Phosphino-enolate ligands) and Drent type catalysts^[22] (Phosphino-sulfonate ligands) (**Figure 3**). These catalysts have been shown to be quite effective at producing both oligomers of ethylene (SHOP) or high molar mass polyethylene, through the use of bulky ligands and phosphine scavengers. By playing with the nature of the ligands, PE with a high (30 to 100 branches per 1000 C atoms) or low branching degree (1 to 10 branches per 1000 C atoms) can be obtained with these catalysts, which are also efficient at copolymerizing ethylene with other α -olefins. Group 10 metals being moderately oxophilic, they have also been successfully used to copolymerize ethylene with polar monomers^[23] or polymerize ethylene in water.^[24–26]

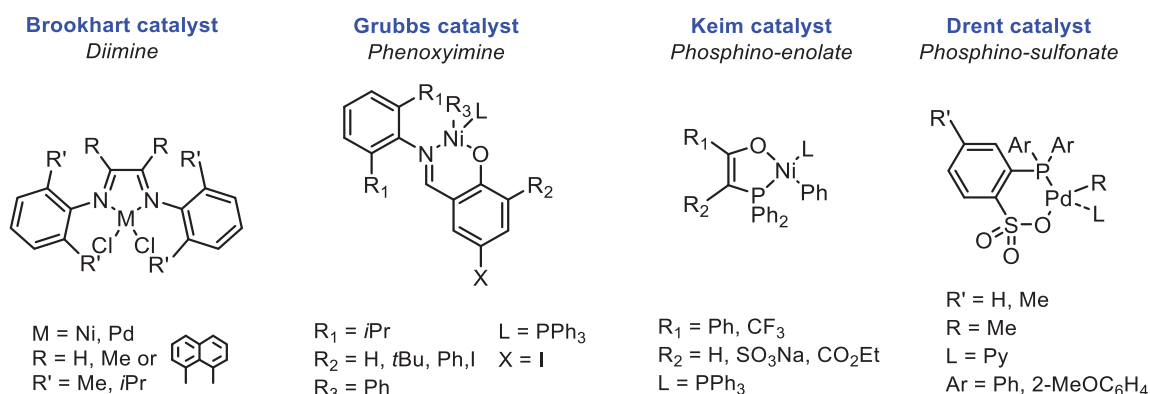
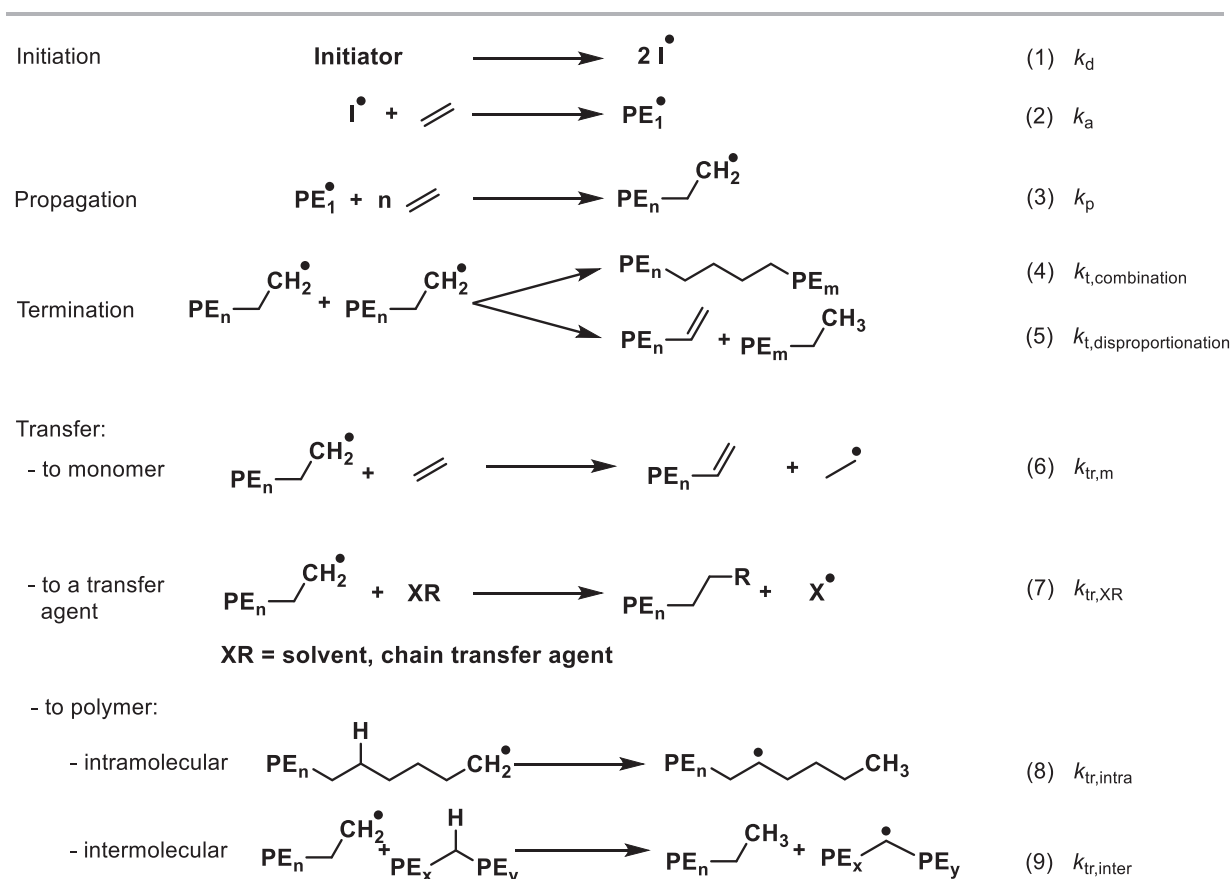


Figure 3. Grubbs, Brookhart, Keim and Drent type catalysts and pre-catalysts.

1.2.2. Radical polymerization of ethylene

The radical polymerization of ethylene can be classified into two categories: the industrial process for ethylene polymerization, specific to large-scale production and not really suited for R&D works, and the laboratory production of PE, carried out in small-scale reactor and suited for R&D. In this paragraph, some generalities about radical polymerization will be presented, and the differences between the two processes will be outlined. A more in-depth explanation of the laboratory production of PE *via* a radical process will then be conducted, as it will be the preferred method of synthesis for PE throughout this PhD work.

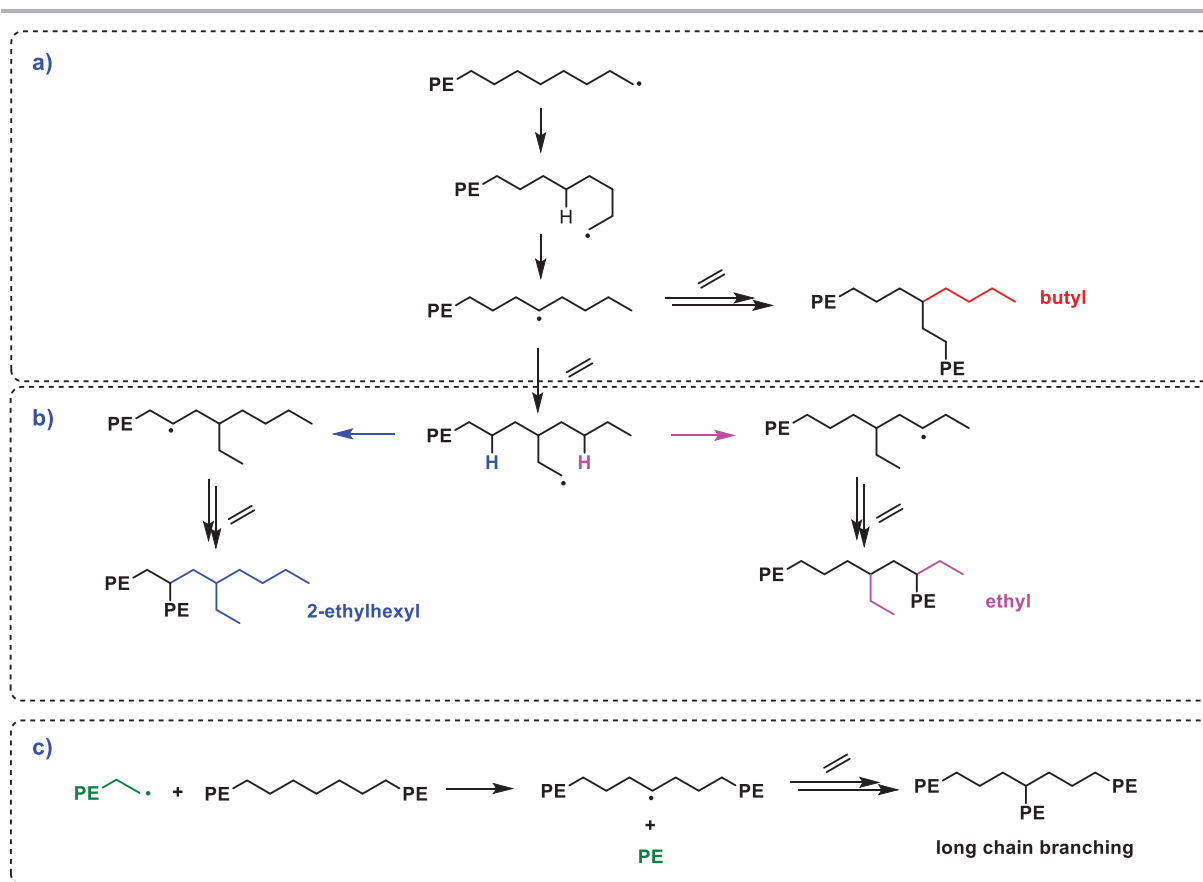
The typical mechanism for the radical polymerization of ethylene (**Scheme 4**) involves the classic steps governing the radical polymerization of vinylic monomers: initiation (**1,2**), propagation (**3**), termination (**4-5**) and transfer (**6-9**). The different transfer reactions do not necessarily occur at the same time and depend largely on the pressure and the temperature.



Scheme 4. Comprehensive mechanism of the radical polymerization of ethylene.^[27]

Naturally, to create a polymer of high molar mass, the propagation rate constant (k_p) must be greater than the termination rate constant (k_t). The addition of a radical onto an ethylene monomer creates an unstable primary $-\text{CH}_2^{\bullet}$ radical. For this reason, the radical polymerization of ethylene is not thermodynamically favored unless the temperature is high enough (*vide infra*) and the system is especially prone to transfer.

Although instinctively random, intramolecular transfer (**8**) leading to short chain branching is in fact very selective in the case of ethylene.^[28] This transfer mostly results in ramifications containing two or four carbon atoms. The mechanism underpinning those ramifications is easily explained by the formation of a stable cyclic intermediate with 6 carbon atoms^[29] leading to butyl (**Scheme 5a**) and 2-ethylhexyl (**Scheme 5b**) branches. The formation of butyl ramifications proceeds by a mechanism referred to as *backbiting*. The formation of long chain branches (> 6 carbon atoms) is mainly the result of intermolecular transfer (**Scheme 5c**). PE produced by a radical process typically contains a total number of 10 to 50 branches per 1000 C atoms. Of these, 10 % are ethyl, 50 % are butyl and 40 % are longer side chains.^[30]



Scheme 5. Formation of ethyl, butyl, 1-ethylhexyl and long chain branching.

1.2.2.1. Industrial production of PE

In the industry, the radical polymerization of ethylene yields LDPE. LDPE represented 24 % of all the PE produced in 2016.^[1] The severe reaction conditions used ($T > 200$ °C, $P > 2000$ bar) bring ethylene above its critical point ($T_{\text{crit}} = 9.2$ °C, $P_{\text{crit}} = 50.4$ bar).^[31] The monomer thus becomes solvent of the polymer, easing the polymerization process. The polymerization is usually conducted in an autoclave or tubular reactor.^[32]

The harsh conditions used in the industry to polymerize ethylene can be explained by the inherent low reactivity of the ethylene monomer. The activation energy for the propagation of

ethylene ($E_a = 34.3 \text{ kJ mol}^{-1}$) is higher than for other monomers ($E_a = 32.5 \text{ kJ mol}^{-1}$ for styrene and $E_a = 20.4 \text{ kJ mol}^{-1}$ for vinyl acetate for example).^[33] A kinetic study by Ehrlich^[34] showed through the determination of the $k_p/k_t^{1/2}$ values for ethylene that the free radical polymerization of ethylene was only favorable under high pressure and high temperature (the higher the $k_p/k_t^{1/2}$ value, the more favorable the polymerization, **Table 1** and **2**).

Table 1. Influence of pressure on $k_p/k_t^{1/2}$ values at 129 °C.

Pressure (bar)	$k_p/k_t^{1/2}$ ($\text{l mol}^{-1/2} \text{ s}^{-1/2}$)
750	0.22
1 000	0.30
1 500	0.40
2 000	0.54
3 000	0.73

Table 2. Influence of temperature on $k_p/k_t^{1/2}$ values, extrapolated at 1 bar.

Temperature (°C)	$k_p/k_t^{1/2}$ ($\text{l mol}^{-1/2} \text{ s}^{-1/2}$)
-20	0.009
83	0.15
129	0.17
130	0.21
250	1.7

Interestingly, the number of ramification increases as the temperature increases or as the pressure diminishes.^[35,36] It is thus possible to produce a highly linear PE (branching degree below 1 branch per 1000 carbon atoms) exhibiting a high melting point (132 °C) and a high density (0.955) under extreme pressure conditions ($P > 5\,000 \text{ bar}$) and relatively low temperature ($T < 60 \text{ °C}$).

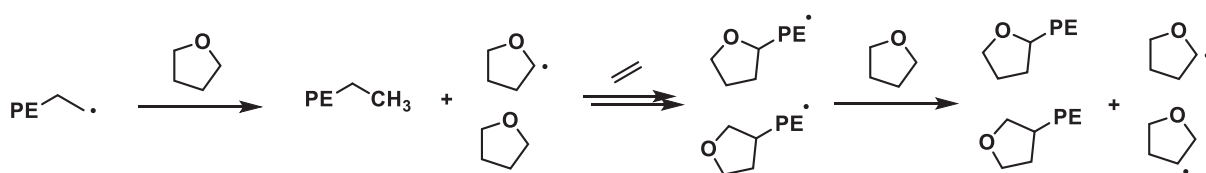
Despite being less energy-efficient than the catalytic polymerization of ethylene, radical polymerization of ethylene is still extensively used nowadays as it is the only way to achieve LDPE.

1.2.2.2. Laboratory synthesis of PE

The conditions required by the industrial production of PE are very hard to reproduce in an academic laboratory. This partly explains the lack of research and development in the FRP of ethylene since its discovery. Only a few other groups are or have been working on PE synthesis at an academic level.^[37-39] Some years ago, Grau *et al.*^[40] demonstrated that the efficacy of the radical polymerization of ethylene can be drastically improved by the use of different solvent, thus enabling the FRP of ethylene under much milder conditions ($T < 100 \text{ °C}$, $P < 200 \text{ bar}$). Originally, Grau *et al.* studied the effect of two common organic solvents for radical polymerization: tetrahydrofuran (THF) and toluene.^[40] It was shown that the polymerization kinetics follows a first order law. The rate of polymerization in THF was found to be about 6 times higher than in toluene, clearly indicating an activating effect of the solvent. In short, the results were as follows:

- **In THF:** Yield of 3.9 g of PE (100 bar of ethylene, 70 °C, 4 hours, 50 mg of azobisisobutyronitrile (AIBN) as initiator. $M_n = 1\ 200\ \text{g mol}^{-1}$, melting temperature (T_m) = 115 °C, crystallinity (X_c) = 58 %.
- **In toluene:** Yield of 0.7 g of PE (same conditions). $M_n = 2\ 300\ \text{g mol}^{-1}$, $T_m = 116\ \text{°C}$, $X_c = 63\ \%$.

The yield in THF is about 6 times higher than in toluene, which is consistent with the kinetic study. The main difference in the PE produced lies in the molar masses M_n . THF yields PE of substantially lower M_n than toluene. This was explained by extensive transfer to solvent in the case of THF (**Scheme 6**), less pronounced with toluene.



Scheme 6. Transfer to THF during ethylene radical polymerization.

The effect of three solvents (THF, toluene and diethyl carbonate) on yield and molar mass is illustrated in **Figure 4a** and **4b**, respectively. Following these results, Grau *et al.* conducted a more thorough study on the effect of the solvent, encompassing a large variety of common organic solvents.^[41] The results are presented in **Table 3**.

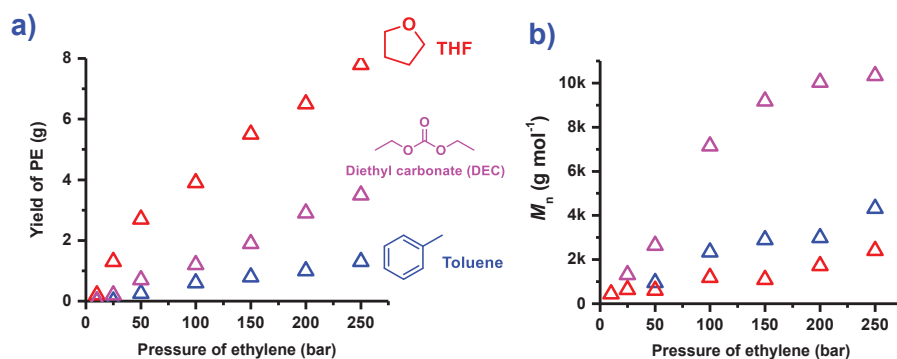


Figure 4. Influence of solvent on the yield (a) and on the molar mass of PE obtained by FRP (b).

Table 3. Solvent influence on the radical homopolymerization of ethylene.

Entry	Solvent	Yield (g)	T _m ^a (°C)	X _c ^a (%)	M _n ^b (g mol ⁻¹)	D ^{b,c}
1	Supercritical ethylene	0.1	105	46	3 000	1.3
2	Cyclohexane	0.6	115	58	4 800	2.2
3	Heptane	0.65	116	55	4 700	2.1
4	Toluene	0.7	115	63	2 300	1.9
5	DMSO	1	112	43	1 900	3.5
6	Acetonitrile	1.1	115	59	1 400	2.2
7	Diethyl carbonate	1.2	117	62	7 200	2.5
8	DMF	1.3	108	47	500	2.9
9	Diethyl ether	1.3	109	52	1 400	1.4
10	Ethanol	1.4	117	63	2 100	2.4
11	Acetone	1.5	115	62	1 700	2.0
12	Dimethyl carbonate	1.6	117	57	11 700	2.5
13	Butanone	1.8	61	nd	400	1.2
14	Butyrolactone	1.8	nd	nd	600	1.4
15	Butan-2-ol	1.9	116	68	2 100	2.8
16	Cyclohexanone	2.1	nd	nd	1 800	1.5
17	Butan-1-ol	2.2	117	58	4 100	2.4
18	Ethyl acetate	2.3	115	54	3 800	3.3
19	Dichloromethane	2.7	105	46	1 100	1.6
20	1,4-dioxane	3.2	118	65	1 300	2.2
21	THF	3.9	115	58	1 200	1.9

Polymerization conditions: 4 h, T = 70 °C, P = 100 bar, AIBN: 50 mg, solvent: 50 mL. ^a: determined by differential scanning calorimetry (DSC), ^b: determined by high temperature size exclusion chromatography (HT-SEC) in 1,2,4-trichlorobenzene (TCB) at 150 °C with a conventional PE calibration, ^c: $D = M_w/M_n$; DMSO: Dimethyl sulfoxide, DMF: *N,N*-dimethylformamide,

In brief, the solvent presenting the best compromise between yield of PE and M_n is dimethyl carbonate (DMC), with a M_n of 11 700 g mol⁻¹, substantially higher than that of other investigated solvents, thus indicating a lower propensity to transfer.

Apart from a clear effect of the solvent on the polymerization of ethylene, previously identified for other monomers,^[42] the precise reason behind this activation is still not yet clear. Grau *et al.* managed to show a relation between the yield of polymer x , the dipole momentum μ and the dielectric constant ε of the solvent (**Equation 1** and **Figure 5**) following the theory of the activated complex.

$$\ln \left[\ln \left(\frac{1}{1-x} \right) \right] \propto \left(\frac{\mu}{\varepsilon} \right)^2$$

Equation 1. Relation between yield of polymer x , dipole momentum μ and dielectric constant ε of the solvent.

The Λ -shape curve obtained clearly shows three extrema, obtained for alkanes (cyclohexane and heptane), THF and diethyl carbonate (DEC). To validate this model, experiments using different ratios of these three solvents were conducted and all points fit nicely to the Λ -shape obtained using pure solvents. The activation of the polymerization by the solvent has been attributed to a caging effect. It is hypothesized that the solvent creates a “cage” around the radical species and the monomer molecules, for which the stability depends on the $(\mu/\varepsilon)^2$ value. The higher the $(\mu/\varepsilon)^2$ value, the longer the lifetime of the cage and the higher the probability of

addition of a propagating radical onto a monomer. This “caging” effect is still under study through a collaboration with S. Marque at the Aix-Marseille university.

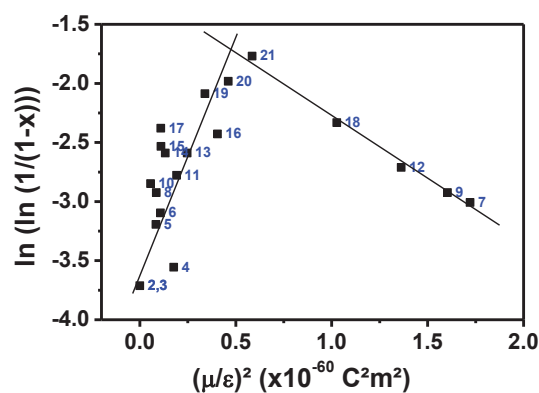


Figure 5. Effect of solvent on yield of PE (x). Polymerization conditions: 4h, 70 °C, 100 bar, 50 mg AIBN, 50 mL DMC. Numbers correspond to entries in Table 3. Extracted from ref [41]

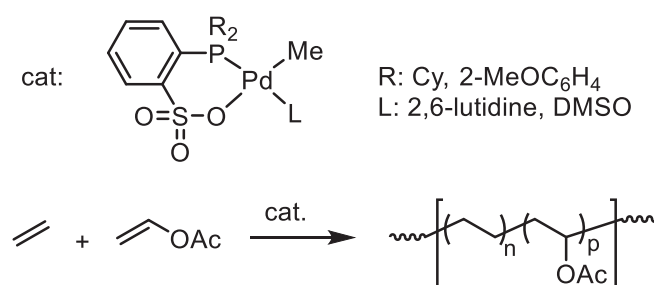
Ethylene can be copolymerized with other monomers (polar or apolar) to afford materials with different properties. The radical statistical copolymerization of ethylene with α -olefins is not efficient because allylic protons are readily abstracted by transfer reactions leading to unreactive allylic radicals.^[43] On the other hand, catalytic coordination-insertion copolymerization of ethylene with α -olefins is well-established^[44] and is used to adjust the mechanical properties of PE by tuning its crystallinity. The statistical copolymerization of ethylene with polar monomers is more challenging and leads to the synthesis of a broad range of materials. It will be discussed in the following section.

I.3. Copolymerization of ethylene with polar monomers

PE (and polyolefins in general) exhibits excellent mechanical properties and chemical resistance, which can also be a drawback when it comes to surface properties. A solution consists in randomly inserting polar units into the polymer backbone, which drastically changes its polarity and potential applications, even at low co-monomer content. The random copolymerization of two monomers yields a polymer with properties intermediate to that of the otherwise two homopolymers. Hence, a high polar monomer content will afford a polymer with mechanical properties very far from that of a PE homopolymer.

I.3.1. Catalytic copolymerization

The statistical copolymerization of ethylene with polar monomers by catalytic coordination-insertion has long been studied.^[23,45,46] As mentioned above, early transition metals suffer from catalyst poisoning issues, but late transition metals (group 10 mostly) allow for the statistical insertion of polar monomer units into the PE backbone. The polar monomer insertion remains quite low (~10-20 mol%) and their presence tremendously reduces the catalytic activity. Nozaki *et al.* copolymerized ethylene with vinyl acetate using palladium-phosphine-sulfonate catalysts (**Scheme 7**) but with VAc insertion not exceeding 2 mol%.^[47] It should be noted that VAc is among the most challenging monomers for metal-catalyzed coordination-insertion polymerization as it causes the most catalyst deactivation.^[48]



Scheme 7. Statistical copolymerization of ethylene and vinyl acetate using a Pd catalyst.^[47]

This type of catalyst has also enabled the statistical copolymerization of ethylene with MMA,^[22,49,50] vinyl ethers,^[51] AN^[52] and vinyl fluoride.^[53] Even in the most recent studies, the low catalytic activities and low molar masses achieved remain a major obstacle. For example, palladium-phosphine-sulfonate and α -diimine palladium complexes were used to copolymerize ethylene with several polar monomers with insertions up to 10 mol%,^[54] but the activities and M_n were reduced by a factor of between 4 and 20 (depending on the polar monomer) compared to ethylene homopolymerization. Interestingly, a recent study shows that the copolymerization of ethylene with a vinyl trialkylsiloxane monomer in the presence of either a α -diimine palladium or α -diimine nickel based catalyst produces, respectively, highly branched or linear copolymers with

activities comparable to that of ethylene homopolymerization. The same study showed that when the polar monomer used is MMA, the catalytic activity is greatly reduced and no catalytic activity is reported when the polar monomer is VAc, AN or a vinyl halide.^[55] Another obstacle to copolymerization of ethylene with polar vinyl monomers by coordination-insertion is the price of the catalyst, hampering their industrial development.

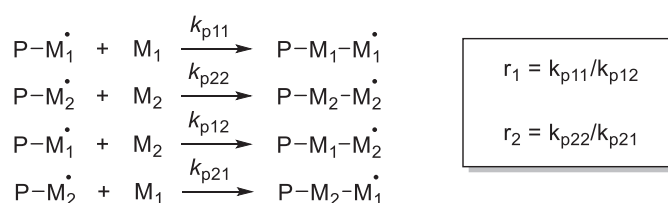
I.3.2. Radical copolymerization

The statistical copolymerization of ethylene with polar vinyl monomers consists essentially in a free radical process performed under harsh conditions (high temperature, high pressure). The reaction conditions used for such copolymerization depend on the polar monomer used and on the desired proportions of each monomer in the final polymer. The statistical radical copolymerization of ethylene with different polar monomers was studied in 1970, giving access to a few reactivity ratios (**Table 4**).^[34]

Table 4. Monomer reactivity ratios between ethylene and various polar monomers.^[34]

Polar comonomer	r_{ethylene}	$r_{\text{comonomer}}$	Pressure (bar)	Temperature (°C)
vinyl acetate	0.82	0.99	1 020-2 040	120
methyl acrylate	0.042	5.5	1 360	130-152
<i>n</i> -butyl acrylate	0.052	3	1 360	130-152
methyl methacrylate	0.03	18	1 360	130
<i>n</i> -butyl methacrylate	0.04	25	1 360	130
acrylic acid	0.02	4	1 160-2 040	140-226
methacrylic acid	0.008	4	2 040	160-200
styrene	0.04	2	1 500-2 500	100-280
1-butene	3.4	0.86	1 020-1 700	130-220

Reactivity ratios r_1 and r_2 (**Scheme 8**) are defined as the ratio between the rate constant for the addition of a monomer to a macro-radical terminated with the same monomer (k_{p11} , homopropagation) to the one for the addition of a monomer to a macro-radical terminated by the second monomer (k_{p12}).



Scheme 8. Definition of reactivity ratios.

It is clear from **Table 4** that reactivity ratios are always in favor of the polar monomer. Thus, in order to get an ethylene-rich copolymer, very high pressures of ethylene are required. Attempts to synthesize statistical copolymers at low ethylene pressure have often resulted in polar homopolymers with only a few isolated ethylene units into the polymer backbone.^[56,57] The use of Lewis acids, such as aluminum oxide (Al_2O_3) or scandium triflate ($\text{Sc}(\text{OTf})_3$) increases slightly the quantity of ethylene inserted.^[56,57]

Among statistical copolymers between ethylene and polar monomers, ethylene – vinyl acetate copolymers (EVA) are by far the most industrially produced and have numerous applications. EVAs can be divided into different categories, depending on their VAc content. For a low VAc content (< 40 weight%), the polymer is semicrystalline and has thermoplastic properties. It has applications as films, foams or fuel additives.^[58] These EVAs are usually produced by the same process used for the synthesis of LDPE: high pressure and high temperature. Processes in organic solution allow for milder synthetic conditions (30-150 °C, 200-700 bar) and cover EVA containing between 40 and 80 weight%. EVAs with a high VAc content (> 60 %) are obtained through radical emulsion polymerization (30-70 °C, 10-200 bar). These EVAs have applications as adhesives, paints or in concrete formulations.

Reversible-deactivation radical polymerization techniques have also been used to copolymerize ethylene with polar monomers. These methods will be surveyed in the part **III** of this chapter.

I.4. Conclusion

PE has numerous applications thanks to its outstanding mechanical properties, chemical resistance and low production costs. Still, the apolar character of PE can be problematic when it comes to surface properties and can be solved by the addition of polar functions. Catalytic coordination-insertion polymerization is efficient for ethylene polymerization, but the addition of polar monomers greatly hampers the catalytic activity, making this technique poorly adapted for the introduction of polar functions into PE. On the other hand, radical polymerization of polar vinyl monomers is highly efficient and statistical copolymers with ethylene can be obtained. This is however hampered by the unfavorable reactivity ratios between ethylene and most polar monomers. An alternative to polar-apolar statistical copolymers with ethylene is block copolymers.

II. Block copolymers synthesis based on a preformed PE segment obtained by catalytic polymerization

Statistical copolymers between ethylene and polar monomers allow for the introduction of polar functions into an otherwise completely apolar polymer. However, the introduction of polar monomers means that the material properties of the PE block, in particular its semicrystalline character, are lost. It is often interesting to synthesize block copolymers to retain the physical properties of both segments. The direct synthesis of PE-*b*-PX copolymers by the same polymerization mechanism, in which PX is a polar segment, is best achieved *via* a reversible-deactivation radical polymerization (RDRP, *vide infra*) mechanism. It necessitates the control over the polymerization of both ethylene and the polar monomer, which is especially challenging in the case of ethylene. The specificities and difficulties associated with the RDRP of ethylene will be presented in the part III of this chapter.

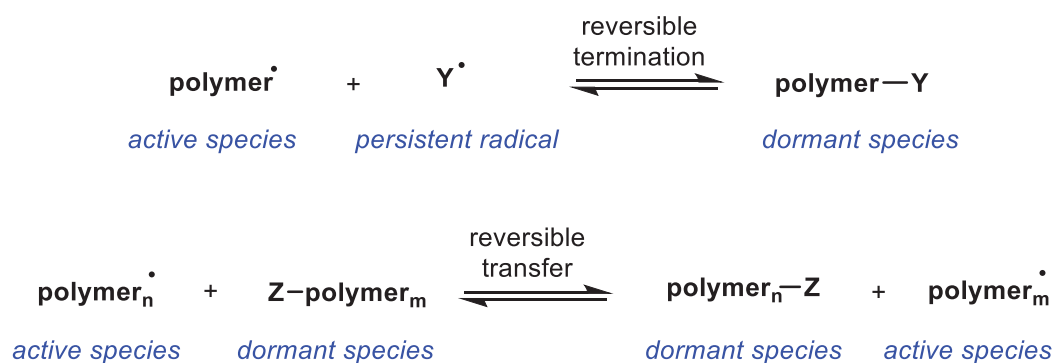
Before moving on to this subject, a non-exhaustive overview of the other methods developed to obtain PE-*b*-PX copolymers will be conducted. These methods mostly involve the synthesis of a PE segment by catalytic coordination-insertion polymerization with a reactive chain-end. The latter can be obtained *in situ* or by post-modification of the preformed PE segment. This reactive chain-end is then used to initiate the polymerization of a polar monomer to obtain the desired PE-*b*-PX copolymer *via* an anionic or radical pathway (*i.e.* indirect block copolymer synthesis).^[59,60] A few examples of catalytic coordination-insertion polymerization of ethylene followed by group transfer polymerization of a polar monomer will also be presented.

Research groups have often functionalized the PE segments with a moiety that can be used for a RDRP process, permitting the controlled growth of the polar segment.^[61] For the sake of clarity, a rapid presentation of the most common RDRP processes will thus be conducted beforehand. This foreword will also serve as an introduction into the following parts dealing with RDRP of ethylene (part III). The use of a preformed PE segment to initiate the polymerization of a polar monomer will then be surveyed. Eventually, some examples of the use of click chemistry to obtain PE-*b*-PX copolymers by the coupling of two preformed blocks will be given.

II.1. Foreword on reversible deactivation radical polymerization

The most common RDRP processes will be presented in the following. Conventional FRP suffers from irreversible termination reactions, transfer to monomer, polymer or solvent, and lack of control on the molar mass, the architecture and the composition of the polymer chains. The addition of a chain controlling agent in conventional radical polymerization allows for the controlled growth of the polymer chains by the rapid equilibrium between dormant (polymer

chains capped with a reactivatable end) and active species. When the equilibrium is strongly in favor of the dormant species, only a few radical centers are active at any given time, favoring propagation over irreversible termination reactions leading to the formation of dead chains. This pseudo-living process is then called reversible-deactivation radical polymerization. RDRP operates via two mechanisms: reversible termination and reversible transfer, of which a simplified schematic mechanism is presented in **Scheme 9**.



Scheme 9. Schematic mechanism of reversible transfer and reversible termination for RDRP.

RDRP by reversible termination (RT) is based on the persistent radical effect, first described by Fischer.^[62] In contrast to the active propagating **polymer**[•], the persistent radical **Y**[•] does not undergo irreversible self-termination and is not capable of initiating the monomer polymerization. Hence, **Y**[•] accumulates and the probability for **polymer**[•] to reversibly react with **Y**[•] rather than irreversibly with another **polymer**[•] increases. Prominent examples of RT are nitroxide-mediated polymerization (NMP)^[63] and atom transfer radical polymerization (ATRP).^[63]

Contrary to reversible termination, RDRP based on reversible transfer (also called degenerative transfer (DT)) is based on the addition of an active **polymer**_n[•] to a dormant species **Z-polymer**_m, resulting in the formation of a new dormant species **polymer**_n-**Z** and another active species **polymer**_m[•]. Examples of DT processes include cobalt-mediated radical polymerization (CMRP),^[64] iodine transfer polymerization (ITP),^[65] tellurium-mediated radical polymerization (TERP)^[66] and the well-known reversible addition-fragmentation chain transfer (RAFT).^[67] In principle, there is no change in the overall number of radicals during the process, so an external source of radicals is required, which in most cases is a typical radical initiator.

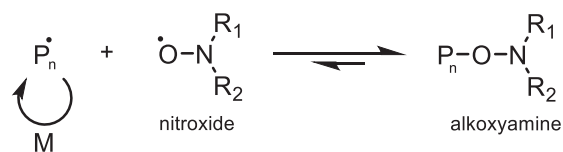
The main features of RDRP techniques are the linear increase of the polymer molar masses upon monomer conversion, associated with low dispersity values. Their pseudo-living character means that chains terminated by a reactive chain-end can be used as macro-control agent for chain-extension with the same monomer or block copolymerization with another monomer.

In the following, only RDRP methods used for the chain-extension of a preformed PE block by a polar segment will be succinctly presented. These methods include NMP, ATRP and RAFT. Other

RDRP techniques (TERP, ITP, CMRP) that have been specifically used for the controlled radical polymerization of ethylene will be presented in section III. Specificities of RAFT, in particular for the synthesis of block copolymers, will also be presented with more details in a separate paragraph in section III.

Nitroxide-mediated polymerization

NMP relies on the dynamic equilibrium between dormant alkoxyamines and active propagating radicals (**Scheme 10**).^[68,69]

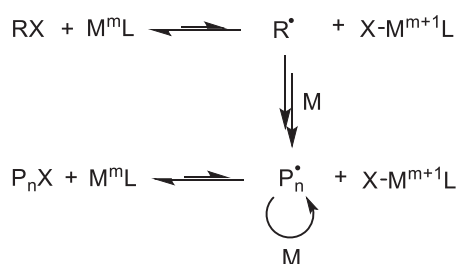


Scheme 10. Equilibrium in nitroxide-mediated polymerization.

The homolytic cleavage of the C-O bond that results in the release of the propagating species occurs upon temperature increase. If the nitroxide species is carefully chosen, the position of the equilibrium in Scheme 10 is such that the dormant alkoxyamine $\text{P}_n\text{ONR}_1\text{R}_2$ is the dominant species at polymerization temperature. The release of the propagating species P_n^\bullet ensures the growth of the polymer chains. The initiation of a controlled radical polymerization mediated by nitroxides can be performed using (i) a bimolecular system composed of a radical initiator and a nitroxide, or (ii) a monomolecular system based on an alkoxyamine which acts as both initiator and control agent.

Atom transfer radical polymerization

ATRP was first used in 1995 by the groups of Sawamoto^[70] and Matyjaszewski.^[71] It is one of the most widely used RDRP method.^[63] The use of a transition metal complex (M^mL , **Scheme 11**) is responsible for the homolytic cleavage of a carbon halogen bond (R-X) which generates the corresponding metal halide complex at a higher oxidation degree ($\text{X-M}^{m+1}\text{L}$) and an organic radical R^\bullet capable of initiating the polymerization of a vinyl monomer (M). The equilibrium between active species P_n^\bullet and dormant species P_nX is responsible for the control growth of the polymer chains.



Scheme 11. Schematic mechanism and equilibrium in atom transfer radical polymerization.

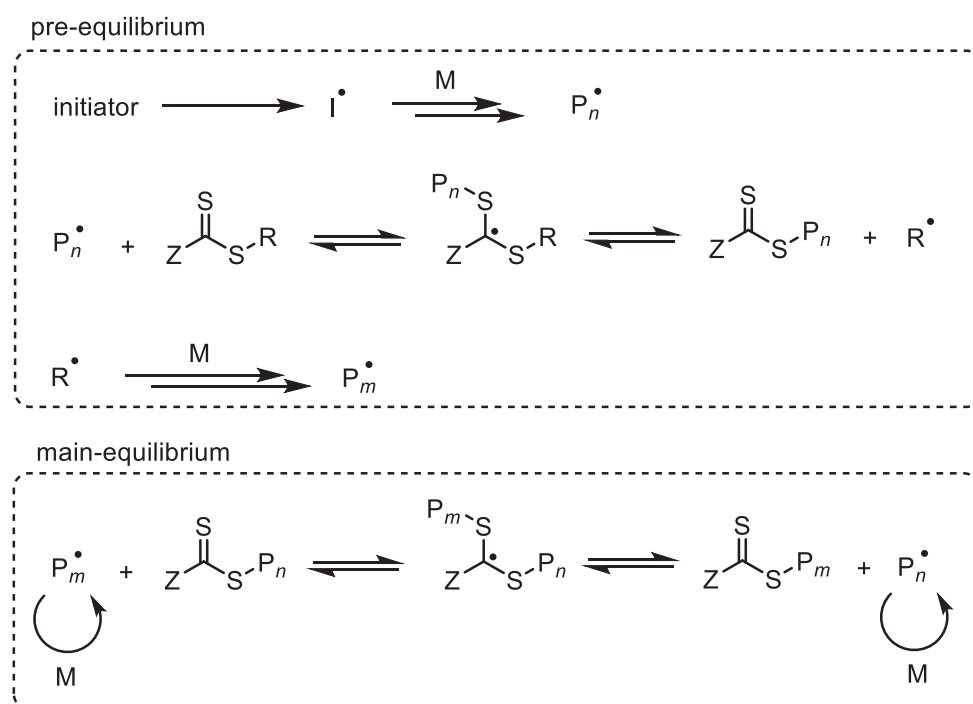
Complexes of Cu have been found to be the most effective for the control of a broad range of monomers, including in water,^[72] but other metals, such as Fe,^[69] Ni^[70] and Ru^[73] have also been used. The main downside of ATRP was its sub-stoichiometric use of transition metal complex. This was overcome with the use of either reducing agent with ARGET (activator regenerated by electron transfer) ATRP^[74] or conventional radical initiators with ICAR (initiator for continuous activator regeneration) ATRP.^[75] These two developments of ATRP enable the use of catalytic quantities of transition metal, down to ppm quantities. In addition, the use of zero valent copper (Cu⁰) has attracted significant attention for the fast and efficient controlled synthesis of high to ultra-high molar masses polymers with the concept of single electron transfer living radical polymerization (SET-LRP).^[76]

Reversible addition-fragmentation chain transfer polymerization

RAFT polymerization is one of the most versatile techniques for the synthesis of polymers with controlled architecture and monomer distribution.^[67] It was discovered almost simultaneously in 1998 by the groups of Moad and Rizzardo in Australia^[77] and of Charlot and Zard in France.^[78] It relies on the addition of a chain transfer agent (CTA) to an otherwise conventional FRP system. Moad *et al.* published their first example of RAFT with the use of dithioester CTAs, whereas Charlot *et al.* used xanthates. Accordingly, the latter ones did not designate their process as RAFT, but as macromolecular design via the interchange of xanthates, or MADIX. Although both terminologies are accepted when the CTA is a xanthate, only the RAFT terminology will be used for the rest of this manuscript.

In a RAFT process (**Scheme 12**), a thiocarbonylthio compound is used as CTA (**Z-C(S)S-R**). It reacts with either a radical derived from the initiator or a propagating polymer chain (**P_n•**), forming a new dormant species and releasing **R•**, in turn capable of re-initiating the polymerization of the monomer **M**. The control over chain-growth is then assured by the rapid exchange between dormant and active species.

Over the last 20 years, RAFT polymerization has been successfully employed for the controlled polymerization of a large variety of monomers, including but not limited to styrenics, acrylates, methacrylates, vinyl esters and more specific monomers such as fluoro-monomers.^[67,79-81]



Scheme 12. RAFT process mechanism.

II.2. Indirect block copolymer synthesis involving a PE block

To this day, one of the most used method for the synthesis of PE-*b*-PX relies on the prior synthesis of a functionalized PE made by a coordination-insertion mechanism, followed by the addition of the polar monomer by another polymerization mechanism, typically anionic or radical. Several reviews have been written on the subject.^[59,82,83] In this chapter, only some of the most important published works in which PE, obtained solely by polymerization of ethylene, is the apolar segment, will be presented. Works in which the polar segment is another polyolefin, or in which the PE block – or PE-like block – is obtained using another monomer than ethylene, will be omitted. Those works include, for example, the synthesis of a PE-like block by ring opening metathesis polymerization (ROMP),^[84–87] using ylides monomers^[88] or by hydrogenation of poly(butadiene) obtained by anionic polymerization.^[89,90] For the sake of conciseness, the synthesis of graft copolymers will not be discussed in this chapter.

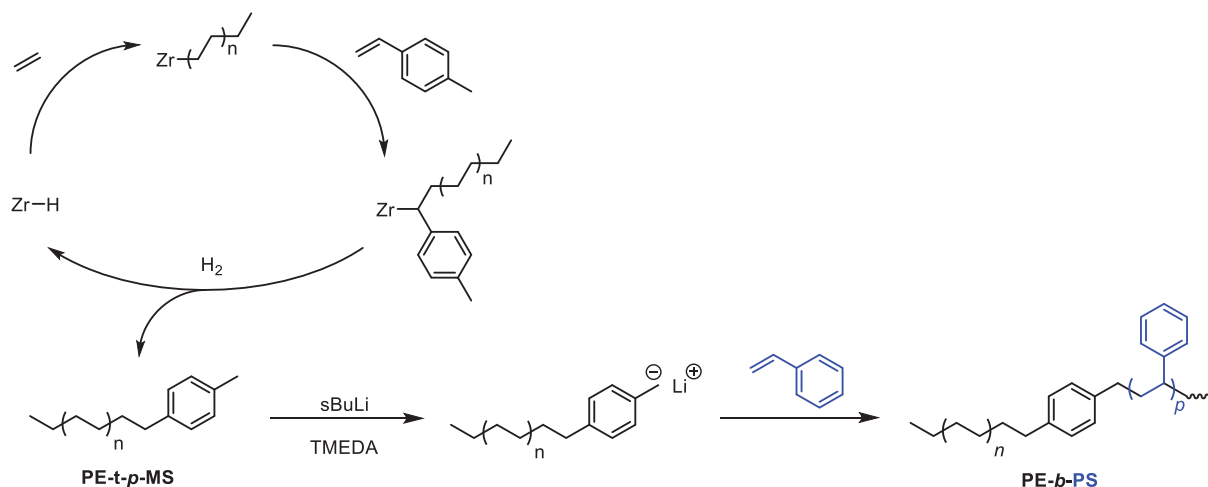
II.2.1. Synthesis by anionic polymerization methods

This paragraph is dedicated to the synthesis of diblock copolymers in which the polar block is added by anionic polymerization. Regular anionic polymerization and anionic ring opening polymerization (ROP) will be dealt with separately.

II.2.1.1. Anionic polymerization

Anionic polymerization is a chain growth polymerization. It is a living polymerization technique in which the active species is a nucleophilic anion and the monomers contain an alkene moiety. The absence of transfer and termination steps (omnipresent in radical polymerization) makes it a robust living polymerization process that continues until all monomer is consumed. Because of the high reactivity of the anionic chain ends, it requires drastic synthetic conditions and the total absence of impurities (e.g. water, oxygen) in the polymerization medium. The scope of monomers polymerizable by this method is thus limited.

Anionic polymerization was successfully used by Chung *et al.* for the synthesis of a PE-*b*-PS copolymer.^[91] To achieve this, ethylene and *p*-methylstyrene (*p*-MS) were copolymerized with a metallocene Cp₂ZrCl₂ in the presence of MAO and hydrogen (**Scheme 13**). It was shown that the catalytic system was able to selectively form PE chains with one terminal *p*-MS group (PE-*t-p*-MS) after transfer to hydrogen. This terminal *p*-MS group can in turn be deprotonated by *s*-butyllithium (*s*-BuLi) in the presence of *N,N,N',N'*-tetramethylethylenediamine (TMEDA) to initiate the polymerization of styrene, hence affording the diblock copolymer PE-*b*-PS. The same strategy was recently used by Lee and coworkers.^[92]



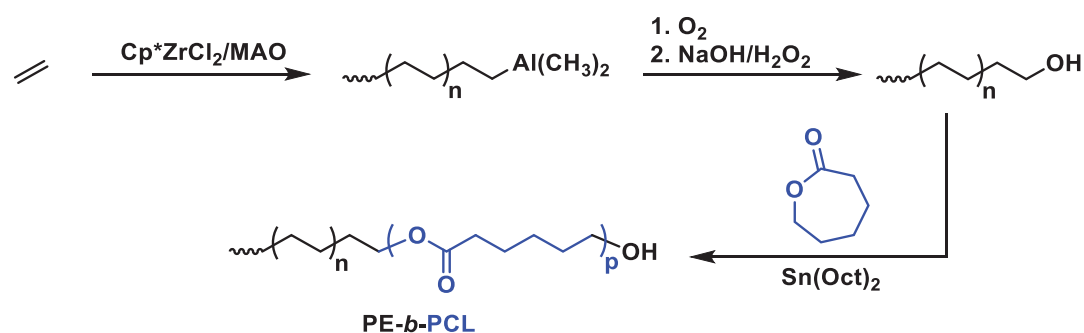
Scheme 13. Synthesis PE-*b*-PS by coordination-insertion of ethylene and subsequent anionic polymerization of styrene.^[91]

II.2.1.2. Anionic ring opening polymerization

Anionic ROP is a form of chain growth polymerization. It is useful to introduce various functional groups such as ether or ester into the polymer backbone. In this technique, the monomers are necessarily cyclic, and the end of the growing polymer behaves as the nucleophile responsible for the opening of the monomer ring.

Successful synthesis of a polyethylene-*block*-polycaprolactone (PE-*b*-PCL) was achieved by anionic ROP of ϵ -caprolactone initiated by an hydroxyl functionalized PE (PE-OH).^[93] PE-OH was

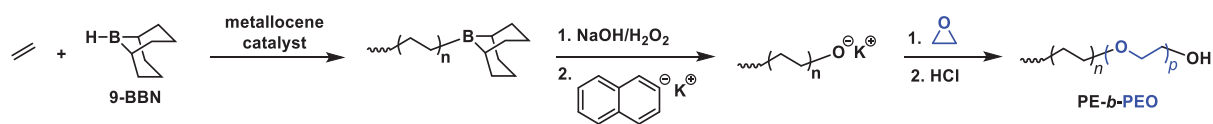
synthesized by catalytic polymerization using a metallocene complex Cp^*ZrCl_2 in the presence of MAO. The presence of MAO induces a transfer of the growing PE chains to aluminum. This results in almost all of the PE chains bearing an Al atom at the end of the polymer chain. Subsequent hydrolysis of the Al chain-end yields the desired PE-OH that can in turn initiate the anionic ROP of ϵ -caprolactone in the presence of a stannate complex (activated ROP, **Scheme 14**). The tin atom is complexed to the oxygen atoms to favor $\text{S}_{\text{N}}2$ addition and ring opening.



Scheme 14. Synthesis of polyethylene-*block*-polycaprolactone via coordination-insertion polymerization of ethylene and subsequent anionic ring opening polymerization of ϵ -caprolactone.^[93]

This kind of approach is still investigated nowadays. A very recent study showed the synthesis of the same block copolymer in a one-pot synthesis.^[94] The functionalization of the PE block is this time achieved with a hydroformylation/hydrogenation step in the presence of carbon monoxide and dihydrogen.

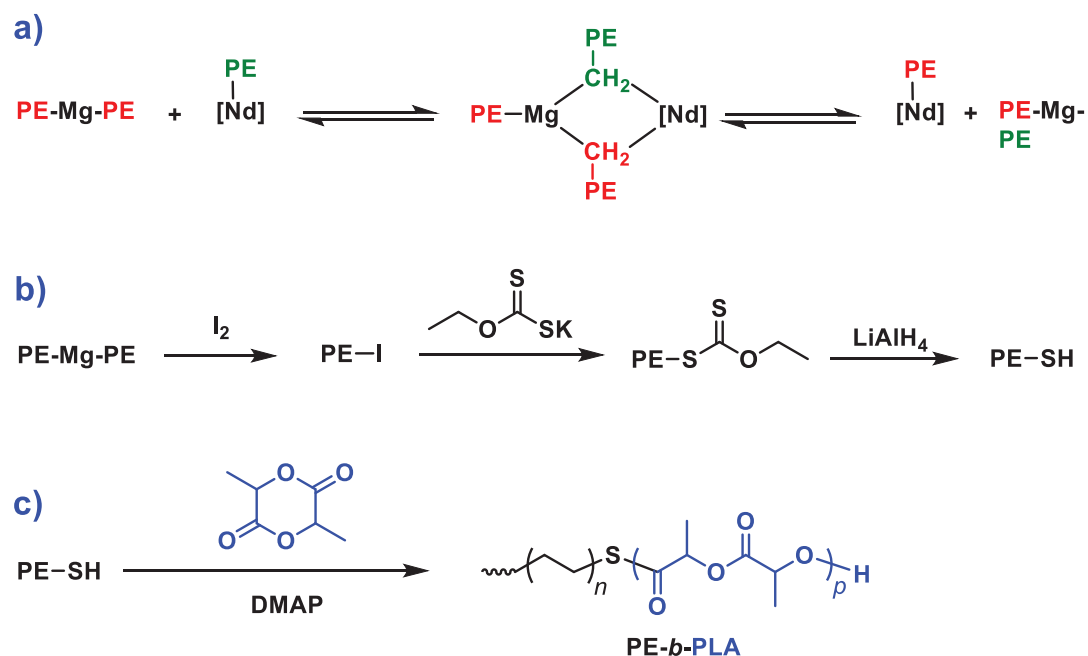
The synthesis of a polyethylene-*b*-poly(ethylene oxide) (PE-*b*-PEO) copolymer was also achieved through the use of a PE-OH, obtained from a borane-terminated PE (PE-*t*-B) synthesized by metallocene catalysis.^[95] The resulting PE-*t*-B was then hydrolyzed and subsequent deprotonation of PE-OH enabled the anionic ROP of ethylene oxide to afford PE-*b*-PEO (**Scheme 15**).



Scheme 15. Synthesis of PE-*b*-PEO via coordination-insertion polymerization of ethylene and subsequent anionic ring opening polymerization of ethylene oxide.^[95]

The synthesis of thiol functionalized PE (PE-SH) was also studied in our laboratory.^[96] Such PE-SH was subsequently used for the synthesis of a polyethylene-*block*-polylactide (PE-*b*-PLA) copolymer.^[97] PE-SH was obtained in a multi-step synthesis. First, dipolyethylenylmagnesium (PE-Mg-PE) was formed by a pseudo-living catalytic polymerization of ethylene with a Nd complex $\text{Cp}^*\text{NdCl}_2\text{Li}(\text{OEt})_2$ in the presence of dialkyl magnesium^[98] (**Scheme 16a**). The M_n of the PE chains can be tuned by the ratio Nd/Mg and the dispersities remain low with $D < 1.5$. PE-Mg-PE was then treated with iodine, potassium xanthic salt and LiAlH_4 (**Scheme 16b**) to afford PE-

SH with a high chain end functionality (88%). This material was ultimately used to initiate the anionic ROP of *D,L*-lactide in the presence of dimethylaminopyridine (DMAP) affording the targeting block copolymer (**Scheme 16c**).



Scheme 16. Synthesis of PE-*b*-PLA via pseudo-living catalytic polymerization of ethylene and subsequent anionic ring polymerization of *D,L*-lactide.^[97]

This PE-Mg-PE species was also used in our laboratory to synthesize diblock copolymers of ethylene with *n*-butyl acrylate (*n*BuA)^[61] by another polymerization technique, which will be discussed in the following part **III.2.2**.

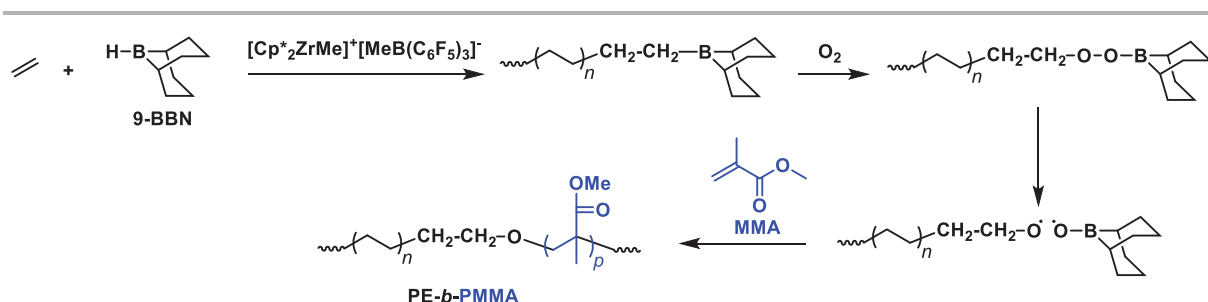
II.2.2. Synthesis by radical polymerization methods

In this paragraph, synthetic methods to grow a polar block onto a PE block by a radical pathway will be discussed. The examples presented will be sorted depending on the radical polymerization process used for the growth of the polar block, namely free radical polymerization or RDRP.

II.2.2.1. Free radical polymerization

In 1999, Chung *et al.* were the first to report the successful synthesis of a PE-*b*-PMMA using a PE-*t*-B species.^[99] They copolymerized ethylene in the presence of 9-borabicyclo[3.3.1]nonane (9-BBN) with a metallocene catalyst $[\text{Cp}^*_2\text{ZrMe}]^+[\text{MeB}(\text{C}_6\text{F}_5)_3]^-$ to afford the PE-*t*-B species. The plot of the polymer molar mass was found to be almost linearly proportional to the molar ratio between ethylene and 9-BBN, thus indicating that the chain transfer reaction to 9-BBN is the dominant process compared to conventional chain transfer via β -H elimination. The majority of

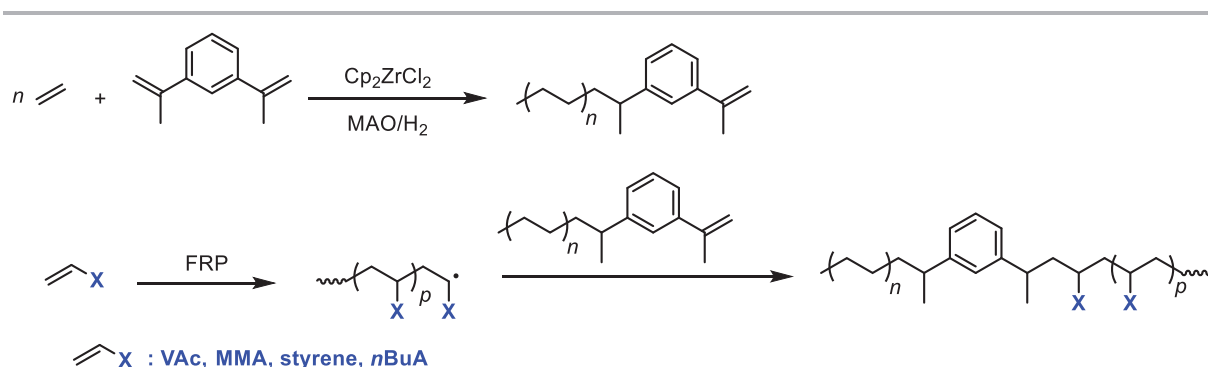
PE chains thus bears a borane moiety at one chain end. The subsequent oxidation of the borane-terminated PE afforded a stable polymeric radical capable of initiating the radical polymerization of MMA to yield the desired diblock copolymer (**Scheme 17**).



Scheme 17. Synthesis of PE-*b*-PMMA via coordination-insertion polymerization of ethylene and subsequent free radical polymerization of MMA.^[99]

Interestingly, it was found that the molar mass of the PMMA segment increases with the reaction time, implying a pseudo-living process. The major disadvantage of this method is that the borane moiety of PE-*t*-B is not stable to air and all reactions and polymer handling have to be done under anaerobic and anhydrous conditions.

Recently, Kay and coworkers reported the synthesis of polar olefin block copolymers by successive catalytic coordination-insertion polymerization of ethylene and FRP of VAc, *n*BuA, MMA and styrene.^[100] They copolymerized ethylene in the presence of 1,3-diisopropenylbenzene (DIB) with a metallocene catalyst Cp₂ZrCl₂ to obtain a DIB terminated PE. The resulting PE-DIB macromonomer was then used during the conventional free radical polymerization of polar monomers, affording PE-*b*-PVAc, PE-*b*-*n*BuA, PE-*b*-PMMA and PE-*b*-PS copolymers (**Scheme 18**).

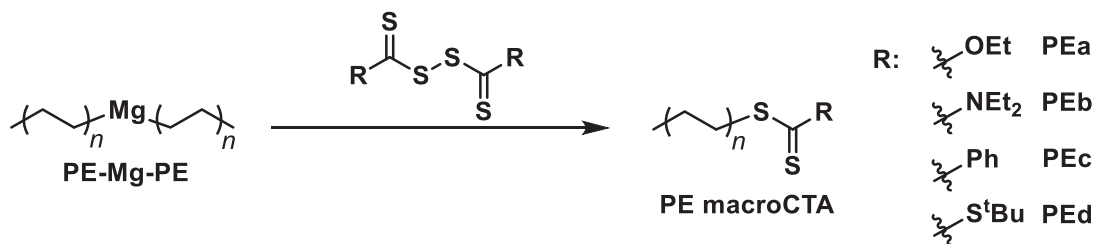


Scheme 18. Synthesis of PE-*b*-PVAc, PE-*b*-PMMA, PE-*b*-PS and PE-*b*-*n*BuA by successive metallocene catalyzed coordination-insertion polymerization of ethylene and free radical polymerization of the polar monomer.^[100]

II.2.2.2. Reversible addition-fragmentation chain transfer

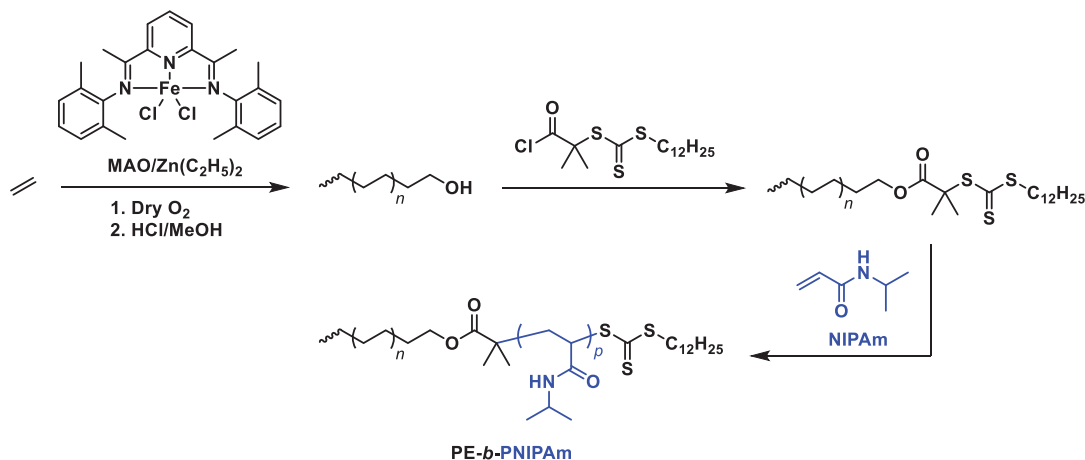
Thiocarbonylthio terminated PE can be obtained by the use of either PE-SH^[96] or Grignards PE-Mg-PE. Using the latter method (**Scheme 19**), our group was able to successfully introduce dithiocarbonate (**PEa**), dithiocarbamate (**PEb**), dithioester (**PEc**) and trithiocarbonate (**PEd**)

moieties at the end of the polymer chain with functionalization yields ranging from 40 % (**PEc**) up to 90 % (**PEb**)^[82].



Scheme 19. Synthesis of thiocarbonylthio terminated-PE.^[82]

PE-*b*-PNIPAm block copolymers were obtained by successive coordination-insertion and RAFT polymerization using ethylene and *N*-isopropylacrylamide (NIPAm).^[101] A PE-OH was obtained by coordination chain transfer polymerization of ethylene using a bis(imino)pyridine iron/MAO/ZnEt₂ catalytic system followed by *in situ* oxidation and hydrolysis. The trithiocarbonate functionalized PE was obtained after esterification of the hydroxyl chain-end as depicted in **Scheme 20**. A similar strategy was employed by Kashiwa *et al.* to obtain PE-*b*-PMMA copolymers using a dithioester chain-end.^[102]



Scheme 20. Synthesis of PE-*b*-PNIPAm via insertion-coordination of ethylene followed by RAFT polymerization of NIPAm.^[101]

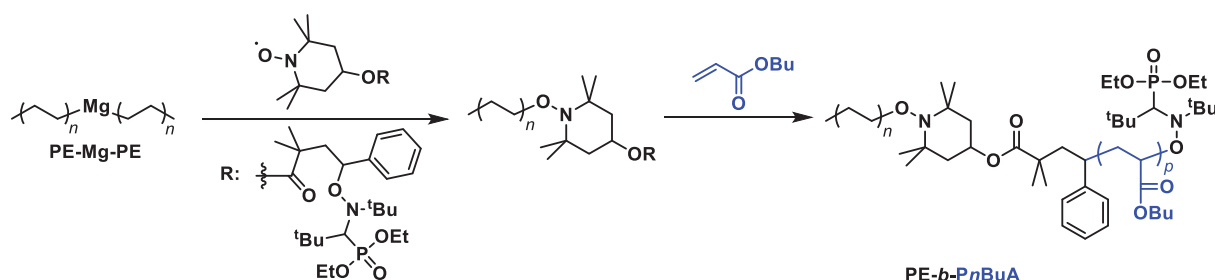
This method allowed for the synthesis of PE-*b*-PNIPAm copolymers that exhibit self-assembly properties in water. The molar masses of the diblock copolymers ranged between 6 and 17 kg mol⁻¹ with $\bar{D} < 1.2$. However, due to solubility issues, the PE block did not exceed 900 g mol⁻¹ ($\bar{D} = 1.08$).

One of the reasons that could explain the very limited number of examples of diblock copolymers obtained after functionalization of a PE with a thiocarbonylthio end group to form a macromolecular CTA (*i.e.* macro-CTA) might stem from the inherent reactivity of such macro-CTAs. Mechanistic considerations on the phenomenon will be thoroughly explained in section **IV.2**. In short, a PE macro-CTA obtained using PE-SH or Grignard reagents will have the general

structure PE-CH₂-CH₂-S-C(S)-Z. The presence of a secondary carbon in α position to the thioester group is less favorable for chain extension with polar vinyl monomers than a tertiary or quaternary carbon. In the example depicted above (**Scheme 20**), a quaternary carbon occupies the α position to the thioester group, thus permitting the successful chain extension with NIPAm.

II.2.2.3. Nitroxide-mediated polymerization

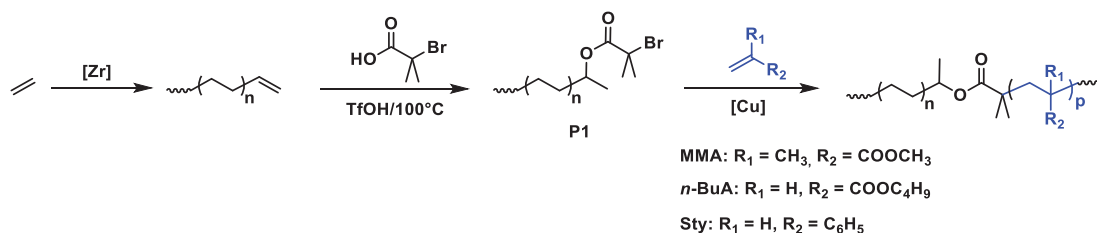
To the best of our knowledge, there exists only one published work on the chain extension of a PE block with a polar monomer by a NMP process. This is explained by the fact that a PE segment functionalized by a common nitroxide group, such as 2,2,6,6-tetramethylpiperidiny-1-oxyl (TEMPO) or *N*-(2-methyl-2-propyl)-*N*-(1-diethylphosphono-2,2-dimethylpropyl)-*N*-oxy (DEPN) would require a cleavage temperature of 180 and 160 °C, respectively, which is not ideal for copolymerization with polar monomers.^[103] However, our group used a specifically designed alkoxyamine for the synthesis of a polyethylene-*b*-poly(*n*-butyl acrylate) diblock copolymer at lower temperature (**Scheme 21**). This method is however largely limited by the low functionalization degree (45%) of the PE block and by the use of an exotic alkoxyamine.



Scheme 21. Synthesis of PE-*b*-P*n*BuA with a nitroxide-terminated PE.^[103]

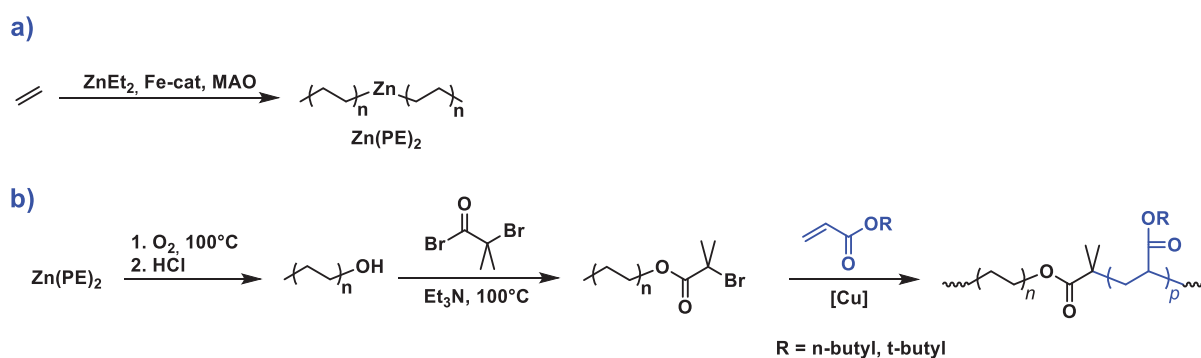
II.2.2.4. Atom transfer radical polymerization

ATRP has often been used to make diblock copolymers with ethylene and activated monomers, such as methacrylates, acrylates or styrenic monomers. Matyjaszewski used a rather straightforward method for the synthesis of such diblock copolymers.^[104] A vinyl terminated PE ($M_n = 1\,800\text{ g mol}^{-1}$, $D = 1.7$), obtained by catalytic polymerization using a phenoxyimine zirconium catalyst, was reacted with 2-bromopropanoic acid in the presence of trifluoromethanesulfonic acid (TfOH) to obtain the ATRP precursor P1 (**Scheme 22**). The chain extension of P1 (in chlorobenzene at 100 °C) was then performed with MMA, *n*BuA or styrene in the presence of a copper complex [Cu] to afford PE-*b*-PMMA, PE-*b*-P*n*BuA and PE-*b*-PS, respectively. The downside of this method is the limited functionalization of the PE block (75 %) and the limitation to activated monomers (*vide infra*) for the polar block.



Scheme 22. Synthesis of PE-*b*-PMMA, PE-*b*-PnBuA and PE-*b*-PS via catalytic coordination-insertion polymerization of ethylene followed by ATRP.^[104]

A different approach consists in reacting a functionalized PE-OH with 2-bromo-2-methylpropionyl bromide to afford the ATRP precursor. It was done by Matyjaszewski to obtain PE-*b*-PnBuA and PE-*b*-PtBuA copolymers (**Scheme 23b**).^[105] The PE-OH block was obtained after oxidation and hydrolysis of a Zn(PE)₂ species, obtained by degenerative transfer polymerization of ethylene in the presence of dialkyl zinc, an iron catalyst and MAO (**Scheme 23a**).



Scheme 23. Synthesis of PE-*b*-PnBuA and PE-*b*-PtBuA via catalytic coordination-insertion polymerization of ethylene followed by ATRP.^[105]

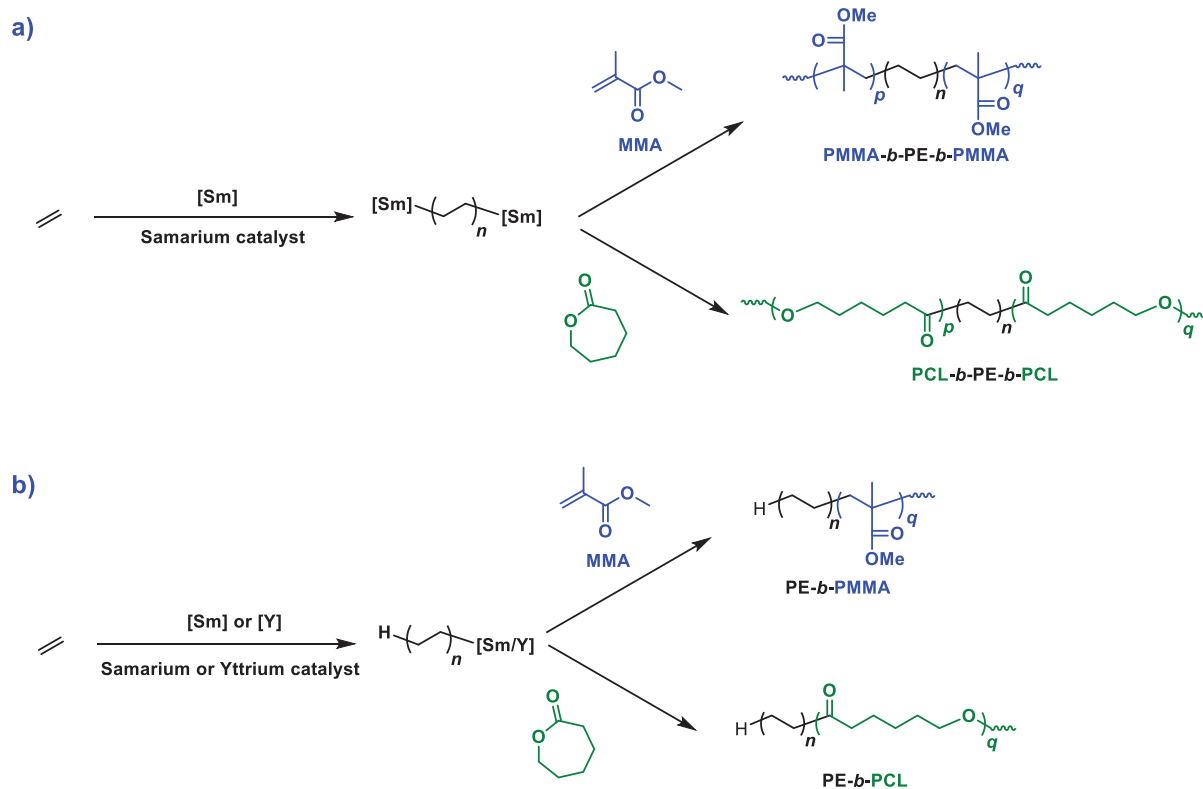
More recently, Wang *et al.* described the synthesis by ATRP of PE-*b*-PMMA and PE-*b*-PS using chloromethyl styrene-capped hyperbranched polyethylene obtained using a Palladium-diimine complex.^[106]

II.3. Block copolymer synthesis by successive coordination-insertion of ethylene and group transfer polymerization of the polar monomer

There exists only a handful of examples of more or less direct block copolymerization routes between ethylene and polar monomers. These rely on the catalytic coordination-insertion polymerization of ethylene to obtain a metal-terminated PE segment. The polar block is then added by metal-catalyzed group transfer polymerization (GTP)^[107] of a polar monomer.

Yasuda studied the block copolymerization of ethylene with rare-earth metal catalysts.^[108] He reported the block copolymerization of ethylene with MMA, δ -valerolactone and ϵ -caprolactone to obtain A-B and B-A-B type block copolymers using Yttrium and Samarium complexes^[109] (where A = PE, **Scheme 24**). The polar monomer is then added by GTP. The reverse addition of

monomers (polar monomer first) induced no block copolymerization and only homopolymers of the polar monomer were obtained. Although very elegant, the use of exotic and expensive lanthanides has greatly hampered the development of these systems for further applications.



Scheme 24. Synthesis of B-A-B (a) and A-B (b) block copolymers with ethylene and MMA/ ϵ -caprolactone using lanthanides complexes.^[109]

Frauenarth *et al.* synthesized PE-*b*-PMMA copolymers using a metallocene catalyst.^[110] The use of a *in situ* generated catalyst from $\text{Me}_2\text{C}(\text{Cp})(\text{Ind})\text{ZrMe}_2$ and $\text{B}(\text{C}_6\text{F}_5)_3$ in toluene allowed for the block copolymerization, starting with ethylene by a coordination-insertion mechanism, and followed with MMA by GTP (**Scheme 25**).



Scheme 25. Ethylene-MMA block copolymerization by crossover from coordination-insertion polymerization to addition polymerization with a zirconocene complex.^[110]

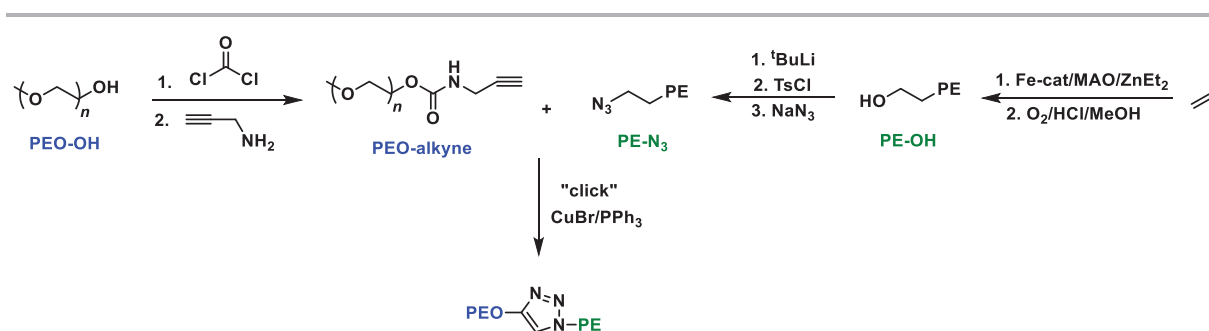
Although very simple and efficient, this route has the major drawback of using one equivalent of metal atom per polymer chain. The sequence of the monomer addition is also not reversible, meaning that when the PMMA polymerization is triggered, it is not possible to switch back to ethylene polymerization.

II.4. Synthesis of diblock copolymers by coupling two preformed blocks

This section will describe the synthesis of block copolymers including a PE segment, where the two blocks are made separately by different polymerization methods, then assembled using a simple and efficient coupling method such as click chemistry.^[111]

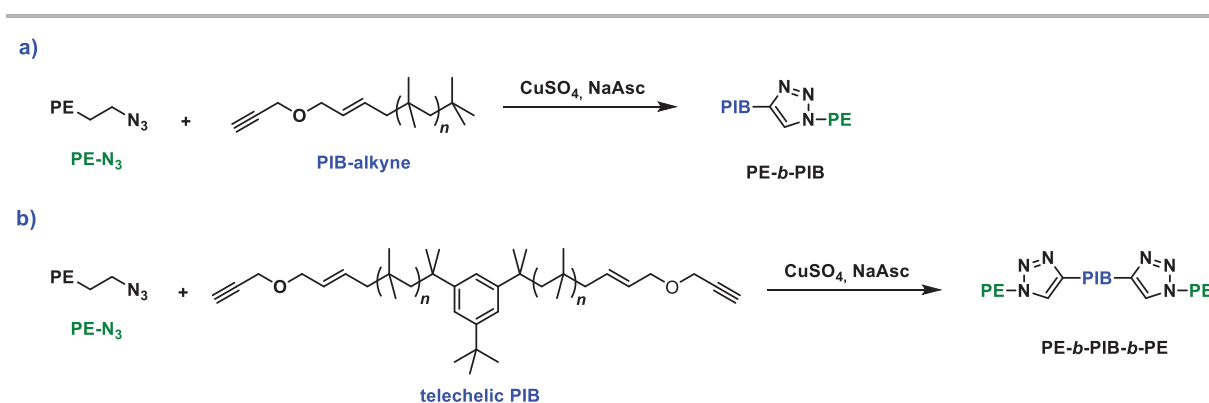
Even with click chemistry being now widely available and efficient,^[112] there exist only few examples reporting its use for making diblock copolymers with PE. An efficient coupling requiring both blocks to be soluble in the reaction solvent, this is often an issue with a PE block, largely insoluble in most solvents.

Li *et al.* reported the synthesis of PE-*b*-PEO by coupling between an azide-terminated PE and an alkyne-terminated PEO (**Scheme 26**).^[113] PE-*b*-PEO copolymers were also obtained by Zhang *et al.* via epoxide ring-opening and thiol-ene addition.^[114]



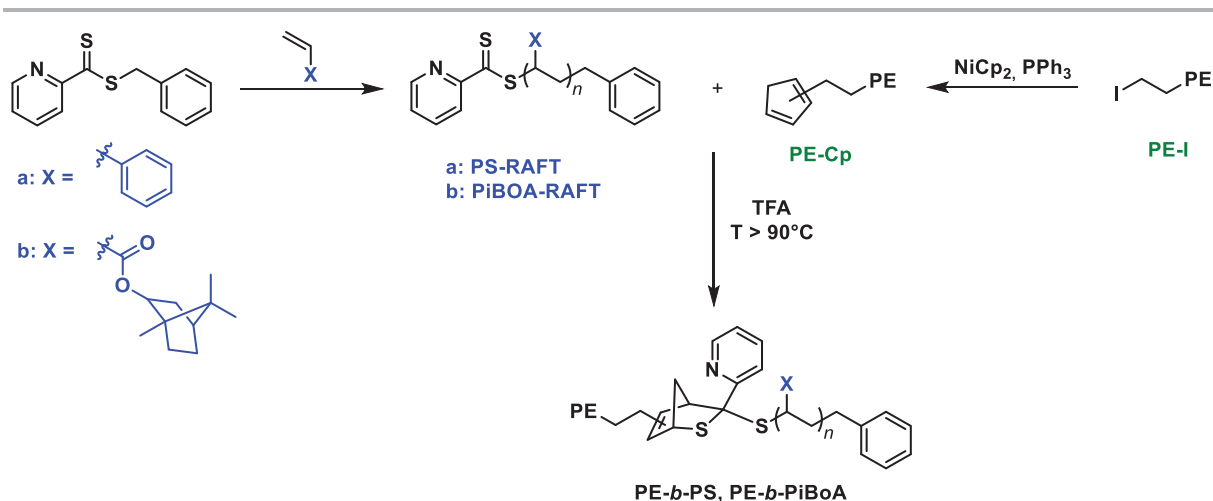
Scheme 26. Synthesis of PE-*b*-PEO by click chemistry.^[113]

In our group, Espinosa *et al.* reported the use of telechelic polyisobutene (PIB) for the synthesis of PE-*b*-PIB and PE-*b*-PIB-*b*-PE diblock and triblock copolymers by coupling between azides and alkynes^[115] (**Scheme 27a** and **27b**, respectively).



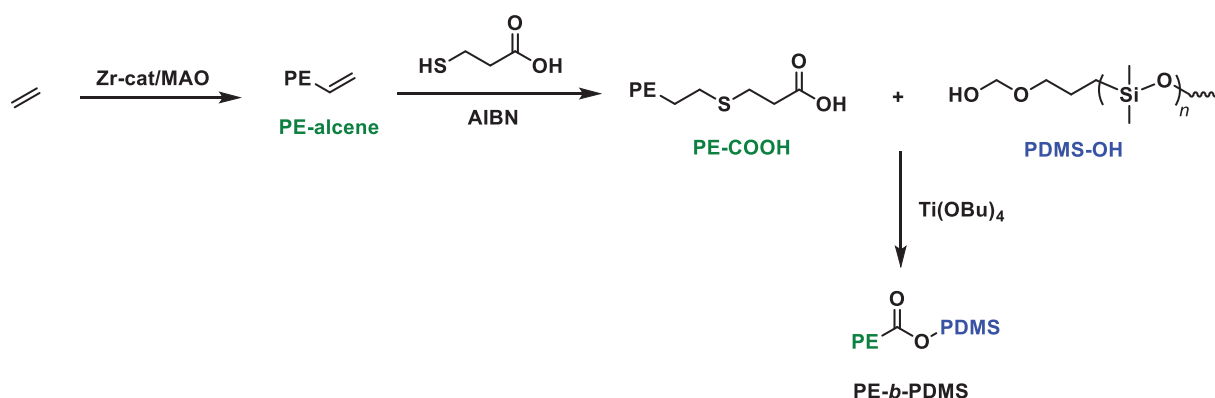
Scheme 27. Synthesis of PE-*b*-PIB and PE-*b*-PIB-*b*-PE by click chemistry.^[115]

Thiocarbonylthio-terminated PS and poly(isobornyl acrylate) (PiBoA) were used by our group for the synthesis of PE-*b*-PS and PE-*b*-PiBoA copolymers by Diels-Alder coupling (**Scheme 28**).^[116]



Scheme 28. Synthesis of PE-*b*-PS and PE-*b*-PiBoA by Diels-Alder coupling.^[116]

More recently, Xu *et al.* applied thiol-ene coupling to a vinyl-terminated PE for the synthesis of polyethylene-*block*-poly(dimethylsiloxane) (PE-*b*-PDMS, **Scheme 29**).^[117] This block copolymer was subsequently used as compatibilizing agent for a HDPE/Silicone blend.



Scheme 29. Synthesis of PE-*b*-PDMS block copolymer via thiol-ene chemistry.^[117]

These examples show that relatively simple and efficient click chemistry reactions can be used to obtain a variety of copolymers including a PE block, affording both apolar-apolar and polar-polar block copolymers. The main disadvantages of these examples are the use of low molar mass PE ($M_n < 3\,000\text{ g mol}^{-1}$, for ease of solubility) and the sometimes tedious post-modification step(s) of either block.

II.5. Conclusion

The incompatibility of polymerization techniques to obtain PE-*b*-PX has been historically circumvented by the synthesis of a PE block by catalytic coordination-insertion polymerization, carrying a reactive chain-end obtained either by the addition of a functional monomer during ethylene polymerization or by post-modification. The polar segment is then added using a

different polymerization chemistry: anionic or radical. This has proved to be mostly limited to low M_n PE and lacks simplicity and efficiency. The synthesis of polar OBCs using only one chemistry (*i.e.* one polymerization mechanism and no intermediate steps) is much more attractive but requires the control over ethylene polymerization.

Despite being still in its infancy, the controlled radical polymerization of ethylene by RDRP appears to be the most attractive way to achieve PE-*b*-PX copolymers in a simple and efficient way. In this context, the next part of this chapter will be focused on RDRP techniques successfully used for ethylene and their applications for copolymerization with polar monomers.

III. Reversible-deactivation radical polymerization of ethylene

In the following, RDRP techniques specifically used for the control over ethylene (co)polymerization will be surveyed. The very low stability of the propagating polyethylenyl PE-CH₂-CH₂• radical and its high propensity to transfer are reasons for the notorious difficulty over the control of its radical polymerization. In addition, the harsh synthetic conditions usually depicted to be required to form PE by a radical process, the difficulty in handling the gaseous ethylene monomer and its polymerization are major obstacles to the investigation of the RDRP of this monomer.

In a RDRP process, the monomer nature greatly influences its reactivity towards radical polymerization. Vinyl monomers can be classified either as more activated monomers (MAMs) or less activated monomers (LAMs), depending on the substituents in α position to the double bond. The reactivity of a vinyl monomer will generally greatly influence the RDRP technique used to mediate its polymerization, as well as the structure of the controlling agent. It also has an importance when considering the synthesis of block copolymers (*vide infra*). After a brief introduction on MAMs and LAMs, the different techniques that have been used to mediate the RDRP of ethylene will be surveyed. These techniques include ITP, TERP, organometallic-mediated radical polymerization (OMRP), NMP and RAFT. Eventually, RAFT polymerization will be presented in more detail as it has been the RDRP method of choice during this PhD work. In particular, the challenges and strategies developed for the synthesis of block copolymers between LAMs and MAMs will be highlighted.

III.1. More activated monomers and less-activated monomers

Vinyl monomers can be divided into two families based on their reactivity: MAMs and LAMs. MAMs have their vinyl group conjugated to a double bond (e.g. butadiene), an aromatic ring (e.g. styrene), a carbonyl group (e.g. (meth)acrylates, (meth)acrylamides) or a nitrile (e.g. acrylonitrile). LAMs exhibit a double bond adjacent to oxygen (e.g. vinyl acetate), nitrogen (e.g. NVP) or an unsaturated carbon (e.g. α -olefins). In this context, ethylene can be considered as a non-activated monomer (**Figure 6**). The classification as MAM or LAM reflects the ability of the considered monomer to react in a free radical process. MAMs react more readily with radicals than LAMs. The reactivity of the propagating radicals derived from these monomers is at odds with this classification. MAMs produce more-stabilized and less reactive radicals (the electron resulting from radical addition is stabilized by resonance and steric factors) than LAMs. These differences in reactivity of both the monomer double bond and the resulting propagating radical

make the copolymerization of MAMs and LAMs no easy task. This concept is particularly important in RAFT polymerization (*vide infra*).

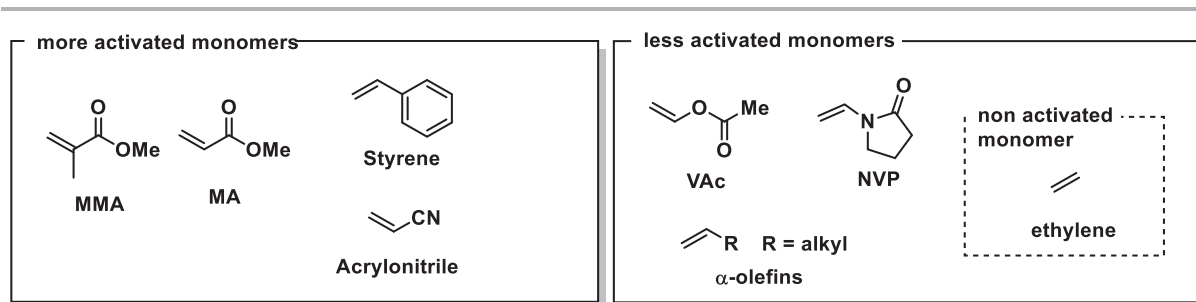
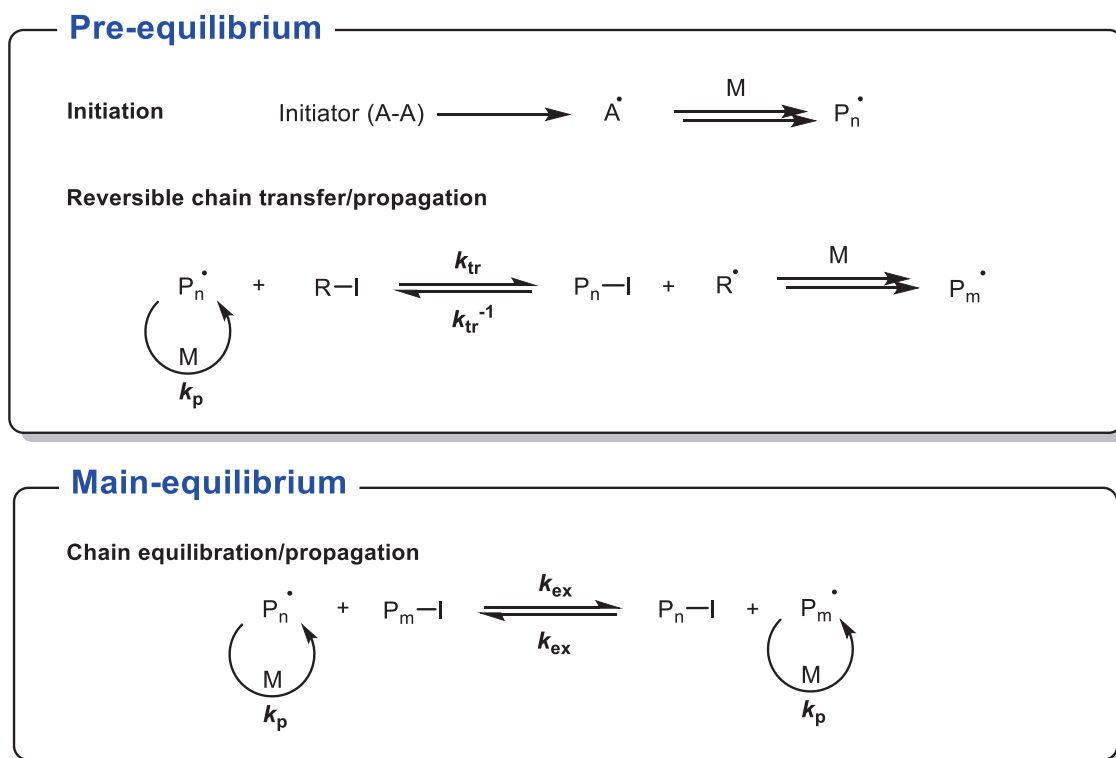


Figure 6. Examples of more activated monomers and less activated monomers.

III.2. RDRP of ethylene *via* ITP

A basic ITP system consists in (i) a conventional radical initiator **A-A**, (ii) a monomer **M** and (iii) an iodo-CTA **R-I** (Scheme 30). During the pre-equilibrium, propagating species P_n^\bullet reversibly react with the iodo-CTA to release a radical R^\bullet capable of reinitiating the polymerization. Once all **R-I** is consumed, the mechanism shifts into the main equilibrium with only active species P_n^\bullet/P_m^\bullet and dormant species P_n-I and P_m-I present in the polymerization medium.



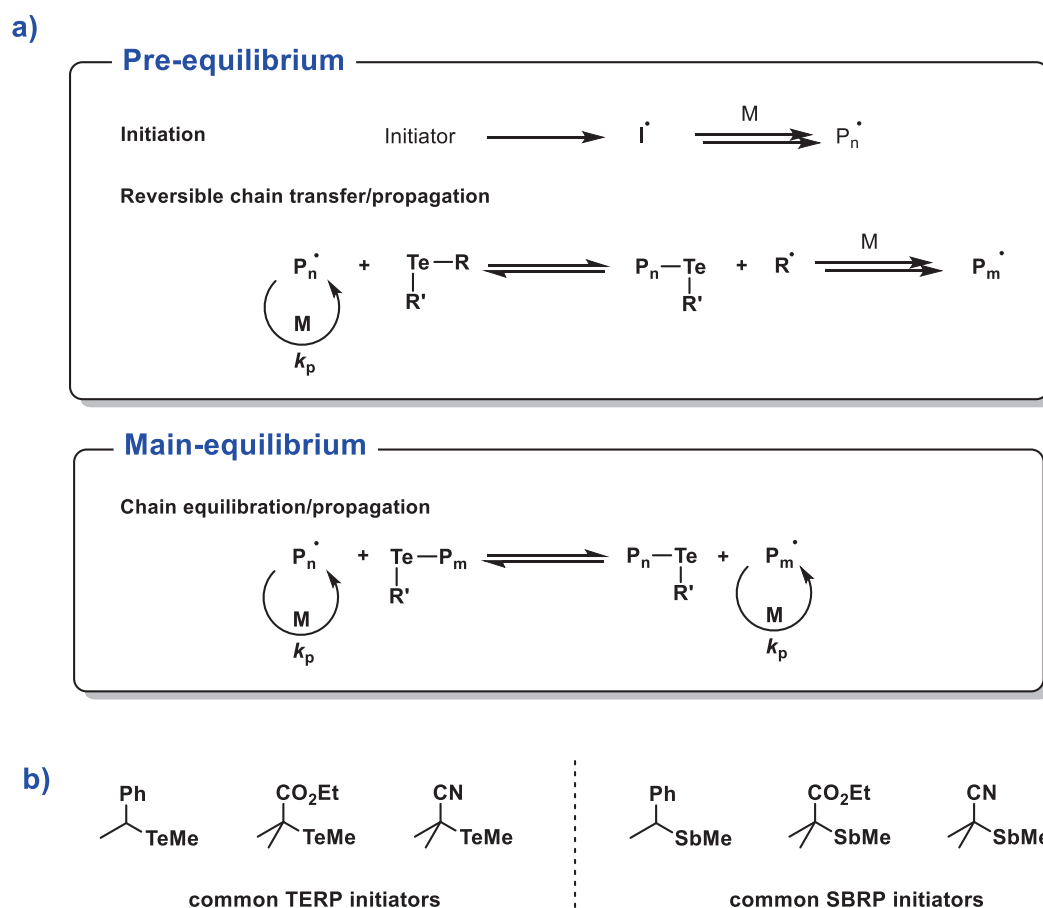
Scheme 30. Simplified mechanism of pre- and main-equilibrium in iodine transfer polymerization.

Over the last two decades, ITP has been used both on activated and non-activated monomers including styrenics, acrylates and methacrylates, vinyl halides and vinyl acetate.^[65] The

homopolymerization of ethylene has not been reported (yet) by ITP, but ITP has been used by Borkar and Sen^[118] to randomly copolymerize ethylene and vinyl acetate under mild conditions (50 bar, 70 °C) to afford statistical copolymers with narrow dispersities ($D < 2$) and M_n up to 22 000 g mol⁻¹. The ethylene content of those copolymers was 40 %.

III.3. RDRP of ethylene *via* TERP

TERP was developed by Yamago in 2002^[119] and is a relatively niche but versatile RDRP technique. It uses an organo-tellurium (**R-Te-R'**) compound as CTA in the presence of a conventional radical initiator (**Scheme 31**). Although TERP mainly proceeds via a DT mechanism, both DT and RT mechanisms can coexist, depending on the temperature.^[120]

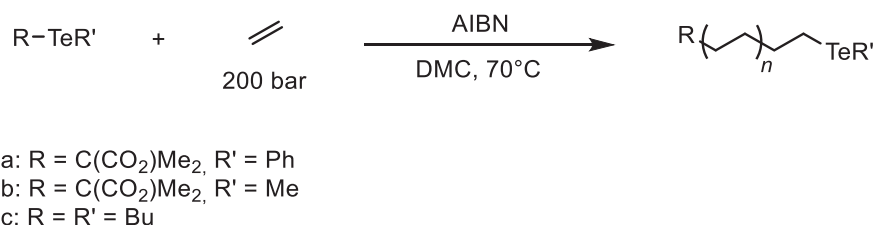


Scheme 31. Simplified mechanism of pre- and main-equilibrium in tellurium-mediated radical polymerization (a) and common CTAs in TERP and SBRP (b).

Stibine-mediated radical polymerization (SBRP) and bismuth-mediated radical polymerization (BIRP) are variant to TERP that employ the metallic species antimony and bismuth respectively, operating under the same conditions and mechanism as TERP. Some commonly used TERP and SBRP initiators are presented in **Scheme 31b**. One advantage of TERP, SBRP and BIRP is their high versatility in polymerizing a variety of monomers including MAMs^[119]

(styrenics, acrylates, methacrylates, acrylamide and AN) and LAMs^[121,122] (NVP, VAc and *N*-vinylcarbazole). Another attractive feature of TERP, SBRP and BIRP is their ability of controlling the polymerization of both LAMs and MAMs without importance of the order of monomer addition. As such, poly(LAM)-*block*-poly(MAM) and poly(MAM)-*block*-poly(LAM) were synthesized with narrow dispersities ($\mathcal{D} < 1.3$), with examples including PS-*b*-PNVP, PMMA-*b*-PNVP and PVNP-*b*-PMMA.^[123]

Although TERP, SBRP and BIRP can rival other RDRP techniques for the preparation of functional materials and block copolymers, the great sensitivity of the CTAs towards oxygen however limits their practical applications. Nonetheless, TERP was very recently used to control the homopolymerization of ethylene through a collaboration between our group and the Yamago group in Japan.^[124] Different CTAs were used at 70 °C in the presence of AIBN as radical initiator, using DMC as solvent (**Scheme 32**).

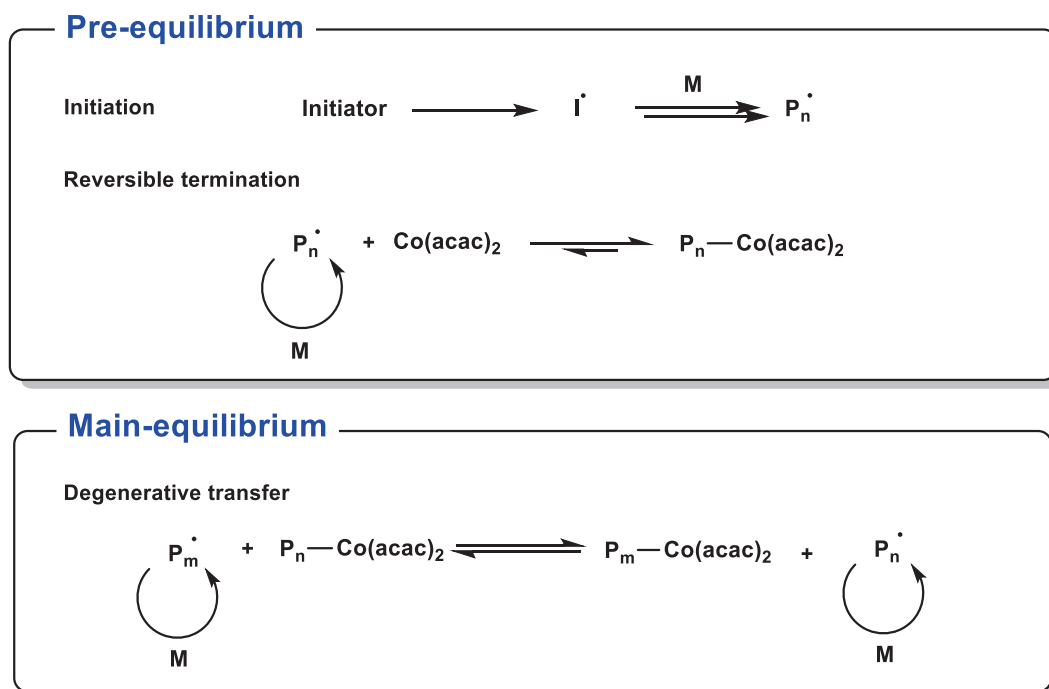


Scheme 32. Tellurium-mediated radical polymerization of ethylene.^[123]

The control of the polymerization was demonstrated up to $M_n = 6\,000 \text{ g mol}^{-1}$ ($\mathcal{D} < 2$) with experimental molar mass values closed to the theoretical ones. A side-fragmentation reaction was observed when R' = alkyl (**b**, **c**), which was not the case when R' = aryl (**a**). This side-fragmentation however did not negatively affect the livingness of the polymerization as the resulting species PE-Te-PE were still active.

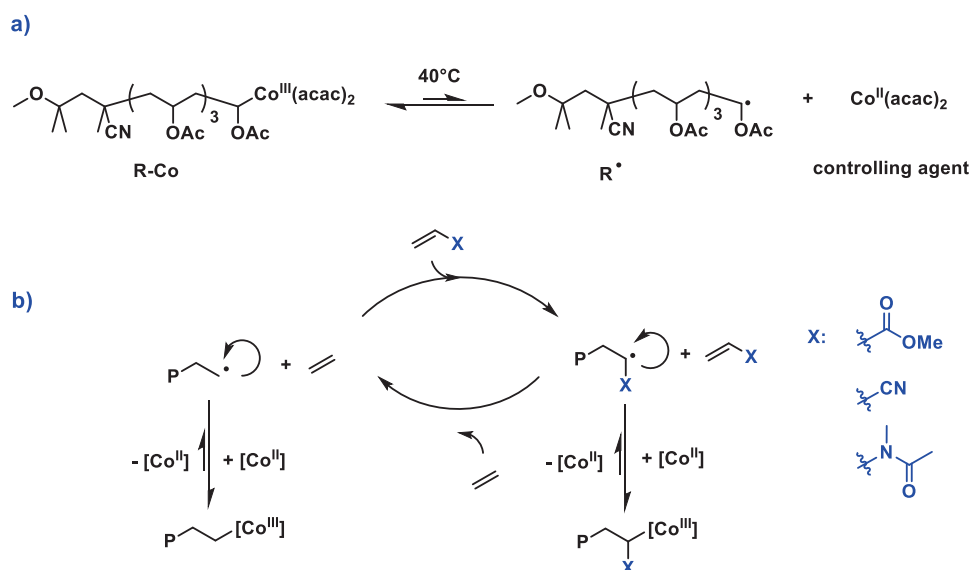
III.4. RDRP of ethylene via OMRP

OMRP is a generic name for RDRP techniques involving the use of metal complexes as CTA. The most well-known OMRP technique is by far the cobalt mediated radical polymerization (CMRP). It was first reported in 1994 simultaneously by Wayland^[125] and Harwood^[126] for acrylates polymerization using porphyrins. Through the work of Detrembleur *et al.*,^[64] CMRP has known a surge in development since 2005 using cobalt bis(acetylacetonate) (Co(acac)₂) to achieve control of VAc homopolymerization with M_n up to 100 000 g mol⁻¹ and \mathcal{D} values between 1.1 and 1.3.^[127] CMRP involves both reversible termination (during pre-equilibrium) and degenerative transfer (during main-equilibrium, **Scheme 33**).



Scheme 33. Simplified CMRP mechanism using $\text{Co}(\text{acac})_2$ as CTA.

A variant of this mechanism consists in preforming VAc oligoradicals trapped by a $\text{Co}(\text{acac})_2$ species and using them as initiator. This was done by Detrembleur *et al.* who developed a system based on organocobalt initiating species^[64] capable of initiating and precisely controlling the growth of the polymer chains, their composition and the monomer distribution to achieve both statistical and block-like copolymers and thus prepare well-defined EVAs.^[128]



Scheme 34. Organocobalt mediated copolymerization of ethylene with polar monomers.^[129]

In their system, the organocobalt initiator (**R-Co**) can homolytically cleave under reaction conditions to produce a radical R^\bullet capable of initiating the vinyl monomer polymerization and a $[\text{Co}^{\text{II}}]$ species that behaves as the chain control agent (**Scheme 34a**). Chain growth occurs

according to a classic radical polymerization process with either ethylene or the polar vinyl comonomer. The [Co^{II}] is able to reversibly trap the growing chains, thus providing chain growth control and a living character to the polymerization. VAc, AN and *N*-methylvinylacetamide have been successfully copolymerized with ethylene using this method (**Scheme 34b**). The copolymers incorporated up to 54 mol% of ethylene. A recent patent^[129] by the same group describes the use of this method to synthesize PVAc-*b*-PE and EVA-*b*-PE copolymers, but the control over ethylene polymerization for the addition of the PE segment is not achieved (molar masses do not increase with ethylene conversion).

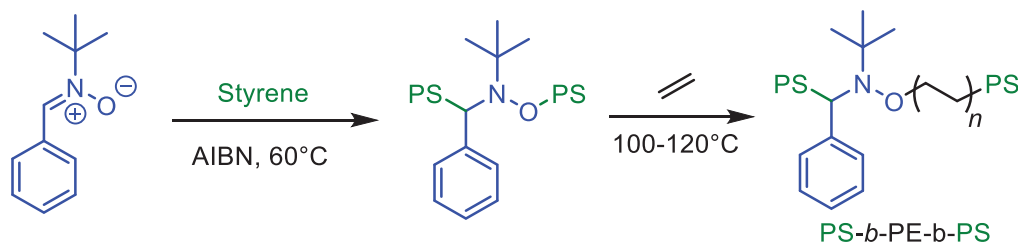
III.5. RDRP of ethylene via NMP

NMP is particularly adapted for the RDRP of activated monomers. For non-activated monomers, such as ethylene, the bond dissociation energy required to break the C-O bond is usually too high. For example, NMP can be used to control the polymerization of *n*BuA or styrene at temperatures as low as 90 °C.^[68] However, for a PE-like propagating radical, such as an hexyl group, a temperature above 150 °C would be required.^[130] It was shown by Gigmes *et al.* that the O-N bond is likely to break before the C-O bond at such temperatures, liberating radicals not capable of initiating the polymerization.^[130] In this context, only two patents report the RDRP of ethylene via NMP. Moffat *et al.*^[131] used TEMPO for the homo and copolymerization of ethylene with various vinyl monomers under harsh conditions (P = 2 500 bar, T = 250 °C) to obtain polymers with narrow dispersity, but the linear increase of the molar masses was not mentioned. Minaux *et al.*^[132] also used TEMPO under somewhat milder conditions (P = 200 bar, T = 160 °C) and the linear increase of the molar masses was observed but dispersity values remained high ($3.7 \leq D \leq 7.4$).

Sen *et al.* have used NMP to control the polymerization under relative mild conditions of several α -olefins (including ethylene, P = 50 bar, T = 120 °C) with MMA,^[133] and even if the control of the polymerization was excellent ($D < 1.2$), the incorporation of olefin remained low (< 15 mol%) and an increase of their concentration led to a dramatic diminution of yields and molar masses.

A variant of NMP, enhanced spin capturing polymerization (ESCP)^[134] was successfully used by Cédric Dommanget in our group (in collaboration with T. Junkers, C. Barner-Kowollik, Y. Guillaneuf and D. Gigmes) to produce PS-*b*-PE-*b*-PS triblock copolymers.^[135] ESCP uses nitrones (that become a nitroxide species upon radical addition) instead of nitroxides as radical traps. The high bond dissociation energy of PE-nitroxide species was circumvented by the initial synthesis of a PS macro-initiator containing a nitroxide bridge. At T > 100 °C, the C-O bond is easily cleaved, releasing a PS• propagating radical capable of initiating ethylene polymerization. The addition of

the PS-*b*-PE• active species onto a nitroxide terminates the polymerization to afford a PS-*b*-PE-*b*-PS triblock copolymer as depicted in **Scheme 35**.



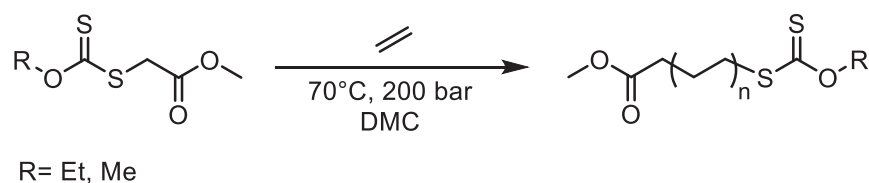
Scheme 35. Synthesis of PS-*b*-PE-*b*-PS triblock copolymers by ESCP.^[136]

III.6. RDRP of ethylene *via* RAFT polymerization

RAFT has proved to be one of the most versatile techniques for the controlled radical polymerization of both LAMs and MAMs^[67,136] and the synthesis of architected polymers.^[137]

Based on theoretical calculations^[138], the RAFT of ethylene was first attempted in 2007 by RAFT with a fluorinated CTA at both high pressure (2 000 bar) and high temperature (175 °C).^[37] The increase of the molar mass with the conversion was not observed and the dispersity values remained quite high ($\mathcal{D} > 2.9$), which indicates that the polymerization was not controlled.

The first example of successful RAFT polymerization of ethylene was recently published by our group. Under the mild conditions successfully used by Grau *et al.* for ethylene radical polymerizations^[40,41] (70 °C, 200 bar), Dommanget *et al.* achieved the control over ethylene polymerization through the use of xanthate chain transfer agents.^[139] *O*-alkyl xanthates (Z = OMe, OEt) were used to successfully control the polymerization in DMC (**Scheme 36**).



Scheme 36. RAFT polymerization of ethylene with *O*-alkyl xanthates.^[140]

The molar mass of the PE synthesized with this method increased linearly with the conversion of ethylene (expressed as the yield of PE, in grams) and the dispersity values remained quite low (**Figure 7a**). Interestingly, the polymerization in the presence of the CTA was slightly but systematically faster than without CTA, a behavior rather untypical (**Figure 7b**).

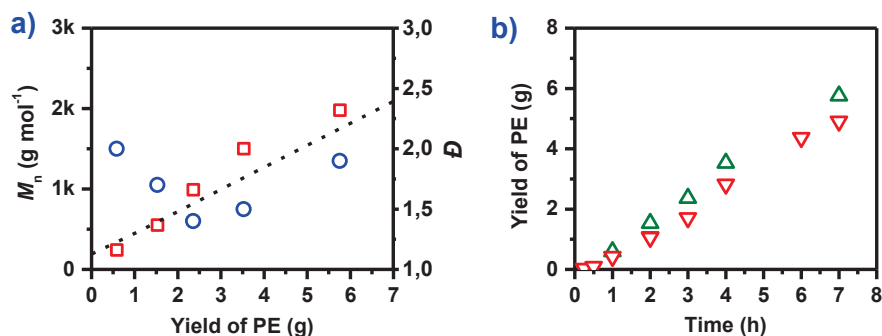


Figure 7. Evolution of M_n (■) and D (○) values with PE yield (a) and comparison between yields obtained by RAFT (with *O*-ethyl xanthate) (△) and FRP (▽) of ethylene (b) at 70 °C and 200 bar.^[140]

SEC analyses showed that the molar mass distributions shifted towards higher molar masses values during the polymerization (Figure 8a) as expected, and the livingness of the chains was ascertained with the chain extension of a low molar mass PE macro-CTA into a PE-*b*-PE copolymer (Figure 8b).

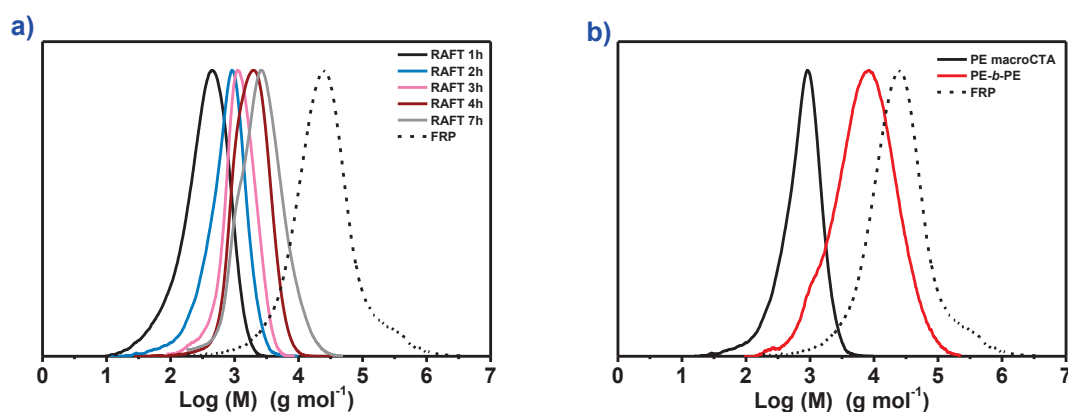
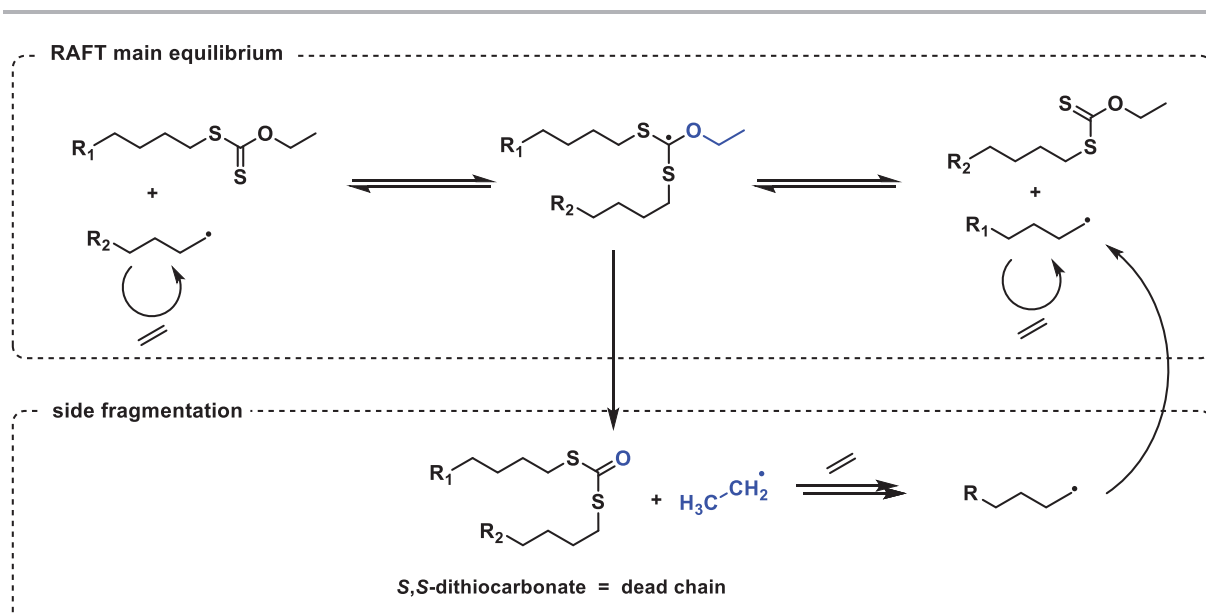


Figure 8. MMD evolution during RAFT polymerization of ethylene in the presence *O*-ethyl xanthate (a) and chain extension of PE macro-CTA with ethylene (b).^[140]

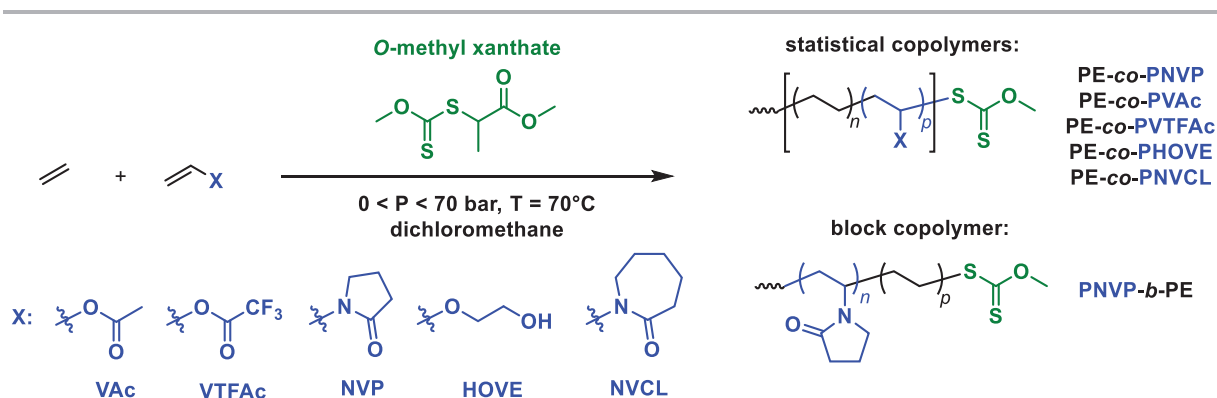
The shoulder observed for the PE-*b*-PE *via* HT-SEC trace corresponds to a fraction of the PE macro-CTA that is not functionalized by a xanthate chain-end. Indeed, a detrimental side fragmentation reaction was found to occur during the polymerization, leading to the formation of a *S,S*-dithiocarbonate species that is not active for polymerization and accumulates (Scheme 37).



Scheme 37. Mechanism of side fragmentation when *O*-ethyl xanthate is used for the RAFT polymerization of ethylene.

The extent of side fragmentation could be quantified by $^1\text{H-NMR}$. Interestingly, it was found to be reduced by a factor of almost two when $Z = \text{OMe}$ compared to $Z = \text{OEt}$. This was attributed to the lesser stability of the methyl radical CH_3^\bullet compared to that of the ethyl radical $\text{CH}_3\text{-CH}_2^\bullet$. Indeed, the methyl radical being less stable, it is less prone to be released than the ethyl radical, the side fragmentation is therefore disfavored and the RAFT main equilibrium dominates. Well defined EVAs ($1.5 < D < 2$) with VAc contents of 2 and 9 mol% could also be obtained, but the same side fragmentation was observed.

Recent work from You *et al.* showed the RAFT copolymerization of ethylene with several vinyl monomers (**Scheme 38**).^[140]



Scheme 38. RAFT copolymerization of ethylene with various polar monomers for the synthesis of statistical and block copolymers.^[141]

The authors claim a polar monomer insertion between 30 and 90 % for the statistical copolymers with remarkably low dispersities (**Table 5**), and the synthesis of well-defined PNVP-*b*-PE block copolymers, supported by SEC, NMR and water contact angle analyses. The use of

dichloromethane as solvent, a CTA:AIBN ratio of 1 and the absence of full NMR attributions are however somewhat surprising, not to mention the complete omission of the side-fragmentation mechanism previously observed with *O*-alkyl xanthates. Noteworthy, the molar mass of the PE segment added after block copolymerization using a PNVP macro-CTA was quite low ($M_{n,PE} = 400 \text{ g mol}^{-1}$).

Table 5. Copolymerization of ethylene with various polar monomers by RAFT.^[141]

Entry	Ethylene pressure (bar)	Polar monomer	M_w (g mol ⁻¹)	\bar{D}	X (%)
1	0	NVP	30 100	1.43	100
2	5	NVP	40 000	1.38	90.1
3	20	NVP	44 000	1.45	75.7
4	35	NVP	47 200	1.48	62.3
5	60	NVP	59 000	1.38	47.0
6	70	NVP	66 600	1.47	36.1
7	5	VAc	16 300	1.40	79.1
8	15	VAc	15 500	1.37	62.7
9	20	VAc	19 900	1.35	45.2
10	30	VAc	15 800	1.37	34.0
11	40	VAc	17 100	1.33	26.2
12	10	HOVE	16 500	1.19	69.9
13	20	HOVE	17 700	1.17	52.2
14	30	HOVE	15 600	1.25	47.3
15	40	HOVE	18 300	1.25	38.9
16	20	VTFAc	7 500	1.05	32.0
17	75	NVCL	19 600	1.31	33.8

HOVE: 2-hydroxyethyl vinyl ether, VTFAc: vinyl trifluoroacetate, X: polar monomer insertion. Reaction conditions: polar monomer (1 mL), dichloromethane (2 mL), AIBN (5 mg), CTA (7.5 mg). M_w and \bar{D} determined by LiBr-DMF SEC (PS standards).

These two examples are, to the best of our knowledge, the only examples of RAFT polymerization of ethylene and other polar monomers to make architected materials (either statistical or block copolymers).

III.7. Conclusion

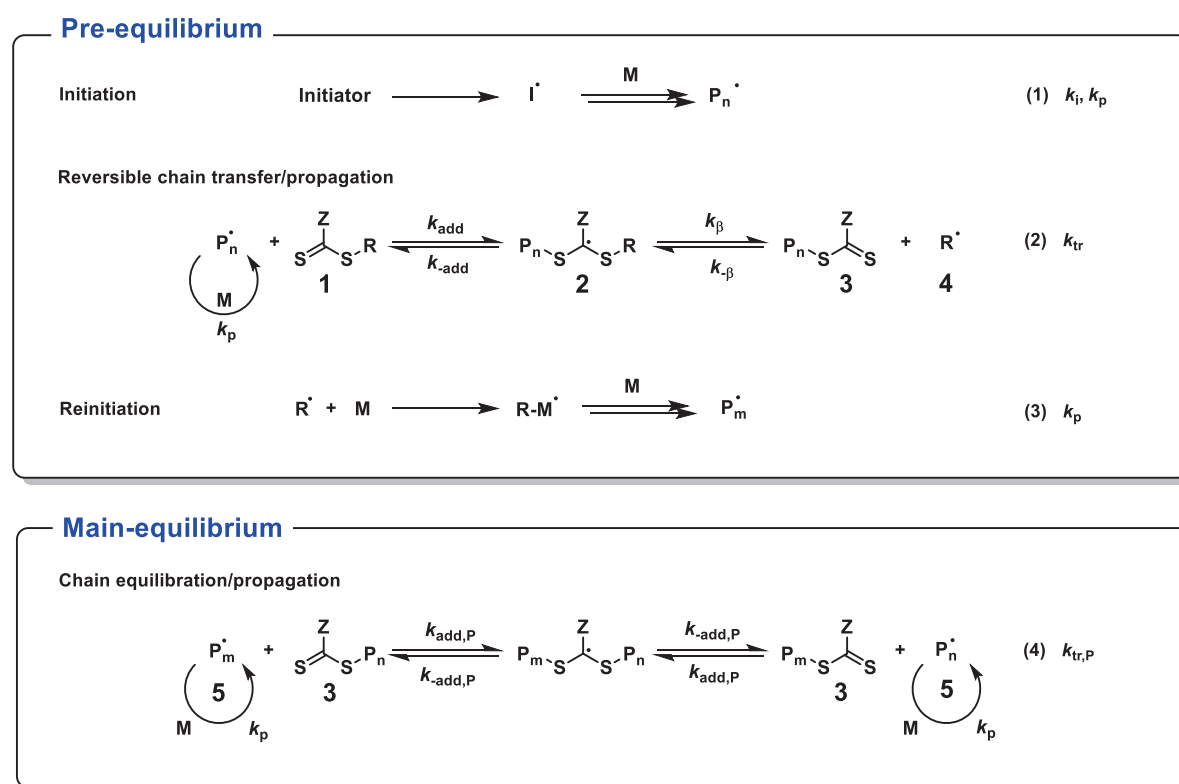
At the time of the start of the present PhD work, Dommaget et al.'s work was the only example clearly establishing the successful RDRP of ethylene *via* a RAFT process and appeared promising for further development. Building on the expertise of the C2P2 group in RAFT and ethylene polymerization, this technique was thus chosen for the simple and efficient synthesis of PE-*b*-PX copolymers. Hence, a more detailed presentation of RAFT polymerization will be conducted in the following section. Its specificities, especially towards the choice of the nature of the CTA for the synthesis of block copolymers based on monomers with disparate reactivities (LAMs vs MAMs) will be highlighted.

IV. Specificities of RAFT polymerization

IV.1. RAFT polymerization

The complete mechanism of RAFT is recalled in **Scheme 39**. At the beginning of the polymerization (pre-equilibrium), the decomposition of the initiator (often a diazo compound, such as AIBN) will produce a radical capable of initiating the polymerization of the desired monomer **M**. The addition of a propagating radical **P•** onto a thiocarbonylthio compound **1** will result in the formation of a non-propagating radical intermediate **2**. One of the following will then occur:

- Reverse addition, thus releasing the same propagating radical **P•** and the same Z-C(S)-S-R species **1**.
- Fragmentation of the S-R bond of the CTA, thus creating a new species Z-C(S)-S-P **3** and releasing a R• **4** capable of re-initiating the polymerization.



Scheme 39. Mechanism of RAFT polymerization

After all the starting CTA **1** is consumed, the polymerization shifts into the main equilibrium phase, where only propagating macro-radicals **5** and dormant species **3** are present in the polymerization medium. The equilibrium between dormant species **3** and active species **5** ensures the simultaneous growth of all polymer chains in a controlled fashion.

As in any RDRP, RAFT polymerization cannot prevent undesired irreversible termination reactions that lead to the formation of dead chains. Those are directly related to the quantity of initiator used and thus a minimum amount is preferable. High CTA:initiator molar ratios are generally used, although this has the antagonist effect of decreasing the polymerization rate (Figure 9).

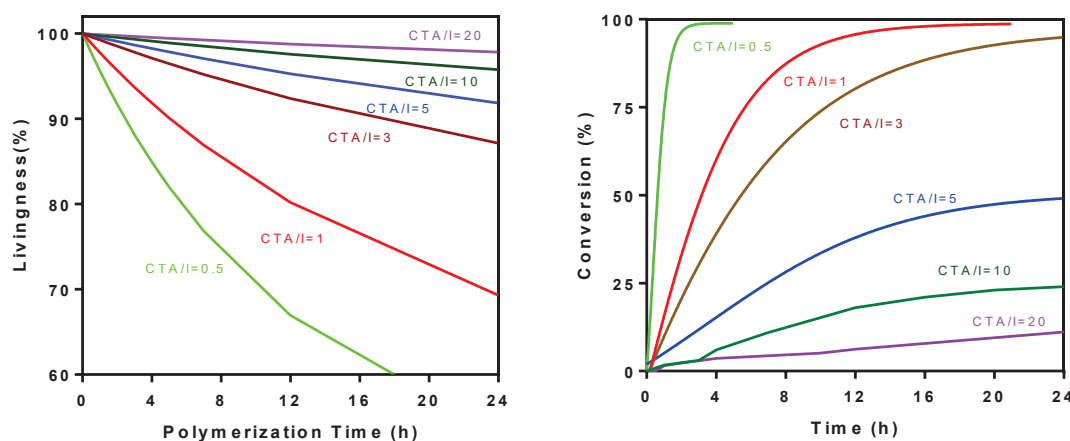


Figure 9. Illustration of the influence of the CTA:initiator ratio on livingness and polymerization kinetics.

The efficiency of the RAFT process is determined by the chain transfer constant value C_{tr} ($C_{tr}=k_{tr}/k_p$). The rate coefficient for chain transfer (k_{tr}) is given by **Equation 2**. As a general rule, the higher the C_{tr} value, the better the control of the polymerization.

$$k_{tr} = k_{add} \frac{k_{\beta}}{k_{-add} + k_{\beta}}$$

Equation 2. Expression used for the determination of k_{tr} .

The importance of the C_{tr} value over M_n and \mathcal{D} values is illustrated by **Figure 10**.^[141] A low C_{tr} value (≤ 2) will result in the non-linear increase of M_n values and dispersity values that remain high throughout the polymerization.

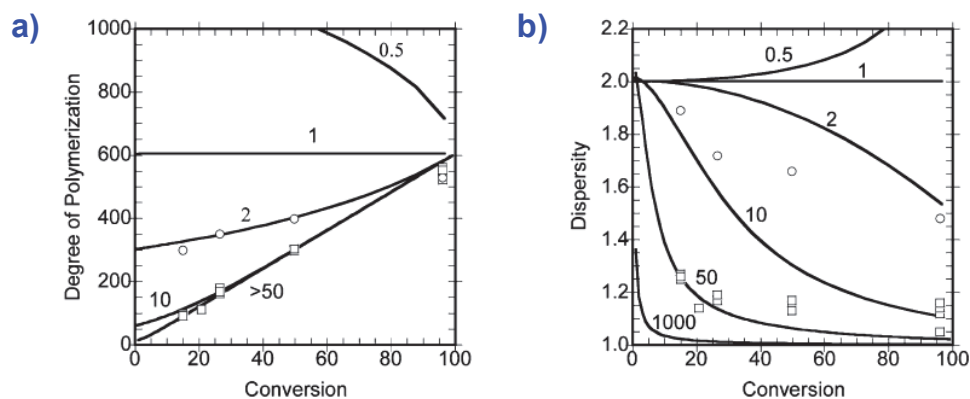


Figure 10. Predicted dependence of (a) the degree of polymerization and (b) the dispersity on conversion in polymerizations involving reversible chain transfer as a function of the chain transfer constant (C_{tr}). Predictions are based on equations proposed by Müller *et al.*^[142,143] with the concentration of active species = 10^{-7} mol L⁻¹, C_{tr} as indicated and the ratio of monomer to transfer agent = 605. Experimental data points shown are for methyl methacrylate (7.02 M) polymerization in presence of dithiobenzoate esters (0.0116 M) where R is $-C(Me)_2CO_2Et$ (O) or $-C(Me)_2Ph$ (□). Reproduced with permission from ref [142]. Copyright 2019 American Chemical Society.

Assuming that the CTA behaves as an ideal chain transfer agent – *i.e.* is rapidly consumed during the polymerization and $k_{tr} > k_p$ – and that all polymer chains are bearing a thiocarbonylthio chain-end, the M_n of the polymer chains formed during a RAFT process can be predicted with **Equation 3**. In this equation, $\Delta[M]_t$ is the consumption of monomer M at a given time t and the number of chains resulting solely from initiation from the decomposition of the initiator is assumed to be negligible.

$$M_n = MW(\text{monomer}) * DP_n = MW(\text{monomer}) * \frac{\Delta[M]_t}{[RAFT]_0}$$

Equation 3. Simplified formula used for the determination of M_n during a RAFT polymerization.

Thus, in an ideal RAFT experiment, the plot of the molar mass *versus* the conversion gives a straight line, and – once the equilibrium state is achieved – the dispersity D values diminish towards the lowest theoretical value of 1 as the conversion goes up (**Figure 11**).

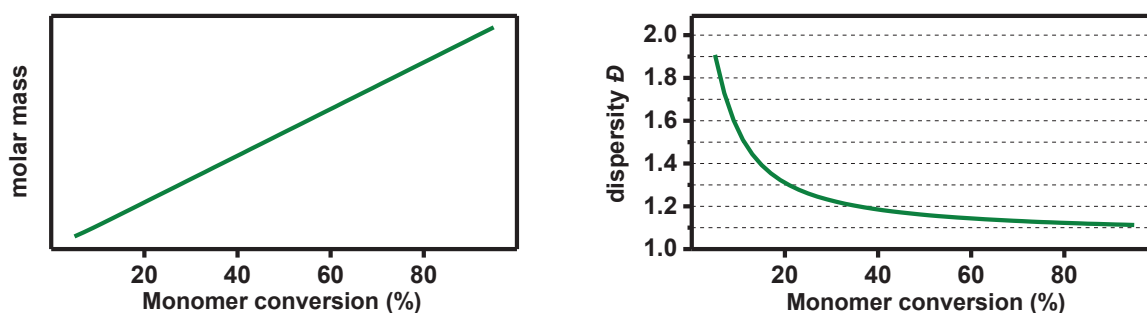


Figure 11. Representation of ideal evolution of molar mass (a) and dispersity (b) during a RAFT experiment.

IV.1.1. Choice of Z- and R-groups

The careful choice of the Z and R groups is of paramount importance in RAFT. The nature of the CTA used, determined by the Z group, will greatly influence which monomer can be controlled. These compounds include dithioesters (Z = alkyl or aryl), trithiocarbonates (Z = SR'), xanthates/dithiocarbonates (Z = OR') and dithiocarbamates (Z = NR'R''). Recently, more exotic CTAs have been studied, such as Selenium^[144] (Z-C(Se)-Se-R), Phosphorus^[145] (Z = PR') and Stannate-based^[146] (Z = SnR') CTAs, but their reactivity will not be discussed in this section.

IV.1.1.1. Role of the Z-group

The efficiency of the addition of a propagating radical onto the thiocarbonylthio moiety of the CTA largely depends on the reactivity of the carbon-sulfur double bond, which is tuned by the Z-group. CTAs which have a carbon or a sulfur adjacent to the thiocarbonylthio (*i.e.* dithioesters and trithiocarbonates) are the most reactive towards a propagating radical. CTAs which have a lone pair on the nitrogen or oxygen adjacent to the thiocarbonylthio (*i.e.* dithiocarbamates and xanthates, respectively) have a dramatically lower reactivity towards radical addition. This is predicted by molecular orbital calculations^[147] and can be viewed as the relative importance of the resonance forms of the CTA. **Figure 12** illustrates the case of two dithiocarbamates: in one case the lone pair is available (**a**) and in the other case the lone pair is not available as it is involved in an aromatic ring system (**b**).

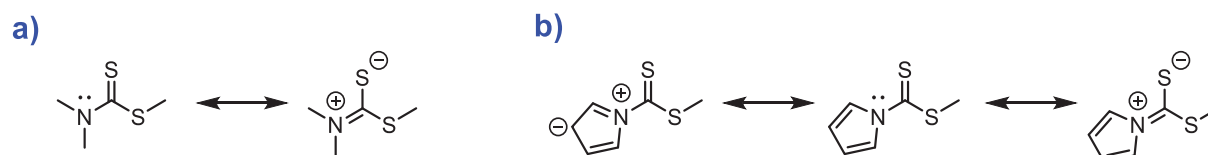


Figure 12. Resonance forms of dithiocarbamates in which **a)** the nitrogen lone pair is available and **b)** the nitrogen lone pair is not available.

The interaction between a lone pair and the C=S double bond reduces the double-bond character of the thiocarbonylthio group, making the CTA less prone to radical addition. Dithiocarbamates in which the lone pair is not available (whether by being part of an aromatic system or where a carbonyl is in α position to the nitrogen) have reactivities similar to that of dithioesters and trithiocarbonates.^[148] Propagating radicals resulting from MAMs are less reactive in radical addition (lower k_p , lower k_{add}) and the most reactive CTAs (dithioesters, trithiocarbonates) are required for good control. Propagating radicals resulting from LAMs are highly reactive in radical addition (higher k_p , higher k_{add}) and the less reactive CTAs (xanthates, dithiocarbamates) are required for good control. However, as poly(LAMs) are poor leaving group, when a most reactive CTA is used, fragmentation is very slow and inhibition or retardation is likely. General guidelines for the selection of the Z-group are shown in **Figure 13**.

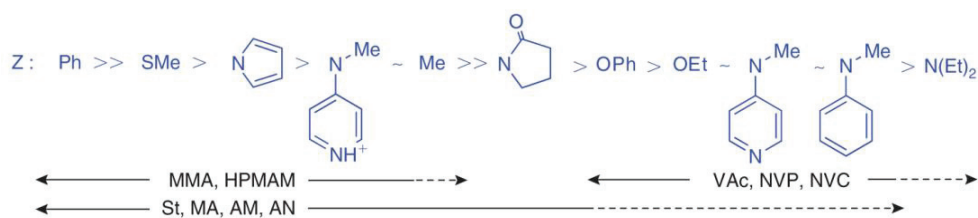


Figure 13. Guidelines for selection of the Z group of RAFT agents Z-C(S)-SR. Addition rate decreases and fragmentation rates increases from left to right. A dashed line indicates a partial control (i.e. good control of M_n but poor control of \bar{D} , or substantial retardation).

IV.1.1.2. Role of the R-group

The nature of the R group determines the partition coefficient ϕ (Equation 4), which indicates the preference for the intermediate radical (**2** in Scheme 39) to fragment to products (k_β) or return to starting materials (k_{add}).

$$\phi = \frac{k_\beta}{k_{\text{add}} + k_\beta}$$

Equation 4. Definition of partition coefficient ϕ .

For effective fragmentation, R should be a good homolytic leaving group and be more stable than the propagating radical P_n^\bullet resulting from the monomer. In short, if P_n^\bullet is highly stabilized (i.e. from MAMs), R should be a stabilized tertiary carbon. If P_n^\bullet is poorly stabilized (i.e. from LAMs), R should be less stable (secondary or primary carbon) while still being able to re-initiate the polymerization. General guidelines for the selection of the R group are shown in Figure 14. The number of substituents of R and their nature strongly affect the partition coefficient ϕ . For example, electron-withdrawing groups both decrease rates of addition to the thiocarbonyl group and increase rates of fragmentation.

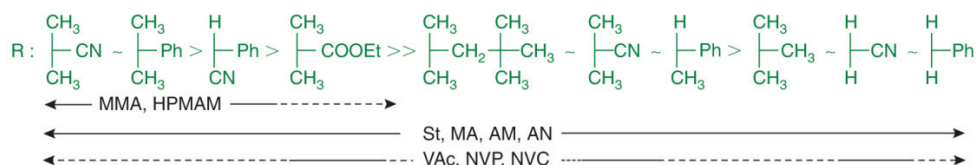


Figure 14. General guidelines for the selection of the R group or RAFT agents Z-C(S)-SR. Partition coefficients decrease from left to right. A dashed line indicates a partial control (i.e. good control of M_n but poor control of \bar{D} , or substantial retardation).

Overall, it is not straightforward to select the right RAFT agent for the right monomer and many factors have to be taken into consideration. Both the nature of the Z- and R-groups have a strong influence on the transfer constant k_{tr} , from which the chain transfer constant value C_{tr}

directly results. **Table 6** collects a few values of experimentally determined C_{tr} for different monomers with different Z- and R-groups.^[67]

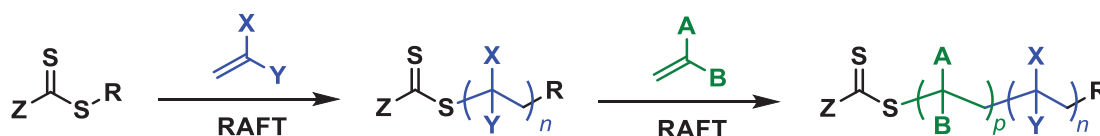
Table 6. Collection of a few chain transfer values of RAFT agents Z-C(S)-SR with different monomers.^[67]

Z	R	Monomer	T (°C)	C_{tr}
PhS	PhCH ₂	S	110	12.4
C ₁₂ H ₂₅ S	PhCH ₂	S	110	9.4
CH ₂ (CO ₂ H)CH ₂ S	CH ₂ (CO ₂ H)CH ₂	S	70	4.3
PhCH(CN)C(S)S(CH ₂) ₄ S	Ph(CH)CN	MMA	70	43
(py)NCH ₃	CH ₂ CN	MA	70	0.9
(py-H ⁺)NCH ₃	CH ₂ CN	MA	70	6.9
(py)NCH ₃	CH ₂ CN	VAc	70	41.7
(py)N(Ph)	CH ₂ CN	VAc	70	124

IV.2. Synthesis of block copolymers via RAFT polymerization

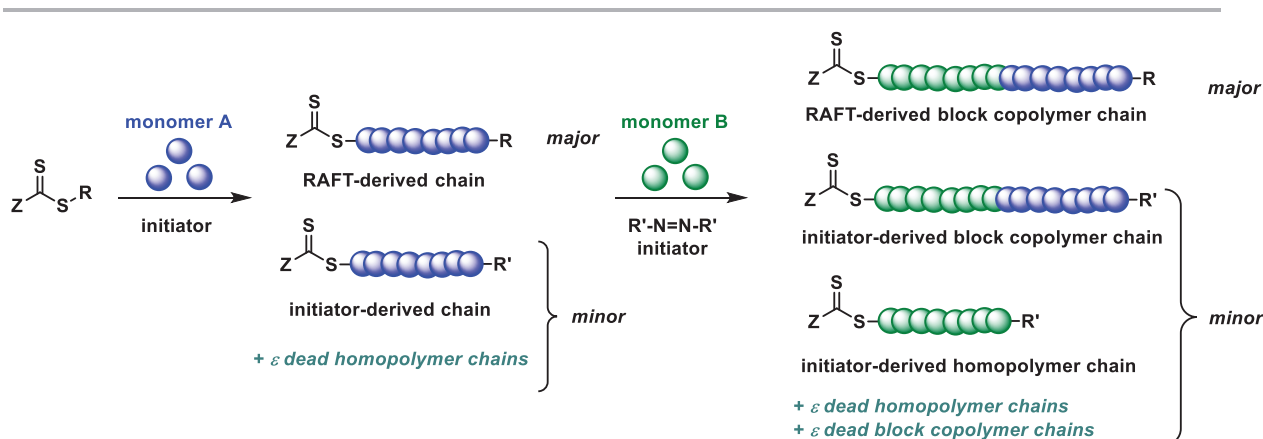
IV.2.1. General guidelines for successful synthesis of block copolymers by RAFT

As previously explained, the nature of the CTA used in RAFT plays a crucial role. Indeed, vinyl monomers are either activated or non-activated. The simplest and most attractive method for the preparation of block copolymers by RAFT is through the incorporation of two (*i.e.* diblock) or more (*i.e.* multiblock) monomers by sequential addition (**Scheme 40**). Considering the above section, the sequential polymerization of monomers with similar reactivities (*i.e.* LAM-LAM or MAM-MAM copolymers) is relatively straightforward, whereas the sequential polymerization of monomers with differing reactivities (*i.e.* LAM-MAM or MAM-LAM) is a lot more challenging.



Scheme 40. Synthesis of block copolymers by RAFT by sequential monomer addition.

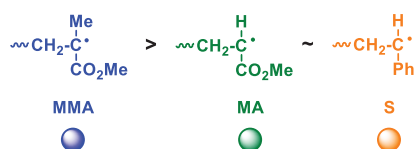
In this context, it should be stated that RAFT polymerization is not perfect and, concomitant to the inevitable formation of dead polymer chains (either by combination, disproportionation or irreversible transfer), the formation of the homopolymer of the monomer used for the second block cannot be avoided (**Scheme 41**). The proportion of homopolymer generated this way depends on the CTA: initiator ratio and is, in most cases, experimentally negligible.^[149]



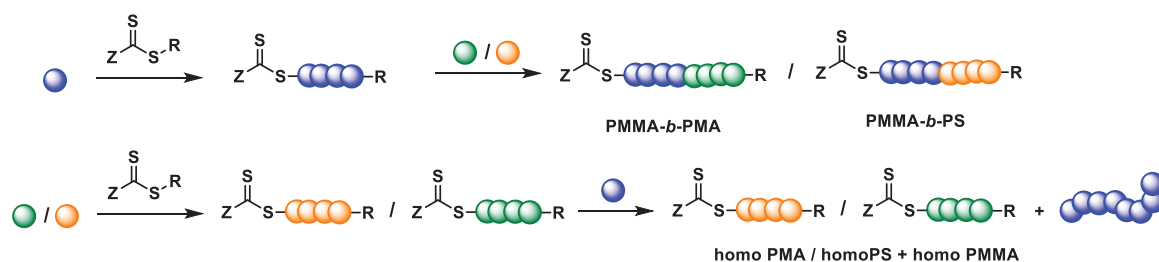
Scheme 41. Schematic representation of the various polymer and copolymer species formed during the synthesis of block copolymer by RAFT.

As well, the order of the polymerization of the different monomers is of great importance. The block copolymer synthesis has to be carefully designed, so that the monomer that gives the most stable propagating radical is polymerized first. This can be exemplified with MMA, MA and S. The propagating radical PMMA• is more stable (tertiary carbon, substituted by electron withdrawing groups (EWGs)) than PS• or PMA• (secondary carbons, substituted by EWGs, **Scheme 42a**). As such, if one wants to make a PMMA-*b*-PS or PMMA-*b*-PMA copolymer by RAFT, the MMA segment should be synthesized first. If not, a mixture of homopolymers will be obtained (**Scheme 42b**). PS• and PMA• have relatively similar reactivities and can be added in either order.

a) relative stability of propagating radical:



b) sequential copolymerization:



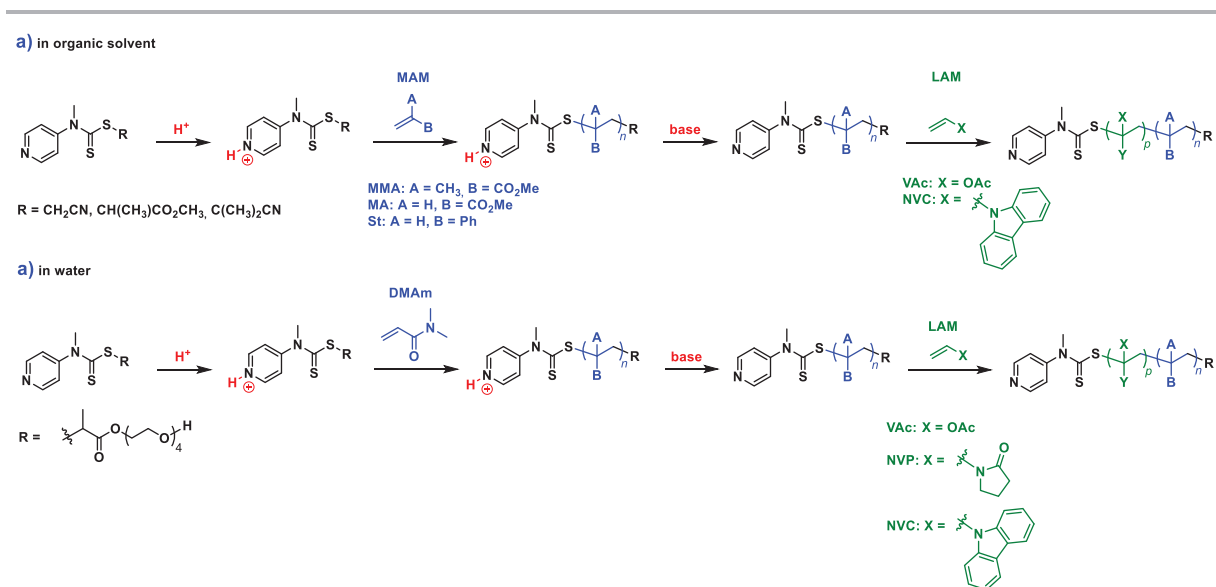
Scheme 42. Relative stability of propagating radicals from MMA, MA and S (a) and illustration of the effect of the order of monomer addition (b).

IV.2.2. Block copolymers between LAMs and MAMs via RAFT polymerization

The efficient block copolymerization of vinyl monomers with different inherent reactivities has long remained a challenge because of the lack of universal character of RAFT agents. Some

groups^[150,151] reported processes using successive ATRP and RAFT to achieve poly(MAM)-*b*-poly(LAM) (e.g. PtBuA)-*b*-PVAc).

Dithiocarbamates have been reported to be able to control both LAMs (VAc) and MAMs (S).^[152] However, the use of the same CTA to control either monomer is somewhat more problematic. In 2009, the CSIRO group reported the first use of switchable *N*-(4-pyridinyl)-*N*-methyldithiocarbamates,^[153] whose reactivity can be selectively tuned through the (de)protonation of a pyridyl ring in the Z-group. Using this new class of pH-responsive CTAs, PMMA-*b*-PVAc, PMA-*b*-PNVC, PS-*b*-PVAc, PDAm-*b*-PNVC, PDAm-*b*-PVAc and PDAm-*b*-PNVP were obtained either in organic solvents (**Scheme 43a**) or in water (**Scheme 43b**).^[153–155] It was shown that the nature of the acid used as well as its quantity relative to the CTA has a great influence on the control of the polymerization (\mathcal{D} ranging from 1.15 to 1.50 for the same monomer with different acids).

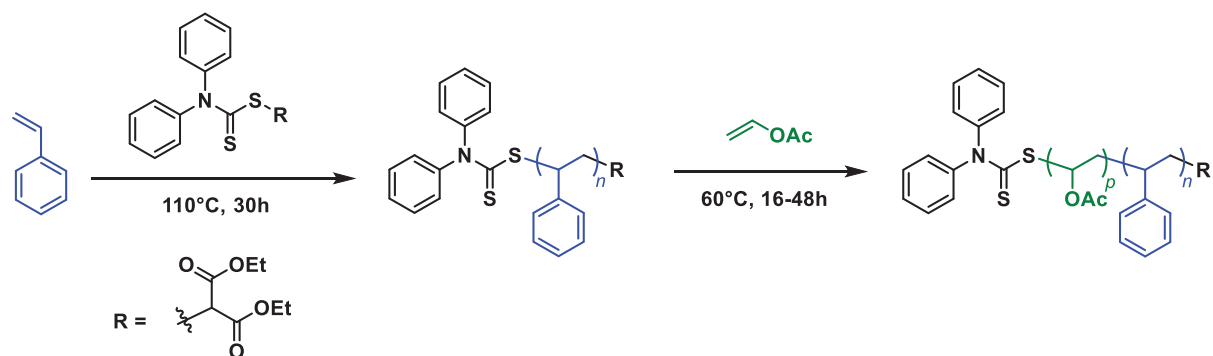


Scheme 43. Synthesis of MAM-LAM block copolymers via switchable dithiocarbamates in organic solvent (a) and in water (b).^[153–156]

Recently, Gardiner *et al.* developed dithiocarbamates with broad applicability, the 3,5-dimethyl-1*H*-pyrazole-1-carbodithioates and 4-halogeno-3,5-dimethyl-1*H*-pyrazole-1-carbodithioates, and showed the successful synthesis of poly(dimethylacrylamide)-*block*-poly(vinyl acetate) copolymers (M_n up to 18 000 g mol⁻¹, $\mathcal{D} < 1.5$).^[156,157] These CTAs provide very good control over MAMs (MA and *N,N*-dimethylacrylamide DMAM, $\mathcal{D} < 1.1$) and LAMs (VAc, $\mathcal{D} < 1.3$). The good control of MMA could be achieved by the introduction of halogens at the 4-position of the pyrazole ring ($1.3 < \mathcal{D} < 1.5$) but this led to a more or less pronounced retardation for VAc. Although the versatility of these CTAs was demonstrated, the synthesis of PMMA-*b*-PVAc has not been reported in their presence.

In some instances, the synthesis of MAM-LAM block copolymers has also been reported with more conventional dithiocarbamates and xanthates. A *N,N*-diphenyldithiocarbamate was used by

Shipp and coworkers to control the polymerization of both S and VAc, and block copolymers could be obtained (**Scheme 44**).^[158]

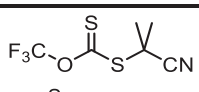
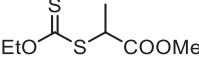
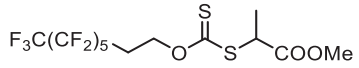
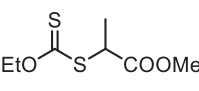


Scheme 44. Synthesis of PS-*b*-PVAc with a *N,N*-diphenyldithiocarbamate CTA.^[159]

The molar mass of the PS block could be increased up to 12 700 g mol⁻¹ ($\mathcal{D} < 1.6$) and the final copolymers had M_n up to 47 000 g mol⁻¹ ($\mathcal{D} < 1.8$). The long polymerization times, high temperature for the styrene block, and low conversion of VAc (< 10%) are all factors that could explain the very limited number of examples of MAM-LAM copolymers with this dithiocarbamate.

Destarac and coworkers reported the use of *O*-alkyl xanthates and *O*-fluoroalkyl xanthates in semi-batch emulsion processes,^[159] organic solvent^[160] or aqueous media^[161] to control both LAMs and MAMs. For these systems, the polymerization conditions were specifically optimized for the desired MAM, but molar masses of the MAM segment remained low ($M_n < 1\,000$ g mol⁻¹, $\mathcal{D} < 1.5$), except in the case of MMA ($M_n = 15\,250$ g mol⁻¹, $\mathcal{D} = 1.28$), for which the semi-batch emulsion conditions favored the polymerization of MMA by keeping its concentration to a minimum. The results of the synthesis of the MAMs macro-CTAs and their subsequent chain extension with LAMs by Destarac *et al.* are presented in **Table 7**.

Table 7. Synthesis of MAM-LAM copolymers using xanthates.^[161-163]

CTA	MAM	$M_{n,macro-CTA}$ g mol ⁻¹ (\bar{D})	LAM	$M_{n,diblock}$ g mol ⁻¹ (\bar{D})
	MMA	15 250 (1.28)	VAc	41 850 (1.27)
	DMAm	1 000 (1.56)	VAc	4 600 (1.24)
	DMAm	1 300 (1.11)	VAc	4 500 (1.21)
	Am	950 (1.07)	NVP	10 500 (1.59)
	AA	1 020 (1.29)	NVP	10 600 (1.25)
	AMPS	1 035 (1.33)	NVP	10 000 (-)
	APTAC	1 010 (1.49)	NVP	10 300 (-)

AMPS: 2-acrylamido-2-methyl-1-propanesulfonic acid, APTAC: 3-acrylamidopropyltrimethylammonium chloride, AA: acrylic acid

*The direct block copolymerization via RAFT of ethylene with a polar monomer was recently reported for the first time by You and coworkers using a PNVP macro-CTA. However, the authors did not mention the occurrence of side-fragmentation with the O-methyl xanthate CTA used during their work, and their results are questionable regarding SEC and NMR analyses. The direct synthesis of PE-*b*-PX copolymers by RAFT, with either LAMs or MAMs, has otherwise never been reported.*

V. Conclusion and positioning of this work

RDRP polymerization techniques allow for the synthesis of complex block copolymers with tailored architecture and tuned properties. Until recently, this was inaccessible for polyethylene because the controlled radical polymerization of ethylene could not be achieved. The high attractiveness of such materials, with one block consisting of pure PE, led research groups around the world to develop alternative pathways to obtain these materials, with the chemical post-modification of a preformed PE block by a coordination-insertion mechanism at the spearhead of the proposed alternatives. The tediousness and limited efficacy of the alternatives proposed have failed to provide a satisfactory solution to the synthesis of polar-apolar olefin block copolymer (PE-*b*-PX copolymers).

Recent developments in the RAFT polymerization of ethylene, as well as the versatility of this technique for the synthesis of block copolymers, have led our group to focus on this polymerization technique to propose a direct, simple and efficient synthesis of PE-*b*-PX copolymers. Through the careful choice of chain transfer agents, we endeavored to solve the issue of the side-fragmentation reaction identified and complete our mastering of the RDRP of ethylene. This will be described in Chapter **II**. Chapter **III** will focus on the relatively straightforward synthesis of block copolymers between ethylene and vinyl acetate, another less activated monomer. The complexity of the synthesis will be further increased with the use of methyl methacrylate, a more activated monomer, for the polar block. A part of this work was done in collaboration with Prof. M. Destarac and Dr. S. Harrisson at the IMRCP laboratory in Toulouse. The synthesis of PMMA-*b*-PE block copolymers, a material with potential interesting applications, such as compatibilizing agent in epoxy polymer blends, will be covered by Chapter **IV**. Chapter **V** will eventually focus on the synthesis of amphiphilic block copolymers in water. The investigation of the polymerization-induced self-assembly (PISA) of ethylene in water, using poly(ethylene oxide) as hydrophilic macro-CTA will be described.

VI. References

- [1] PTT, *Polymer Marketing Company - Current PE Market Situation and Production Capacity Outlook*, **2017**.
- [2] R. Muellhaupt, *Macromol. Chem. Phys.* **2013**, *214*, 159–174.
- [3] E. W. Fawcett, R. O. Gibson, M. W. Perrin, *Polymerization of Olefins. US2153553*, **1939**.
- [4] A. J. Peacock, *Handbook of Polyethylene*, Marcel Dekker Inc., **2000**.
- [5] S. M. Kurz, *UHMWPE Handbook*, Academic Press, **2004**.
- [6] K. Ziegler, *Angew. Chemie* **1952**, *64*, 323–329.
- [7] J. P. Hogan, R. L. Banks, *Polymers and Production Thereof. US2825721*, **1958**.
- [8] K. Ziegler, E. Holzkamp, H. Breil, H. Martin, *Angew. Chem.* **1955**, *67*, 541–547.
- [9] W. Kaminsky, *J. Polym. Sci. Part A Polym. Chem.* **2004**, *42*, 3911–3921.
- [10] V. C. Gibson, S. K. Spitzmesser, *Chem. Rev.* **2003**, *103*, 283–316.
- [11] J.J. Boor, *Ziegler-Natta Catalysts and Polymerizations*, **1979**.
- [12] R. F. Jordan, *Proc. Publ. 2006 by Am. Chem. Soc.* **2006**, 4–5.
- [13] P. Aaltonen, G. Fink, B. Löfgren, J. Seppälä, *Macromolecules* **1996**, *29*, 5255–5260.
- [14] M. R. Kesti, G. W. Coates, R. M. Waymouth, *J. Am. Chem. Soc.* **1992**, *114*, 9679–9680.
- [15] L. S. Boffa, B. M. Novak, *Chem. Rev.* **2000**, *100*, 1479–1493.
- [16] G. J. P. Britovsek, V. C. Gibson, S. J. McTavish, G. A. Solan, A. J. P. White, D. J. Williams, G. J. P. Britovsek, B. S. Kimberley, P. J. Maddox, *Chem. Commun.* **2002**, *311*, 849–850.
- [17] B. L. Small, M. Brookhart, A. M. a Bennett, *J. Am. Chem. Soc.* **1998**, *120*, 4049–4050.
- [18] F. C. Rix, M. Brookhart, *J. Am. Chem. Soc.* **1995**, *117*, 1137–1138.
- [19] C. Wang, S. Friedrich, T. R. Younkin, R. T. Li, R. H. Grubbs, D. A. Bansleben, M. W. Day, *Organometallics* **1998**, *17*, 3149–3151.
- [20] L. K. Johnson, C. M. Killian, M. Brookhart, *J. Am. Chem. Soc.* **1995**, *117*, 6414–6415.
- [21] W. Keim, F. H. Kowaldt, R. Goddard, K. Carl, *Angew. Chem. Int. Ed.* **1978**, *17*, 466–467.
- [22] E. Drent, R. van Dijk, R. van Ginkel, B. van Oort, R. I. Pugh, *Chem. Commun.* **2002**, 744–745.
- [23] A. Nakamura, S. Ito, K. Nozaki, *Chem. Rev.* **2009**, *109*, 5215–5244.
- [24] I. Göttker-Schnetmann, B. Korthals, S. Mecking, *J. Am. Chem. Soc.* **2006**, *128*, 7708–7709.
- [25] F. M. Bauers, S. Mecking, *Angew. Chemie - Int. Ed.* **2001**, *40*, 3020–3022.
- [26] R. Spitz, J. Claverie, R. Soula, A. Guyot, *Macromolecules* **2001**, *34*, 2022–2026.
- [27] D. B. Malpass, in *Introd. to Ind. Polyethyl. Prop. Catal. Process.*, **2010**, pp. 85–97.
- [28] M. J. Roedel, *J. Am. Chem. Soc.* **1953**, *75*, 6110–6112.
- [29] D. A. Boyle, W. Simpson, J. D. Waldron, *Polymer*, **1961**, *2*, 323–334.
- [30] R. S. Porter, *Handbook of Polymer Synthesis*, **2005**.
- [31] R. C. Reid, J. M. Prausnitz, T. K. Sherwood, *McGraw-Hill (1977)* **1987**, 741.
- [32] B. Levresse, *Techniques de l'ingénieur - Polyethylene Basse Densité*, **1993**.
- [33] T. P. Davis, *Handbook of Radical Polymerization*, **2013**.
- [34] P. Ehrlich, G. A. Mortimer, *Adv. Polym. Sci.* **1970**, *7*, 386–448.
- [35] G. A. Mortimer, W. F. Hamner, *J. Polym. Sci. Part A Polym. Chem.* **1964**, *2*, 1301–1309.
- [36] J. C. Woodbrey, P. Ehrlich, *J. Am. Chem. Soc.* **1963**, *85*, 1580–1584.
- [37] M. Busch, M. Roth, M. H. Stenzel, T. P. Davis, C. Barner-Kowollik, *Aust. J. Chem.* **2007**, *60*, 788.
- [38] S. Machi, T. Tamura, M. Hagiwara, M. Gotoda, T. Kagiya, *J. Polym. Sci. Part A-1 Polym. Chem.* **1966**, *4*, 283–291.
- [39] S. Machi, M. Hagiwara, M. Gotoda, T. Kagiya, *J. Polym. Sci. Part A Gen. Pap.* **1965**, *3*, 2931–2934.
- [40] E. Grau, J. P. Broyer, C. Boisson, R. Spitz, V. Monteil, *Macromolecules* **2009**, *42*, 7279–7281.
- [41] E. Grau, J. P. Broyer, C. Boisson, R. Spitz, V. Monteil, *Polym. Chem.* **2011**, *2*, 2328–2333.
- [42] V. F. Gromov, P. M. Khomikovskii, *Russ. Chem. Rev.* **2005**, *48*, 1040–1054.
- [43] J. Merna, P. Vlček, V. Volkis, J. Michl, *Chem. Rev.* **2016**, *116*, 771–785.
- [44] Y. Imanishi, N. Naga, *Prog. Polym. Sci.* **2001**, *26*, 1147–1198.
- [45] L. K. Johnson, S. Mecking, M. Brookhart, *J. Am. Chem. Soc.* **1996**, *118*, 267–268.
- [46] S. Mecking, L. K. Johnson, L. Wang, M. Brookhart, *J. Am. Chem. Soc.* **1998**, *120*, 888–899.
- [47] S. Ito, K. Munakata, A. Nakamura, K. Nozaki, *J. Am. Chem. Soc.* **2009**, *131*, 14606–14607.
- [48] H. W. Boone, P. S. Athey, M. J. Mullins, D. Philipp, R. Muller, W. A. Goddard, *J. Am. Chem. Soc.* **2002**, *124*, 8790–8791.
- [49] T. Kochi, K. Yoshimura, K. Nozaki, *Dalt. Trans.* **2006**, 25–27.
- [50] K. M. Skupov, P. R. Marella, M. Simard, G. P. A. Yap, N. Allen, D. Conner, B. L. Goodall, J. P. Claverie, *Macromol. Rapid Commun.* **2007**, *28*, 2033–2038.
- [51] S. Luo, J. Vela, G. R. Liet, R. F. Jordan, *J. Am. Chem. Soc.* **2007**, *129*, 8946–8947.
- [52] T. Kochi, S. Noda, K. Yoshimura, K. Nozaki, *J. Am. Chem. Soc.* **2007**, *129*, 8948–8949.

- [53] W. Weng, Z. Shen, R. F. Jordan, *J. Am. Chem. Soc.* **2007**, *129*, 15450–15451.
- [54] Y. Na, S. Dai, C. Chen, *Macromolecules* **2018**, *51*, 4040–4048.
- [55] Z. Chen, M. Brookhart, *Acc. Chem. Res.* **2018**, *51*, 1831–1839.
- [56] M. Nagel, D. Poli, A. Sen, *Macromolecules* **2005**, *38*, 7262–7265.
- [57] R. Luo, A. Sen, *Macromolecules* **2006**, *39*, 7798–7800.
- [58] A. Zarrouki, E. Espinosa, C. Boisson, V. Monteil, *Macromolecules* **2017**, *50*, 3516–3523.
- [59] N. M. G. Franssen, J. N. H. Reek, B. de Bruin, *Chem. Soc. Rev.* **2013**, *42*, 5809–5832.
- [60] E. Passaglia, S. Coiai, F. Cicogna, F. Ciardelli, *Polym. Int.* **2014**, *63*, 12–21.
- [61] R. Godoy Lopez, F. D'Agosto, C. Boisson, *Prog. Polym. Sci.* **2007**, *32*, 419–454.
- [62] H. Fischer, *J. Polym. Sci. Part A Polym. Chem.*, **1999**, *37*, 1885–1901.
- [63] K. Matyjaszewski, *Macromolecules* **2012**, *45*, 4015–4039.
- [64] J. Demarteau, A. Debuigne, C. Detrembleur, *Chem. Rev.* **2019**, *119*, 6906–6955.
- [65] G. David, C. Boyer, J. Tonnar, B. Ameduri, P. Lacroix-Desmazes, B. Boutevin, *Chem. Rev.* **2006**, *106*, 3936–3962.
- [66] S. Yamago, *J. Polym. Sci. Part A Polym. Chem.* **2006**, *44*, 1–12.
- [67] G. Moad, E. Rizzardo, S. H. Thang, *Aust. J. Chem.* **2012**, *65*, 985.
- [68] J. Nicolas, Y. Guillauneuf, D. Bertin, D. Gigmes, B. Charleux, *Prog. Polym. Sci.* **2013**, *38*, 63–225.
- [69] M. K. Georges, R. P. N. Veregin, P. M. Kazmaier, G. K. Hamer, *Macromolecules* **1993**, *26*, 2987–2988.
- [70] M. Kato, M. Kamigaito, M. Sawamoto, T. Higashimura, *Macromolecules* **1995**, *28*, 1721–1723.
- [71] K. Matyjaszewski, J. Wang, *J. Am. Chem. Soc.* **1995**, *117*, 5614.
- [72] G. R. Jones, A. Anastasaki, R. Whitfield, N. Engelis, E. Liarou, D. M. Haddleton, *Angew. Chemie - Int. Ed.* **2018**, *57*, 10468–10482.
- [73] Y. Kotani, M. Kato, M. Kamigaito, M. Sawamoto, *Macromolecules* **1996**, *29*, 6979–6982.
- [74] K. Matyjaszewski, W. Jakubowski, K. Min, *Macromolecules* **2006**, *39*, 39–45.
- [75] L. Mueller, W. Jakubowski, W. Tang, K. Matyjaszewski, *Macromolecules* **2007**, *40*, 6464–6472.
- [76] A. Anastasaki, V. Nikolaou, D. M. Haddleton, *Polym. Chem.* **2016**, *7*, 1002–1026.
- [77] J. Chiefari, Y. K. B. Chong, F. Ercole, J. Krstina, J. Jeffery, T. P. T. Le, R. T. A. Mayadunne, G. F. Meijs, C. L. Moad, G. Moad, et al., *Macromolecules* **1998**, *31*, 5559–5562.
- [78] P. Corpart, D. Charmot, S. Z. Zard, T. Biadatti, D. Michelet, *Method for Block Polymer Synthesis by Controlled Radical Polymerization W09858974*, **2000**.
- [79] R. Devasia, R. L. Bindu, R. Borsali, N. Mougín, Y. Gnanou, in *Macromol. Symp.*, **2005**, pp. 8–17.
- [80] M. Destarac, W. Bzducha, D. Taton, I. Gauthier-Gillaizeau, S. Z. Zard, *Macromol. Rapid Commun.* **2002**, *23*, 1049–1054.
- [81] B. Ameduri, *Macromolecules* **2010**, *43*, 10163–10184.
- [82] R. G. Lopez, C. Boisson, F. D'Agosto, R. Spitz, F. Boisson, D. Gigmes, D. Bertin, *Macromol. Rapid Commun.* **2006**, *27*, 173–181.
- [83] T. C. Chung, *Prog. Polym. Sci.* **2002**, *27*, 39–85.
- [84] M. K. Mahanthappa, F. S. Bates, M. A. Hillmyer, *Macromolecules* **2005**, *38*, 7890–7894.
- [85] S. M. Banik, B. L. Monnot, R. L. Weber, M. K. Mahanthappa, *Macromolecules* **2011**, *44*, 7141–7148.
- [86] S. B. Myers, R. A. Register, *Macromolecules* **2008**, *41*, 5283–5288.
- [87] S. Xu, C. Zhang, L. Li, S. Zheng, *Polymer*, **2017**, *128*, 1–11.
- [88] H. Wang, F. Xu, K. Cui, H. Zhang, J. Huang, Q. Zhao, T. Jiang, Z. Ma, *RSC Adv.* **2017**, *7*, 42484–42490.
- [89] C. Auschra, R. Stadler, *Polym. Bull.* **1993**, *30*, 257–264.
- [90] N. Petzetakis, G. M. Stone, N. P. Balsara, *Macromolecules* **2014**, *47*, 4151–4159.
- [91] J. Y. Dong, T. C. Chung, *Macromolecules* **2002**, *35*, 1622–1631.
- [92] C. S. Kim, S. S. Park, S. D. Kim, S. J. Kwon, J. W. Baek, B. Y. Lee, *Polymers.* **2017**, *9*, 1–14.
- [93] C. J. Han, M. S. Lee, D.-J. Byun, S. Y. Kim, *Macromolecules* **2002**, *35*, 8923–8925.
- [94] T. Yan, D. J. Walsh, C. Qiu, D. Guironnet, *Macromolecules* **2018**, *51*, 10167–10173.
- [95] Y. Lu, Y. Hu, Z. M. Wang, E. Manias, T. C. Chung, *J. Polym. Sci. Part A Polym. Chem.* **2002**, *40*, 3416–3425.
- [96] J. Mazzolini, I. Mokthari, R. Briquel, O. Boyron, F. Delolme, V. Monteil, D. Bertin, D. Gigmes, F. D'Agosto, C. Boisson, *Macromolecules* **2010**, *43*, 7495–7503.
- [97] C. Lefay, D. Glé, M. Rollet, J. Mazzolini, D. Bertin, S. Viel, C. Schmid, C. Boisson, F. D'Agosto, D. Gigmes, et al., *J. Polym. Sci. Part A Polym. Chem.* **2011**, *49*, 803–813.
- [98] S. Bogaert, T. Chenal, A. Mortreux, J. F. Carpentier, *J. Mol. Catal. A Chem.* **2002**, *190*, 207–214.
- [99] G. Xu, T. C. Chung, *J. Am. Chem. Soc.* **1999**, *121*, 6763–6764.
- [100] C. J. Kay, P. D. Goring, C. A. Burnett, B. Hornby, K. Lewtas, S. Morris, C. Morton, T. McNally, G. W. Theaker, C. Waterson, et al., *J. Am. Chem. Soc.* **2018**, *140*, 13921–13934.
- [101] Y. Zhao, X. Shi, H. Gao, L. Zhang, F. Zhu, Q. Wu, *J. Mater. Chem.* **2012**, *22*, 5737–5745.
- [102] N. Kawahara, S. I. Kojoh, S. Matsuo, H. Kaneko, T. Matsugi, J. Saito, N. Kashiwa, *Polym. Bull.* **2006**, *57*, 805–812.

- [103] R. G. Lopez, C. Boisson, F. D'Agosto, R. Spitz, F. Boisson, D. Bertin, P. Tordo, *Macromolecules* **2004**, *37*, 3540–3542.
- [104] Y. Inoue, K. Matyjaszewski, *J. Polym. Sci. Part A Polym. Chem.* **2004**, *42*, 496–504.
- [105] H. Kaneyoshi, Y. Inoue, K. Matyjaszewski, *Macromolecules* **2005**, 5425–5435.
- [106] W. J. Wang, L. Pingwei, B. G. Li, Z. Shiping, *J. Polym. Sci. Part A Polym. Chem.* **2010**, *48*, 3024–3032.
- [107] S. Collins, D. G. Ward, K. H. Suddaby, *Macromolecules* **1994**, *27*, 7222–7224.
- [108] H. Yasuda, E. Ihara, T. Hayakawa, T. Kakehi, *J. Org. Chem.* **2002**, *647*, 128–138.
- [109] G. Desurmont, M. Tanaka, Y. Li, H. Yasuda, T. Tokimitsu, S. Tone, A. Yanagase, *Polymer* **2000**, 4095–4109.
- [110] H. Frauenrath, S. Balk, H. Keul, H. Höcker, *Macromol. Rapid Commun.* **2001**, *22*, 1147–1151.
- [111] H. C. Kolb, M. G. Finn, K. B. Sharpless, *Angew. Chemie - Int. Ed.* **2001**, *40*, 2004–2021.
- [112] K. Kempe, A. Krieg, C. R. Becer, U. S. Schubert, *Chem. Soc. Rev.* **2012**, *41*, 176–191.
- [113] T. Li, W. J. Wang, R. Liu, W. H. Liang, G. F. Zhao, Z. Y. Li, Q. Wu, F. M. Zhu, *Macromolecules* **2009**, *42*, 3804–3810.
- [114] Y. Zhang, H. Li, J. Y. Dong, Y. Hu, *Polym. Chem.* **2014**, *5*, 105–115.
- [115] E. Espinosa, B. Charleux, F. D'Agosto, C. Boisson, R. Tripathy, R. Faust, C. Soulié-Ziakovic, *Macromolecules* **2013**, *46*, 3417–3424.
- [116] E. Espinosa, M. Glassner, C. Boisson, C. Barner-Kowollik, F. D'Agosto, *Macromol. Rapid Commun.* **2011**, *32*, 1447–1453.
- [117] Z. Xu, S. Jie, B. G. Li, *J. Polym. Sci. Part A Polym. Chem.* **2014**, *52*, 3205–3212.
- [118] S. Borkar, A. Sen, *J. Polym. Sci. Part A Polym. Chem.* **2005**, *43*, 3728–3736.
- [119] S. Yamago, K. Iida, J. I. Yoshida, *J. Am. Chem. Soc.* **2002**, *124*, 2874–2875.
- [120] S. Yamago, *Chem. Rev.* **2009**, *109*, 5051–5068.
- [121] S. I. Yusa, S. Yamago, M. Sugahara, S. Morikawa, T. Yamamoto, Y. Morishima, *Macromolecules* **2007**, *40*, 5907–5915.
- [122] S. Yamago, B. Ray, K. Iida, J. I. Yoshida, T. Tada, K. Yoshizawa, Y. Kwak, A. Goto, T. Fukuda, *J. Am. Chem. Soc.* **2004**, *126*, 13908–13909.
- [123] B. Ray, M. Kotani, S. Yamago, *Macromolecules* **2006**, *39*, 5259–5265.
- [124] Y. Nakamura, B. Ebeling, A. Wolpers, V. Monteil, F. D'Agosto, S. Yamago, *Angew. Chem. Int. Ed.* **2018**, *57*, 305–309.
- [125] B. B. Wayland, G. Poszmik, S. Mukerjee, *J. Am. Chem. Soc.* **1994**, *116*, 7943–7944.
- [126] L. D. Arvanitopoulou, M. P. Gruel, H. J. Harwood, *Polym. Prepr. (American Chem. Soc. Div. Polym. Chem.)* **1994**, *35*, 549–550.
- [127] A. Debuigne, J. R. Caille, C. Detrembleur, R. Jérôme, *Angew. Chemie - Int. Ed.* **2005**, *44*, 3439–3442.
- [128] A. Kermagoret, A. Debuigne, C. Jérôme, C. Detrembleur, *Nat. Chem.* **2014**, *6*, 179–187.
- [129] C. Detrembleur, J. Demarteau, A. Debuigne, A. Kermagoret, *WO 2019/121409A1 - Block Copolymerization of Ethylene by Cobalt-Mediated Radical Polymerization*, **2019**.
- [130] D. Gignes, A. Gaudel-Siri, S. R. A. Marque, D. Bertin, P. Tordo, P. Astolfi, L. Greci, C. Rizzoli, *Helv. Chim. Acta* **2006**, *89*, 2312–2326.
- [131] K. A. Moffat, M. D. Saban, R. P. N. Veregin, M. K. Georges, G. K. Hamer, P. M. Kazmaier, *Stable Free Radical Polymerization Process and Thermoplastic Materials Produced Therefrom - US5449724*, **1995**.
- [132] E. Minaux, L. Greci, M. Buback, P. Tordo, T. Senninger, P. Stipa, P. Carloni, E. Damiani, G. Tommasi, *Process for the Controlled Radical Polymerization or Copolymerization of Ethylene under High Pressure in the Presence of Initiating Free Radicals and of Controlling Indoline Nitroxide Radicals - US6706832B2*, **2004**.
- [133] B. Gu, S. Liu, J. D. Leber, A. Sen, *Macromolecules* **2004**, *37*, 5142–5144.
- [134] E. H. H. Wong, M. H. Stenzel, T. Junkers, C. Barner-Kowollik, *Macromolecules* **2010**, *43*, 3785–3793.
- [135] C. Dommanget, C. Boisson, B. Charleux, F. D'Agosto, V. Monteil, F. Boisson, T. Junkers, C. Barner-Kowollik, Y. Guillaneuf, D. Gignes, *Macromolecules* **2013**, *46*, 29–36.
- [136] G. Moad, E. Biccocchi, M. Chen, J. Chiefari, C. Guerrero-sanchez, M. Haeussler, S. Houshyar, D. Keddie, E. Rizzardo, S. H. Thang, et al., **2012**, 1998.
- [137] S. Perrier, *Macromolecules* **2017**, *50*, 7433–7447.
- [138] M. L. Coote, E. I. Izgorodina, G. E. Cavigliasso, M. Roth, M. Busch, C. Barner-Kowollik, *Macromolecules* **2006**, *39*, 4585–4591.
- [139] C. Dommanget, F. D'Agosto, V. Monteil, *Angew. Chem. Int. Ed.* **2014**, *53*, 6683–6686.
- [140] Q. B. Chen, T. Y. Zeng, L. Xia, Z. Zhang, C. Y. Hong, G. Zou, Y. Z. You, *Chem. Commun.* **2017**, *53*, 10780–10783.
- [141] D. J. Keddie, G. Moad, E. Rizzardo, S. H. Thang, *Macromolecules* **2012**, *45*, 5321–5342.
- [142] A. H. E. Müller, R. Zhuang, D. Yan, G. Litvinenko, *Macromolecules* **1995**, *28*, 4326–4333.
- [143] G. Litvinenko, A. H. E. Müller, *Macromolecules* **1997**, *30*, 1253–1266.

- [144] D. Matioszek, O. Brusylovets, D. James Wilson, S. Mazières, M. Destarac, *J. Polym. Sci. Part A Polym. Chem.* **2013**, *51*, 4361–4368.
- [145] S. Mazières, I. Kulai, R. Geagea, S. Ladeira, M. Destarac, *Chem. - A Eur. J.* **2015**, *21*, 1726–1734.
- [146] I. Kulai, O. Brusylovets, Z. Voitenko, S. Harrisson, S. Mazières, M. Destarac, *ACS Macro Lett.* **2015**, *4*, 809–813.
- [147] M. L. Coote, D. J. Henry, *Macromolecules* **2005**, *38*, 1415–1433.
- [148] J. Chiefari, R. T. A. Mayadunne, C. L. Moad, G. Moad, E. Rizzardo, A. Postma, M. A. Skidmore, S. H. Thang, *Macromolecules* **2003**, *36*, 2273–2283.
- [149] D. J. Keddie, *Chem. Soc. Rev.* **2014**, *43*, 496–505.
- [150] H. Hussain, B. H. Tan, C. Gudipati, Y. Liu, C. B. He, B. T. P. Davis, *J. Polym. Sci. Part A Polym. Chem.* **2008**, *46*, 5604–5615.
- [151] V. Malepu, C. D. Petruczok, D. A. Shipp, *J. Polym. Sci. Part A Polym. Chem.* **2008**, 7200–7206.
- [152] M. Destarac, D. Charmot, X. Franck, S. Z. Zard, *Macromol. Rapid Commun.* **2000**, *21*, 1035–1039.
- [153] M. Benaglia, J. Chiefari, Y. K. Chong, G. Moad, E. Rizzardo, S. H. Thang, *J. Am. Chem. Soc.* **2009**, *131*, 6914–6915.
- [154] G. Moad, M. Benaglia, M. Chen, J. Chiefari, Y. K. Chong, D. J. Keddie, E. Rizzardo, S. H. Thang, *ACS Symp. Ser.* **2011**, *1066*, 81–102.
- [155] G. Moad, D. Keddie, C. Guerrero-Sanchez, E. Rizzardo, S. H. Thang, *Macromol. Symp.* **2015**, *350*, 34–42.
- [156] J. Gardiner, I. Martinez-Botella, J. Tsanaktsidis, G. Moad, *Polym. Chem.* **2016**, *7*, 481–492.
- [157] J. Gardiner, I. Martinez-Botella, T. M. Kohl, J. Krstina, G. Moad, J. H. Tyrell, M. L. Coote, J. Tsanaktsidis, *Polym. Int.* **2017**, *66*, 1438–1447.
- [158] L. A. Dayter, K. A. Murphy, D. A. Shipp, *Aust. J. Chem.* **2013**, *66*, 1564–1569.
- [159] M. Destarac, D. Matioszek, X. Vila, J. Ruchmann-Sternchuss, S. Z. Zard, *ACS Symp. Ser.* **2018**, *1284*, 291–305.
- [160] E. Girard, T. Tassaing, J. D. Marty, M. Destarac, *Polym. Chem.* **2011**, *2*, 2222–2230.
- [161] A. Guinaudeau, O. Coutelier, A. Sandeau, S. Mazières, H. D. Nguyen Thi, V. Le Drogo, D. J. Wilson, M. Destarac, *Macromolecules* **2014**, *47*, 41–50.

Chapter II

RAFT polymerization of ethylene

I. Introduction.....	98
II. Context of ethylene RAFT homopolymerization	99
II.1. RAFT polymerization of ethylene with <i>O</i> -ethyl xanthate	99
II.2. RAFT polymerization of ethylene with <i>O</i> -methyl xanthate	101
II.3. Z-groups with aromatic substituents to suppress side-fragmentation.....	101
II.3.1. Xanthates with aromatic substituents.....	101
II.3.2. <i>N,N</i> -dithiocarbamates with aromatic substituents.....	104
III. RAFT polymerization of ethylene with <i>O</i>-aryl xanthates	105
III.1. RAFT homopolymerization of ethylene.....	105
III.1.1. Polymerization at 70°C and 200 bar	105
III.1.2. Polymerization at 80°C and 200 bar	110
III.1.3. Rationalization of the emergence of free radical polymerization at a pressure of 200 bar in the presence of aromatic xanthates.....	115
III.1.4. Ethylene homopolymerization at 80°C and 80 bar.....	117
III.1.5. Origin of new side-products from cross-termination.....	119
III.2. RAFT copolymerization of ethylene in the presence of vinyl acetate: Synthesis of EVA copolymers.....	122
III.3. Conclusion on the use of xanthates for ethylene RAFT polymerization	123
IV. RAFT polymerization of ethylene with <i>N</i>-aryl carbamates.....	125
IV.1. Ethylene homopolymerization in the presence of 3,5-dimethyl-1H-pyrazole- 1-carbodithioate (4).....	125
IV.2. Ethylene homopolymerization in the presence of <i>N</i> -methylphenyl (3) and switchable <i>N</i> -methylpyridyl (5-7) dithiocarbamates	126
IV.2.1. Kinetics of the polymerizations	126
IV.2.2. Chain-ends analysis.....	128
V. Conclusion	132
VI. Experimental section	134
VII. References	138

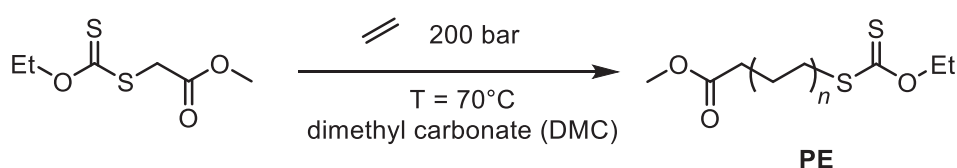
I. Introduction

The work performed during this thesis is focused on the synthesis of polar-apolar diblock copolymers (PE-*b*-PX copolymers) by a RAFT process. This is ultimately achieved through the controlled growth of both blocks through radical polymerization. This is generally easily achieved for the polar segment thanks to well-established and mature RDRP processes,^[1,2] but the control over the PE segment is more problematic. Among the available RDRP techniques, and as mentioned in Chapter I, RAFT has been selected in this work. To obtain well-defined PE-*b*-PX copolymers, RAFT homopolymerization of ethylene must thus be mastered beforehand. As such, this chapter will briefly recall the pre-existing work done by Cédric Dommanget during his PhD work in the C2P2 group on the controlled radical polymerization of ethylene using *O*-alkyl xanthates as chain transfer agent (CTA). The strategy adopted to suppress the side-fragmentation observed in these first systems will be presented and the RAFT homopolymerization of ethylene with aromatic xanthates and aromatic dithiocarbamates will be studied. The CTAs presented in this study were all selected according to their potential ability to control the synthesis of both the PE and the polar block.

II. Context of ethylene RAFT homopolymerization

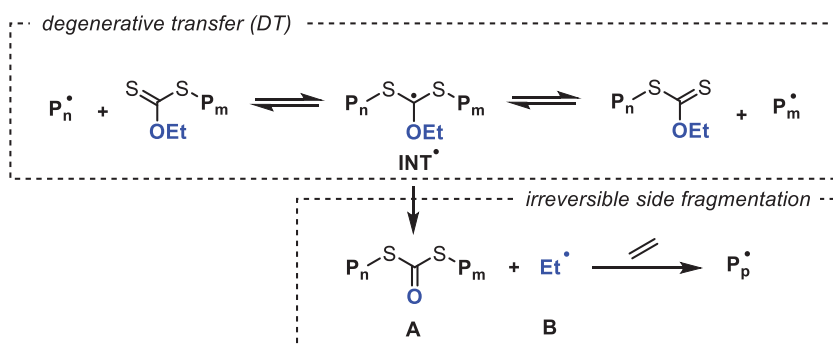
II.1. RAFT polymerization of ethylene with *O*-ethyl xanthate

The radical polymerization of ethylene was controlled for the first time by our group in 2014 through RAFT polymerization.^[3,4] Cédric Dommanget showed that *O*-ethyl xanthate could provide control over the molar mass. The polymerization was performed at 70 °C, under an ethylene pressure of 200 bar and using dimethyl carbonate (DMC) as a low transferring organic solvent (**Scheme 1**). The polyethylene (PE) thus obtained has low dispersity values ($\mathcal{D} < 2$) and its molar mass increases linearly with conversion up to 2 000 g mol⁻¹.



Scheme 1. RAFT polymerization of ethylene with *O*-ethyl xanthate as CTA.^[3]

As previously stated in Chapter I, this system features – along with chain growth control – a side-fragmentation reaction that competes with the usual fragmentation within the degenerative transfer (DT) equilibrium (**Scheme 2**). The intermediate radical **INT**[•] can undergo side-fragmentation giving an ethyl radical **B** and the polymeric species **A**, that consists of two PE chains linked together by a dithiocarbonate SC(=O)S bridge. As the C=O double bond is much less reactive towards radical addition than a C=S double bond, species **A** accumulates in the polymerization mixture as dead chains. While this reaction is already known and used in organic chemistry,^[5] it was only anticipated by a single study based on *ab initio* molecular orbital calculations of RAFT polymerization of VAc.^[6] In the case of PVAc, this side-fragmentation has however never been experimentally observed. It is observed in the case of PE because the low stability of the propagating PE[•] promotes side-fragmentation as a competitive reaction to DT.



Scheme 2. Irreversible side-fragmentation with *O*-ethyl xanthate

The extent of this side-fragmentation can be easily quantified by $^1\text{H-NMR}$ (**Figure 1**). The loss of the ethoxy group protons (**a** and **b**) is concomitant with the loss of the protons in α position to the xanthate moiety (**c**) and proportional to the emergence of the protons in α position to the dithiocarbonate bridge (**z**). The relative integration between protons **a** and **z** gives access to the percentage of dead chains that accumulate during the polymerization.

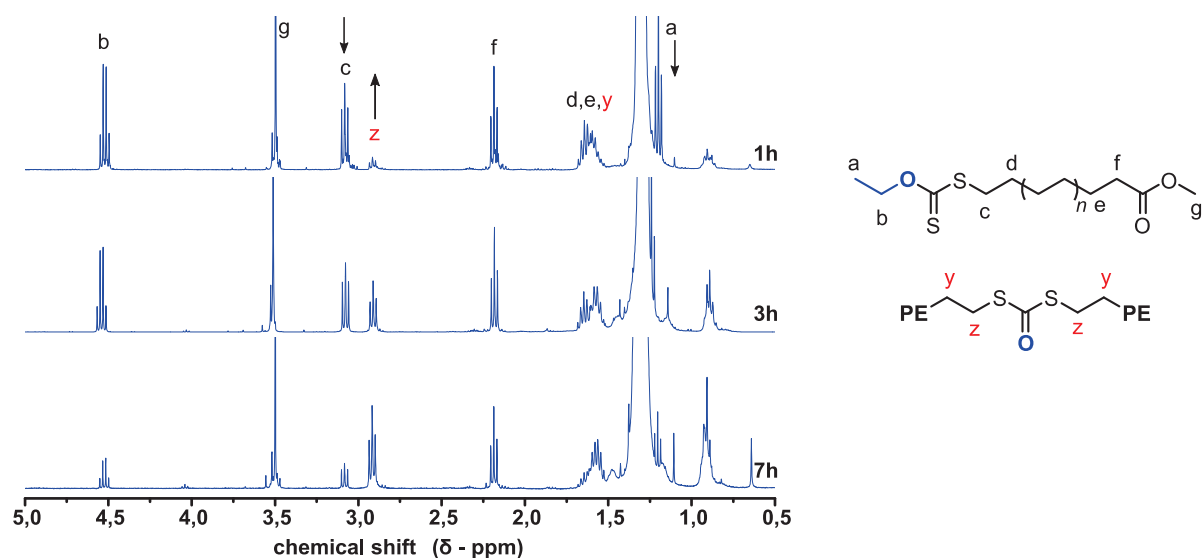


Figure 1. $^1\text{H-NMR}$ spectra of PE obtained by RAFT polymerization in the presence of *O*-ethyl xanthate (70 °C, 200 bar, DMC: 50 mL), AIBN: 50 mg), CTA:AIBN molar ratio = 10:1).^[4]

This side-fragmentation is also observed during the synthesis of ethylene-vinyl acetate (EVA) statistical copolymers with different VAc contents, but not in the case of VAc homopolymerization (**Figure 2**). This confirms that side-fragmentation only occurs in the presence of PE•:

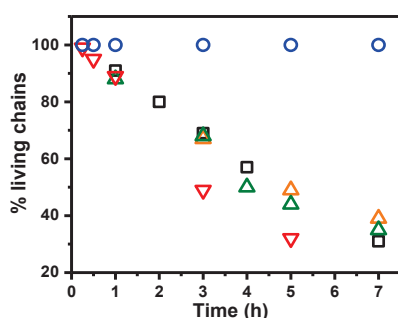


Figure 2. Loss of living chains with polymerization time in the presence of *O*-ethyl xanthate. PE homopolymer (□), EVA 2% (△), EVA 10% (▽), EVA 80% (∇), PVAc homopolymer (○).^[4]

Side-fragmentation was hypothesized to be favored by the similar stability between the PE• leaving group and the ethyl radical released if Z = OEt. Indeed, considering the penultimate unit effect^[7] to be minimal for PE, the stability of $\text{CH}_3\text{-CH}_2\cdot$ and $\text{PE-CH}_2\text{-CH}_2\cdot$ radicals can be considered equivalent. To confirm this theory, *O*-methyl xanthate was investigated as CTA for the RAFT polymerization of ethylene. The lower stability of the $\cdot\text{CH}_3$ radical was expected to reduce the extent of side-fragmentation observed with *O*-ethyl xanthate.

II.2. RAFT polymerization of ethylene with *O*-methyl xanthate

The control over the polymerization of ethylene is similar using either *O*-methyl or *O*-ethyl xanthate CTAs (**Figure 3a** – \bar{D} slightly higher with $Z = \text{OMe}$). As anticipated, the side-fragmentation is effectively reduced with *O*-methyl xanthate (**Figure 3b** – twice the amount of living chains remains after 7 hours of polymerization).

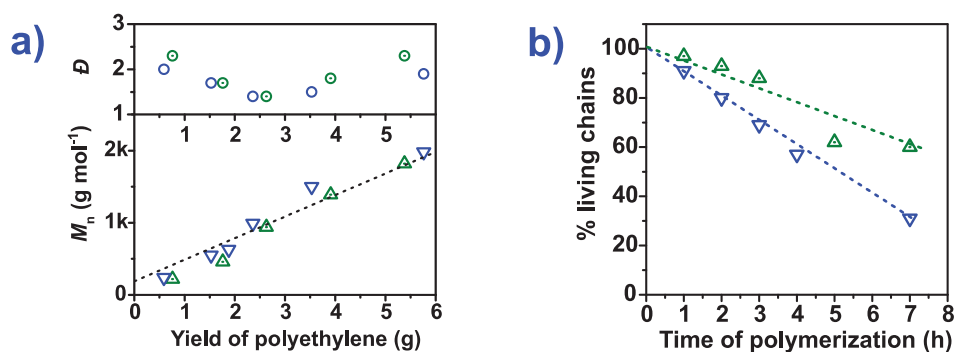


Figure 3. Evolution of M_n and \bar{D} values vs. PE yield (a) and extent of living chains loss during polymerization (b) with $Z = \text{OMe}$ (Δ, \circ) and $Z = \text{OEt}$ (∇, \circ).^[4]

In this context, it is worth mentioning that You *et al*^[8] did not report or mention the occurrence of side-fragmentation when they used *O*-methyl xanthate for the homopolymerization or copolymerization of ethylene with polar monomers (VAc, NVP). Nevertheless, the straightforward strategy of reducing the side-fragmentation reaction by choosing a Z group that releases a less stable radical is promising. It was anticipated that the use of a CTA with Z -group even less prone to release a radical than $Z = \text{OMe}$ could, in principle, completely suppress the side-fragmentation and offer the most efficient system to control ethylene to date.

II.3. Z -groups with aromatic substituents to suppress side-fragmentation.

II.3.1. Xanthates with aromatic substituents

The absence of literature on the RAFT polymerization of ethylene has led us to base our reasoning on vinyl acetate, another less activated monomer (LAM). Barner-Kowollik and coworkers^[9] studied the ability of eight xanthates ($Z = \text{OZ}'$) to control the polymerization of VAc (**Figure 4**). As the propagating radical resulting from VAc is highly reactive (*i.e.* not stable), the resulting intermediate radical will be relatively stable with respect to fragmentation. Efficient control on VAc will only be obtained when the radical intermediate is destabilized (*i.e.* is a xanthate/dithiocarbamate), which is achieved by increasing the electron density at the radical center.

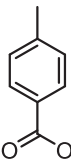
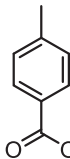
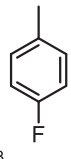
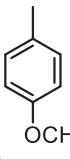
	A	B	C	D	E	F	G	H
								
δ (ppm)	4.83	4.83	4.62	4.02	3.89	3.89	3.87	3.80

Figure 4. Structures of Z' substituents A-H in xanthates Z'OC(S)SCH₂COOMe used for the polymerization of VAc^[9] and associated chemical shifts of the methylene protons.

The ¹H-NMR chemical shifts of the methylene protons adjacent to the sulfur in CTAs **A-H** were measured. When going from **A** to **H**, the chemical shift steadily decreases from 4.83 to 3.80 ppm, which can be correlated to the electron-withdrawing ability of the Z' groups. As expected, xanthates substituted with the more electron-withdrawing phenyl groups have a lower electron density at the methylene group. Consequently, the electron density at the carbon that will be the radical center after addition is lower. Accordingly, those xanthates afford radical intermediates that are more stable than their alkyl counterpart is. It was experimentally found that xanthates **A-C** are not suitable for the control of VAc polymerization. This was attributed to the high stability of the intermediate radical when using **A-C**, not allowing for effective fragmentation, making the main equilibrium too slow to compete with the fast VAc radical propagation. Xanthates **D-G** provided good molar mass control and low dispersity values, with more or less pronounced retardation. Xanthate **H** completely inhibited the polymerization. This inhibition was rationalized with high-level *ab initio* calculations^[6] and attributed to preferential side-fragmentation when Z' = *tert*-Bu, releasing a very stable *tert*-butyl radical. Following those results, it appears that only xanthate **D** would be suitable for the control of ethylene. Xanthates **G-H** would result in an even more pronounced side-fragmentation, whereas **A-C** would likely fail to provide control over the polymerization as it was the case with VAc.

In the case of ethylene, xanthate **D** features a second advantage. The phenyl radical that would be released upon side-fragmentation is unstable. The *O*-aryl substituent of the xanthate would therefore be even less prone to undergo side-fragmentation. The low stability of the phenyl radical can be rationalized with simple orbital considerations. Exemplified with Z=OPh, the homolytic C-O bond cleavage occurring during side-fragmentation would result in a lone electron located in a σ orbital in the plane (*xy*) of the aromatic ring (**Figure 5**). The electrons in the π orbitals (represented as p_z orbitals) of the aromatic ring are located in the (*xz*) and (*yz*) planes. The lone electron therefore cannot participate in resonance forms with the electrons in the π orbitals as they are not in the same plane.

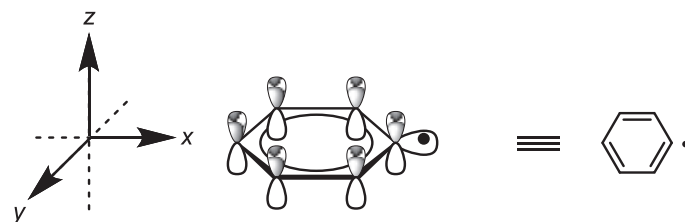


Figure 5. Illustration of a phenyl radical resulting from side-fragmentation of a xanthate when $Z = \text{OPh}$.

Accordingly, we selected two aromatic xanthates (*O*-aryl xanthate) as potential candidates to suppress the side-fragmentation reaction, the methyl phenoxycarbonothioylsulfanyl acetate and the methyl (4-methoxyphenoxy)carbonothioylsulfanyl acetate (**1** and **2**, respectively, in **Figure 6**). Those xanthates will also be referred to as phenoxy xanthate and phenoxymethoxy xanthate, respectively.

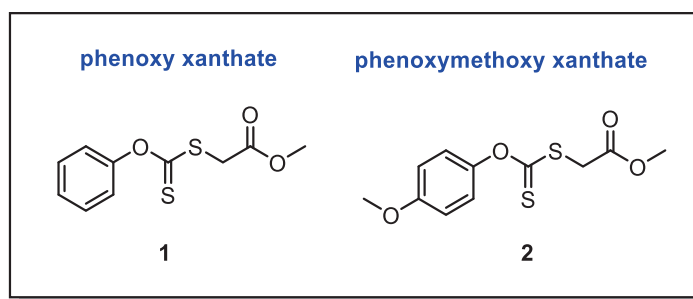


Figure 6. Structures of the *O*-aryl xanthate selected as candidates to suppress the side-fragmentation reaction observed in RAFT polymerization of ethylene.

II.3.2. *N,N*-dithiocarbamates with aromatic substituents.

N,N-dithiocarbamates are also effective at controlling the polymerization of vinyl acetate.^[10,11] Cédric Dommanget thus investigated a *N,N*-methylphenyldithiocarbamate (**3**, **Figure 7**) for the RAFT polymerization of ethylene. This work is not published but is described in his PhD dissertation.^[4]

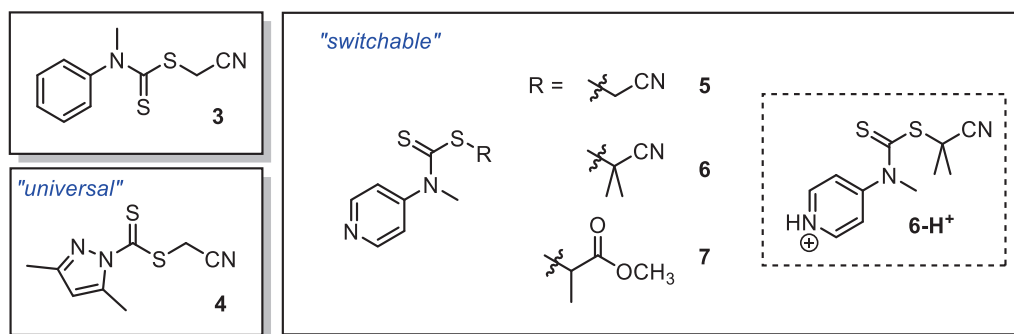


Figure 7. Structures of dithiocarbamates investigated for the RAFT polymerization of ethylene.

Based on the same reasoning as with xanthates, the presence of the aromatic ring on the Z group in carbamate **3** should stabilize the intermediate radical and restrain side-fragmentation. Preliminary results showed that **3** provokes retardation of polymerization (about 2.5 times slower compared to FRP or when *O*-ethyl xanthate is used) and the control over M_n is poor. Dispersity values are however substantially lower than when a xanthate is used ($\mathcal{D} < 1.9$).

The molar masses values are systematically higher than the theoretical ones but tend to get closer as the yield of PE increases (*i.e.* as the conversion of ethylene goes up). This behavior is rather typical for RAFT agents with a low chain transfer constant.^[12] The low chain transfer constant means that the RAFT agent is consumed slowly during the polymerization. This was confirmed with $^1\text{H-NMR}$ measurements that showed 35% of remaining CTA even after 7h of polymerization at 70°C. The most important feature of CTA **3** is that no side-fragmentation (either between the N-Ph or N-Me bonds) was detected by $^1\text{H-NMR}$.

Those results show that dithiocarbamates are promising RAFT agents for ethylene polymerization. We elected to pursue the study of compound **3** for the control of ethylene *via* RAFT polymerization. Compound **4** has been described as a "universal" CTA that controls both MAMs and LAMs^[13] and was also investigated. Switchable carbamates^[14] were also investigated with a systematic variation in the nature of the R group (Compounds **5**, **6**, **7**). Throughout this manuscript, compounds with one aromatic ring in the Z group (either phenyl or pyridinyl, **3**, **4**, **5**, **6**, **7**) will be referred to as *N*-aryl carbamate.

III. RAFT polymerization of ethylene with *O*-aryl xanthates

The phenoxy xanthate (**1**, **Figure 6**) and the phenoxy methoxy xanthate (**2**, **Figure 6**) were investigated as RAFT agent to suppress the side-fragmentation observed with *O*-alkyl xanthates. Those two xanthates are not commercially available and therefore have been synthesized in-house prior to their use. The protocols of their synthesis are described in the experimental section at the end of this chapter. Their ability to control ethylene at different pressures and temperatures will be assessed, with a special focus on whether side-fragmentation is suppressed or not. The synthesis of statistical ethylene-vinyl acetate copolymers using those xanthates will also be described.

III.1. RAFT homopolymerization of ethylene

III.1.1. Polymerization at 70 °C and 200 bar

Polymerizations were conducted at 70 °C and 200 bar of ethylene pressure using 2,2'-azobis(2-methylpropionitrile (AIBN (50 mg, 6.09 mmol L⁻¹)) as radical initiator in DMC (50 mL). These conditions are consistent with Cédric Dommanget's work using *O*-alkyl xanthates. However, using a ratio [CTA]:[AIBN] of 10:1, we observed a significant retardation with both aromatic xanthates, hence a [CTA]:[AIBN] ratio of 3:1 was preferred for the course of this study. **Table 1** presents the results of the polymerizations using either **1** or **2** as CTA (18.3 mmol L⁻¹), the yields obtained, the theoretical and experimental molar masses ($M_{n,theo}$ and M_n respectively), the dispersity values (\mathcal{D}) and the chain-end fidelity (f). f is calculated using the following method: the integration of the CH₂ protons at the α extremity of the chain (**i** in **Figure 10**, $\delta = 2.13$ ppm) is set at a value of 2 and the resulting integral value of the CH₂ protons at the ω extremity (i.e. adjacent to the xanthate, **l** in **Figure 10**, $\delta = 3.10$ ppm) is divided by 2. f thus corresponds to the percentage of PE chains functionalized by a xanthate chain-end, *i.e.* chain-end fidelity. It should be stated that f does not take into consideration chains initiated with an AIBN moiety, as it is not possible to properly integrate the corresponding characteristic protons. As a result, f can sometimes be slightly overestimated ($f > 100\%$).

Table 1. Homopolymerization of ethylene with CTAs 1 and 2 at 70 °C and 200 bar.

Entry	CTA	Time (h)	Yield (g)	$M_{n,theo}^a$ (g mol ⁻¹)	M_n^b (g mol ⁻¹)	\bar{D}^b	f^c (%)
1	1	1	0.14	400	340	1.26	110
2	1	2	0.25	510	490	1.23	100
3	1	4	0.35	620	700	1.24	95
4	1	5	0.38	650	1 000	1.21	90
5	1	6	0.82	1 130	1 600	1.98	70
6	2	1	0.18	470	440	1.34	110
7	2	2	0.32	620	550	1.34	105
8	2	3	0.40	700	1 130	1.33	95
9	2	5	1.14	1 520	1 420	2.95	85
10	FRP	3	1.94	-	13 260	2.15	-

Polymerization conditions: T = 70 °C, P = 200 bar, DMC: 50 mL, AIBN: 50 mg, [CTA]:[AIBN] = 3.

^a: Determined using a derived form of equation 3, chapter I: $M_{n,theo} = \text{Yield(g)} / \text{CTA(mol)} + MW_{CTA}(\text{g mol}^{-1})$.

^b: Determined by HT-SEC using a conventional PE standards calibration.

^c: Determined by ¹H-NMR in TCE/C₆D₆ (2/1 v/v) at 363 K.

Polymerizations using either CTAs **1** or **2** feature a substantial decrease in polymer yield (*i.e.* polymerization rate) compared to free radical polymerization (FRP) (**Figure 8a**) and polymerization proceeds slightly faster with **2** than with **1**. This retardation is very likely to stem from the expected strong retardation of the intermediate radical in RAFT equilibrium by aromatic Z groups. The molar masses using either **1** or **2** increase linearly with conversion and stay close to the theoretical values. Dispersity values for the lower yields (< 0.7 g) are remarkably narrow ($1.21 < \bar{D} < 1.34$), which is a feature of a controlled polymerization (**Figure 8b**). However, for yields greater than 0.7 g (and $M_n > \sim 1\,000 \text{ g mol}^{-1}$), \bar{D} increases dramatically for both CTAs (with **1**: $M_n = 1\,600 \text{ g mol}^{-1}$ $\bar{D} = 1.98$, with **2**: $M_n = 1\,420 \text{ g mol}^{-1}$ $\bar{D} = 2.95$). This indeed corresponds to the formation of a second molar-mass distribution (MMD) detected by HT-SEC for the last polymerization times with both CTAs.

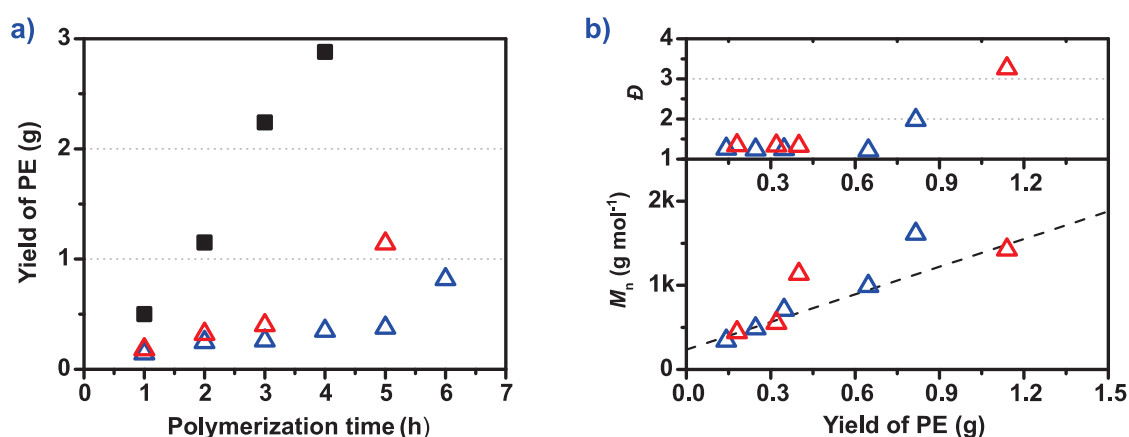
**Figure 8. a) Yield of PE vs polymerization time; b) Evolution of M_n and \bar{D} vs yield of PE. CTA 1 (Δ), CTA 2 (Δ), FRP (\blacksquare). P = 200 bar, T = 70 °C.**

Figure 9 exemplarily shows the MMD of PE obtained with **1** at different polymerization times. For the last polymerization time (6 h), the second MMD is detected as a shoulder towards higher molar masses. It appears to overlap with a MMD of a PE obtained by free radical polymerization,

which suggests that for $M_n > 1\,000\text{ g mol}^{-1}$, the polymerization does not proceed in a controlled fashion anymore and free radical polymerization mechanism takes over the RAFT process. Interestingly, the last points in **Figure 8a** (6 hours for CTA **1** and 5 hours for CTA **2**) feature a substantially higher yield than what is expected from the trend of their respective previous points. This corroborates the assumption that, for the highest polymerization times (*i.e.* highest yields and highest M_n), a free radical polymerization takes over the RAFT process, the former being sensibly faster. The formation of this second MMD will be discussed more in detail later in this manuscript. Considering only the MMD and \mathcal{D} values, those two CTAs appear to be very effective at controlling the polymerization of ethylene at the beginning of the polymerization (*i.e.* for low PE yields and low M_n), but the control is lost at high conversion with the emergence of the second MMD. To investigate whether the side-fragmentation reaction is suppressed or not, $^1\text{H-NMR}$ analyses were carried out on the PE thus obtained.

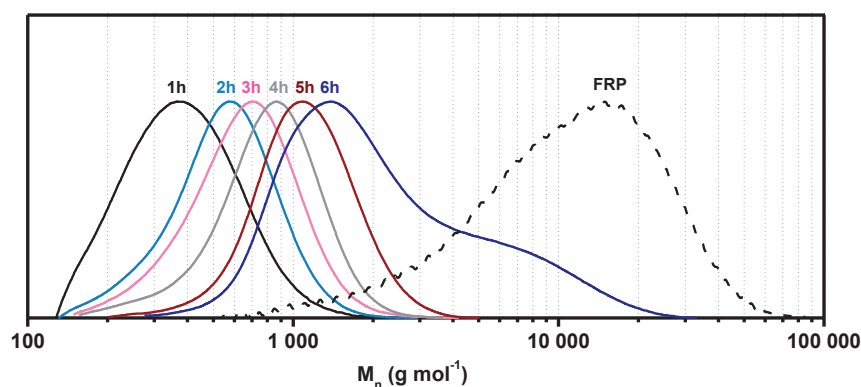


Figure 9. Evolution of MMD of PE obtained after different polymerization times with CTA **1** at 70°C and 200 bar. The dotted line corresponds to a PE obtained by FRP.

Figure 10a shows an exemplary $^1\text{H-NMR}$ spectrum of a PE obtained with *O*-ethyl xanthate (by Cédric Dommanget during his PhD work) at 70 °C after 3 hours of polymerization, featuring the side-fragmentation product (characteristic protons **z**). **Figure 10b** shows an exemplary $^1\text{H-NMR}$ spectrum of a PE obtained with CTA **2** after 5 hours of polymerization (entry 9 of Table 2). Upon side-fragmentation, PE derived from both *O*-ethyl xanthate and CTA **2** (or CTA **1**), would afford the same product of two PE chains connected by one $\text{SC}(=\text{O})\text{S}$ bridge, with identical chain ends. However, PE obtained with **2** shows no sign of the characteristic protons **z**, indicating that side-fragmentation does not occur with CTA **2**. This observation applies for any PE synthesized with **1** or **2**. As it was anticipated, the aromatic substituent on the xanthate has indeed suppressed the side-fragmentation reaction. However, several new signals (labelled with *) in the region 2.3-2.8 ppm are detected, of which a zoom is presented in **Figure 10c**. Our first hypothesis was that the emergence of the second MMD detected by HT-SEC and those new $^1\text{H-NMR}$ signals were related. However, further experiments at higher temperature, lower pressure and the synthesis of EVAs have ruled out this possibility (*vide infra*). The $^1\text{H-NMR}$ spectra also reveal the characteristic

signals of PE chains resulting from transfer to solvent, labelled with o in **Figure 10**, which was already observed in the presence of *O*-alkyl xanthates.

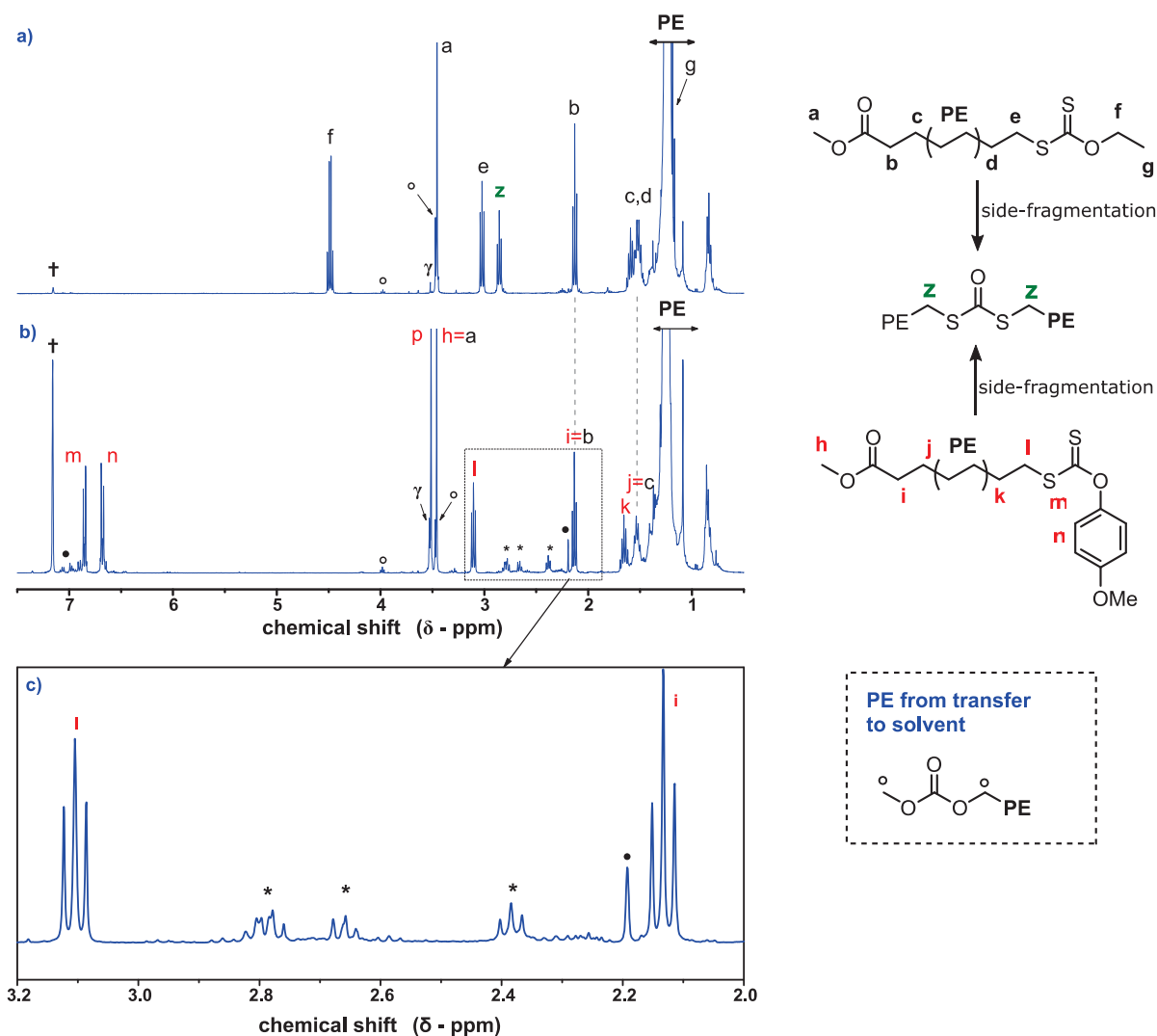


Figure 10. ¹H-NMR spectra of a PE obtained with *O*-ethyl xanthate after 3 hours of polymerization (a), with CTA 2 after 5 hours of polymerization (b) and zoom on the 2.0-3.2 ppm region (c). P = 200 bar, T = 70 °C. †: NMR residual solvent benzene, •: collecting solvent toluene, γ: polymerization solvent DMC, *: new unidentified signals.

As a brief anticipation of part II.1.5, we believe those signals (*) correspond to new products, resulting from cross-termination reactions happening on the intermediate radical. As mentioned earlier, the stabilization of the intermediate radical is expected to be much greater with *O*-aryl xanthates than with *O*-alkyl xanthates, which is experimentally traduced by a strong retardation of the polymerization. It is our belief that the lifetime of the intermediate radical is long enough so that it can undergo cross-termination reactions (*vide infra*). Such cross-termination products, of which a general example is given in **Figure 11**, give simulated chemical shifts within the 2.3-2.8 ppm region, which corresponds to what is experimentally observed. The formation of such cross-termination products will be discussed more in details later in this manuscript.

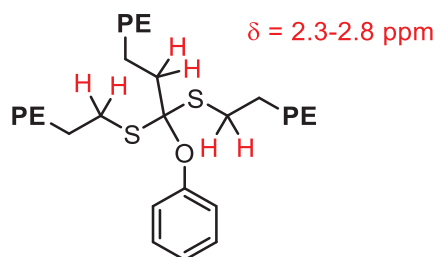


Figure 11. General structure of a potential cross-termination product obtained with CTA 1.

The intensity of the CH₂ protons at the ω chain-end gradually decreases as the polymerization time increases, while the intensity of the protons corresponding to the cross-termination side-products gradually increase (**Figure 12**), indicating an accumulation of side-products, detrimental to chain-end fidelity. This also hints that chain-end degradation happens exclusively at the ω chain-end of the polymer and is therefore influenced by the nature of the Z-group.

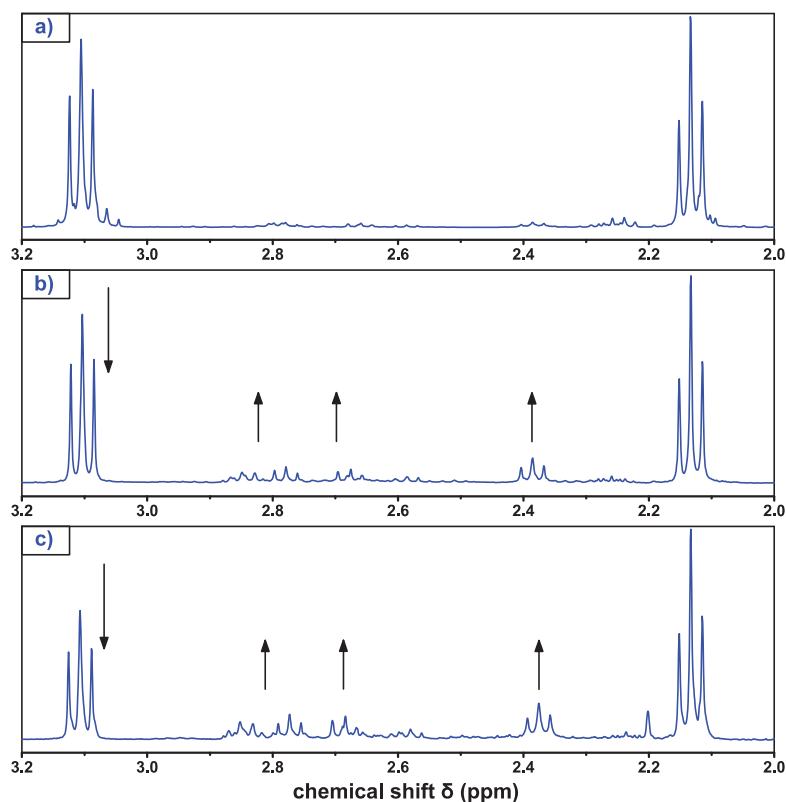
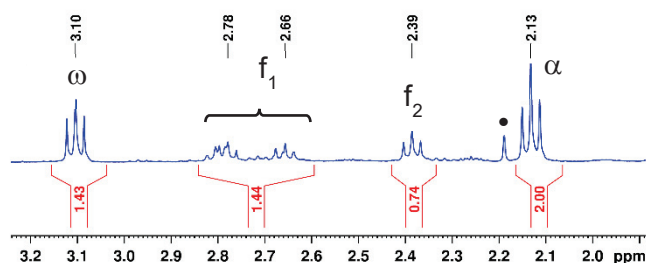


Figure 12. Zoomed ¹H-NMR spectra on the 2.0-3.2 ppm region and accumulation of side-products during ethylene homopolymerization with 1 at different polymerization time: a) 1h, b) 4h, c) 6h. P = 200 bar, T = 70 °C.

From these ¹H-NMR spectra, one can quantify the amount of side-products generated during the polymerization. The value Ξ was defined to quantify those side-products (**Equation 1**). Ξ is calculated by dividing the sum of the integral values of the side-products (f₁ and f₂ regions, δ = 2.6-2.85 and δ = 2.39 ppm respectively) by the sum of integrals of ω, f₁, f₂ and α (**Figure 13**), where ω and α corresponds to the CH₂ protons at each extremity of the polymer chain. This value can be regarded as the amount of side-products resulting from xanthate degradation compared to the

total amount of xanthate in the polymerization medium. It has no physical meaning but it gives an idea on how much and how fast the products accumulate during the polymerization. The Ψ values obtained at 70 °C and 200 bar of ethylene pressure for CTAs 1 and 2 are compiled in **Table 2**.



$$\Psi = \frac{\text{Int}(f_1 + f_2)}{\text{Int}(\omega + f_1 + f_2 + \alpha)}$$

Equation 1. Calculation of Ψ .

Figure 13. Chemical shifts of integrals used for the calculation of Ψ . (•) collecting solvent toluene.

Table 2. Chain-end fidelity and quantification of side-products accumulation during ethylene homopolymerization with CTAs 1 and 2 at 70 °C and 200 bar.

Entry	CTA	Time (h)	Yield (g)	f^a (%)	Ψ^a (%)
1	1	1	0.14	110	10
2	1	2	0.25	100	16
3	1	4	0.35	95	22
4	1	5	0.38	90	23
5	1	6	0.82	70	35
6	2	1	0.18	110	8
7	2	2	0.32	105	13
8	2	3	0.40	95	24
9	2	5	1.14	85	31

Polymerization conditions: T = 80 °C, P = 200 bar, DMC: 50 mL, AIBN: 50 mg, [CTA]:[AIBN] = 3.

^a: Determined by ¹H-NMR in TCE/C₆D₆ (2/1 v/v) at 363K.

The functionality of the polymers slowly decreases as the polymerization yields increase. In the meantime, side-products appear to accumulate at roughly the same rate in the reactor. These results hint that chain-end degradation of the polymer and the formation of those side products must be closely related. Further discussion on this matter will be provided later in the manuscript. As the yield of PE obtained with *O*-aryl xanthates is drastically lower than with *O*-alkyl xanthates, experiments were carried out at a temperature of 80 °C in order to increase the polymer yield, under otherwise identical conditions.

III.1.2. Polymerization at 80 °C and 200 bar

Polymerizations were conducted at 80 °C and 200 bar of ethylene pressure using AIBN (50 mg, 6.09 mmol L⁻¹) in DMC (50 mL). As for the polymerizations at 70 °C, a CTA:AIBN ratio of 3:1 (CTA: 18.3 mmol L⁻¹) was adopted. **Table 3** presents the results of the polymerizations using CTAs 1 or 2, as well as those of FRP of ethylene at 80 °C as reference.

Table 3. Ethylene homopolymerization at 80 °C and 200 bar with CTA 1 and CTA 2

Entry	CTA	Time (h)	Yield (g)	$M_{n,theo}^a$ (g mol ⁻¹)	M_n^b (g mol ⁻¹)	\bar{D}^b	f^c (%)
11	1	1	0.40	680	690	1.22	100
12	1	2	0.59	890	1 020	1.25	85
13	1	3	1.29	1 650	1 420	2.73	80
14	1	4	1.65	2 040	2 300	2.21	60
15	1	5	2.09	2 530	2 860	2.31	40
16	1	6	2.43	2 900	2 860	2.48	40
17	2	1	0.35	840	710	1.43	105
18	2	2	0.93	1 470	1 550	1.81	95
19	2	3	2.13	2 600	2 950	2.20	65
20	2	6	2.99	3 550	3 230	2.38	65
21	FRP	3	4.31	-	9 700	3.38	-

Polymerization conditions: T = 80 °C, P = 200 bar, DMC: 50 mL, AIBN: 50 mg, [CTA]:[AIBN] = 3.

^a: Determined using a derived form of equation 3, chapter I: $M_{n,theo} = \text{Yield(g)} / \text{CTA(mol)} + MW_{CTA}(\text{g mol}^{-1})$.

^b: Determined by HT-SEC using a conventional PE standards calibration.

^c: Determined by ¹H-NMR in TCE/C₆D₆ (2/1 v/v) at 363K.

As expected, the yields are significantly higher at 80 °C than at 70 °C (**Figure 14a**). The polymerization appears to proceed slightly faster with CTA 2 than with CTA 1, as already observed at 70 °C. Molar masses increase again linearly with conversion and are remarkably close to the expected values. \bar{D} values are low for the lowest polymerization times and yields ($\bar{D} < 1.4$ for yields < 1 g and $M_n < 1\,000$ g mol⁻¹, **Figure 14b**) and greatly increase for yields > 1 g and $M_n > 1000$ g mol⁻¹.

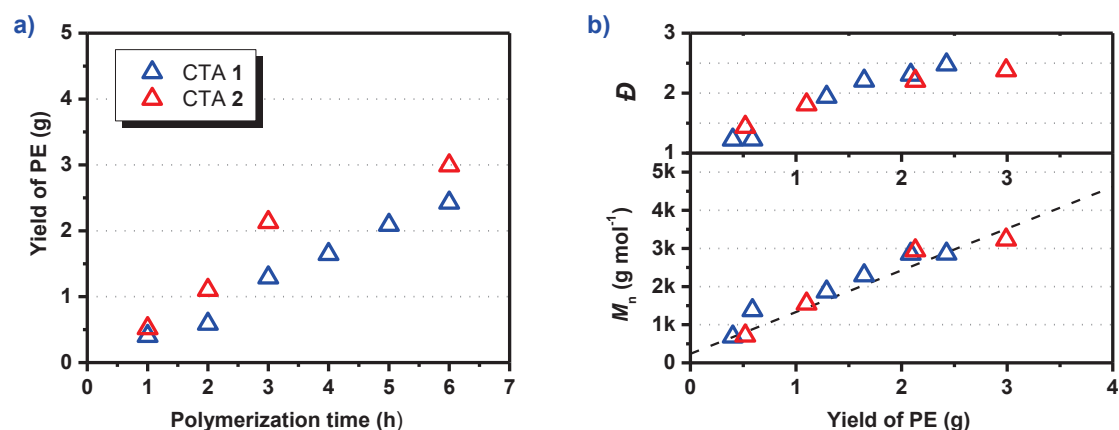


Figure 14. Polymerization kinetics and evolution of M_n and \bar{D} versus yield of PE (T = 80°C, P = 200 bar) obtained with CTA 1 (Δ) and CTA 2 (Δ). The dotted line corresponds to theoretical M_n values.

All effects described for 70 °C are also observed at 80 °C, with the difference that the emergence of the second MMD (for yields > 1 g and $M_n > 1000$ g mol⁻¹) appears at shorter polymerization times. For the higher polymerization times, the shoulder previously observed at 70 °C clearly becomes a distinct second MMD at 80°C that overlaps with the MMD of a PE obtained by FRP under the same pressure and temperature conditions (**Figure 15a** with CTA 1 and **15b** with CTA 2). The second MMD stays at similar molar masses and only increases in intensity, while the shift of MMD of the original PE macroCTA completely stops once the second distribution appears. This strongly suggests that participation of the RAFT agent is not involved for the

formation of this second population. Intuitively, the emergence of FRP would be the direct result of the loss of the xanthate moiety. This is not the case since xanthate chain-ends are still detected by $^1\text{H-NMR}$ even after FRP takes over RAFT (the xanthate chain-end is detected in **Figure 16a**, the corresponding PE is the green trace (after 3 hours) in **Figure 15a**).

As a brief anticipation, this has been attributed to a segregation of the polymer particles that result in the xanthate chain-ends being inaccessible to growing radicals (*vide infra*, part II.1.3).

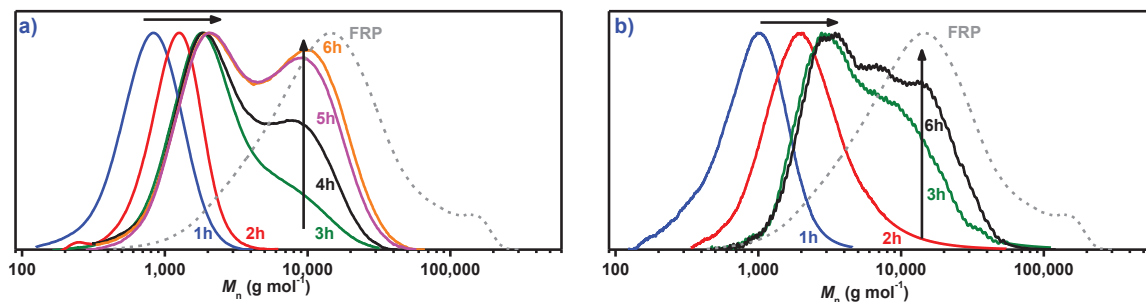


Figure 15. MMD evolutions for PE obtained with CTA 1 (a) and CTA 2 (b) after different polymerization times at 80 °C and 200 bar. The dotted line corresponds to a PE obtained by FRP.

Figure 16 shows an exemplary $^1\text{H-NMR}$ spectrum of PE obtained after 3 hours of polymerization at 80 °C with CTA 1 ((a), corresponding to entry 13 in Table 3) and after 2 hours of polymerization with CTA 2 ((b), corresponding to entry 18 in Table 3).

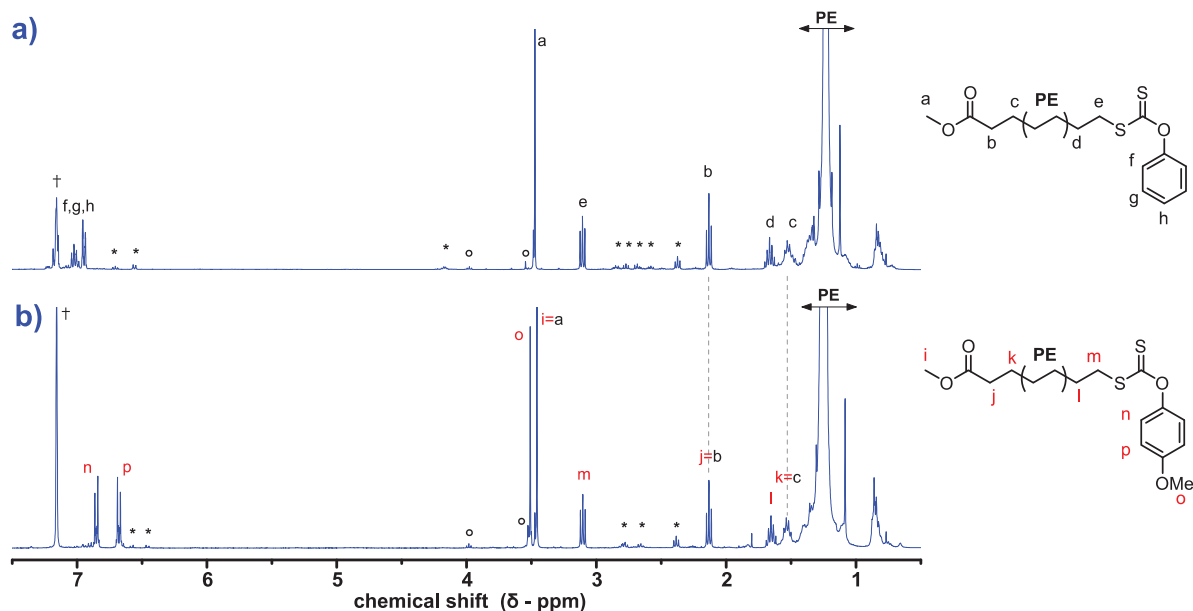


Figure 16. $^1\text{H-NMR}$ spectra for PE obtained after 3 hours of polymerization at 80 °C with CTA 1 (a) and after 2 hours of polymerization at 80 °C with CTA 2 (b). P = 200 bar.

The product of side-fragmentation is again not detected, confirming the absence of side-fragmentation with *O*-aryl xanthates at both 70 and 80 °C. The same new signals in the region 2.3-2.8 ppm previously detected at 70 °C are present for CTA 2. CTA 1 features both identical signals

(e.g. $\delta = 2.39$ ppm) and a few new signals (e.g. $\delta = 4.18$, $\delta = 6.57$ ppm). CTA **1** and **2** have the same structure at the α chain-end, but different structures at the ω chain-end, confirming that the *locus* of the side-reactions is at the ω chain-end. **Table 4** compiles the f and Ψ values for both CTAs at 80 °C. Graphic representations of the evolution of f and Ψ at both temperatures versus the yield of polyethylene for CTA **1** and CTA **2** are presented in **Figure 17**.

Table 4. Chain-end fidelity and quantification of side-products accumulation during ethylene homopolymerization with CTAs 1 and 2 at 80 °C and 200 bar.

Entry	CTA	Time (h)	Yield (g)	f^a (%)	Ψ^a (%)
11	1	1	0.40	100	16
12	1	2	0.59	85	26
13	1	3	1.29	80	38
14	1	4	1.65	60	47
15	1	5	2.09	40	52
16	1	6	2.43	40	49
17	2	1	0.35	105	18
18	2	2	0.93	95	23
19	2	3	2.13	65	39
20	2	6	2.99	65	60

Polymerizations performed at T = 80 °C and P = 200 bar

^a: Determined by ¹H-NMR in TCE/C₆D₆ (2/1 v/v) at 363K

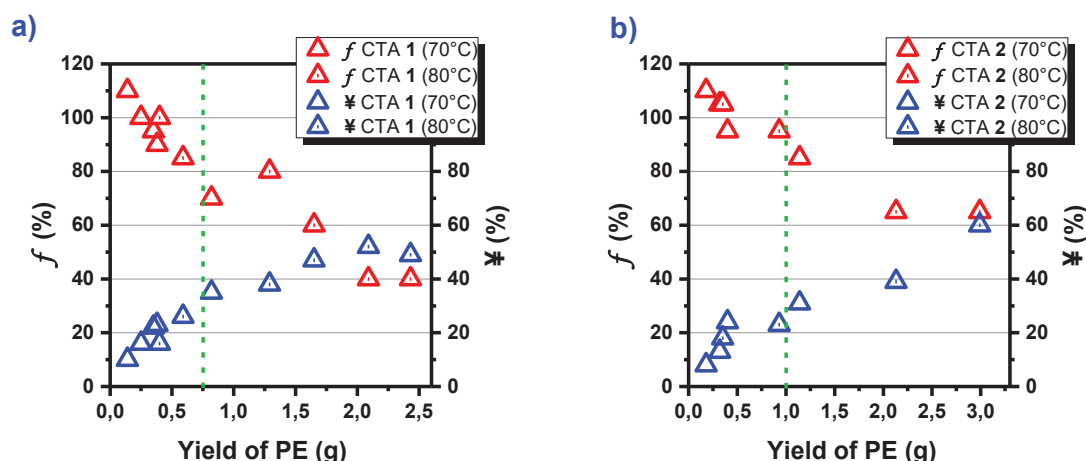


Figure 17. Evolution of chain-end fidelity (f (Δ , Δ)) and accumulation of side products (Ψ (Δ , Δ)) versus yield of PE with CTA **1 (a) CTA **2** (b) at 70 and 80 °C and P = 200 bar. The green dotted line corresponds to the emergence of the second MMD in SEC.**

Regardless of the temperature, the same trend is observed with both CTAs. Chain-end fidelity steadily decreases as the yield of PE increases, while the side-products accumulate at roughly the same speed. Chain-end fidelity appears to be lost slightly faster with **1** than with **2** ($f = 40$ % for yield > 2 g and $f = 65$ % for yield > 2 g respectively). Accordingly, **1** also features a slightly higher accumulation of side-products than **2** at comparable yields. As **1** and **2** have the same R-group but different Z-group, this implies that the nature of the Z group plays a role in the degradation mechanism. It is also confirmed that, although side-fragmentation is suppressed, another mechanism is happening with *O*-aryl xanthates that results in equivalent chain-end fidelity loss.

Surprisingly, the chain-end degradation appears to happen at more or less the same speed before and after the emergence of the second MMD (green dotted line in **Figure 17**). One would expect that chain-end degradation happens through the addition of a radical onto the xanthate moiety. As the xanthate chain-ends are inaccessible to radical after that point (traduced by the polymerization becoming uncontrolled), another mechanism might participate in this degradation.

Even though CTA **2** provides slightly lesser control on ethylene polymerization than **1** for the lowest yields ($\bar{D} \approx 1.3$ vs. $\bar{D} \approx 1.2$ respectively), it features the lowest chain-end fidelity loss accompanied with the slowest accumulation of side-products. Regardless of the emergence of FRP, **2** also appears to feature a slightly increase polymerization rate compared to **1**. Recalling that a higher polymerization rate is (partly) the consequence of a lower stabilization of the intermediate radical, it can be assumed that, the longer the lifetime of the intermediate radical, the more severe the loss of functionality and accumulation of side products. This supports our theory that the observed degradation of the xanthate chain-end and the accumulation of side-products stem from side-reactions happening with the intermediate radical (*vide infra*).

The apparition of a second MMD, the loss of chain-end fidelity and the accumulation of new side-products do not bode well for the synthesis of block copolymers with these CTAs. As a result, we endeavored to try to explain those phenomena and find a way to avoid them if possible. This will be treated in the following section.

As CTA **2** appears to provide the best results regarding polymerization rate and chain-end fidelity, it will be the preferred xanthate used for the rest of this study.

III.1.3. Rationalization of the emergence of free radical polymerization at a pressure of 200 bar in the presence of aromatic xanthates.

At 200 bar of ethylene pressure, it is known that the polymerization medium is monophasic and made of a supercritical mixture of ethylene and solvent (DMC in our case).^[15] From experimental observations and theoretical calculations, it was shown that a phase transition occurs around 100 bar for a solvent volume of 50 mL at a temperature range of 70-80 °C. Below 100 bar, the mixture is biphasic and consists of a bottom liquid DMC phase in which the radical initiator and ethylene are dissolved, and a top ethylene phase (gaseous or supercritical, depending on the pressure). The polymerization occurs in the liquid phase. Above 100 bar, the polymerization occurs in the single supercritical DMC/ethylene phase. These two phases (liquid and supercritical) have distinct solvent and polarity properties which can affect the polymerization yield.

Experiments were then conducted around the phase transition pressure under standard conditions using CTA 2 (DMC: 50 mL, AIBN: 50 mg, CTA:AIBN = 3:1, polymerization time = 4 hours and T = 80 °C) at 60, 80, 100 and 120 bar. The HT-SEC traces of the polymers obtained are presented in **Figure 18**.

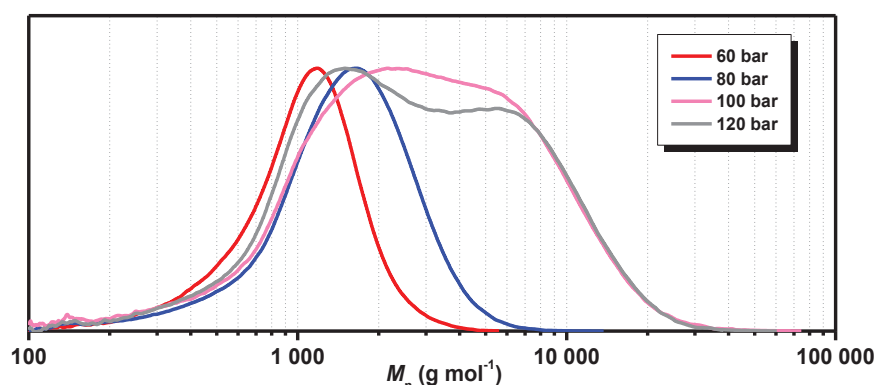


Figure 18. HT-SEC traces of polyethylene obtained after 4 hours of polymerization at different pressures using CTA 2. Polymerization conditions: T = 80 °C, DMC : 50 mL, AIBN : 50 mg, [CTA]:[AIBN] = 3:1. 60 bar: yield = 1.03 g, $M_n = 840 \text{ g mol}^{-1}$, $\mathcal{D} = 1.35$; 80 bar: yield = 1.37 g, $M_n = 1\,120 \text{ g mol}^{-1}$, $\mathcal{D} = 1.52$; 100 bar: yield = 1.50 g, $M_n = 1\,400 \text{ g mol}^{-1}$, $\mathcal{D} = 2.65$; 120 bar: yield = 1.72 g, $M_n = 1\,650 \text{ g mol}^{-1}$, $\mathcal{D} = 2.58$.

It is clear that when the polymerization takes place in the liquid phase (60 and 80 bar), no conventional radical polymerization occurs and the control is ensured by the expected RAFT process (narrow unimodal distribution) even with yields > 1 g. When the polymerization takes place in the supercritical ethylene/DMC mixture (100 and 120 bar), the second MMD corresponding to conventional radical polymerization appears, to the detriment of the RAFT process. It is then clear that the phase transition around 100 bar has a strong impact on the polymerization process. However, the explanation to this phenomenon goes beyond simple solubility considerations.

In order to get a better understanding of the physical behavior of the polymerization medium, one experiment was conducted during which the ethylene pressure was gradually increased. Other conditions were otherwise standard: CTA **2**, $T = 80^{\circ}\text{C}$, DMC: 50 mL, AIBN: 50 mg, $[\text{CTA}]:[\text{AIBN}] = 3:1$. For this experiment, a reactor equipped with a sapphire window (**Figure 19a,b**) replaced the standard stainless steel polymerization reactor (**Figure 19c**). This windowed reactor was not routinely used for polymerization as its use is not convenient.

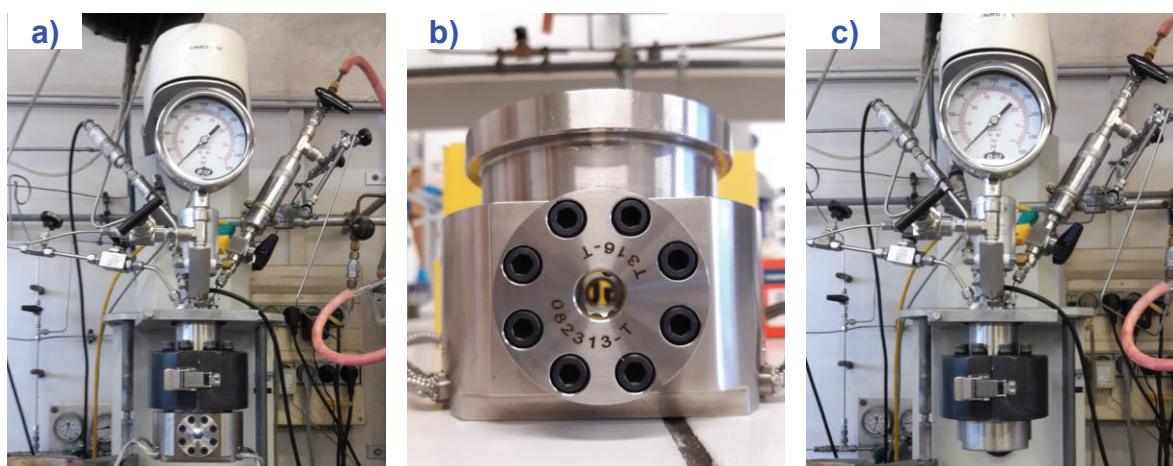


Figure 19. Polymerization setup using a reactor equipped with a sapphire window (a,b) and polymerization setup using the regular reactor (c).

It was visually observed that, at the pressure range of 20-80 bar, the polymerization mixture is a stable dispersion of free-flowing white particles. The particles do not appear to stick to each other or to the reactor walls/windows. At the range 90-100 bar, the particles start to stick to each other and the reactor window becomes rapidly obscured. Above 100 bar, nothing can be seen through the window anymore. The polymerization thus behaves as a slurry process at any pressure between 20 and 200 bar. The only visible difference at the phase transition from biphasic to monophasic medium is the stability of the dispersion. We believe that this segregation prevents the solvent from effectively accessing and swelling the particles in the region of the living chain-ends. They will therefore no longer participate in the reaction, leaving the system with a conventional radical polymerization. The fact that the xanthate chain-ends are trapped and not simply degraded is corroborated by $^1\text{H-NMR}$ analyses mentioned above that show that xanthate chain-ends are still detected after FRP takes over the RAFT process (**Figures 16**). The fact that such a behavior is not observed at all with *O*-alkyl xanthates is remarkable and can be attributed to the difference in polarity of the aromatic chain-end compared to the alkyl chain-end.

III.1.4. Ethylene homopolymerization at 80 °C and 80 bar.

A pressure of 80 bar was chosen as it is the best compromise to maximize polymerization yield while avoiding getting too close to the phase transition of the polymerization medium. CTA 2 was preferred for this study to minimize chain-end degradation and accumulation of side-products. Except for the ethylene pressure, reaction conditions were identical to the previously described polymerization: T = 80 °C, DMC: 50 mL, AIBN: 50 mg, [CTA]:[AIBN] = 3:1. The results of the polymerizations are presented in **Table 5**.

Table 5. Ethylene homopolymerization at 80 bar and 80 °C with CTA 1.

Entry	Time (h)	Yield (g)	$M_{n,theo}^a$ (g mol ⁻¹)	M_n^b (g mol ⁻¹)	\mathcal{D}^b	f^c (%)	Ψ^c
22	2	0.69	1 030	880	1.22	100	18
23	4	1.32	1 720	1 350	1.28	95	29
24	6	1.63	2 060	1 500	1.32	72	39
25	7	1.93	2 400	1 980	1.38	-	-
26	16	2.37	2 900	2 050	1.63	95	30

Polymerization conditions using CTA 2: T = 80°C, P = 80 bar, DMC: 50 mL, AIBN: 50 mg, [CTA]:[AIBN] = 3.

^a: Determined using a derived form of equation 3, chapter I: $M_{n,theo} = \text{Yield(g)} / \text{CTA(mol)} + \text{MW}_{\text{CTA}}(\text{g mol}^{-1})$.

^b: Determined by HT-SEC using a conventional PE standards calibration.

^c: Determined by ¹H-NMR in TCE/C₆D₆ (2/1 v/v) at 363K.

The linear increase of the molar masses is again observed, although the values are surprisingly systematically lower than expected (**Figure 20b**). M_n values obtained with the same CTA at 80 °C and 200 bar are plotted for comparison. Dispersity values remain narrow during the first 7 hours of polymerization ($\mathcal{D} < 1.4$). The slight increase in the dispersity value after 16 hours of polymerization (entry 26, $\mathcal{D} = 1.6$) is likely due to slight variations in reaction conditions (temperature and pressure cannot be maintained constant overnight) and transfer reactions. The MMDs remain unimodal throughout the polymerization (**Figure 21**) and no second MMD at higher molar mass values is detected.

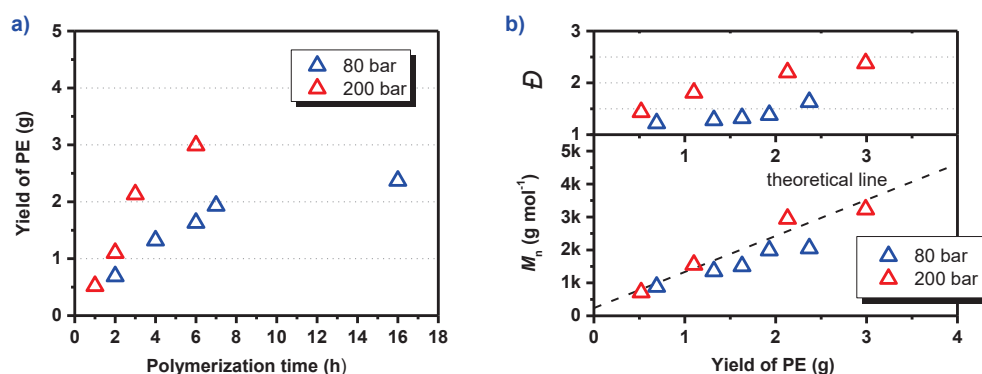


Figure 20. Kinetics of polymerization of ethylene (a) and M_n and \mathcal{D} evolution (b) at 80 bar and 80°C with CTA 2 (Δ). Data obtained at 200 bar and 80°C (Δ) are plotted for comparison.

As anticipated, performing the polymerization below 100 bar prevented the segregation of the polymer particles and the RAFT process endured for yields up to 2.37 g and M_n up to 2 000 g mol⁻¹. This is a serious improvement compared to the same polymerization performed at 200 bar

where the RAFT process was lost for yields and M_n as low as 1 g and 1 500 g mol⁻¹, respectively. The lower yields obtained at 80 bar compared to 200 bar can be explained by (i) the lower pressure of ethylene and (ii) the fact that the FRP mechanism (faster) does not take over RAFT (slower) during the polymerization (**Figure 20a**).

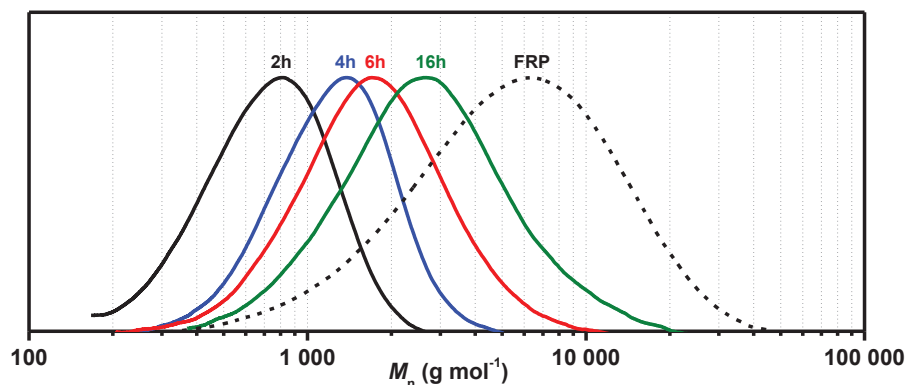


Figure 21. MMD evolution of PE obtained at 80 bar and 80°C with CTA 2.

An exemplary ¹H-NMR spectrum of a PE obtained at 80 bar after 16 hours of polymerization is presented in **Figure 22** (corresponding to entry 26 in **Table 6**). The α and ω chain-ends are detected (protons **b** and **e**), confirming the livingness of the polymerization at 80 bar. Side products (labelled with *) are detected at the same chemical shifts, with the same multiplicities and similar intensities as when the polymerization was performed at 200 bar using the same CTA (**Figure 16b**). This means that the same side-reactions are occurring while MMDs stay unimodal, confirming that the two phenomena are not related.

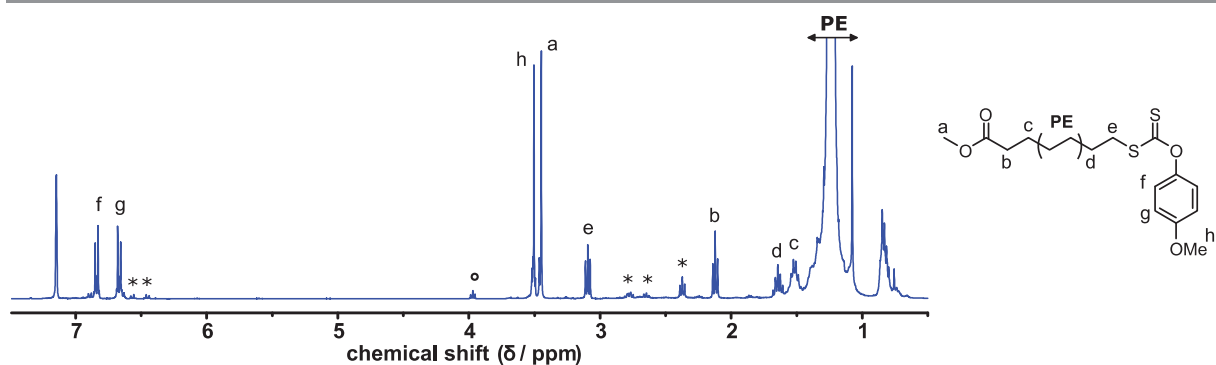


Figure 22. ¹H-NMR spectrum of a PE obtained after 16 hours of polymerization at 80 bar with CTA 2 corresponding to entry 25 of Table 6.

Functionalities f and the accumulation of side products \mathbb{Y} for PE prepared at 80 bar are shown in **Table 5**. While the same tendency is observed (f diminishes and \mathbb{Y} increases) for the first 3 entries (22-24) compared to the polymerizations performed at 200 bar (*vide supra*), the longest polymerization time (16h) features a remarkably high functionality and an amount of side products comparable to that of entry 23 (4 hours, $f = 95\%$, $\mathbb{Y} = 29\%$). Although this result is

surprising and against the tendency, several aliquots of this PE were analyzed and the same results were obtained, confirming this chain-end fidelity value.

III.1.5. Origin of new side-products from cross-termination

Polyethylene generated from aromatic xanthates **1** and **2** suffers from a loss of chain-end functionality during the polymerization. This loss of functionality happens at both 200 bar and 80 bar, whereas the emergence of the aforementioned FRP, taking over the RAFT process, happens only at 200 bar. The two phenomena are thus unrelated and the explanation for this degradation has to be found somewhere else. Conventional side-fragmentation happening with *O*-alkyl xanthates has already been ruled out, so another mechanism must be taking place. **Figure 23** recalls the characteristic signals observed for these side-products for a PE generated in the presence of **2** after 3 hours at 70 °C and 200 bar.

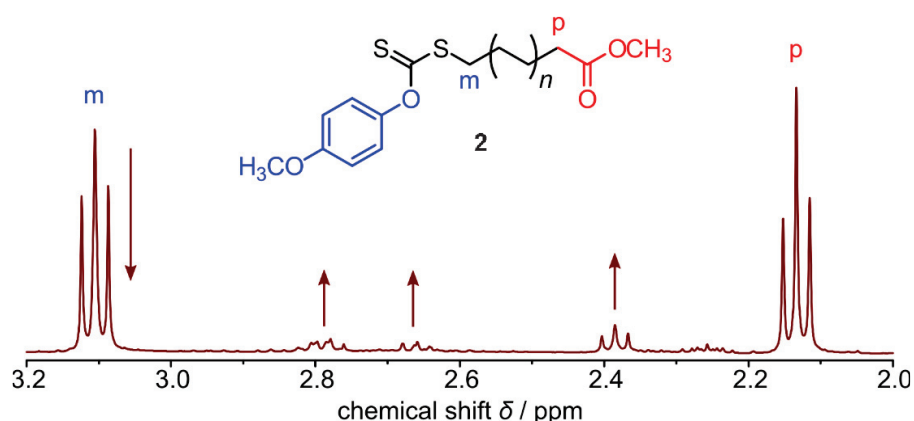
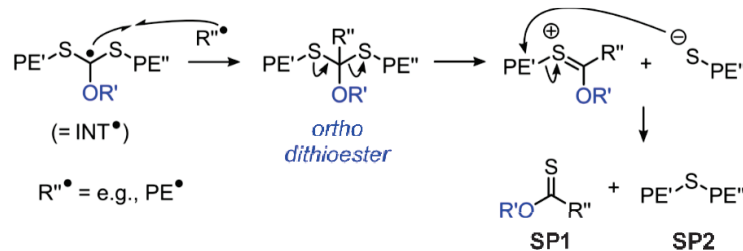


Figure 23. Zoomed ^1H -NMR spectrum on the 2.0-3.2 ppm region of a PE obtained with CTA **2** (corresponding to entry 8 of Table 2).

The chemical shifts of the new side-products are in the range 2.2 - 3.0 ppm, which corresponds to methylene protons in α position to heteroatoms such as S or O. ^1H - ^{13}C heteronuclear single quantum coherence (HSQC) NMR spectroscopy resolved the signals at 2.66 and 2.76 ppm to be a collection of superimposed triplets corresponding to both CH_2 and CH protons (HSQC-NMR spectrum in Figure S4 in the experimental section at the end of this chapter). The triplet at 2.38 ppm can be assigned to CH_2 protons and shows a ^{13}C coupling at 32.7 ppm, which is very characteristic for a CH_2 unit neighboring the S atom in a PE-S-PE thioether species.^[16] Taking into account all these data, a possible mechanism to explain the formation of such thioether species is proposed in **Scheme 3**.



Scheme 3. Potential mechanism of cross-termination and subsequent degradation of the cross-termination products with xanthates.

The aromatic xanthates were chosen to stabilize the intermediate radical (INT[•]) to prevent side-fragmentation. It is possible that the lifetime of this intermediate radical is long enough so that it can undergo cross-termination with a radical species R''[•], generating an ortho dithioester species. If R''[•] is a growing PE macroradical, then the ortho dithioester species would have the general structure presented in **Figure 24**, which features simulated triplets in the region 2.2-2.6 ppm. Those triplets could (partly) correspond to what is experimentally observed.

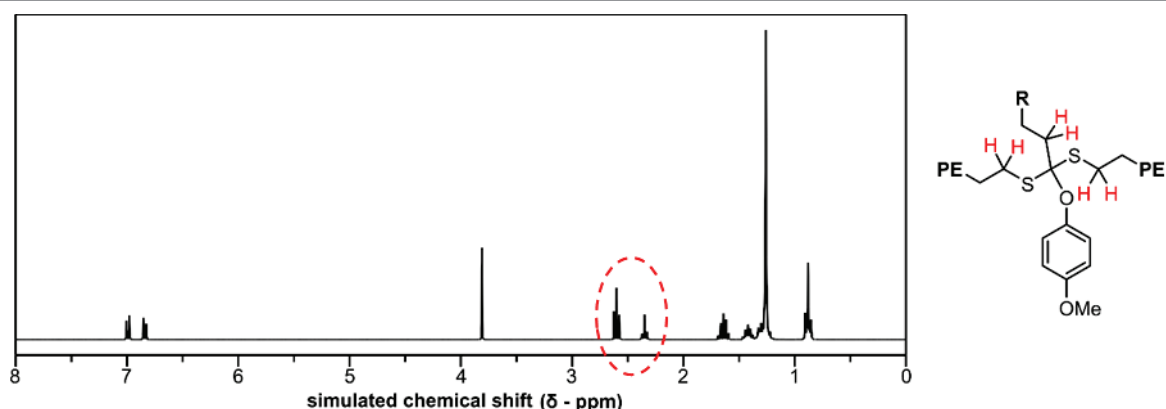


Figure 24. Simulated ¹H chemical shifts of a cross-termination product with CTA 2.

The occurrence of cross-termination in RAFT has been frequently studied – both experimentally and by simulations – mainly for the role it plays in observed rate-retardation effects for systems with dithiobenzoate RAFT agents.^[17,18] For xanthates, cross-termination is normally not even discussed, as the intermediate radical INT[•] is destabilized and its lifetime is short. In our system, the very low stability of the polyethylenyl radical PE[•] (already responsible for side-fragmentation) counters this effect and increases the lifetime of INT[•]. This might be sufficient so that cross-termination becomes a reasonable assumption with a xanthate CTA. The formed ortho dithioester in **Scheme 3** has the potential to decompose, eventually resulting in the PE-S-PE thioether (**SP2**) and a monothioester (**SP1**). Analogous other esters (R₁O)₃CR₂ are known for their propensity to decompose to an ether and an ester species upon catalytic activation.^[19,20] A monothioester with different R'' moieties (e.g. PE, oligomeric PE, small radicals from the radical

initiator or from transfer reactions) might (partly) give rise to the observed signals between 2.60 and 2.85 ppm.

The thioether **SP2** species is expected to have a higher molar mass than the monothioester **SP1**. That is because **SP2** is composed of two PE chains, while there is only one for **SP1**. In this context, some studies suggest that cross-termination happens exclusively with very short oligomeric radicals. In polymerizations of styrene, for example, cross-termination is expected to mainly happen with chains up to two monomer units.^[21,22] Assuming that R'' is indeed a rather short oligomeric species, the molar mass difference between **SP1** and **SP2** should be even greater. While the complete isolation of these two species has not been possible, a protocol of long-chains enrichment and short-chains depletion was designed. PE from **Figure 23** (obtained after 3 hours of polymerization at 70 °C and 200 bar) was stirred in DMC at room temperature for three days and subsequently filtered. Under these conditions, only short polymer chains and small molecules will be solubilized and end-up in the filtrate, whereas long polymeric species will be retained in the filter cake. This is confirmed by the MMD of the filtrate and the filter cake presented in **Figure 25**. Their respective ¹H-NMR spectra are presented in **Figure 26**. The filtrate shows indeed an enrichment of the species responsible for the signals at 2.60-2.85 ppm compared to the filter cake. The characteristic signal of the thioether at 2.39 ppm is much more intense in the filter cake, just as expected from the suggested mechanism and reasoning.

Eventually, it should be stated that the stoichiometry of the observed ¹H-NMR signals indicates that chain-end decomposition does not happen exclusively through the mechanism presented in **Scheme 3**.

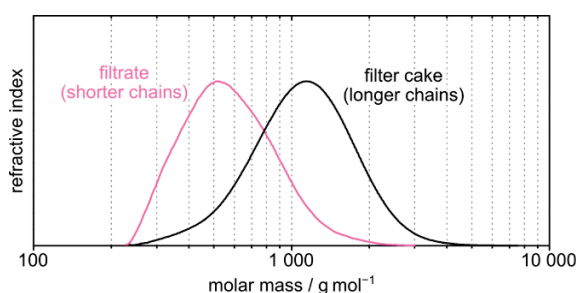


Figure 25. MMD of PE residue from the filtrate (shorter chains) and of PE from the filter cake (longer chains).

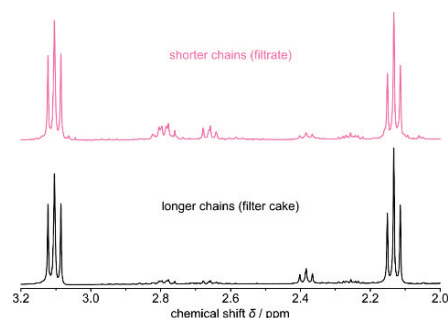


Figure 26. ¹H-NMR spectra of low molar-mass PE recovered in the filtrate and high molar-mass PE recovered in the filter cake.

III.2. RAFT copolymerization of ethylene in the presence of vinyl acetate: Synthesis of EVA copolymers.

The copolymerization of ethylene at a pressure of 200 bar with VAc (12.5 mL) in DMC (37.5 mL) leads to the formation of statistical EVAs that incorporate 10 mol% of VAc in the polymer backbone, as detected by $^1\text{H-NMR}$. The polymerization was carried out in conditions similar to ethylene homopolymerization using CTA 2: $T = 70\text{ }^\circ\text{C}$, AIBN (50 mg), $[\text{CTA}]:[\text{AIBN}] = 3$. The results of the polymerization are presented in **Table 6**. Noteworthy, EVAs with 10 mol% VAc content remain constant throughout the entire polymerization at 200 bar. The incorporation of VAc (%VAc, in mol%), chain-end fidelity (f) and Ψ were determined by $^1\text{H-NMR}$. %VAc was calculated by relative integration of the VAc repeating unit compared to the integration of the ethylene repeating unit, given by **Equation 2**

$$\%VAc = \frac{\int_{4.65}^{5.05} (\text{CH}_2\text{CH}(\text{OAc}))}{\int_{4.65}^{5.05} (\text{CH}_2\text{CH}(\text{OAc})) + \frac{1}{4} \int_{1.10}^{1.36} (\text{CH}_2\text{CH}_2)}$$

Equation 2. Calculation of VAc mol% in EVAs.

Cédric Dommanget showed that the EVA chains with 10 mol% VAc exclusively have an ethylene unit adjacent to the xanthate chain-end.^[3] f and Ψ can thus be calculated according to the previously described method.

Table 6. Ethylene-VAc copolymerization at 200 bar and 70°C with CTA 2.

Entry	Time (h)	Yield (g)	$M_{n,\text{theo}}^a$ (g mol $^{-1}$)	M_n^b (g mol $^{-1}$)	\mathcal{D}^b	%VAc ^c (mol%)	f^c (%)	Ψ^c (%)
27	1	0.20	490	360	1.23	11	110	4
28	2	0.65	990	630	1.31	10	100	13
29	3	0.81	1 150	690	1.31	9	90	14
30	4	0.93	1 300	740	1.33	9	95	19
31	6	1.31	1 630	1 120	1.31	10	80	30
32	18	4.07	4 540	3 450	1.77	9	65	40

T = 70 °C, P = 200 bar, DMC: 37.5 mL, VAc: 12.5 mL, AIBN: 50 mg, [CTA]:[AIBN] = 3.

^a: Determined using a derived form of equation 3, chapter I: $M_{n,\text{theo}} = \text{Yield}(\text{g}) / \text{CTA}(\text{mol}) + \text{MW}_{\text{CTA}}(\text{g mol}^{-1})$.

^b: Determined by HT-SEC using a conventional PE standards calibration.

^c: Determined by $^1\text{H-NMR}$ in TCE/ C_6D_6 (2/1 v/v) at 363K.

The molar masses found by HT-SEC are systematically lower than the theoretical values, which can be explained by the PE standards calibration used. The EVA copolymers being more polar than PE, they are more retained on the columns used for HT-SEC analyses and thus have a higher retention volume, hence a lower M_n . However, M_n values increase indeed linearly with polymer yield (**Figure 28a**) and the dispersities are remarkably narrow over the first 6 hours of polymerization ($\mathcal{D} \leq 1.33$). The broadening of the MMD (entry 32, $\mathcal{D} = 1.77$) after 18 hours of polymerization can be explained for the reasons stated above and by the accumulation of side products, resulting from the observed loss of functionality ($f = 65\%$).

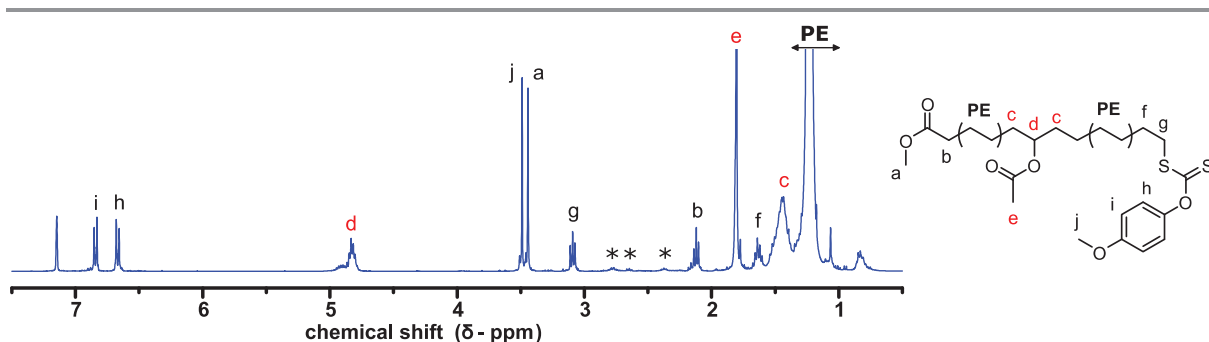


Figure 27. $^1\text{H-NMR}$ spectrum of an EVA after 4 hours of polymerization with CTA 2 at 70 °C and 200 bar (entry 30 table 6).

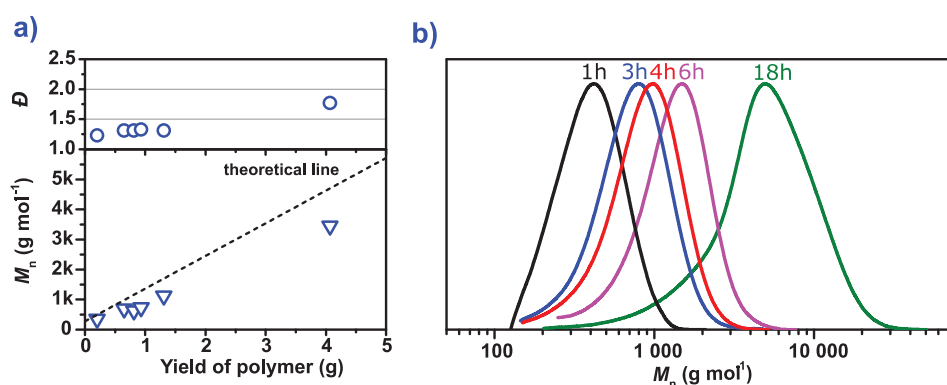


Figure 28. M_n (∇) and \bar{D} (\circ) evolution versus yield of polymer (a) and MMDs evolution (b) for ethylene-VAc copolymerization at 70 °C and 200 bar with CTA 2.

Interestingly, the second MMD is not observed for the synthesis of EVAs at a pressure of 200 bar at 70 °C, as it was the case for the homopolymerization of ethylene (at both 70 and 80 °C) using the same CTA at 200 bar (Figure 28b). The fact that cross-termination products and chain-end loss are still observed (* markers in Figure 27) confirms that the two phenomena are independent. The absence of high-molar-mass chains arising from conventional radical polymerization with CTA 2 at 200 bar is attributed to the better solubility of EVAs in the polymerization mixture. It could indeed be observed that EVAs with of VAc content of 10 mol% remain entirely soluble throughout the entire polymerization. No segregation occurs and the xanthate chain-ends (even linked to an ethylene repeating unit) remain accessible to growing radicals.

III.3. Conclusion on the use of xanthates for the RAFT polymerization of ethylene

Aromatic xanthates 1 and 2 have both shown the ability to suppress the side-fragmentation reaction observed with alkyl xanthates. Unprecedented control over ethylene homopolymerization at 200 bar ($1.2 \leq \bar{D} \leq 1.3$) could be achieved for molar masses up to

1 000 g mol⁻¹ but a segregation phenomenon occurred at that pressure, resulting in the loss of control for higher molar masses. This segregation could be avoided by performing the polymerization at a lower pressure (80 bar) and the control could be maintained for molar masses up to 3 000 g mol⁻¹ ($1.2 \leq D \leq 1.6$).

On the downside, CTAs **1** (phenoxy xanthate) and **2** (phenoxy methoxy xanthate) feature a pronounced rate retardation and ethylene homopolymerization proceeds substantially slower than when their alkyl counterparts are used. Chain-end degradation was found to occur with both CTAs and the functionality was gradually lost during polymerization. While the exact mechanism behind this degradation is not fully demonstrated, it is believed that a longer lifetime of the intermediate radical might result in new cross-termination reactions happening at the intermediate radical. Chain-end degradation is less pronounced with CTA **2** (up to 95 % of chain-end fidelity after 16 hours of polymerization at 80 bar) than with CTA **1**, hinting at an influence of the nature of the Z-group and supporting cross-termination reactions at the intermediate radical. CTA **2** is known to provide good control over vinyl acetate at moderate temperatures (60 °C), it was thus decided to use it nonetheless to mediate the block copolymerization between VAc and ethylene (see Chapter **III**).

IV. RAFT polymerization of ethylene with *N*-aryl carbamates

N-aromatic dithiocarbamates were investigated as alternatives to xanthates for the RAFT polymerization of ethylene. Their structures are recalled in **Figure 29**. These CTAs are commercially available and their ability to control ethylene at 200 bar and either 70 or 80 °C has been assessed in the following.

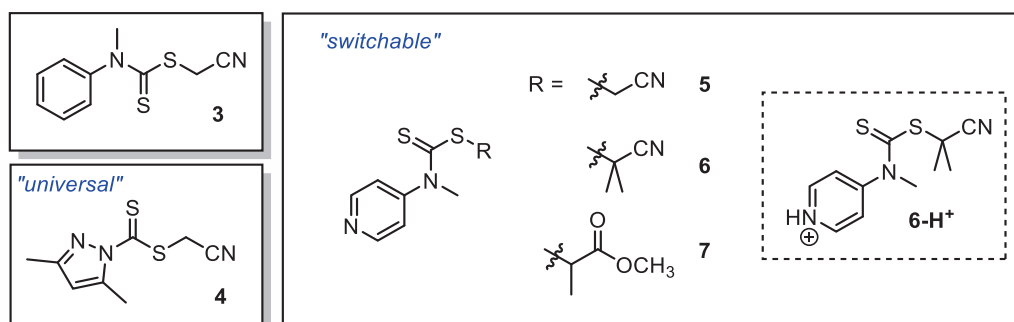


Figure 29. Structures of the *N*-aryl dithiocarbamates used for ethylene homopolymerization.

Among those CTAs, **4** is known to have a broad applicability to control both LAMs and MAMs,^[13,23] although its control over MMA is somewhat limited. As it requires no external stimuli to switch between either LAMs or MAMs as **5-7** do, this dithiocarbamate is of utmost interest and its ability to control the polymerization of ethylene will be presented first. CTA **3** has already been shown to be able to control the polymerization of ethylene without side-fragmentation by Cédric Dommanget during his thesis work.^[4] **3** is known to provide good control over the polymerization of LAMs and, to a lesser extent, MAMs.^[10] It was thus decided to pursue its investigation by confirming Cédric Dommanget's results and to compare it with its switchable counterpart **5**. Switchable dithiocarbamates **5-7** have shown by far the greatest ability to control both LAMs and MAMs depending on whether they are protonated or not^[14] and represent promising candidates for the ultimate goal of block copolymers synthesis.^[24] The results using **3,5-7** will be presented altogether as they all have analogous structures and the direct effects of different Z/R-groups can be rationalized.

IV.1. Ethylene homopolymerization in the presence of 3,5-dimethyl-1H-pyrazole-1-carbodithioate (**4**)

Ethylene polymerization was performed first under standard polymerization conditions ($T = 70\text{ °C}$, $P = 200\text{ bar}$, DMC: 50 mL, AIBN: 50 mg, [CTA]:[AIBN] = 3:1) with **4**. Those conditions yielded no polymer at all after 6 hours of polymerization (**Table 7**, entry 33). The [CTA]:[AIBN] was reduced to 1:1 under otherwise identical conditions and still no polymer was obtained after 6

hours (entry 34). **4** thus features a strong inhibition for the polymerization of ethylene, which was to be expected as intermediate radicals with Z = dimethylpyrazoyl show by far the lowest propensity to undergo fragmentation of all the RAFT agents used in the present work.^[13] This behavior is reinforced in the case of ethylene because the low stability of the polyethylenyl propagating radical further decreases the propensity of the intermediate radical to undergo fragmentation and release PE•. This illustrates how the careful choice of the chain transfer agent is of paramount importance when it comes to controlled radical polymerization of ethylene. CTAs that have shown good control over the polymerization of other LAMs, such as VAc, are not necessarily suitable for ethylene.

Table 7. Homopolymerization of ethylene at 200 bar in the presence of CTA **4.**

Entry	Time of polymerization (h)	Yield (g)	[CTA]:[AIBN] ratio	$M_{n,theo}^c$ (g mol ⁻¹)	M_n^d (g mol ⁻¹)	\bar{D}^d
33	6 ^a	0.00	3	-	-	-
34	6 ^a	0.00	1	-	-	-
35	3 ^b	1.53	0.5	5 220	5 700	2.47
36	6 ^b	4.58	0.5	15 240	9 500	2.62

^a: Polymerization performed at 70 °C using 50 mg of AIBN in DMC (50 mL).

^b: Polymerization performed at 80 °C using 100 mg of AIBN in DMC (50 mL).

^c: Determined using a derived form of equation 3, chapter I: $M_{n,theo} = \text{Yield(g)} / \text{CTA(mol)} + \text{MW}_{\text{CTA}}(\text{g mol}^{-1})$.

^d: Determined by HT-SEC using a conventional PE standards calibration.

PE was only obtained after doubling the AIBN quantity (100 mg) and for a [CTA]:[AIBN] ratio of 0.5:1 at 80 °C (entries 35-36). Those polymerization conditions are far from standard RAFT conditions and SEC analysis showed rather high \bar{D} values ($\bar{D} > 2.47$), comparable with what is obtained for a conventional free radical polymerization process. Besides, ¹H-NMR analysis did not show any of the characteristic signals expected for PE functionalized with **4**. There is consequently a complete inhibition of the polymerization in the presence of **4** and, when polymerization indeed occurs, there is no participation of the CTA and the polymerization occurs *via* conventional free radical polymerization.

IV.2. Ethylene homopolymerization in the presence of *N*-methylphenyl (3) and switchable *N*-methylpyridyl (5-7) dithiocarbamates

IV.2.1. Kinetics of the polymerizations

Ethylene polymerization was performed with **3,5-7** under standard polymerization conditions (T = 70 or 80 °C, P = 200 bar, DMC: 50 mL, AIBN: 50 mg, [CTA]:[AIBN] = 3:1). As with the aromatic xanthates, aromatic dithiocarbamates showed substantial retardation (compared to FRP) and a [CTA]:[AIBN] ratio of 3:1 was preferred for satisfactory polymerization kinetics and yields. The polymerization results at 70 °C and 80 °C are presented in **Figure 30**. The same trend is observed at both temperatures, with polymerization rates decreasing in the following order: **3**

$7 > 5 \approx 6$. CTAs **3** and **5** have identical R-group ($R = \text{CH}_2\text{CN}$) but different Z-group. The pronounced difference in polymerization rates can thus be attributed to a higher stabilization of the intermediate radical by the Z-group of **5** ($Z = \text{PyrN}(\text{Me})$) compared to **3** ($Z = \text{PhN}(\text{Me})$). A faster addition (k_{add}) of PE^{\bullet} to **5** is also a possibility. The trend $7 > 5 \approx 6$ (identical Z-group, different R-group) might stem for different affinities of the released radical R^{\bullet} to (re)initiate polymerization. All CTAs show very good agreement with expected M_n values, while D values remain rather similar for all systems ($1.40 < D < 1.80$).

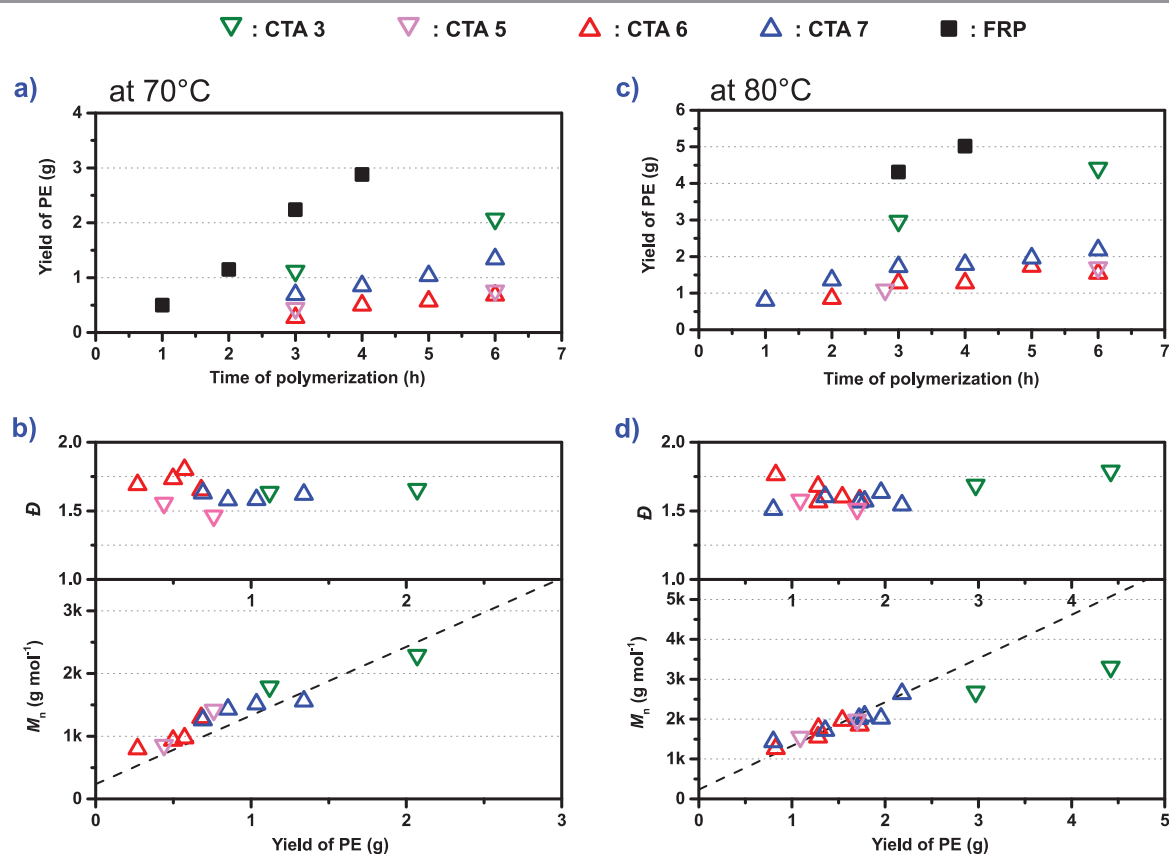


Figure 30. Ethylene homopolymerization in the presence of CTAs **3**, **5**, **6** and **7** at 200 bar. a) Polymerization kinetics at 70 °C. b) M_n and D evolution versus of yield of PE at 70 °C. c) Polymerization kinetics at 80 °C. d) M_n and D evolution versus of yield of PE at 80 °C

A downward deviation of M_n for **3** is clearly visible when the polymerization is performed at 80 °C (highest PE yields). It is mainly assigned to the inevitable irreversible termination of PE as well as continuous initiation of new chains by AIBN and was equally observed in earlier works by our group.^[25]

Noteworthy, a control experiment was performed using the protonated form of **6** (**6-H⁺**) to mediate ethylene polymerization. In principle, no polymerization should occur as this CTA is known in its protonated to provide control over MAMs and the inhibit the polymerization of LAMs.^[14] No polymer was obtained after 5 hours of polymerization at 80 °C and 200 bar, which is consistent with the expected behavior of this CTA in its protonated form. **Figure 31** exemplarily

shows the MMD evolution obtained with **7** at 80 °C and 200 bar after 1h to 6h. Similar MMDs evolutions could be observed for **3,5-7** at both 70 and 80 °C.

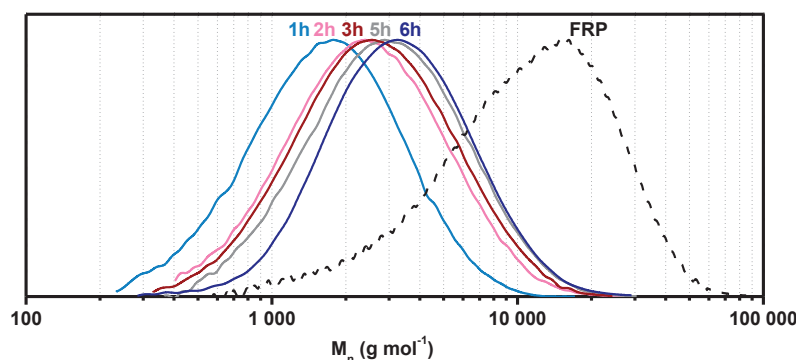
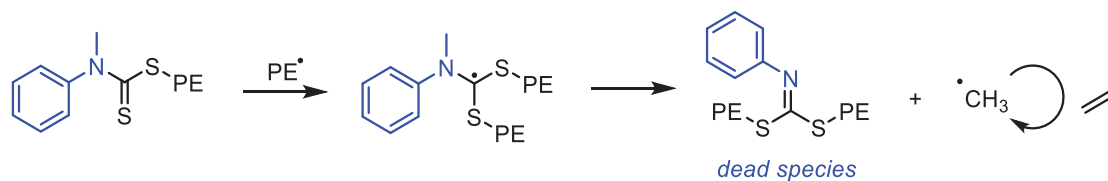


Figure 31. MMDs evolution of PE obtained with **7 at 80 °C at different polymerization times.**

In contrast to aromatic xanthate systems, MMDs stay unimodal throughout the entire polymerization to M_n up to 3 000 g mol⁻¹ (and yields up to 4.42 g). This clarifies that the loss of control (traduced by the emergence of FRP and bimodal SEC traces) in previous experiments is specific to aromatic xanthates when the polymerization is performed at 200 bar. The difference (even so slight) of the nature of the chain-end (xanthate vs carbamate) is surprisingly sufficient to avoid the previously described segregation effect. On the downside, the remarkably low \bar{D} values achieved for the lowest polymerization times with *O*-aryl xanthates ($1.22 < \bar{D} < 1.30$) cannot be attained with *N*-aryl dithiocarbamates regardless of the yield or the nature of the CTA ($\bar{D} > 1.40$).

IV.2.2. Chain-ends analysis

¹H-NMR analysis was recorded for each polymerization time and each CTA at both temperature. An exemplary spectrum for PE obtained after 3 hours of polymerization at 80 °C in the presence of **3**, **5**, **6** and **7** is presented in **Figure 32a**, **32b**, **32c** and **32d**, respectively. Side-fragmentation with the considered *N*-aryl carbamates could, in principle, happen through the release of a •CH₃ radical affording the corresponding dead polymer bearing a C=N double bond. Just as with *O*-alkyl xanthates, this dead polymer species would feature two PE chains linked together by a dithioiminocarbonate S(C=NPh)S bridge (**Scheme 4**). The expected chemical shift of such side-fragmentation would be similar to that of two PE chains linked by a dithiocarbonate S(C=O)S bridge ($\delta = 2.92$ ppm). As ¹H-NMR shows no signals in that region, side-fragmentation with *N*-aryl carbamates is indeed ruled out.



Scheme 4. Side-fragmentation with *N*-aryl dithiocarbamates.

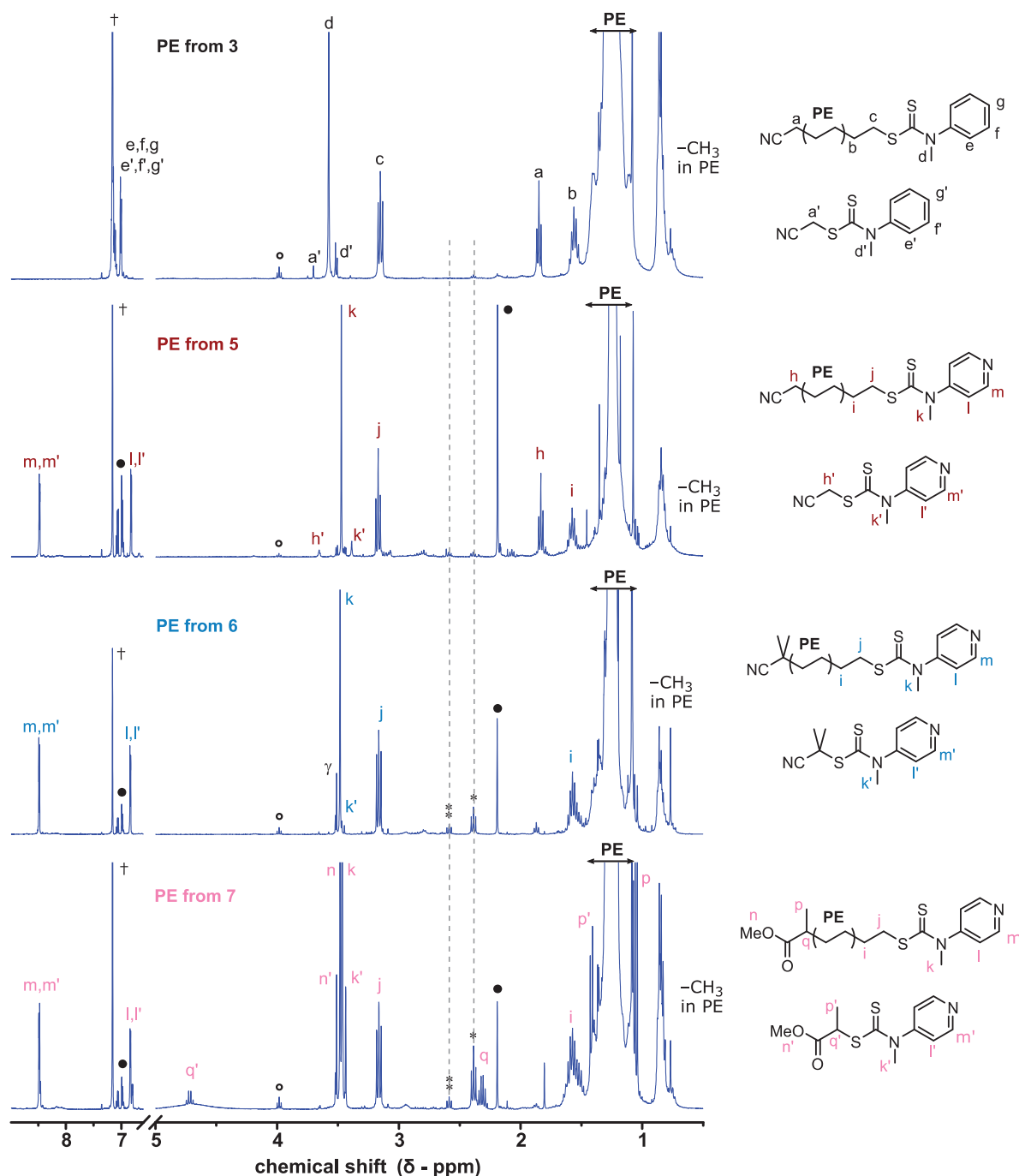
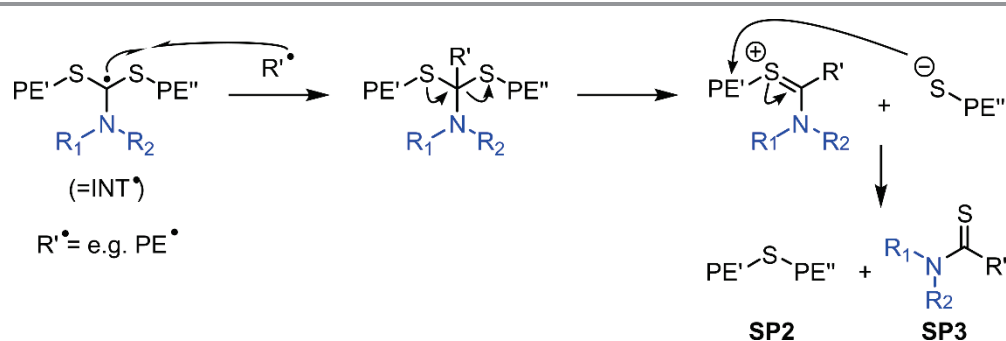


Figure 32. ¹H-NMR spectra of PE obtained after 3 hours of polymerization at 80 °C with 3 (a), 5 (b), 6 (c) and 7 (d). †NMR residual solvent benzene, °collecting solvent toluene, γpolymerization solvent DMC, °transfer to DMC.

Surprisingly, PE from 7 features a particularly intense triplet at 2.38 ppm (*), which corresponds to the PE-S-PE thioether species previously identified (**SP2**, **Scheme 3**), that would

indicate the probable occurrence of cross-termination at the intermediate radical *via* the same mechanism. **6** shows the same triplet with a lesser intensity, whereas it is of equivalent intensity and barely detectable with **5** and **3**. As **7**, **6** and **5** have the same Z-group but different R-group, a strong dependency on the nature of the R-group can be deduced. This clarifies that both the Z-group and the R-group play a role in cross-termination. This leads to the reasonable assumption that cross-termination happens indeed with rather short chains, for which the R-group is sufficiently close to the radical center to have a significant impact.

PE from **6** and **7** also display two new distinct triplets at $\delta = 2.59$ ppm (\ddagger), indicating new side-products (which have yet to be fully identified). A signal at the same chemical shift is also detected in PE from **5** at very low intensity, while PE from **3** has a remarkably flat baseline in that region. This chemical shift could, in principle, correspond to the methylene protons in α position to the monothiocarbamate **SP3** (**Scheme 5**) generated during the potential cross-termination mechanism, and accompanying the production of **SP2**, as simulated by Chemdraw.



Scheme 5. Potential mechanism of cross-termination and subsequent degradation of the cross-termination products with dithiocarbamates.

The intensity of the triplet from **SP3** should be half of that of **SP2** (assuming that $R'^{\bullet} = \text{PE}^{\bullet}$), which is indubitably not the case for PE from **5-7**. In this context, it should be stated that a second $^1\text{H-NMR}$ analysis was done on another aliquot of PE from **7** and the triplet at 2.59 ppm was not detected, whereas the triplet 2.38 ppm had the same intensity.

The detection of signals from new side-products is even more peculiar as, when integration of both the α and the ω chain-ends is possible (for example, the α chain-end signal overlaps with $-\text{CH}_2-$ and $-\text{CH}_3$ signals of PE for **6** and integration is not possible), chain-end fidelity (f) is always equal or close to 100 %. While this is intuitive for PE obtained with **3**, which arguably features the cleanest $^1\text{H-NMR}$ spectrum, it is somewhat more surprising for PE obtained with **7**, which contains several degradation products. That being said, it should be stated that the signal of characteristic proton **q** of **7** overlaps with the triplet at 2.38 ppm and its integration is not accurate.

All investigated dithiocarbamates have in common to be slowly consumed during the polymerization process, which was not observed with xanthates. All $^1\text{H-NMR}$ spectra (**Figure 32**) show the presence of unconsumed CTA. The integration of their respective characteristic protons

permits the determination of the CTA consumption. The consumption of **3** is especially slow at 70 °C, with 71 % and 92 % consumption after PE yields of, respectively, 1.1 and 2.1 g at 70 °C. **5** is consumed about three times faster (74 % and 92 % for PE yields of 0.4 and 0.8 g, respectively, at 70 °C). As **3** and **5** have the same R-group, this indicates that the pyridyl moiety of the Z-group significantly increases the reactivity of the RAFT agent toward PE[•] compared to a phenyl moiety. As a result, faster addition of PE[•] is expected with **5** during the main equilibrium (k_{add}), which goes hand in hand with the lower polymerization rate observed with **5** compared to **3**. The fastest consumption of the CTA is observed with **6** (95 % after 0.3 g at 70 °C), which is straightforward as its tertiary R-group is more readily released than the primary one of **5**. This slow consumption of all CTAs explains why all M_n are systematically higher than the expected values at 70 °C (**Figure 30b**) for the lowest polymerization yields.

The consumption rate of all dithiocarbamates is enhanced by performing the polymerization at 80 °C (traded by M_n values much closer to theoretical values for the lowest yields, **Figure 30d**). **Table 8** collects the f and consumption values for each CTA after 3 hours and 6 hours of polymerization at 80 °C. f values superior to 100 % are due to (i) chains resulting from initiation by AIBN and (ii) difficulty of integration due to overlapping signals.

Table 8. Chain-end fidelity f and consumption of CTAs 3, 5-7 after 3 and 6 hours of polymerization at 80 °C.

Entry	CTA	Time (h)	Yield (g)	f^a (%)	CTA consumption (%) ^a
36	3	3	2.97	100	96
37	3	6	4.42	105	>99
38	5	3	1.09	105	93
39	5	6	1.70	110	97
40	6	3	1.28	-	>99
41	6	6	1.54	-	>99
42	7	3	1.72	130	95
43	7	6	2.18	90	>99

Polymerizations performed at T = 80 °C and P = 200 bar

^a: Determined by ¹H-NMR in TCE/C₆D₆ (2/1 v/v) at 363K

V. Conclusion

Ethylene homopolymerization could be successfully controlled using aromatic xanthates and aromatic dithiocarbamates *via* a RAFT process. The side-fragmentation reaction previously identified with alkyl xanthates could be completely suppressed by incorporating an aromatic ring in the Z-group of the CTA. On the downside, all investigated CTAs provoke strong retardation. Acceptable polymerization rates are only obtained at higher temperature (80 °C vs. 70 °C) and with a lower [CTA]:[AIBN] ratio (3 vs. 10) compared to our previous work with alkyl xanthates.

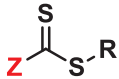
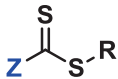
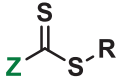
Phenoxy and phenoxymethoxy xanthates (**1** and **2**) produced PE with unprecedentedly low \bar{D} values (down to 1.2). However, a severe loss of chain-end functionality was observed using those CTAs leading to the accumulation of new side-products. These side-products have been attributed to new cross-termination mechanisms involving rather short polymeric species, for which both R/Z-groups play a role. The detrimental impact of a supercritical DMC/ethylene phase for polymerization at 200 bar using those aromatic xanthates could be circumvented by performing the polymerization at 80 bar. The use of **2** resulted in a lesser loss of chain-end fidelity and fewer side-products, while giving the highest yields.

The use of the pyrazole CTA (**4**) resulted in the complete inhibition of the polymerization and PE was only obtained for low CTA and high AIBN quantities. HT-SEC and ¹H-NMR analysis showed that the polymerization occurred exclusively by a conventional free radical mechanism.

N-methylphenyl and *N*-methylpyridinyl CTAs (**3**, **5-7**) were efficient at controlling the RAFT polymerization of ethylene and no significant chain-end functionality loss was detected. In particular, CTAs **3** and, to a lesser extent, **5** have shown the greatest ability to control the polymerization of ethylene while minimizing the generation of side-products. All dithiocarbamates feature a slow consumption during polymerization at 70 °C. This slow consumption is less pronounced when the polymerization is performed at 80 °C.

All investigated aromatic xanthates and dithiocarbamates feature advantages and disadvantages compared to alkyl xanthates, which are listed in the following **Table 9**.

Table 9. Advantages and disadvantages of the xanthates and dithiocarbamates used for ethylene RAFT polymerization.

 Z = OEt, OMe		 Z = OPh, OPhOMe		 Z = N(Ph)Me, N(Pyr)Me	
✓	No rate retardation	✗	Rate retardation	✗	Rate retardation
✗	Side-fragmentation	✓	No side-fragmentation	✓	No side-fragmentation
		✓	Instantaneous consumption at 70 °C	✗	Slow consumption at 70 °C
		✗	Cross-termination	✗/✓	Cross-termination depending on Z/R-group
✗	Loss of chain-end fidelity	✗	Loss of chain-end fidelity	✓	Chain-end fidelity retained

Despite the more or less pronounced loss of chain-end fidelity observed with **2**, this CTA will be investigated for the synthesis of block copolymers with vinyl acetate (Chapter III). The loss of chain-end fidelity with this CTA is indeed lower than with CTA **1** or with the more conventional *O*-alkyl xanthates. Moreover, CTA **2** has been shown to be especially efficient at controlling VAc polymerization and unprecedented low \bar{D} ($1.2 \leq \bar{D} \leq 1.6$) values are obtained when it is used to mediate ethylene polymerization. The high chain-end fidelity obtained with dithiocarbamates and their switch ability will be used for the synthesis of diblock copolymers with methyl methacrylate (Chapter IV) and poly(ethylene oxide) (Chapter V).

A part of the work presented in this chapter has been published:

Angew. Chem. Int. Ed. **2019**, *58*, 14295.

VI. Experimental section

Materials and Methods

The comprehensive list of materials and analytical methods used for this work are presented at the end of this manuscript.

Typical ethylene polymerization procedure

The employed autoclave reactor (160 mL) was equipped with a mechanical stirring apparatus, a thermometer and a pressure sensor (**Figure S1**). A solution of AIBN (50 mg, 0.30 mmol, 6.09 mmol L⁻¹, 1 equiv) and the RAFT agent (0.91 mmol, 18.3 mmol L⁻¹, 3 equiv) in DMC (50 mL) (or a mixture of DMC (38 mL) and VAc (12 mL) for the synthesis of statistical EVAs) was added to the reactor preheated to 70 or 80 °C under argon atmosphere with a mechanical stirring of 600 rpm. Immediately after the injection port was closed, ethylene gas was fed into the reactor until the envisaged pressure of either 80 or 200 bar was reached. This took a few seconds for experiments at 80 bar and about 4 min for experiments at 200 bar. If necessary, additional ethylene gas was introduced to keep a constant pressure during the polymerization. After a predetermined period of time, the stirring was slowed down and the reactor was cooled with iced water. When the temperature inside the reactor dropped below 30 °C, the remaining pressure was carefully released. The content of the reactor was collected with toluene, and evaporation of the solvent gave the polymeric product.



Figure S1. Autoclave used for ethylene polymerization.

Synthesis of methyl 2-(phenoxy-carbonothioylthio)acetate **1**

The synthesis was inspired by and adapted from several works from the literature.^[9,26] Phenol (10 g, 106 mmol, 1 equiv) was dissolved in dimethyl sulfoxide (DMSO) (100 mL) at 40 °C. *N,N*-Diisopropylethylamine (19 mL, 106 mmol, 1 equiv) was added, followed by carbon disulfide (40 mL, 638 mmol, 6 equiv). The mixture was then stirred at 40 °C for 24 h. Methyl 2-bromoacetate (10 mL, 106 mmol, 1 equiv) was added dropwise to the dark red solution which was then stirred at 40 °C for an additional 24 h. The volatiles were removed *in vacuo* and cold H₂O (300 mL) was added. The aqueous phase was extracted three times with ethyl acetate (1x100 mL, 2x50 mL) and the combined organic phases were washed with H₂O (50 mL), 1M HCl (50 mL), 1M NaOH (50 mL), H₂O (50 mL), and a saturated aqueous solution of NaCl (50 mL). The organic phase was dried over MgSO₄ and the solvent removed *in vacuo*. The crude mixture was purified by flash chromatography on silica gel (dichloromethane/petroleum ether 40:60 by volume) to yield the *O*-phenyl xanthate **1** as a yellow oil (7.57 g, 31 mmol, 29%). ¹H-NMR (CDCl₃): δ (ppm) = 7.35 (m, 2H) 7.20 (m, 1H) 7.03 (m, 2H) 3.98 (s, 2H) 3.72 (s, 3H). Spectrum of isolated product is shown in **Figure S2**.

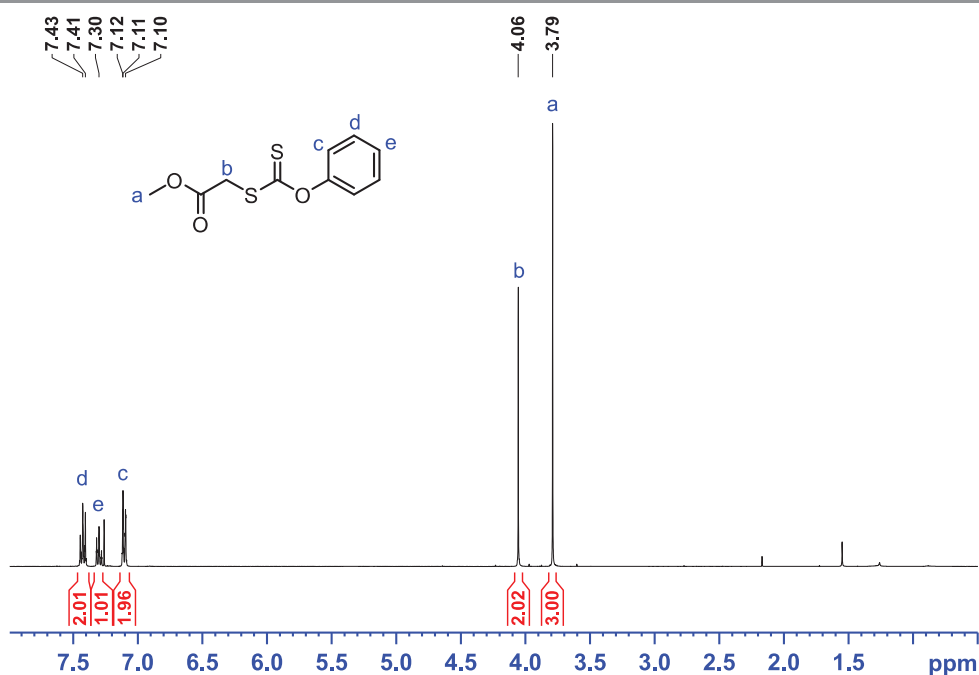


Figure S2. ¹H-NMR spectrum of CTA **1** in CDCl₃.

Synthesis of methyl 2-(4-methoxyphenoxycarbonothioyl)acetate **2**

The synthesis was inspired by and adapted from several works from the literature.^[9,26] 4-Methoxy phenol (10 g, 81 mmol, 1 equiv) was dissolved in carbon disulfide (100 mL) at room temperature. *N,N*-Diisopropylethylamine (15 mL, 90 mmol, 1.1 equiv) was added and the yellow solution was stirred at 40 °C for 24 h. Methyl 2-bromoacetate (4 mL, 41 mmol, 0.5 equiv) was added dropwise and the resulting orange suspension was stirred at 40 °C for an additional 24 h. The rest of the methyl 2-bromoacetate (4 mL, 41 mmol, 0.5 equiv) was added and the mixture was again stirred at 40 °C for 24 h. The volatiles were removed *in vacuo* and the residue was dissolved in ethyl acetate (200 mL). A white precipitate was removed by filtration. The resulting clear orange solution was washed with H₂O (50 mL), 1M HCl (50 mL), 1M NaOH (50 mL), H₂O (50 mL) and a saturated aqueous solution of NaCl (50 mL). The organic phase was dried over MgSO₄ and the solvent removed *in vacuo*. The resulting dark oil was purified by flash chromatography on silica gel (toluene/petroleum ether 80:20 by volume) to yield the *O*-phenoxymethoxy xanthate **2** as a yellow oil (6.40 g, 23 mmol, 29%). ¹H-NMR (CDCl₃): δ (ppm) = 7.02 (m, 2H) 6.92 (m, 2H) 4.05 (s, 2H) 3.82 (s, 3H) 3.79 (s, 3H). Spectrum of isolated product is shown in **Figure S3**.

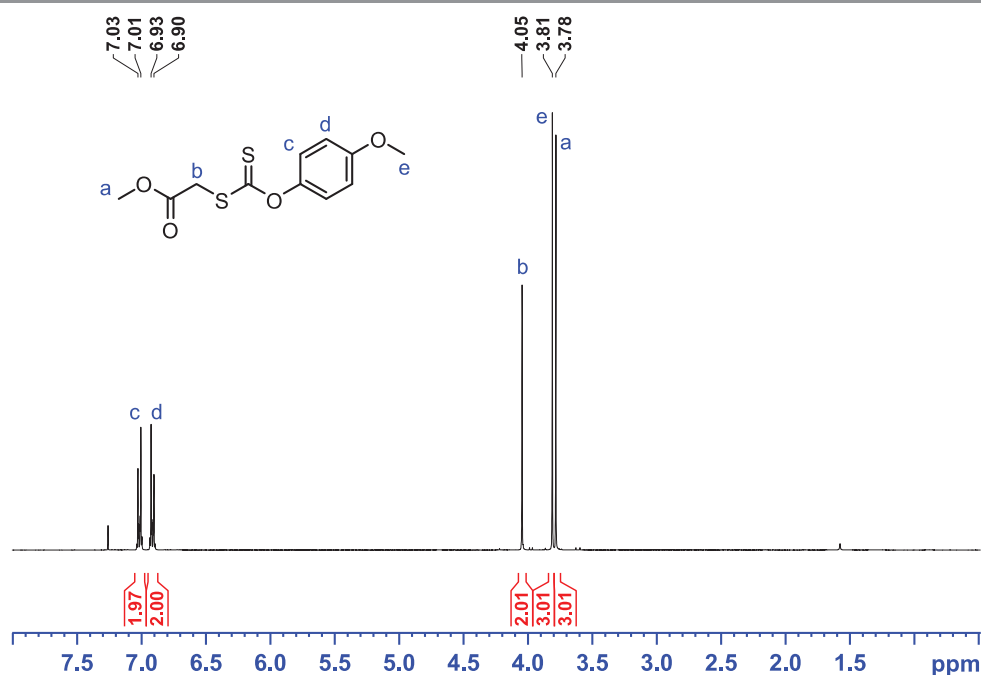


Figure S3. ¹H-NMR spectrum of CTA 1 in CDCl₃.

HSQC-NMR analysis of a PE synthesized with CTA 2

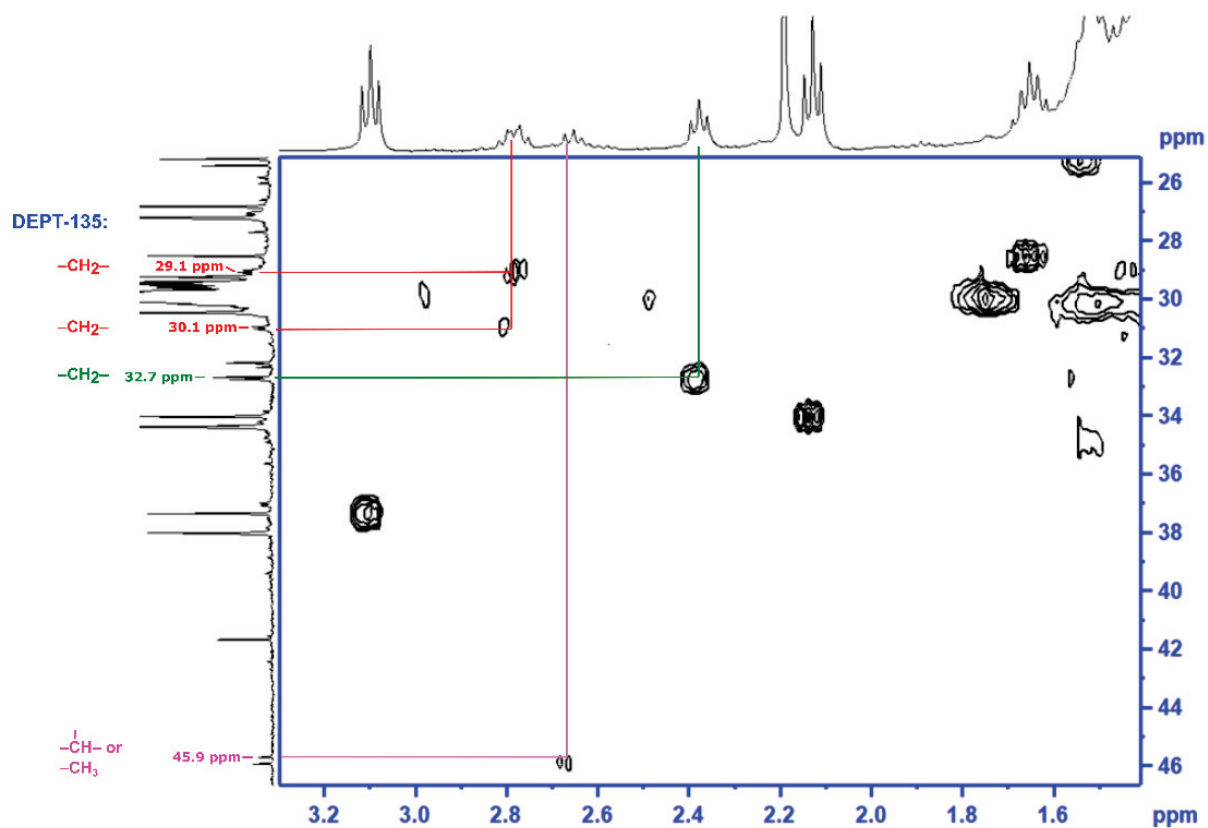


Figure S4. HSQC-NMR analysis of a PE synthesized with CTA 2 (corresponding to entry 8 of Table 2).

VII. References

- [1] S. Perrier, *Macromolecules* **2017**, *50*, 7433–7447.
- [2] D. J. Keddie, *Chem. Soc. Rev.* **2014**, *43*, 496–505.
- [3] C. Dommaget, F. D'Agosto, V. Monteil, *Angew. Chem. Int. Ed.* **2014**, *53*, 6683–6686.
- [4] C. Dommaget, Polymérisation Radicalaire Contrôlée : Le Défi de l'éthylène, **2013**. Thèse université Lyon 1.
- [5] D. H. R. Barton, D. Crich, A. Löbberding, S. Z. Zard, *Tetrahedron* **1986**, *42*, 2329–2338.
- [6] M. L. Coote, L. Radom, *Macromolecules* **2004**, *37*, 590–596.
- [7] J. P. A. Heuts, G. Gilbert, I. A. Maxwell, *Macromolecules* **1997**, *30*, 726–736.
- [8] Q. B. Chen, T. Y. Zeng, L. Xia, Z. Zhang, C. Y. Hong, G. Zou, Y. Z. You, *Chem. Commun.* **2017**, *53*, 10780–10783.
- [9] M. H. Stenzel, L. Cummins, G. E. Roberts, T. P. Davis, P. Vana, C. Barner-Kowollik, *Macromol. Chem. Phys.* **2003**, *204*, 1160–1168.
- [10] M. Destarac, D. Charmot, X. Franck, S. Z. Zard, *Macromol. Rapid Commun.* **2000**, *21*, 1035–1039.
- [11] G. Moad, E. Rizzardo, S. H. Thang, *Aust. J. Chem.* **2012**, *65*, 985.
- [12] G. Moad, C. Barner-Kowollik, *The Mechanism and Kinetics of the RAFT Process: Overview, Rates, Stabilities, Side Reactions, Product Spectrum and Outstanding Challenges*, **2008**.
- [13] J. Gardiner, I. Martinez-Botella, J. Tsanaktisidis, G. Moad, *Polym. Chem.* **2016**, *7*, 481–492.
- [14] M. Benaglia, J. Chiefari, Y. K. Chong, G. Moad, E. Rizzardo, S. H. Thang, *J. Am. Chem. Soc.* **2009**, *131*, 6914–6915.
- [15] E. Grau, J. P. Broyer, C. Boisson, R. Spitz, V. Monteil, *Phys. Chem. Chem. Phys.* **2010**, *12*, 11665–11669.
- [16] J. Mazzolini, I. Mokthari, R. Briquel, O. Boyron, F. Delolme, V. Monteil, D. Bertin, D. Gimes, F. D'Agosto, C. Boisson, *Macromolecules* **2010**, *43*, 7495–7503.
- [17] G. Moad, *Macromol. Chem. Phys.* **2014**, *215*, 9–26.
- [18] N. De Rybel, P. H. M. Van Steenberge, M. F. Reyniers, C. Barner-Kowollik, D. R. D'hooge, G. B. Marin, *Macromol. Theory Simulations* **2017**, *26*, 1–19.
- [19] H. Staudinger, G. Rathsam, *Helv. Chim. Acta* **1922**, *5*, 645–655.
- [20] E. Márquez, J. R. Mora, T. Cordova, G. Chuchani, *J. Phys. Chem. A* **2009**, *113*, 2600–2606.
- [21] D. Konkolewicz, B. S. Hawkett, A. Gray-Weale, Perrier, *J. Polym. Sci. Part A Polym. Chem.* **2008**, *47*, 3455–3466.
- [22] S. R. S. Ting, T. P. Davis, P. B. Zetterlund, *Macromolecules* **2011**, *44*, 4187–4193.
- [23] J. Gardiner, I. Martinez-Botella, T. M. Kohl, J. Krstina, G. Moad, J. H. Tyrell, M. L. Coote, J. Tsanaktisidis, *Polym. Int.* **2017**, *66*, 1438–1447.
- [24] G. Moad, D. Keddie, C. Guerrero-Sanchez, E. Rizzardo, S. H. Thang, *Macromol. Symp.* **2015**, *350*, 34–42.
- [25] Y. Nakamura, B. Ebeling, A. Wolpers, V. Monteil, F. D'Agosto, S. Yamago, *Angew. Chem. Int. Ed.* **2018**, *57*, 305–309.
- [26] C. A. Bell, G. G. Hedir, R. K. O'Reilly, A. P. Dove, *Polym. Chem.* **2015**, *6*, 7447–7454.

Chapter III
**Synthesis of block copolymers based
on ethylene and vinyl acetate**

I. Introduction.....	142
II. Synthesis of PVAc macro-CTAs	144
III. Synthesis of PVAc-<i>b</i>-PE copolymers.....	147
III.1. Block copolymerizations at 200 bar	147
III.2. Block copolymerizations at 80 bar	149
III.3. Thermal properties of PVAc- <i>b</i> -PE copolymers.....	154
IV. Conclusion	156
V. Experimental section	157
VI. References	158

I. Introduction

To the best of our knowledge, the direct block copolymerization (*i.e.* by sequential monomer addition) of ethylene and vinyl acetate has never been reported. Their statistical copolymerization by radical processes is however largely documented.^[1-5] There exists one example of indirect block synthesis, in which the PE-like block is in fact formed of methylene $-(CH_2)-$ repeating units and is obtained by polyhomologation of ylides followed by chain-end functionalization with iodine. The block copolymer with VAc is then obtained by ITP initiated *via* visible light.^[6]

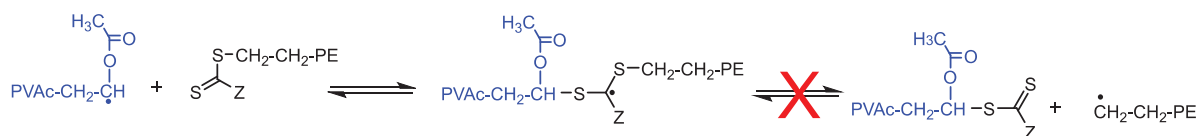
VAc is a less-activated monomer. Its polymerization *via* RAFT is therefore controlled by xanthate or dithiocarbamate CTAs. In Chapter II, it was shown that the phenoxymethoxy xanthate (referred to as CTA 2) is capable of controlling ethylene polymerization while minimizing the loss of chain-end fidelity and the formation of side-products. This CTA has been studied by Stenzel *et al.*^[7] for VAc homopolymerization and, while a strong inhibition was observed by the authors for high CTA concentration, remarkably low dispersities were obtained ($\mathcal{D} < 1.10$, lower than with more conventional *O*-alkyl xanthates). Based on these results, CTA 2 was chosen to mediate VAc RAFT polymerization in order to achieve a PVAc macro-CTA that could be further used in ethylene polymerization for the formation of the targeted diblock copolymers.

While such a block copolymer synthesis is also possible with dithiocarbamates, experiments performed during this work revealed that VAc homopolymerization with *N*-aryl dithiocarbamates (CTAs 3, 5-7 from Chapter II) featured a particularly strong inhibition and the control over molar masses was poor. In this context, Destarac *et al.*^[8] reported excellent control over VAc polymerization with dithiocarbamates ($Z = N(Ph)_2$, $R = CH(COOEt)_2$), whereas Shipp *et al.*^[9] noted a strong influence of both the Z/R-groups and effective control over VAc homopolymerization was not achieved with $Z = N(Ph)Me$, $R = CH_2COOEt$ and $Z = N(Ph)_2$, $R = CH_2COOEt$. In light of all these data, the synthesis of well-defined PVAc macro-CTAs with a dithiocarbamate chain-end was thus not further investigated and the use of dithiocarbamates was preferred for the synthesis of PMMA-*b*-PE and PEO-*b*-PE copolymers (Chapters IV and V). For these reasons, only works with the phenoxymethoxy xanthate (CTA 2 in Chapter II) will be described in this chapter.

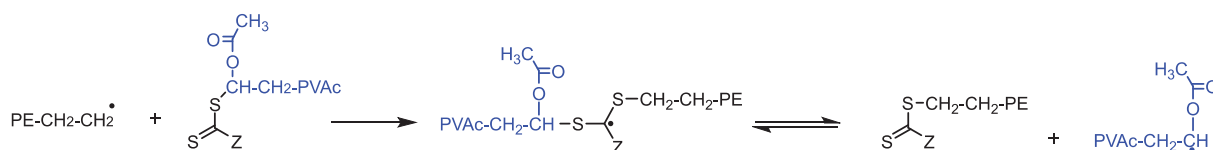
As stated in chapter I, the polymerization order is important in obtaining well-defined block copolymers. The more activated monomer has to be polymerized first as the resulting macro-CTA will produce a more stable propagating radical. This was observed by Shipp and coworkers^[9] for the synthesis of PVAc-*b*-PMA copolymers. VAc and ethylene are both less activated monomers, but ethylene produces the least stable propagating radical ($PE-CH_2\cdot$ vs $PVAc-CH(OAc)\cdot$). Indeed, apart from solubility issues, if the PE block is synthesized first, the difference in stability of propagating radicals of PE and PVAc will result in PVAc homopolymerization and a mixture of homopolymers will be obtained (**Scheme 1a**). This was confirmed experimentally by Cédric

Dommanget with the CTA *O*-ethyl xanthate during his PhD work.^[10] The PVAc block will thus be synthesized first and used as macro-CTA for chain-extension with ethylene in an attempt to obtain the desired block copolymers (**Scheme 1b**).

a) Start with PE macro-CTA: a mixture of homopolymers is obtained



b) Start with PVAc macro-CTA: block copolymers are obtained

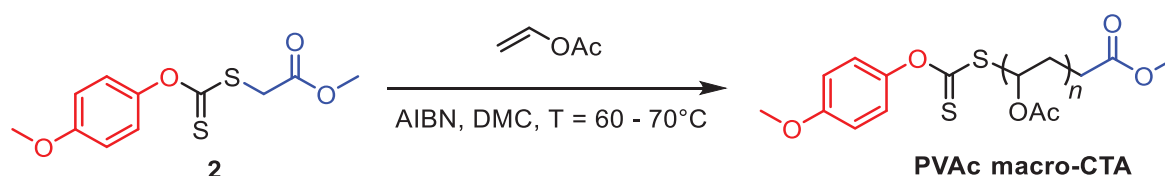


Scheme 1. Illustration of the importance of polymerization order for the synthesis of PVAc-*b*-PE copolymers: start with a PE macro-CTA (a) to obtain PE-*b*-PVAc or start with a PVAc macro-CTA (b) to obtain PVAc-*b*-PE copolymers.

As a general comment, the characterization of the polar-apolar block copolymers obtained during this work was not trivial. The analysis of polymers by SEC or ¹H-NMR requires their complete dissolution. This is easily achieved in THF or CDCl₃ at room temperature for polar polymers, such as PVAc or PMMA but the dissolution of semi-crystalline polyolefins such as PE requires elevated temperatures (HT-SEC, 1,2,4-trichlorobenzene, 150 °C). HT-SEC is however not adapted for polar polymers and the analysis of the same sample *via* SEC-THF and HT-SEC results in the determination of completely different molar masses, even with the same calibration. In some cases, a polar segment of low molar mass was found to be highly retained on the columns and almost “invisible” *via* HT-SEC. The HT-SEC analyses of polar-apolar block copolymers with ethylene gave a molar mass equal to that of the PE segment alone (*vide infra*). This problem is worsened by the formation of aggregates, clearly observed for PMMA-*b*-PE copolymers in chapter **IV**. Although the amount of aggregates (proportional to the intensity of the refractive index in HT-SEC) is low in the conditions under which HT-SEC is carried out, ¹H-NMR analyses are conducted at a substantially lower temperature (90 °C). This could result in a non-negligible fraction of PE blocks being not completely dissolved during the analysis, inducing bias in the integration of the corresponding resonances.

II. Synthesis of PVAc macro-CTAs

The PVAc macroCTAs were synthesized using the phenoxy methoxy xanthate CTA according to **Scheme 2**. The polymerization was performed at either 60 °C or 70 °C in DMC with a [CTA]:[AIBN] ratio of 5:1. The results of the RAFT homopolymerizations of VAc are presented in **Table 1**.



Scheme 2. Synthesis of PVAc macro-CTA with CTA 2.

Table 1. RAFT polymerization of vinyl acetate (VAc) with the phenoxy methoxy xanthate CTA.

Entry	[VAc] (mol L ⁻¹)	T (°C)	Time (min)	Conv. ^e (%)	<i>M</i> _{n,SEC-THF} ^f (g mol ⁻¹)	<i>D</i> ^f	<i>M</i> _{n,HT-SEC} ^g (g mol ⁻¹)	<i>D</i> ^g
1	11	60	60	0	-	-	-	-
2	11	60	120	0	-	-	-	-
3	11	60	180	24	5 550	1.18	-	-
4	11	60	250	34	7 450	1.33	-	-
5	11	60	320	71	13 900	1.69	-	-
6	6.7	70	240	77	11 700	1.77	3 180	1.79
7	2.5	70	100	20	1 350	1.14	330	1.13
8	2.5	70	140	30	1 600	1.17	340	1.08
9	7.7	70	300	86	3 200	1.50	540	1.18

Polymerization conditions: [CTA]:[AIBN] = 5:1, ^a: Bulk, AIBN: 8 mg, ^b: DMC: 50 mL, AIBN: 110 mg, ^c: DMC: 15 mL, AIBN: 110 mg, ^d: DMC: 3 mL, AIBN: 85 mg. ^e: Determined by ¹H-NMR in CDCl₃. ^f: Determined by SEC-THF using conventional PS calibration, corrected by Mark-Houwink parameters. ^g: Determined by HT-SEC using conventional PE calibration.

The controlled character of the polymerization was ascertained (entries 1-5) and different batches of PVAc macroCTAs (with different *M*_n) were synthesized (entries 6-9) for subsequent chain extension. The molar masses of the polymers were determined by SEC-THF using a conventional polystyrene (PS) calibration. *M*_n values were corrected using Mark-Houwink (M-H) parameters of PS ($\alpha = 0.7$, $K = 1.41 \times 10^{-5} \text{ L g}^{-1}$) and PVAc ($\alpha = 0.7$, $K = 1.60 \times 10^{-5} \text{ L g}^{-1}$).^[11] The M-H equation^[12] was then used (**Equation 1**), simplified equation if $\alpha_1 = \alpha_2$ (**Equation 2**).

$$\log(M_2) = \frac{1}{1 + \alpha_2} \log\left(\frac{K_1}{K_2}\right) + \frac{1 + \alpha_1}{1 + \alpha_2} \log(M_1)$$

Equation 1. M-H equation.

$$\log\left(\frac{M_2}{M_1}\right) = \frac{1}{1 + \alpha_2} \log\left(\frac{K_1}{K_2}\right)$$

Equation 2. Simplified M-H equation if $\alpha_1 = \alpha_2$.

A relatively strong inhibition is observed when the polymerization is performed at 60 °C (entries 1-5), which was equally observed by Stenzel *et al.*^[7] with this CTA. The inhibition is slightly less pronounced when the polymerization is performed at 70 °C with lower VAc concentrations (entries 6-9).

Molar masses increase linearly with conversion (**Figure 1a**) and \bar{D} values remain quite low at low conversions. The increase in dispersity value at 71 % conversion ($\bar{D} = 1.69$) is attributed to competitive head-to-head additions that lead to the accumulation of PVAc-CH(OAc)CH₂-SC(=S)-OPh-OMe products as confirmed by ¹H-NMR (**Figure 1b**). A PVAc-CH(OAc)CH₂• radical being less stable than its PVAc-CH₂-CH(OAc)• counterpart, it is less prone to undergo fragmentation upon radical addition. Hence, PVAc-CH(OAc)CH₂-SC(=S)-OPh-OMe accumulates once formed during polymerization. This was not mentioned by Stenzel but is well documented for the RDRP of VAc.^[13-15] In order to limit this phenomenon, keeping a low conversion of VAc is preferable. The analysis of the same PVAc with either SEC-THF or HT-SEC (*via* a conventional calibration using PE standards) gives completely different M_n values (whereas \bar{D} values remain close, **Table 1**). This phenomenon is common when analyzing polar polymer with HT-SEC as it is only adapted for the analysis of apolar polyolefins. The use of calibration using more polar PS standards *via* HT-SEC resulted in absurd \bar{D} values, while the molar masses of the PVAc were too low to be determined with a universal or triple calibration.

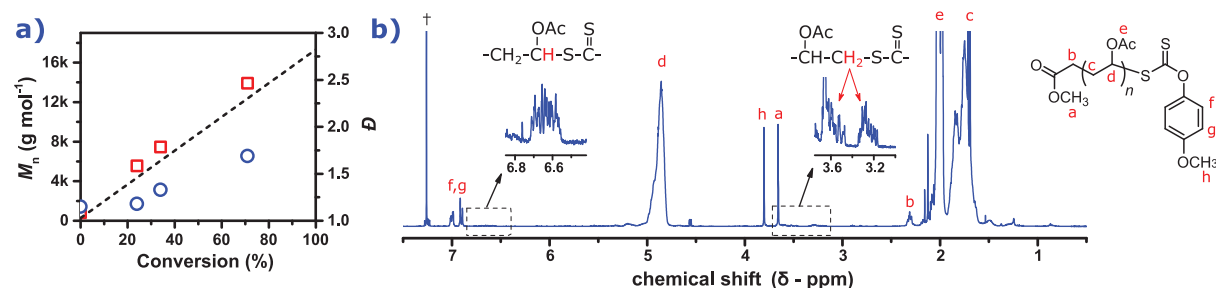


Figure 1. Evolution of M_n (□) and \bar{D} (○) during VAc RAFT homopolymerization corresponding to entries 1-5 in Table 1 (a) and ¹H-NMR analysis of a PVAc macro-CTA (entry 5, Table 1). (†) NMR residual solvent chloroform.

The livingness of the PVAc macro-CTA was ascertained by chain-extension with VAc. PVAc from entry 6 of Table 1 ($M_n = 13\,900$ g mol⁻¹, $\bar{D} = 1.69$) was successfully chain-extended with a second PVAc block after 4 hours of polymerization at 70 °C in bulk using AIBN as initiator [macro-CTA]:[AIBN] ratio = 5). A PVAc-*b*-PVAc polymer was obtained with $M_n = 120\,000$ g mol⁻¹ and $\bar{D} = 2.70$ (**Figure 2**). The apparent large increase in dispersity is most likely again due to head-to-head additions. The MMD obtained after chain-extension is however unimodal and does not show any unreacted PVAc macro-CTA at low molar mass values.

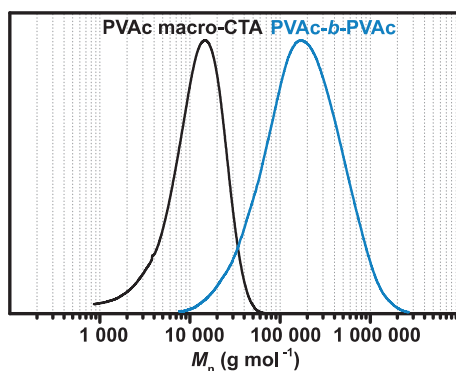


Figure 2. Chain extension of a PVAc macro-CTA (entry 6, Table 1) with another PVAc block to afford a PVAc-*b*-PVAc polymer.

The ease of chain extension of a PVAc macro-CTA obtained with CTA **2** with VAc hints that the chain-extension with ethylene is indeed possible. The propagating macro-radical PVAc• has a reactivity similar to that of an EVA• terminated by a vinyl acetate monomer. In principle, it is therefore possible to initiate ethylene polymerization with PVAc•, hence affording the desired PVAc-*b*-PE copolymer. The presence of PVAc macro-CTAs resulting from both head-to-tail and head-to-head additions (PVAc-CH₂CH(OAc)-SC(S)Z and PVAc-CH(OAc)CH₂-SC(S)Z, respectively) is not expected to be an issue for chain-extension with ethylene as the propagating polyethylenyl radical PE-CH₂CH₂• is the least stable.

III. Synthesis of PVAc-*b*-PE copolymers

III.1. Block copolymerizations at 200 bar

The first attempts to obtain PVAc-*b*-PE copolymers were carried out under similar conditions used for ethylene RAFT homopolymerization in Chapter II: T = 80 °C, P = 200 bar, 50 mL of DMC, [macro-CTA]:[AIBN] ratio of 3:1. The PVAc macro-CTA is completely soluble in DMC at either room temperature or 80 °C. The block copolymerizations were performed using the PVAc from entry 6 in Table 1 ($M_n = 11\,700\text{ g mol}^{-1}$ $\bar{D} = 1.77$. The unreacted VAc was removed under high vacuum) during either 4 or 6 hours. The quantity of AIBN was reduced down to 10 mg to keep the quantity of macro-CTA used for block copolymerization at a reasonable amount.

The HT-SEC traces of the polymers recovered after solvent evaporation are presented in **Figure 3**. The intensity of the MMD corresponding to the PVAc macro-CTA (elution time = 24 minutes) does not decrease as the polymerization proceeds, while a new MMD (elution time = 21 minutes) appears. This new MMD does not shift towards higher values and appears to be similar with that of a PE obtained by conventional FRP at 200 bar. The intensity of this new MMD increases between 4 and 6 hours of polymerization, hinting at an accumulation of dead PE chains. These results indicate that the RAFT chain-end does not participate in the polymerization mechanism. Rather, the PVAc macro-CTA is spectator and only PE homopolymer is produced, as seen *via* HT-SEC.

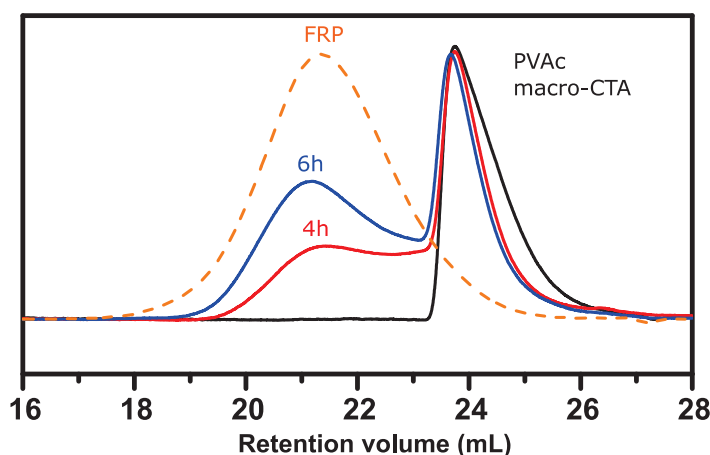


Figure 3. HT-SEC traces of the polymers obtained after chain-extension of a PVAc macro-CTA (from entry 6 of Table 1) with ethylene at 80 °C and 200 bar. AIBN: 15 mg, DMC: 50 mL, PVAc macro-CTA: 4.5 g. (---) corresponds to a PE obtained by FRP after 4 hours of polymerization using 50 mg of AIBN at 80 °C and 200 bar.

While such a phenomenon is typically observed when the order of polymerization is wrong, this is not the case in this instance and the explanation lies elsewhere. This has been attributed to the solubility of the PVAc macro-CTA under the polymerization conditions. Indeed, even though the macro-CTA is completely soluble in DMC at r.t. and 80 °C, the properties of the polymerization

medium dramatically change as ethylene gets dissolved into DMC, in particular above 100 bar, when the ethylene/solvent mixture becomes supercritical.^[16] Experiments performed using the windowed reactor (not routinely used for polymerization) have given insight into what is happening. A solution of PVAc (from entry 6 of Table 1) in DMC (4.5 g PVAc, 50 mL DMC) was transferred into the reactor at 80 °C and ethylene pressure was steadily increased. No AIBN was used for this qualitative experiment. Below 90 bar, the DMC + PVAc solution remains clear and no phase separation occurs. The content of the reactor consists of a liquid phase and a critical ethylene phase (**Figure 4a**). Between 90 and 110 bar, the solution becomes completely turbid and nothing can be seen through the reactor window. Above 110 bar, a demixing occurs and a decanting yellow oil can be observed. The content of the reactor then consists of a supercritical DMC + ethylene phase and a PVAc oil-like phase that accumulates at the bottom of the reactor when the stirring is stopped (**Figure 4b**). The PVAc macro-CTA is thus insoluble in the polymerization mixture when the pressure is above 110 bar, which probably explains why it does not participate during the polymerization and only PE homopolymer is formed.

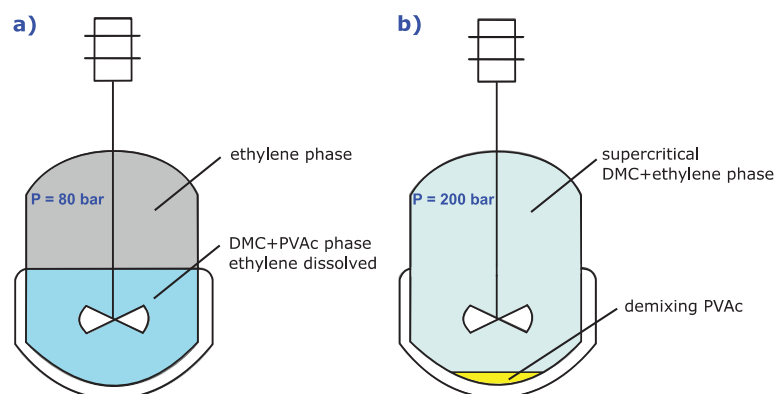


Figure 4. Schematic representation of the physical state of the polymerization mixture at 80 bar (a) and 200 bar (b).

A parallel can be drawn between these observations and the observed segregation of the polymer particles during ethylene homopolymerization with CTA 2 at 200 bar (Chapter II). To address this solubility issue, chain-extensions were attempted at 80 bar, well below the phase transition of the polymerization medium.

The demixing of PVAc was additionally found to be partly related to its molar mass, and block copolymerization could be indeed achieved, to some extent, at 200 bar and using the PVAc macro-CTA with the lowest molar mass (Table 1, entry 7, $M_n = 1\,300\text{ g mol}^{-1}$). The SEC traces are presented in **Figure 5a**. Although the block copolymerization did occur at 200 bar, the tailing at elution volume = 27 mL corresponds to unreacted PVAc macro-CTA, most probably due to incomplete solubility of PVAc at 200 bar, even with such low molar mass. The bimodal aspect of

the PVAc trace is due to the conditions of the HT-SEC on the day of the analysis and was not observed in SEC-THF (**Figure 5b**).

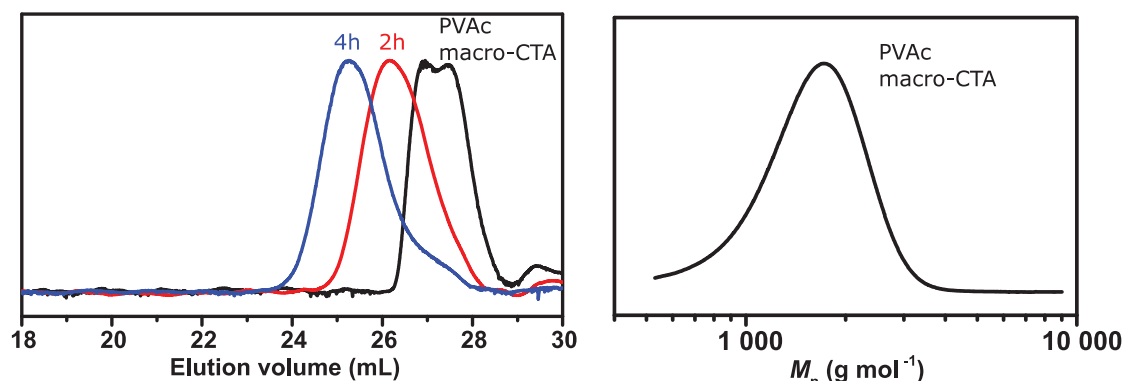


Figure 5. a) HT-SEC traces of PVAc-*b*-PE after chain extension of a low molar mass PVAc macro-CTA (entry 7 of Table 1) at 80 °C and 200 bar. AIBN: 50 mg, DMC: 50 mL, PVAc macro-CTA: 0.95 g. b) MMD of the PVAc macro-CTA obtained *via* SEC-THF.

III.2. Block copolymerizations at 80 bar

Chain extensions of PVAc macro-CTAs with ethylene were then performed at a pressure of 80 bar. Polymerization conditions were otherwise identical than previously: 50 mL of DMC, 25 mg of AIBN, [macro-CTA]:[AIBN] ratio of 3:1. The macro-CTAs used for these experiments have molar masses of $\sim 1\,500\text{ g mol}^{-1}$ and $\sim 3\,200\text{ g mol}^{-1}$, as determined by SEC-THF and $^1\text{H-NMR}$. For the sake of clarity for the rest of this chapter, the PVAc macro-CTA from entry 8 of Table 1 is called **PVAc-1**, whereas the PVAc macro-CTA from entry 9 of Table 1 is called **PVAc-2** (**Figure 6**). The unreacted VAc was removed under high vacuum for these two PVAc.

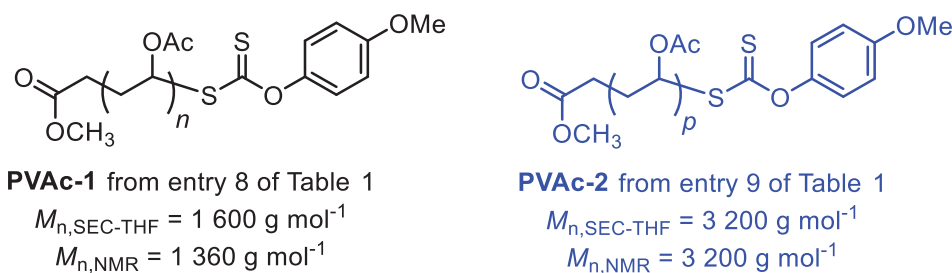


Figure 6. Recall of the characteristics of PVAc-1 (entry 8 of Table 1) and PVAc-2 (entry 9 of Table 1)

The results of the chain-extensions using PVAc-1 and PVAc-2 are presented in **Table 2**.

Table 2. Block copolymerization of ethylene with PVAc macro-CTAs at 80 bar at 80 °C.

Entry	macro-CTA	Time (h)	Yield of PE (g)	$M_{n,theo}^a$ PE block (g mol ⁻¹)	$M_{n,theo}^b$ diblock (g mol ⁻¹)	$M_{n,HT-SEC}^c$ (g mol ⁻¹)	\bar{D}^c	$M_{n,NMR}^d$ (g mol ⁻¹)
10 (8)	PVAc-1	-	-	-	-	340	1.08	1 360
11	PVAc-1	1	0.37	800	2 400	1 100	1.39	2 360
12	PVAc-1	3	1.00	2 200	3 800	2 000	1.51	4 000
13	PVAc-1	5	1.39	3 000	4 600	2 400	1.55	4 850
14 (9)	PVAc-2	-	-	-	-	540	1.18	3 200
15	PVAc-2	1	0.45	1 330	4 500	1 500	1.59	4 550
16	PVAc-2	2	0.60	1 800	5 000	2 100	1.75	4 800
17	PVAc-2	3	0.75	2 200	5 400	2 100	1.82	5 120
18	PVAc-2	4	0.99	3 000	6 200	2 400	1.84	6 450

Block copolymerization conditions: T = 80 °C, P = 80 bar, DMC: 50 mL, AIBN: 25 mg, [macro-CTA]:[AIBN] = 3:1

^a: Determined from yield of PE: $M_n = \text{Yield of PE (g)} / n_{\text{macro-CTA (mol)}}$; ^b: Determined from yield of PE and $M_{n,NMR}$ of PVAc block: $M_n = \text{Yield of PE (g)} / n_{\text{macro-CTA (mol)}} + M_{n,macro-CTA} \text{ (g mol}^{-1}\text{)}$ with $M_{n,macro-CTA}$ determined by SEC-THF using PS calibration and corrected by M-H parameters; ^c: Determined by HT-SEC using conventional PE calibration; ^d: Determined by ¹H-NMR in TCE/C₆D₆ (2:1 v:v) at 90 °C using equation 3.

The polymerization rate of ethylene polymerization using either macro-CTA appears to be roughly the same and is about half the value of the conventional radical polymerization of ethylene using the same AIBN quantity at the same pressure (**Figure 7**). Unsurprisingly, this is similar to what was observed for ethylene homopolymerization using CTA 2 at 80 bar (Chapter II). The presence of PVAc thus appears to have little effect on the polymerization rate.

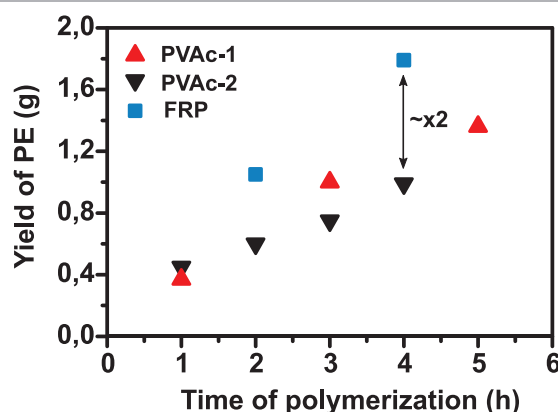
**Figure 7. Yields of PE during polymerization of ethylene in the presence of PVAc macro-CTAs at 80 bar and 80 °C. The yields obtained in the absence of macro-CTA are also plotted for comparison.**

Figure 8 presents the HT-SEC traces of the block copolymerizations using PVAc-1 (**a**) and PVAc-2 (**b**) at a pressure of 80 bar. The clean shift of the MMD towards higher values indicates successful block copolymerization, while the MMD corresponding to the macro-CTAs completely disappears in both cases, even for a polymerization time as low as 1 hour. Nevertheless, the polar-apolar nature of the block copolymers proved to be an issue for the determination of their molar masses by HT-SEC, as already mentioned in paragraph I. Conventional PE calibration tends to give M_n values very close to what is expected for the PE block alone (**Figure 8c, d**) whereas triple and universal calibrations are not adapted for low molar mass polymers. In both cases, \bar{D} values increase at the beginning of the polymerization and reach a plateau value (~ 1.5 with PVAc-1 and ~ 1.8 with PVAc-2). Noteworthy, \bar{D} values are obtained with the PE conventional calibration and

might not be accurate for the block copolymers. The determination of M_n by $^1\text{H-NMR}$ (**Figure 9**) using **Equation 3** eventually gave molar masses values in close agreement with what is theoretically expected for the diblock copolymers (**Figure 8c, d**).

$$M_{n,NMR} = M_{n,PVAc} + \frac{\frac{1}{4} \int_{1.10}^{1.50} (\text{CH}_2\text{CH}_2)_p}{\int_{4.80}^{5.20} (\text{CH}_2\text{CH}(\text{OAc}))_n} * MW(\text{C}_2\text{H}_4)$$

Equation 3. Determination of $M_{n,NMR}$ of PVAc-*b*-PE copolymers by $^1\text{H-NMR}$.

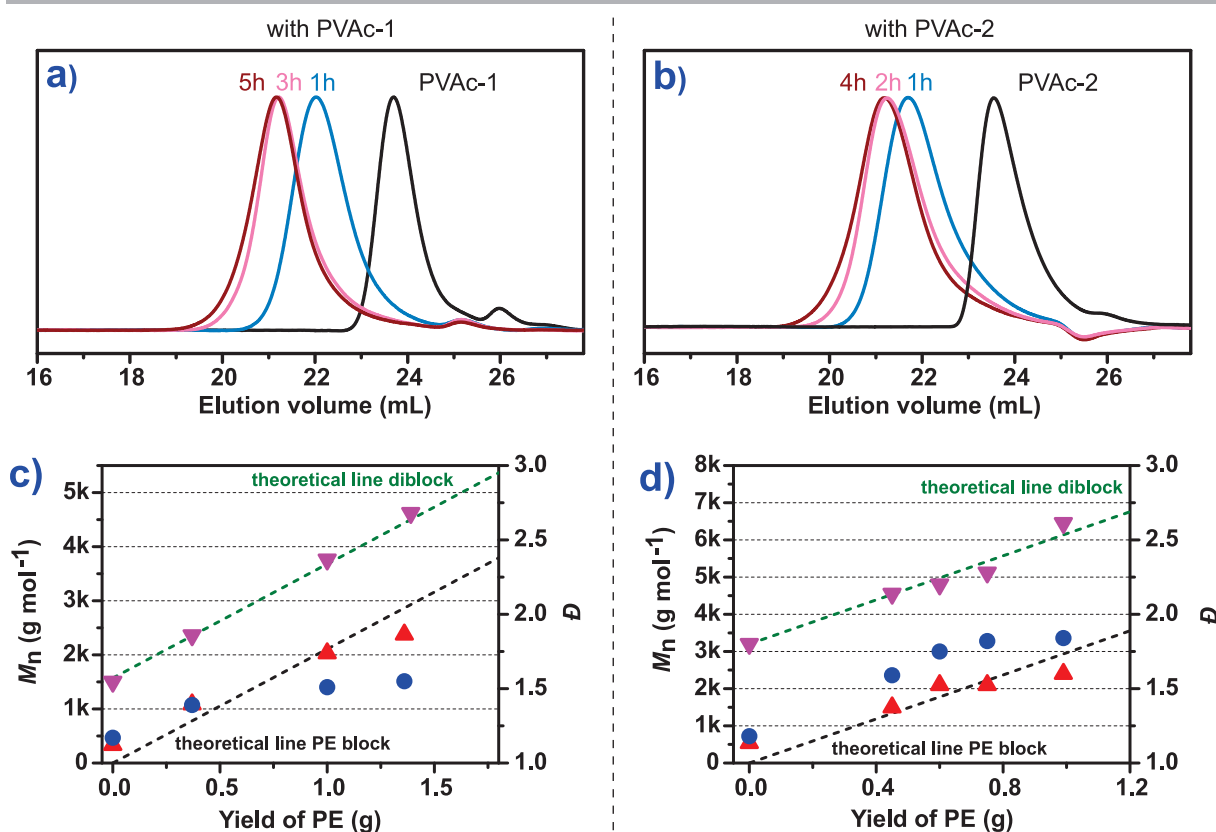


Figure 8. HT-SEC traces of PVAc-*b*-PE copolymers obtained with PVAc macro-CTAS PVAc-1 (a) and PVAc-2 (b), and evolution of their $M_{n,NMR}$ (▼), $M_{n,HT-SEC}$ (▲) and \bar{D} (●) values (c) and (d) for PVAc-1 and PVAc-2, respectively. The dashed lines correspond to $M_{n,theo}$ of the diblock copolymer (---) and $M_{n,theo}$ of the PE block (---).

From these results, it is clear that performing the polymerization at an ethylene pressure of 80 bar instead of 200 bar addressed the solubility issue of the PVAc macro-CTA and block copolymers could be obtained. $^1\text{H-NMR}$ analyses were performed on all PVAc-*b*-PE copolymers, of which an exemplary spectrum is shown in **Figure 9**. $^1\text{H-NMR}$ does not categorically confirm the successful block copolymerization, but strongly hints at its success. Indeed, the characteristic signals of the last VAc unit before the PE block (PVAc-CH₂CH(OAc)-CH₂CH₂-PE, proving the initiation of the PE block by PVAc*) most likely overlaps with other signals (simulated by Chemdraw at the same chemical shift of the VAc repeating units), making its detection impossible.

However, the emergence of the characteristic protons PE-CH₂-CH₂-SC(=S)Z ($\delta = 3.11$ ppm, **d** in **Figure 9a**) proves that at least several ethylene units are linked to a xanthate moiety (while the characteristic proton PVAc-CH₂-CH(OAc)-SC(=S)Z ($\delta = 6.70$ ppm, **d** in **Figure 9b**) disappears. The ratio of the relative integrations of the protons of the α ($\delta = 2.17$ ppm) and ω ($\delta = 3.11$ ppm) chain-ends is close to unity for short polymerization times, greatly hinting at the successful block copolymerization. Cross-termination products (*) are also detected and accumulate during polymerization, which is not surprising as they are formed during RAFT polymerization of ethylene with this CTA. The chain-end fidelity thus decreases as the polymerization proceeds, as it was observed for ethylene RAFT homopolymerization with **2** (see Chapter II). Those observations are applicable for both series of PVAc-*b*-PE copolymers from PVAc-1 and PVAc-2.

The combination of both HT-SEC and ¹H-NMR analyses is a proof that the block copolymerization occurs and that, for the first time, a true PVAc-*b*-PE block copolymer was created by sequential monomer addition and using the same polymerization mechanism.

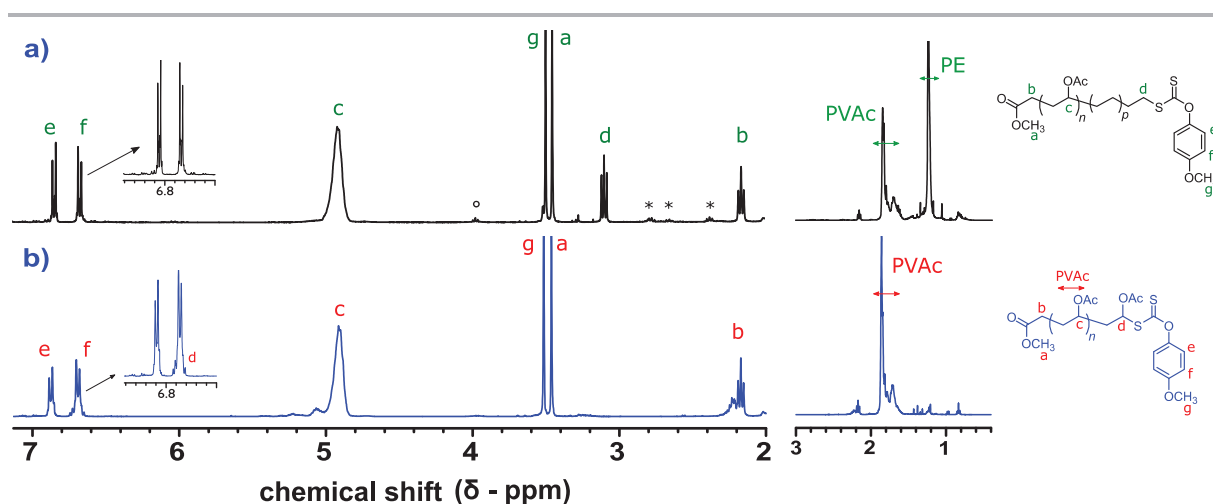


Figure 9. ¹H-NMR analysis of PVAc-*b*-PE obtained after 1 hour of polymerization (entry 11 Table 2) (a) and starting PVAc macro-CTA (entry 10 Table 2) (b).

The PVAc macro-CTA of the highest molar mass (11 700 g mol⁻¹, entry 6 of **Table 1**) that was unsuccessfully used for block copolymerization with ethylene at 200 bar was used for chain-extension at 80 bar during 4 hours to confirm the solubility theory. The quantity of AIBN, macro-CTA and DMC were identical to those used for the experiments at 200 bar (part III.1).

Compared to the block copolymerization at 200 bar that featured a bimodal trace with unreacted PVAc macro-CTA and a new MMD corresponding to PE homopolymer, the trace from the block copolymerization at 80 bar is unimodal and does not show unreacted PVAc macro-CTA (**Figure 10a**). The MMD shifts towards higher values and is intermediate between that of the starting macro-CTA and of a PE homopolymer produced by conventional radical polymerization. The unusual broadness and shape of the distribution the polymer obtained after 4 hours of polymerization can be explained by the fact that HT-SEC analyses were not performed on the same

day. Furthermore, the macro-CTA was stored for nearly two years at room temperature without any particular precautions (e.g. light protection), and a possible degradation cannot be excluded.

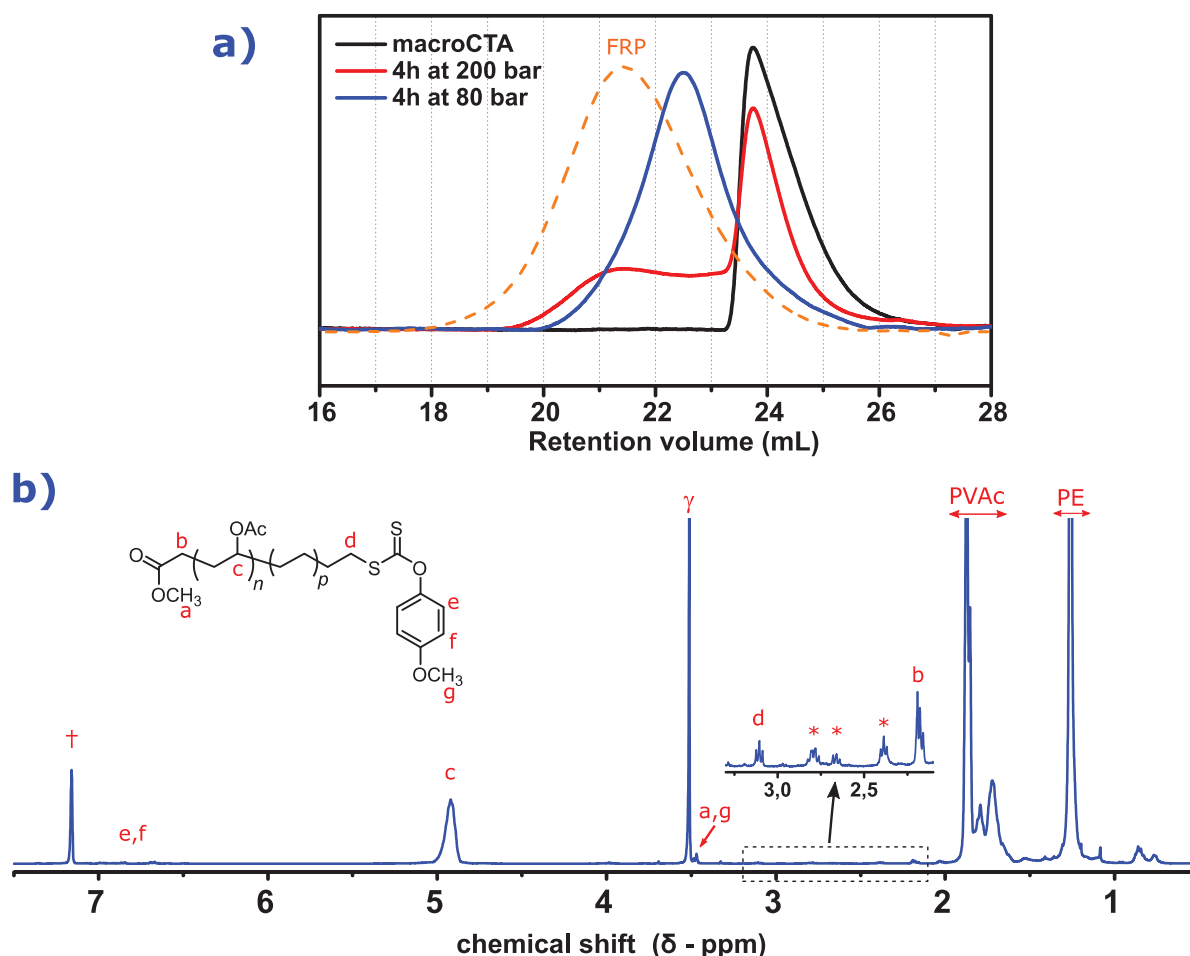


Figure 10. HT-SEC traces of block copolymerizations of the PVAc macro-CTA from entry 6 of Table 1 with ethylene at 80 and 200 bar (a) and $^1\text{H-NMR}$ spectrum of the block copolymer obtained at 80 bar (b). †: NMR residual solvent benzene, γ : polymerization solvent DMC.

$^1\text{H-NMR}$ analysis confirms the emergence of the characteristic protons $\text{PE-CH}_2\text{-CH}_2\text{-SC(=S)Z}$ ($\delta = 3.11$ ppm, **d** in **Figure 10b**). The relative integration of the PVAc block ($\delta = 4.9$ ppm, $DP_{n,\text{PVAc}} = 133$) and of the PE block ($\delta = 1.25$ ppm, $DP_{n,\text{PE}} = 247$) gives a molar mass for the PVAc-*b*-PE copolymer of $M_{n,\text{NMR}} = 18\,350$ g mol $^{-1}$, close to $M_{n,\text{theo}} = 18\,400$ g mol $^{-1}$ calculated from the yield of PE (0.87 g).

III.3. Thermal properties of PVAc-*b*-PE copolymers.

Differential scanning calorimetry (DSC) analyses were performed on PVAc-*b*-PE copolymers. The glass transition temperatures (T_g), melting and crystallization temperatures (T_m/T_c) are reported in **Table 3**. The thermograms of the second heat cycle and second cooling for each series (from macro-CTAs PVAc-1 and PVAc-2) are presented in **Figure 10**.

Table 3. Thermal analysis of PVAc-*b*-PE copolymers via DSC.

Entry	macro-CTA (time of polym.)	Yield of PE (g)	$M_{n,PE}^a$ (g mol ⁻¹)	T_g (°C)	T_m (°C)	T_c (°C)
10 (8)	PVAc-1 (-)	-	-	10	-	-
11	PVAc-1 (1 h)	0.37	800	2	99	92
12	PVAc-1 (3 h)	1.00	2 200	-8	106	98
13	PVAc-1 (5 h)	1.39	3 000	-14	106	98
14 (9)	PVAc-2 (-)	-	-	25	-	-
15	PVAc-2 (1 h)	0.45	1 300	23	105	96
16	PVAc-2 (2 h)	0.60	1 800	22	110	102
17	PVAc-2 (3 h)	0.75	2 200	18	111	102
18	PVAc-2 (4 h)	0.99	3 000	25	112	103

^a: molar mass of the PE block determined by ¹H-NMR

Block copolymers from PVAc with a low molar mass (PVAc-1, $M_n = 1\,600\text{ g mol}^{-1}$) do not have the same thermal behavior as those from a higher molar mass PVAc (PVAc-2, $M_n = 3\,200\text{ g mol}^{-1}$). For the series with PVAc-1, the glass transition temperature of the PVAc block diminishes from 10 to -14 °C as the molar mass of the PE block increases. Similar behavior has been observed for poly(styrene-*co*-butadiene)-*block*-polystyrene copolymers, where the T_g of the polystyrene block decreased by up to 40 °C when its molar mass diminished. This was attributed to decreasing polystyrene domain sizes (proportional to molar mass) and nanoscale confinement.^[17] It is possible that a similar phenomenon happens in this case, with the confinement of the low molar mass PVAc block (or, conversely, the confinement of the PE block) getting more pronounced as the molar mass of the PE block increases. This is further supported by the presence of a small second crystallization peak at 49 and 53 °C (entries 12 and 13, respectively), not present in a typical PE homopolymer (dashed line in **Figure 11a, top**). Polyethylenes with low crystallization temperatures have already been observed for PE confined in small size domains (ZN catalysts pores,^[18] particles from emulsion polymerization,^[19-21] block copolymers^[22-24]). The lower T_c observed for copolymers from entries 10-13 (compared to ~100-110 °C for LDPE^[25]) can be explained by a favored nucleation with respect to crystal growth, resulting in smaller crystalline regions with lower T_c .

This is not observed for the series with PVAc-2, for which the T_g of the PVAc block remains rather constant regardless of the molar mass of the PE block. However, this series features of second small crystallization peak at 69 °C for all block copolymers (**Figure 11b**), indicating probable nano-confinement. This series also features fusion and crystallization temperatures

systematically about 5 °C higher than for the PVAc-1 series at similar molar masses of the PE block. These differences could be due to the change of molar mass of the PVAc block, but a third set of experiments using a PVAc macro-CTA of molar mass either intermediate or higher to PVAc-1 and PVAc-2 would be needed for confirmation.

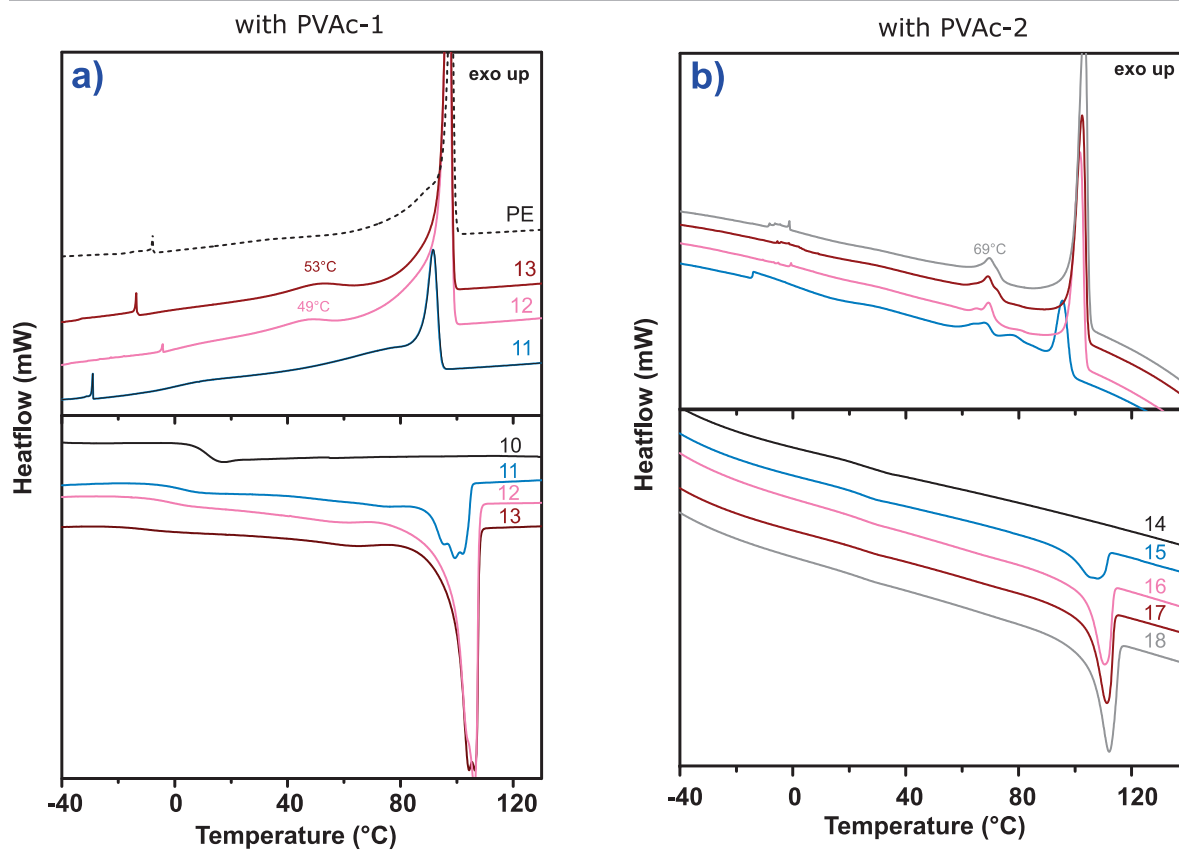


Figure 11. Thermograms of PVAc-*b*-PE copolymers (entries 10-13) of Table 3. Second heating cycle (a) and second cooling cycle (b). The dashed line (---) corresponds to a PE homopolymer obtained by RAFT polymerization (80 °C, 80 bar, 4 h). Numbers correspond to the entries of Table 3.

IV. Conclusion

The synthesis of PVAc-*b*-PE copolymers was achieved at a pressure of 80 bar using a xanthate functionalized PVAc macro-CTA, and well-defined block copolymers were obtained for the first time by sequential monomer addition (VAc then ethylene). The ethylene pressure and physical state of the polymerization medium is of paramount importance for the success of the block copolymerization. At 200 bar, the polymerization medium is in a supercritical state and the polar PVAc macro-CTA is insoluble. This results in the conventional free radical polymerization of ethylene and mixtures of homopolymers are obtained. This was circumvented by performing the block copolymerization at a pressure lower than 100 bar, corresponding to the threshold at which the polymerization medium becomes supercritical.

High temperature size-exclusion chromatography was found to be poorly adapted for the determination of molar masses and dispersity values of the block copolymers created. HT-SEC nevertheless provided valuable information towards the evolution of the molar mass distributions of the polymeric materials. Upon block copolymerization, the MMDs of the PVAc-*b*-PE copolymers cleanly shifted towards higher values and stayed relatively narrow, while the M_n of the block copolymers could be determined by $^1\text{H-NMR}$ analysis and were remarkably close to theoretical values. Thermal analysis of a series of PVAc-*b*-PE copolymers revealed, in some cases, a drop in the T_g value of the PVAc segment as the molar mass of the PE block increases. The presence of two crystallization temperatures ($\sim 50\text{-}70\text{ }^\circ\text{C}$ and $110\text{ }^\circ\text{C}$) is attributed to potential confinement in small size domains.

The difficulty of characterization of the PVAc-*b*-PE copolymers, linked to their incompatible polar-apolar nature, can be of potential interest in other areas. Indeed, incompatible block copolymers are known to exhibit self-assembly properties. While the self-assembly properties of PVAc-*b*-PE copolymers were not investigated in this chapter, they will be developed in the following. Noteworthy, the PVAc block of these copolymers could be potentially hydrolyzed to obtain amphiphilic PVOH-*b*-PE copolymers, materials with *a priori* interesting properties. This was attempted but the resulting materials proved to be completely insoluble in the solvents used for SEC and NMR analyses. This is another example of the difficulty of synthesis and characterization of block copolymers with opposite polarities, especially if one block is a semi-crystalline polyolefin. The hydrolysis of the PVAc block to attain a new class of materials is however an avenue worth exploring.

Ultimately, suitable polymerization conditions for the synthesis of polar olefin block copolymers with ethylene were found. In the following chapters, HT-SEC analysis will be used to follow the MMDs evolution upon block copolymerizations, whereas $^1\text{H-NMR}$ will be used to determine the molar masses of the block copolymers.

V. Experimental section

Materials and methods

The comprehensive list of materials and analytical methods used for this work are presented at the end of this manuscript.

Typical procedure for the synthesis of PVAc macro-CTAs

VAc, AIBN, CTA 2 and DMC were introduced in a Schlenk flask to the desired quantities according to Table 1. The solution was degassed by three freeze-vacuum-thaw cycles, filled with argon and immersed in an oil bath pre-heated to the desired temperature. Where appropriate, aliquots were removed at different time intervals to follow monomer conversion by $^1\text{H-NMR}$ and molar masses evolution by SEC-THF. After the desired time, the reaction mixture was rapidly cooled down in an ice bath and the volatiles were removed *in vacuo*. The resulting PVAc macro-CTAs were analyzed by $^1\text{H-NMR}$, SEC-THF and HT-SEC and used for block copolymerization with ethylene after the complete removal of unreacted VAc under high vacuum.

Typical block copolymerization procedure

The employed autoclave reactor (160 mL) was equipped with a mechanical stirring apparatus, a thermometer, and a pressure sensor. In a typical polymerization procedure, a degassed solution of AIBN (25 mg, 3.1 mmol L⁻¹, 1 eq.) and a PVAc macro-CTA (9.3 mmol L⁻¹, 3 eq.) in DMC (50 mL) was added to the reactor preheated to 80 °C under argon atmosphere with a mechanical stirring of 600 rpm. Immediately after the injection port was closed, ethylene gas was fed into the reactor until the targeted pressure of either 80 or 200 bar was reached. This took a few seconds for experiments at 80 bar and about 4 min for experiments at 200 bar. If necessary, additional ethylene gas was introduced to keep a constant pressure during the polymerization. After a predetermined period of time, the stirring was slowed down and the reactor was cooled with iced water. When the temperature inside the reactor dropped below 25 °C, the remaining pressure was carefully released. The content of the reactor was collected with toluene, and evaporation of the solvent gave the polymeric product.

VI. References

- [1] S. Borkar, A. Sen, *J. Polym. Sci. Part A Polym. Chem.* **2005**, *43*, 3728–3736.
- [2] A. Zarrouki, E. Espinosa, C. Boisson, V. Monteil, *Macromolecules* **2017**, *50*, 3516–3523.
- [3] C. Dommanget, F. D’Agosto, V. Monteil, *Angew. Chem. Int. Ed.* **2014**, *53*, 6683–6686.
- [4] A. Debuigne, J. R. Caille, C. Detrembleur, R. Jérôme, *Angew. Chemie - Int. Ed.* **2005**, *44*, 3439–3442.
- [5] Q. B. Chen, T. Y. Zeng, L. Xia, Z. Zhang, C. Y. Hong, G. Zou, Y. Z. You, *Chem. Commun.* **2017**, *53*, 10780–10783.
- [6] H. Wang, F. Xu, K. Cui, H. Zhang, J. Huang, Q. Zhao, T. Jiang, Z. Ma, *RSC Adv.* **2017**, *7*, 42484–42490.
- [7] M. H. Stenzel, L. Cummins, G. E. Roberts, T. P. Davis, P. Vana, C. Barner-Kowollik, *Macromol. Chem. Phys.* **2003**, *204*, 1160–1168.
- [8] M. Destarac, D. Charmot, X. Franck, S. Z. Zard, *Macromol. Rapid Commun.* **2000**, *21*, 1035–1039.
- [9] V. Malepu, C. D. Petruczok, D. A. Shipp, *J. Polym. Sci. Part A Polym. Chem.* **2008**, 7200–7206.
- [10] C. Dommanget, Polymérisation Radicalaire Contrôlée : Le Défi de l’éthylène, **2013**.
- [11] F. Cane, T. Capaccioli, *Eur. Polym. J.* **1978**, *14*, 185–188.
- [12] R. J. Houwink, *J. Prakt. Chem.* **1940**, *157*, 15–18.
- [13] A. N. Morin, C. Detrembleur, C. Jérôme, P. De Tullio, R. Poli, A. Debuigne, *Macromolecules* **2013**, *46*, 4303–4312.
- [14] N. De Rybel, P. H. M. Van Steenberge, M.-F. Reyniers, D. R. D’hooge, G. B. Marin, *Macromolecules* **2019**, *52*, 4555–4569.
- [15] M. Guerre, S. M. Wahidur Rahaman, B. Améduri, R. Poli, V. Ladmiral, *Polym. Chem.* **2016**, *7*, 6918–6933.
- [16] E. Grau, J. P. Broyer, C. Boisson, R. Spitz, V. Monteil, *Phys. Chem. Chem. Phys.* **2010**, *12*, 11665–11669.
- [17] C. G. Robertson, T. E. Hogan, M. Rackaitis, J. E. Puskas, X. Wang, *J. Chem. Phys.* **2010**, *132*, 1049041–1049045.
- [18] E. Tioni, V. Monteil, T. McKenna, *Macromolecules* **2013**, *46*, 335–343.
- [19] F. M. Bauers, R. Thomann, S. Mecking, *J. Am. Chem. Soc.* **2003**, *125*, 8838–8840.
- [20] C. N. Rochette, S. Rosenfeldt, K. Henzler, F. Polzer, M. Ballauff, Q. Tong, S. Mecking, M. Drechsler, T. Narayanan, L. Harnau, *Nano Lett.* **2007**, *7*, 2024–2029.
- [21] G. Billuart, E. Bourgeat-Lami, M. Lansalot, V. Monteil, *Macromolecules* **2014**, *47*, 6591–6600.
- [22] Y. L. Loo, R. A. Register, A. J. Ryan, *Phys. Rev. Lett.* **2000**, *84*, 4120–4123.
- [23] Y. L. Loo, R. A. Register, A. J. Ryan, G. T. Dee, *Macromolecules* **2001**, *34*, 8968–8977.
- [24] Y. L. Loo, R. A. Register, A. J. Ryan, *Macromolecules* **2002**, *35*, 2365–2374.
- [25] K. M. Drummond, J. L. Hopewell, R. A. Shanks, *J. Appl. Polym. Sci.* **2000**, *78*, 1009–1016.

Chapter IV

Synthesis of block copolymers based on ethylene and methyl methacrylate

I. Introduction.....	162
II. Synthesis of PMMA-<i>b</i>-PE using a switchable dithiocarbamate...	165
II.1. Synthesis of PMMA macro-CTA with 6-H ⁺	165
II.2. Chain extension of PMMA-6 with ethylene.....	167
II.3. Self-assembly of PMMA- <i>b</i> -PE copolymers in DMC.....	170
III. Synthesis of PMMA-<i>b</i>-PE by successive FRP and RAFT polymerization.....	173
III.1. Determination of the chain transfer constant.....	174
III.2. Synthesis of PMMA-T with TD.....	175
III.2.1. Chain-end analysis.....	176
III.2.2. Chain-extension with vinyl acetate.....	178
III.3. Chain extension of PMMA-T with ethylene.....	179
III.4. Self-assembly of PMMA- <i>b</i> -PE.....	184
IV. Conclusion	186
V. Experimental section	188
VI. References	190

I. Introduction

As demonstrated in Chapter II, dithiocarbamate CTAs (**3**, **5-7**, **Figure 1**) proved to be the most efficient for the RAFT polymerization of ethylene. These CTAs were set aside when investigating the synthesis of PVAc-*b*-PE copolymers because the control over the synthesis of the PVAc segment was unsatisfactory. On the other hand, dithiocarbamates, especially the switchable ones (**5-7**), are particularly interesting when it comes to the synthesis of block copolymers employing monomers with different reactivities (MAMs vs. LAMs).^[1] It was thus attempted to use dithiocarbamates to obtain PMMA-*b*-PE copolymers, based on existing works in the literature and the work described in Chapter II. In the following, the methods used in the literature to obtain a PMMA functionalized by a dithiocarbamate (capable of controlling ethylene polymerization) will be surveyed.

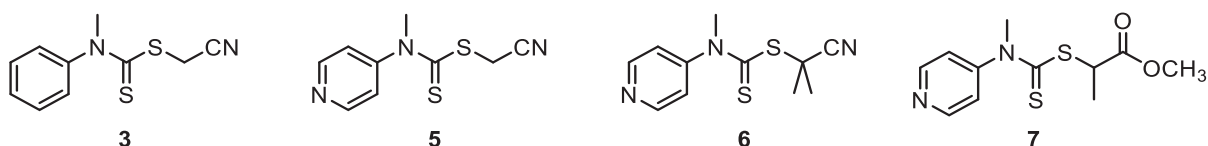
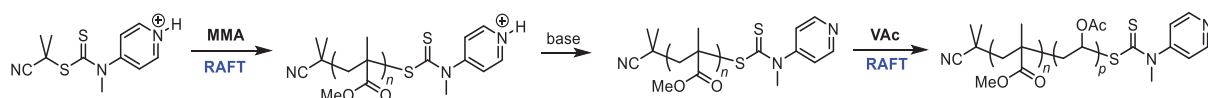


Figure 1. Dithiocarbamates used in Chapter II for the RAFT polymerization of ethylene.

The synthesis of block copolymers based on MAMs (such as MMA) and LAMs (such as ethylene) has long been a challenging area and examples of syntheses of poly(MAM)-*b*-poly(LAM) copolymers *via* RDRP processes are scarce.^[2] TERP and Organostibine/bismuth-mediated living radical polymerization are the most adapted to the synthesis of such block copolymers^[3] and have been used to produce well-defined PS-*b*-PNVP and PMMA-*b*-PNVP.^[4] The use of Te, Sb and Bi atoms however make these techniques quite uncommon. On the other hand, RAFT polymerization has been frequently used and stands out as one of the most robust and versatile processes for the preparation of such block copolymers. Switchable CTAs such as *N*-methyl-*N*-(4-pyridinyl)^[5-7] and *N*-aryl-*N*-(4-pyridinyl)^[1] dithiocarbamates control either MAMs (MMA, MA, DMA and styrene) upon protonation by a strong acid, or LAMs (VAc, NVP and *N*-vinylcarbazole (NVC)) after deprotonation by a base.

Considering that ethylene and VAc have similar reactivities, it can be safe to assume that systems allowing the synthesis of PMMA-*b*-PVAc copolymers might allow to achieve PMMA-*b*-PE copolymers. To the best of our knowledge, only two examples for the synthesis of PMMA-*b*-PVAc by RAFT exist, *via* the use of (i) switchable dithiocarbamates (**Scheme 1**) by Moad *et al.*^[5] or (ii) fluorinated xanthates in a semi-batch emulsion process by Destarac *et al.*^[8] For ethylene, the use of fluorinated xanthates ($Z = \text{OCH}_2\text{CF}_3$) has not been considered as this could potentially lead to the same side-fragmentation than with $Z = \text{OCH}_2\text{CH}_3$. What is more, the conditions used by Destarac *et al.* (semi-batch emulsion) were deliberately tuned and optimized for a system

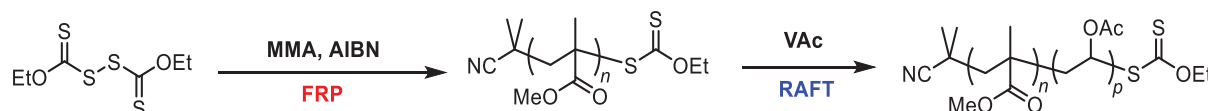
involving the use of MMA in water and would not be suitable for block copolymerization in organic solvent. This limited number of methods to prepare PMMA-*b*-PVAc *via* RDRP (and, consequently, PMMA-*b*-PE) has led us to consider alternative options.



Scheme 1. Synthesis of PMMA-*b*-PVAc by RAFT polymerization with a switchable dithiocarbamate as described by Moad *et al.*^[5]

Early works on iniferters by Otsu^[9,10] have shown that it is possible to use a dithiuram disulfide ($R_1R_2NC(S)SSC(S)NR_3R_4$) or xanthogen disulfide ($R_1OC(S)SSC(S)OR_2$) as irreversible chain transfer agents during conventional free radical polymerizations of vinyl monomers. These CTAs were used to obtain polymers functionalized by either one (ω -functionalized, $f = 1$) or two (α,ω -functionalized, $f = 2$) dithiocarbamate/xanthate chain-end(s). These polymers can then be used as macro-CTA for the synthesis of block copolymers.^[11-14]

Subsequent developments in this field^[15] have made possible the synthesis of PMMA-*b*-PVAc by using a xanthogen disulfide CTA, used to obtain a xanthate-functionalized PMMA *via* FRP and irreversible transfer, subsequently chain-extended with VAc *via* a RAFT mechanism as depicted by **Scheme 2**. Although versatile, this kind of systems have not been studied in detail since. On the side note, conclusions about xanthate functionality f differ depending on authors. Niwa *et al.*^[11] determined a f value close to 2 by UV analysis, whereas Catala^[15] and Zhang *et al.*^[16] hypothesized a f value of 1.

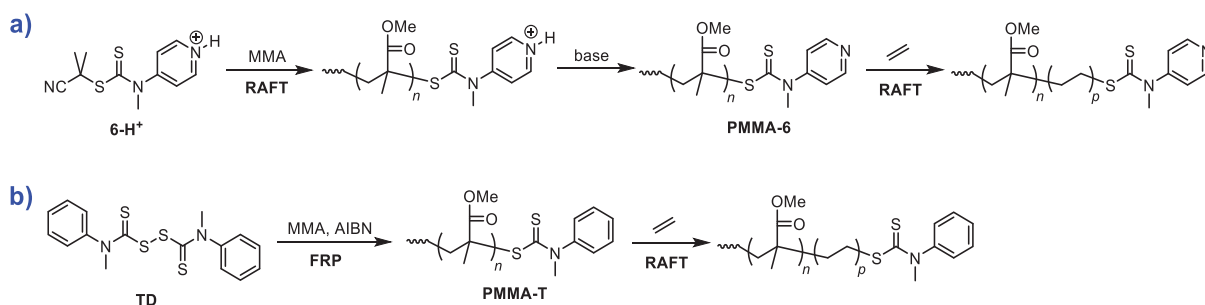


Scheme 2. Synthesis of PMMA-*b*-PVAc by successive FRP of MMA and RAFT polymerization of VAc.^[15]

The use of xanthogen disulfide is not advantageous in our case as this would lead to side-fragmentation when ethylene is used.^[17,18] We thus attempted to use the same strategy as Catala,^[15] but by replacing the xanthogen disulfide by a thiuram disulfide, which has never been described in the literature. The thiuram disulfide investigated (**TD**, **Scheme 3b**) has a Z-group ($Z = N(Ph)Me$) identical to that of CTA **3** used in Chapter II, which has been shown to be efficient at controlling ethylene polymerization. We thus expect that a macro-CTA bearing this Z-group would be suitable for the synthesis of block copolymers with ethylene.

Hence, the synthesis of PMMA-*b*-PE copolymers was attempted using a dithiocarbamate-functionalized PMMA obtained by the two previously described methods:

- (i) use of a switchable dithiocarbamate (**6-H⁺**, **Scheme 3a**) to obtain **PMMA-6** (**Scheme 3a**)
- (ii) use of a thiuram disulfide (**TD**) to obtain **PMMA-T** (**Scheme 3b**)



Scheme 3. Strategies adopted for the synthesis of PMMA-*b*-PE by RAFT polymerization using a switchable dithiocarbamate (a) or by successive FRP and RAFT polymerization using a thiram disulfide (TD) (b).

The first part of this chapter will present the results obtained with the switchable dithiocarbamate, inspired from the work of Moad *et al.*^[5] The synthesis of PMMA-T by conventional FRP was achieved through a collaboration with Prof. Mathias Destarac and Dr. Simon Harrisson at the IMRCP group in Toulouse (Université Paul Sabatier, Toulouse III). The synthesis, determination of functionality and the use of this PMMA macro-CTA for block copolymerization with ethylene will be presented in the second part of this chapter.

The issues evoked in chapter II about the difficulties of characterization of the polar-apolar block copolymers apply in this chapter too. Even more so as aggregates were detected for the first time with PMMA-*b*-PE copolymers. This results in the determination of the molar masses by ¹H-NMR being not completely accurate and trustworthy, especially in the paragraph III.3 of this chapter.

II. Synthesis of PMMA-*b*-PE using a switchable dithiocarbamate

II.1. Synthesis of PMMA macro-CTA with 6-H⁺

The synthesis of the PMMA macro-CTA (**PMMA-6**, **Scheme 3**) using the switchable (and commercially available) dithiocarbamate **6-H⁺** as described by Moad *et al.*^[5] was first attempted using the same experimental conditions: T = 60 °C, [MMA]/[CTA]/[AIBN] ratio = 300/1/0.3, solvent: acetonitrile. The strong acid used (Trifluoromethane sulfonic acid, TfOH) was mistakenly added in a slight excess (1.5 eq. instead of 1.0 eq.). The results of the polymerization are presented in **Table 1** (entries 1-4).

Table 1. Polymerization of MMA in the presence of 6-H⁺ in acetonitrile.

Entry	Time (h)	Conversion ^c (%)	$M_{n,theo}^d$ (g mol ⁻¹)	$M_{n,SEC-THF}^e$ (g mol ⁻¹)	\bar{D}^e
1 ^a	1	0	-	-	-
2 ^a	3	7	2 440	66 590	1.32
3 ^a	5	16	5 250	63 220	1.41
4 ^a	19	100	31 460	66 340	1.40
5 ^b	1.5	37	1 330	2 620	1.50
6 ^b	3	72	2 360	3 620	1.44
7 ^b	4	84	2 700	4 500	1.35
8 ^b	20	100	3 170	5 320	1.31
9 ^b	20	100	3 170	6 250 ^f	1.21 ^f

^a: T = 60°C, [MMA] = 6.57 mmol L⁻¹, [CTA] = 0.021 mmol L⁻¹, [AIBN] = 0.007 mmol L⁻¹, [TfOH] = 0.035 mmol L⁻¹

^b: T = 70°C, [MMA] = 6.25 mmol L⁻¹, [CTA] = 0.21 mmol L⁻¹, [AIBN] = 0.07 mmol L⁻¹, [TfOH] = 0.20 mmol L⁻¹

^c: Determined by ¹H-NMR in CDCl₃

^d: Determined from conversion of MMA: $M_{n,theo} = ([MMA]/[CTA]) * MW(MMA) * Conversion + MW(CTA)$

^e: Determined by SEC-THF using a conventional PMMA calibration

^f: Determined by SEC-THF using a conventional PMMA calibration after neutralization with Hunig's base and precipitation in methanol

When the polymerization is performed at 60 °C (entries 1-4), the molar mass of the polymer stays the same regardless of the conversion ($M_n \sim 65$ kg mol⁻¹) and is roughly twice the value of what is expected at 100% conversion ($M_n = 31$ kg mol⁻¹), while dispersity values remain quite low ($\bar{D} \leq 1.4$). This behavior (constant M_n) is usually seen when the chain transfer is equal to 1. Moad *et al.* investigated the effect of an excess of acid and found that it only influenced the dispersity (\bar{D} increases with the amount of acid), but not the M_n values, which is not the case in our study. After some optimization, the polymerization was performed at 70 °C and using 0.95 equivalent of acid compared to the CTA (entries 5-9). The targeted molar mass at 100 % was lower than for entries 1-4 ($M_n = 3$ kg mol⁻¹ compared to $M_n = 31$ kg mol⁻¹). In this case, the molar masses increase indeed linearly with the conversion (**Figure 2a**) and dispersity values decrease as the polymerization proceeds (\bar{D} down to 1.3), which is a sign of the controlled and living character of the polymerization, traduced by the clean shift of the MMDs towards higher values (**Figure 2b**). The reason why M_n values obtained during this work are systematically twice the expected ones is still

not known to this day. It is possible that only half the CTA reacted during the polymerization, but another polymerization carried out using a CTA synthesized in-house yielded the same results.

At the end of the polymerization, the reaction medium was neutralized with *N,N*-diisopropylethylamine (DIPEA, Hunig's base) and the polymer was precipitated in an excess of cold methanol and filtered to afford the PMMA macro-CTA used for chain extension with ethylene and hereafter referred to as **PMMA-6** (Table 1, entry 9).

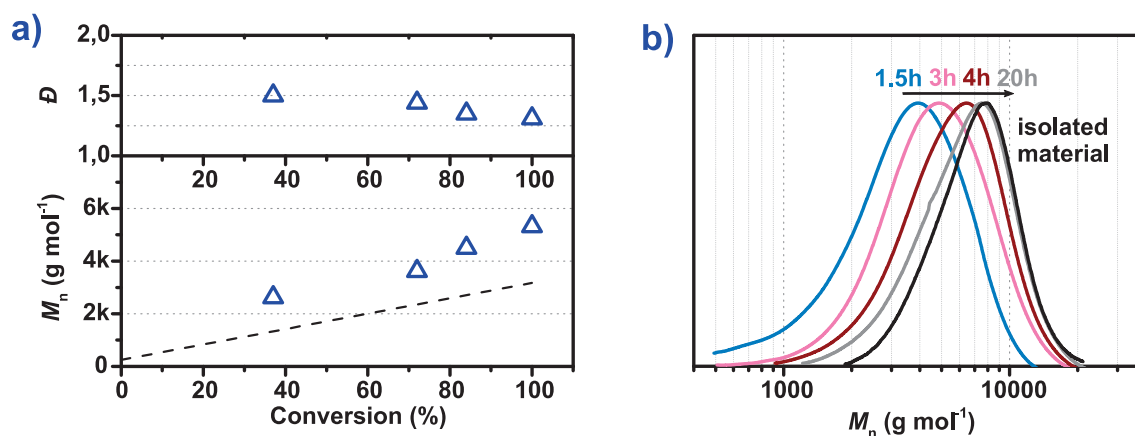


Figure 2. Evolution of M_n and \bar{D} (Δ) (a) and MMDs (b) of PMMA obtained at 70 °C with 6- H^+ (entries 5-8 of Table 1).

$^1\text{H-NMR}$ analysis confirms the presence of the pyridine moiety of the dithiocarbamate chain-end in the final **PMMA-6** (Figure 3). The relative integration of these protons and the methoxy protons corresponding to the MMA repeating units ($\delta = 3.50\text{-}3.75$ ppm) gives $\text{DP}_{n,\text{NMR}} = 80$ ($M_{n,\text{NMR}} = 8\,250$ g mol $^{-1}$), which is in relatively good agreement with SEC-THF values ($\text{DP}_{n,\text{SEC}} = 60$, $M_{n,\text{SEC}} = 6\,250$ g mol $^{-1}$). **PMMA-6** was used as macro-CTA for block copolymerization with ethylene.

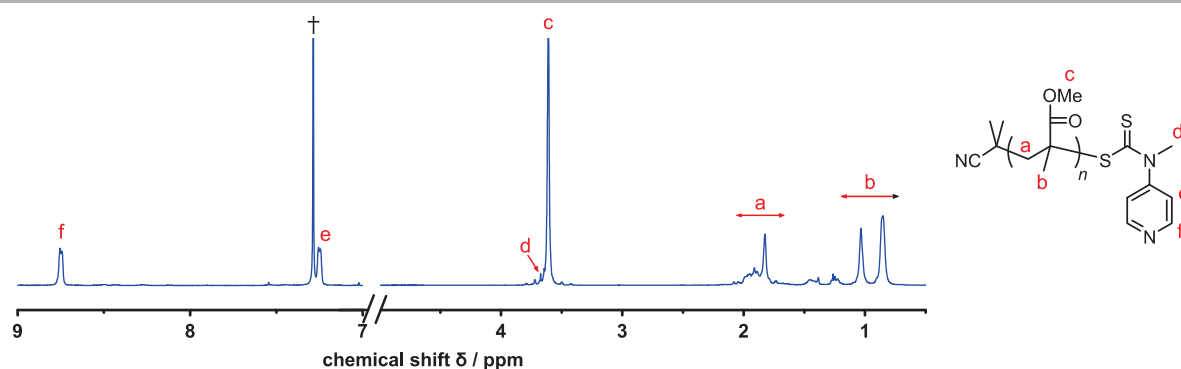


Figure 3. $^1\text{H-NMR}$ spectrum of PMMA macro-CTA obtained with switchable dithiocarbamate 6- H^+ after neutralization and precipitation in methanol (entry 9 in Table 1). (†) NMR residual solvent chloroform.

One explanation for the M_n values systematically twice higher than the expected ones (confirmed by $^1\text{H-NMR}$) could be the incomplete consumption of the CTA during polymerization. It would have been interesting to concentrate the filtrate after precipitation of the polymer in

methanol and analyze it by $^1\text{H-NMR}$. The presence or absence of unreacted CTA would have been a clue, but unfortunately this was not done during this study.

II.2. Chain extension of PMMA-6 with ethylene

Block copolymerization of **PMMA-6** with ethylene was performed at a pressure of 80 bar to avoid any solubility issue. The AIBN quantity was adjusted so that several experiments could be performed with **PMMA-6** from the available quantity. Polymerization conditions were otherwise standard: $T = 80\text{ }^\circ\text{C}$, 50 mL of DMC, 10 mg of AIBN, [macro-CTA]:[AIBN] ratio of 3:1. The results of the chain-extensions are presented in **Table 2**.

Table 2. Block copolymerization of ethylene with switchable PMMA-6 at 80 °C and 80 bar.

Entry	Time (h)	Yield of PE (g)	$M_{n,theo}^a$ PE block (g mol $^{-1}$)	$M_{n,theo}^a$ diblock (g mol $^{-1}$)	$M_{n,HT-SEC}^b$ (g mol $^{-1}$)	\mathcal{D}^b	$M_{n,NMR}^c$ (g mol $^{-1}$)
10	0	-	-	-	950	1.38	8 250 ^d
11	1	0.18	1 000	9 250	1 270	1.96	10 700
12	2	0.44	2 200	10 450	1 540	2.19	11 800
13	3	0.66	3 500	11 750	2 140	2.13	12 400
14	4	0.65	3 300	11 550	1 900	2.31	12 800

Polymerization conditions: $T = 80\text{ }^\circ\text{C}$, $P = 80\text{ bar}$, DMC: 50 mL, AIBN: 10 mg

^a: Determined using a derived form of equation 3, chapter I: $M_{n,theo} = \text{Yield(g)} / \text{CTA(mol)} + MW_{CTA}(\text{g mol}^{-1})$.

^b: Determined by HT-SEC using a conventional PE calibration.

^c: Determined by $^1\text{H-NMR}$ at 363K in TCE/ C_6D_6 (2/1 v/v) with equation 1

The stagnating yield after 3 hours of polymerization (entries 13-14) could be due to the low quantity of AIBN used for these chain-extensions (10 mg) or experimental error. At 80°C, the half-life time of AIBN is 83 minutes (calculated using literature k_d values of AIBN in toluene^[19] and Arrhenius' equation with $t_{1/2}(\text{sec}) = \ln(2)/k_{d,80^\circ\text{C}}$) and it is possible that after 4 hours of polymerization the quantity of AIBN left is not sufficient to compensate radical losses due to termination. This phenomenon was however not observed for experiments using the same AIBN quantity in part **III.3**, which reinforces the hypothesis of experimental error.

$$M_{n,NMR} = M_{n,PMMA} + \frac{DP_{n,SEC}(PMMA) * \frac{1}{4} \int_{1.10}^{1.50} (CH_2CH_2)_p}{\frac{1}{3} \left[\int_{3.30}^{3.60} (CH_2C(Me)C(O)-OCH_3)_n - 3 \right]} * MW(C_2H_4)$$

Equation 1. Calculation of the molar masses of the block copolymers determined by $^1\text{H-NMR}$.

HT-SEC analyses reveal that the MMDs shift towards higher values as the polymerization proceeds, but the presence of a tailing (at the same elution time of **PMMA-6**) enlarges the \mathcal{D} values (**Figure 4a**). This shoulder most likely originates from unconsumed **PMMA-6**, which could be due to low chain transfer constant. The low M_n values determined *via* HT-SEC are again due to poor suitability of this analytic technique for polar/apolar block copolymers. On the other hand, the

determination of M_n values via $^1\text{H-NMR}$ (according to **Equation 1**) reveal that the molar masses increase indeed linearly with the conversion of ethylene, but that they are systematically higher than the expected values (**Figure 4b**). M_n values also tend to get closer to the theoretical line as the conversion goes up, which corroborates the hypothesis of low C_{tr} .^[20,21] The fact that the PMMA macroCTA is slowly consumed during polymerization is however surprising as CTA **6** (closest structure to the PMMA macroCTA) was consumed very rapidly during ethylene homopolymerization at 80°C.

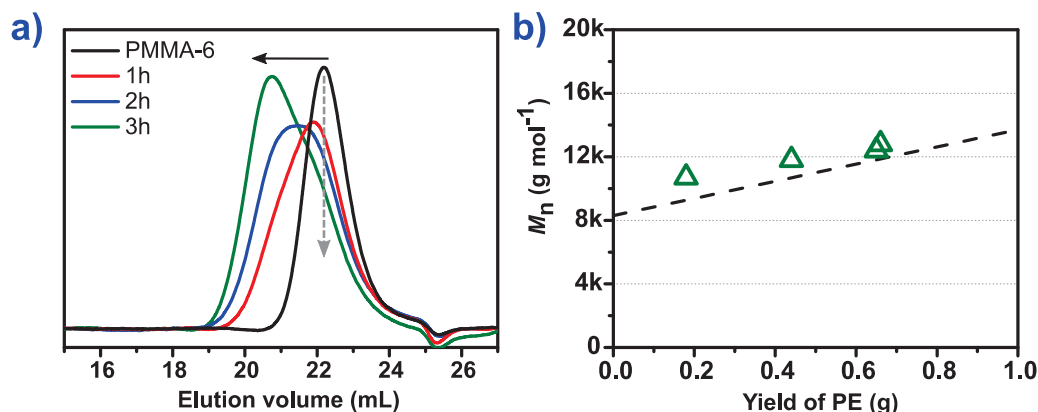


Figure 4. MMD evolution of PMMA-*b*-PE during chain extension of PMMA-6 with ethylene (a) and evolution of M_n (Δ) values determined by $^1\text{H-NMR}$ in TCE/ C_6D_6 (2/1 v/v) at 363K. (---) corresponds to the linear fit of experimental values and (—) is the theoretical line.

An exemplary $^1\text{H-NMR}$ spectrum of the polymeric product obtained after 3 hours of polymerization is presented in **Figure 5**. The presence of the characteristic $-\text{CH}_2\text{-S-C(=S)Z}$ protons **d** confirms the insertion of ethylene between the PMMA block and the dithiocarbamate chain-end, which, along with the increase in M_n values, indicates successful block copolymerization. However, as it was already the case with PVAc-*b*-PE (Chapter III), it is not possible to observe the tying between the last MMA and the first ethylene repeating units as they overlap with other signals (simulated at $\delta = 1.54$ ppm by Chemdraw, same chemical shift as the $-\text{CH}_2\text{-CH}_2\text{-S-C(=S)Z}$ protons). In addition, the pyridinyl protons resonances do not seem to be specific of the type of chain they are carried by (PE or PMMA). As a consequence, the unreacted PMMA observed by HT-SEC cannot be accounted for when calculating the molar mass of the PE segments.

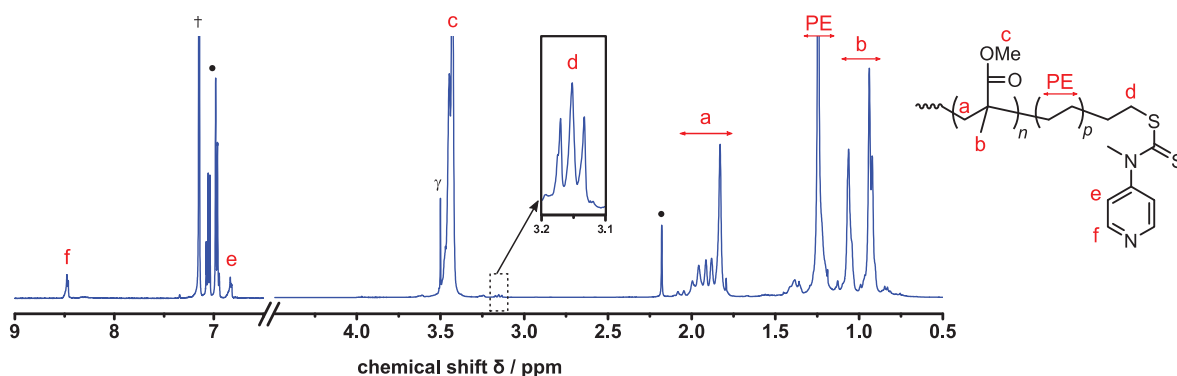


Figure 5. $^1\text{H-NMR}$ spectrum of PMMA-*b*-PE obtained with PMMA-6 after 3 hours of polymerization (entry 13 in Table 2). (+) NMR residual solvent chloroform, (•) collecting solvent toluene, (γ) polymerization solvent DMC.

The separation of unreacted PMMA and PMMA-*b*-PE was thus attempted by (i) centrifugation in DMC and (ii) extraction by THF with a Soxhlet but both methods proved unsuccessful. While it was possible to partially recover the unreacted PMMA by centrifugation and decantation, the complete separation of PMMA and PMMA-*b*-PE could not be achieved. THF proved to be a solvent provoking a fine dispersion of the product that was not recoverable anymore by filtration. This is however a good indication that a block copolymer was formed and that it may act as a stabilizer in THF. The use of the more polar solvent system EtOH/H₂O 80/20 by volume is capable of solubilizing unreacted PMMA^[22] (up to 0.5 wt% and 28 kg mol⁻¹) while the PE block remains completely insoluble, permitting filtration. A 0.013 wt% dispersion of PMMA-*b*-PE obtained after 2 hours of polymerization (entry 12 of Table 2) was prepared in 10 mL of an 80% aqueous ethanolic solution. The dispersion was stirred for 24 hours at 30°C and the insoluble part was filtered off. A large excess of the ethanolic solution was used to wash the filter cake which was then dried until constant weight. 57 % of the material used was recovered on the filter (if the material was a mixture of pure PE and PMMA homopolymers, only PE homopolymer would have been recovered, accounting for 25 wt% of the crude. The 57 wt% recovered on the filter are thus another proof of block copolymerization). The remaining 43% was identified as PMMA without the ω -dithiocarbamate chain-end *via* SEC-THF ($M_n = 6\,000\text{ g mol}^{-1}$, $D = 1.24$) and $^1\text{H-NMR}$ (absence of pyridinyl protons at $\delta = 8.74$ and 7.24 ppm and presence of vinylic protons at $\delta = 5.75$ - 5.55 ppm). Because these vinylic protons were not detected in the starting **PMMA-6**, it is likely that chain-end degradation occurred during polymerization. The quantity of **PMMA-6** that was chain extended with ethylene can then be determined and new theoretical values for molar masses can be re-calculated (**Equation 2**).

$$M_{n,theo}(\text{PE block}) = \frac{\text{yield}(\text{PE}) * M_n(\text{PMMA-6})}{0.57 * m(\text{PMMA-6})}$$

Equation 2. Calculation of theoretical molar mass of PE block taking into consideration the incomplete consumption of PMMA-6.

The new theoretical M_n value for entry 12 is thus 14 500 g mol⁻¹. ¹H-NMR of the purified material gives a new molar mass for the block copolymer of 13 150 g mol⁻¹, quite close to the expected value. HT-SEC analysis of the insoluble clearly shows the presence of one MMD population that is narrow, perfectly fits with the higher molar mass region of the unpurified material (**Figure 6a**) and has a clean shift of MMD towards higher values compared to the starting macroC_TA. This confirms that the PMMA-*b*-PE copolymers are obtained and well-defined once unreacted **PMMA-6** is removed. The purified material has a MMD at substantially lower values than a PE homopolymer obtained by conventional free radical polymerization, confirming that PE homopolymer was not formed during the block copolymerization. Finally, ¹H-NMR confirms the presence of both PMMA and PE in the insoluble as well as the presence of the dithiocarbamate chain-end on the PE block (**Figure 6b**). These results are the first known examples of the direct synthesis of a PMMA-*b*-PE copolymer by sequential monomer addition and RAFT polymerization.

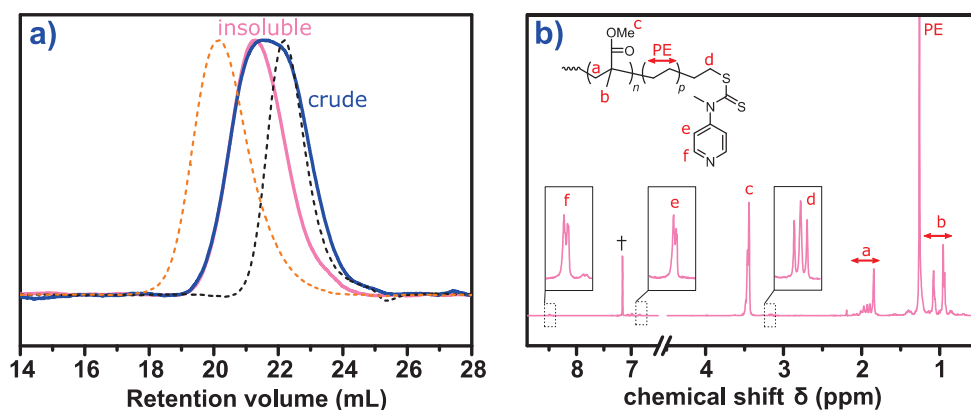


Figure 6. a) HT-SEC traces of the crude polymeric material from entry 12 in Table 2 (—) and its insoluble fraction (—) after purification in EtOH/H₂O (80/20) overlaid with PE homopolymer obtained at 80 bar and 80 °C (---) and the starting PMMA-6 (---). b) ¹H-NMR spectrum of the insoluble fraction. (†) NMR residual solvent benzene.

II.3. Self-assembly of PMMA-*b*-PE copolymers in DMC

The apparent assembly of the diblock copolymers into particles observed when the material is dispersed in THF has led us to consider the potential self-assembly of this block copolymer either during polymerization in DMC or upon crystallization when cooling the polymerization mixture. It was indeed observed that the reactor content after polymerization with **PMMA-6** was systematically a stable white dispersion. **PMMA-6** is completely soluble in the polymerization medium (DMC + ethylene dissolved) and the addition of the second block (PE) leads to solvophobic/solvophilic block copolymer with one block soluble and one block insoluble. Those systems are known to potentially self-assemble into particles after polymerization,^[23,24] during polymerization^[25] or during crystallization.^[26]

Transmission electron microscopy (TEM) analyses were not performed on the dispersions obtained directly after polymerization but on the dried material re-dispersed in DMC. It is however safe to assume that the particle morphologies observed (if any) are the same after re-dispersion because the fusion temperature of the PE segment ($T_f \sim 110\text{ }^\circ\text{C}$) is expected to “freeze” the particle morphologies (samples are dried at a maximum temperature of $60\text{ }^\circ\text{C}$). Crude block copolymers from entry 12 (2 hours of chain extension) and entry 13 (3 hours of chain extension) were re-dispersed in DMC (0.5 wt%) and sonicated at room temperature for 2 hours and observed by TEM (**Figure 7a** and **7b**, respectively).

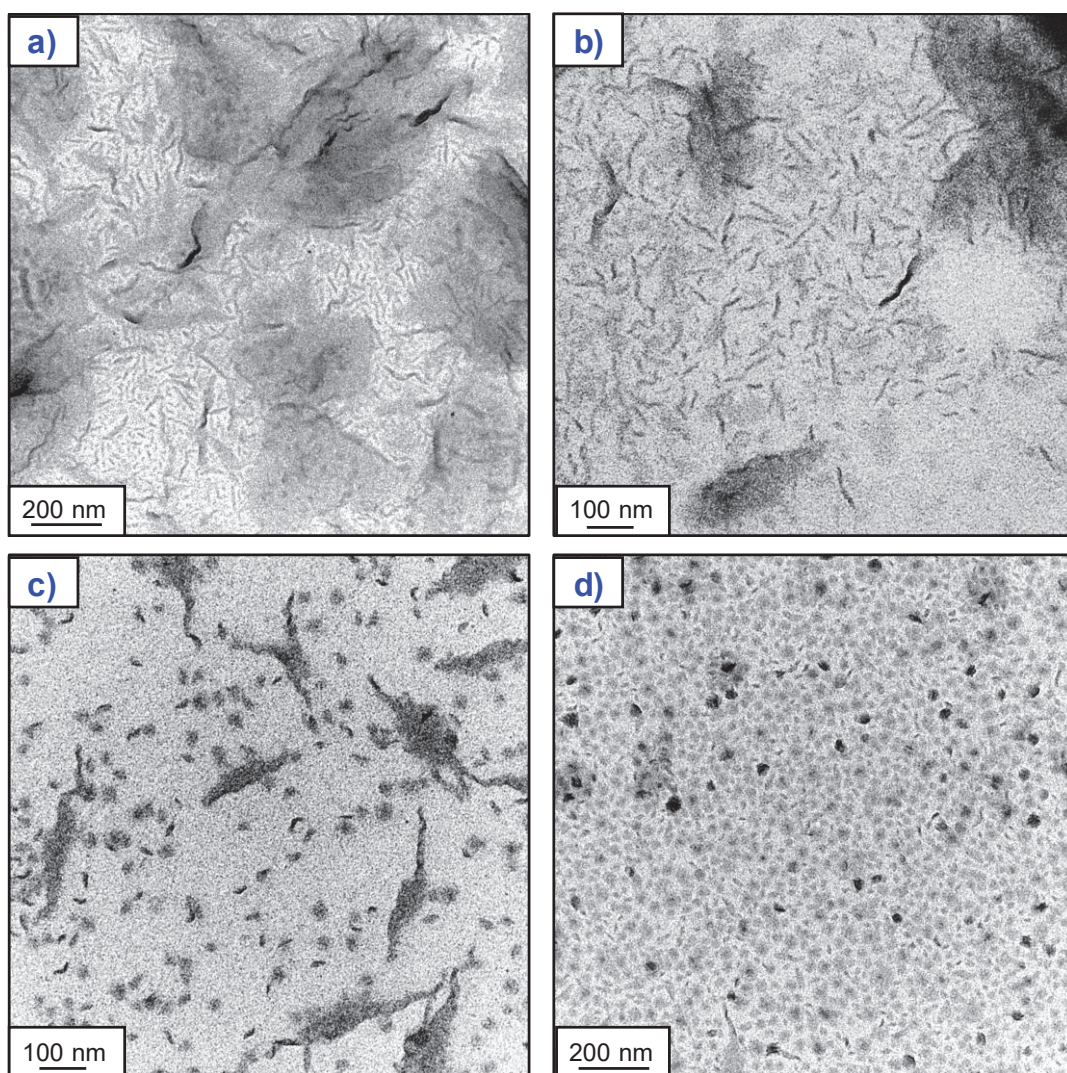


Figure 7. TEM images of PMMA-*b*-PE copolymers re-dispersed in DMC after 2 hours (a) and 3 hours (b) of polymerization. The same dispersions are then heated and analyzed again by TEM ((c) and (d), respectively).

Short fiber-like particles (worms) of $\sim 100\text{ nm}$ are undoubtedly present in these copolymer samples before heating (**Figure 7 a, b**). In those images, the dark parts correspond to the crystalline PE block. The molar mass of the PE block appears to have little impact on the morphology as the worms size is sensibly the same ($\sim 100\text{ nm}$) in the M_n range of the PE block explored (2 200 or 3 500 g mol^{-1}).

In addition, the samples were then gently heated at 120 °C ($T > T_{\text{melt}}$ of PE) until the solution became translucent (PE block melted) and allowed to cool down to room temperature, upon which the solution became cloudy again. The morphology drastically changes after heating above the melting point of the PE block (**Figure 7 c, d**). The worms appear to be broken down into smaller part (**c**), eventually affording small anisotropic olive-like PE lamellas aggregating into spherical particles (**d**). It should be stated that the heating duration and cooling rate were not controlled, which could explain why one sample features mostly intact worms and the other features mostly spherical particles.

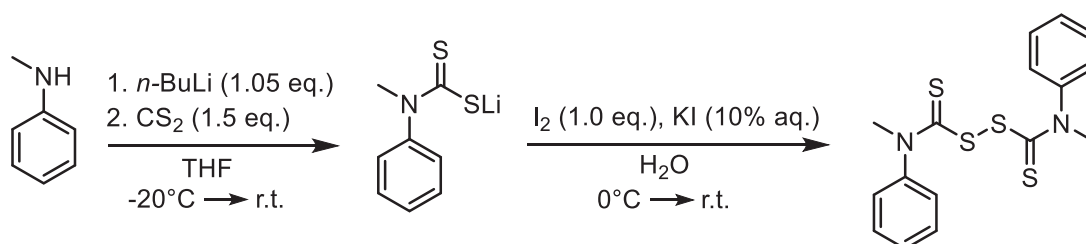
III. Synthesis of PMMA-*b*-PE by successive FRP and RAFT polymerization.

The use of a switchable dithiocarbamate afforded the desired PMMA-*b*-PE copolymer, as the first known example for such a system. It involved the use of a strong acid and the extra protonation/deprotonation step. Although the control over the polymerization of MMA was achieved ($D \leq 1.3$), the systematic higher than expected M_n values, along with a slow consumption of the macro-CTA **PMMA-6** upon chain-extension with ethylene are areas for improvement.

Alternatively, we investigated the synthesis of PMMA carrying a dithiocarbamate chain-end by simply using *N,N'*-dimethyl-*N,N'*-diphenyl thiuram disulfide (**TD**) as irreversible chain transfer agent in the free radical polymerization of MMA. This strategy was used by other groups to obtain a PMMA carrying a xanthate chain-end,^[15,27] but was, to the best of our knowledge, never attempted with a dithiocarbamate. Although the control of the PMMA obtained with this method cannot compete with a RAFT process, the present strategy would lead to similar block copolymers in a more convenient way. This strategy can also be potentially extended to thiuram disulfides with different substituents on the nitrogen to adjust the control of the PE block.

A full investigation of the nature of the α and ω chain-ends of the PMMA thus obtained was performed and the chain transfer constant C_{tr} of **TD** in MMA polymerization was determined. The dithiocarbamate chain-end resulting from **TD** has a Z-group identical to that of CTA **3** from Chapter II (**Figure 1**). The same behavior and the same level of control could then be expected.

TD was synthesized according to **Scheme 4**. The full synthetic procedure is described in the experimental part at the end of this chapter.



Scheme 4. Synthetic route to **TD**.

III.1. Determination of the chain transfer constant.

The chain transfer constant C_{tr} was determined using the simple and well-known method described by Mayo.^[28] In short, Mayo showed that, after some approximation (constant monomer concentration and absence of transfer to solvent), the plot of the inverse of the degree of polymerization $1/DP_n$ against the ratio between the chain transfer agent and the monomer gives a straight line whose slope is the chain transfer constant. An alternative consists in using the degree of polymerization by weight DP_w , as M_w is less entailed with errors in SEC analyses (Equation 3).

$$\frac{1}{DP_n} = \frac{2}{DP_w} = C_{tr} \frac{[CTA]}{[M]}$$

Equation 3. Relationship used for the determination of the chain transfer constant by Mayo plot.

The Mayo equation assumes that the polymerization is performed in bulk and that the monomer conversion remains low. In our case, TD was found to be only partially soluble in MMA at the polymerization temperature (80°C), and a small quantity of toluene was added to ensure the homogeneity of the polymerization medium. The addition of toluene is assumed to have only a very limited impact on the determination of C_{tr} as the chain transfer constant of MMA to toluene is 2×10^{-5} which is very low.^[29] Table 3 presents the polymerization conditions and the results used for the Mayo plot (Figure 8).

Table 3. Experiment details for the Mayo plot experiments used for the determination of C_{tr} of PMMA• to TD.

Entry	MMA/TD/AIBN	[TD] (mol L ⁻¹)	Conv. ^a (%)	M_w , ^b (g mol ⁻¹)	2/ DP_w
15	1000/0/1	-	10.7	98 900	0.0020
16	1000/1/1	0.003	5.7	81 900	0.0024
17	1000/2/1	0.007	9.9	71 500	0.0028
18	1000/5/1	0.017	2.9	45 700	0.0044
19	1000/10/1	0.033	3.9	23 900	0.0084
20	1000/20/1	0.067	2.0	13 800	0.0145

Polymerization conditions: T = 80 °C, MMA: 5 g, AIBN: 8.2 mg, toluene: 10 mL

^a: Determined by ¹H-NMR in CDCl₃

^b: Determined by SEC-THF with a conventional PMMA calibration

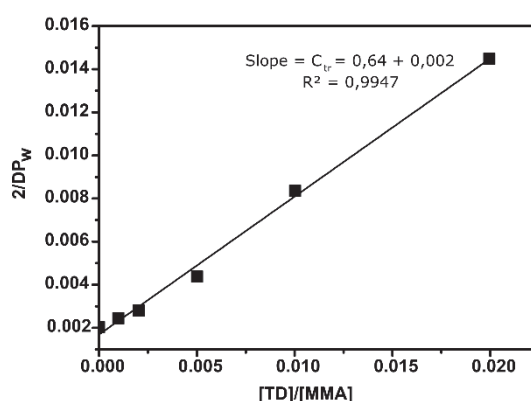


Figure 8. Mayo plot for the determination of C_{tr} of PMMA• to TD.

A C_{tr} value of 0.64 is found, close to the ideal value of 1. A C_{tr} value of 1 means that the ratio between the concentration of the CTA and the monomer remains constant throughout the polymerization.^[30] This means that a polymer with constant molar mass is formed at both low and high monomer conversion. It was reported by Otsu and Matsumoto^[31] that disulfide CTAs with low C_{tr} tend to give short polymer chains with one single CTA chain-end. On the contrary, a high C_{tr} value tends to give telechelic (one CTA at both chain-ends) polymers. We thus expect that PMMAs formed by this method will be monofunctional ($f = 1$).

III.2. Synthesis of PMMA-T with TD

Toluene was initially used as polymerization solvent but unreacted TD was systematically present in the final PMMA. resulted in the systematic presence of unreacted TD in the final PMMA (even after isolation from precipitation in methanol). The presence of unreacted TD could be harmful for subsequent chain-extension. Rather than performing a tedious workup after polymerization in toluene, acetonitrile was preferred as polymerization solvent as it was found that the solubility of TD in cold acetonitrile is minimal. PMMA free of any unreacted TD could thus be obtained. PMMA-T were synthesized with different targeted M_n (determined empirically). The experimental conditions and the polymerization results are presented in **Table 4**.

Table 4. Synthesis of PMMA macro-CTAs of different molar masses with TD in acetonitrile.

Entry	Polymer	[MMA] (mol L ⁻¹)	Conv ^a (%)	$M_{n,target}$ (g mol ⁻¹)	$M_{n,SEC}^b$ (g mol ⁻¹)	\bar{D}^b	f^c	
							1 st precipitation	2 nd precipitation
21	PMMA-T1	4.2	73	10 000	9 800	1.73	0.92	0.90
22	PMMA-T2	2.1	71	5 000	5 600	1.49	0.91	-
23	PMMA-T3	4.2	72	10 000	8 900	1.55	0.92	-
24	PMMA-T4	0.8	71	2 000	1 580	1.79	1.00	-

Polymerization conditions: T = 80 °C, time = 6 h, [TD] = 0.042 mol L⁻¹, [AIBN] = 0.042 mol L⁻¹.

^a: Determined by ¹H-NMR in CDCl₃

^b: Determined by SEC-THF with a conventional PMMA calibration

^c: Functionality f determined by equation 4

The SEC-THF traces of PMMA-T2, PMMA-T3 and PMMA-T4 are presented in **Figure 9**. The presence of a thiocarbonylthio moiety on the entire MMD of PMMA-T2/3/4 is confirmed as the UV absorbance at 300 nm (corresponding to the maximum absorbance of the C=S double bond) overlaps with the refractive index (RI) trace. The shoulder seen in all UV traces in the low M_n area of the MMDs is due small polymer chains having a higher UV absorption for the same concentration. A small quantity of unreacted TD is detected in the case of PMMA-T4 at high elution volume. This quantity was however too small to be quantified by ¹H-NMR.

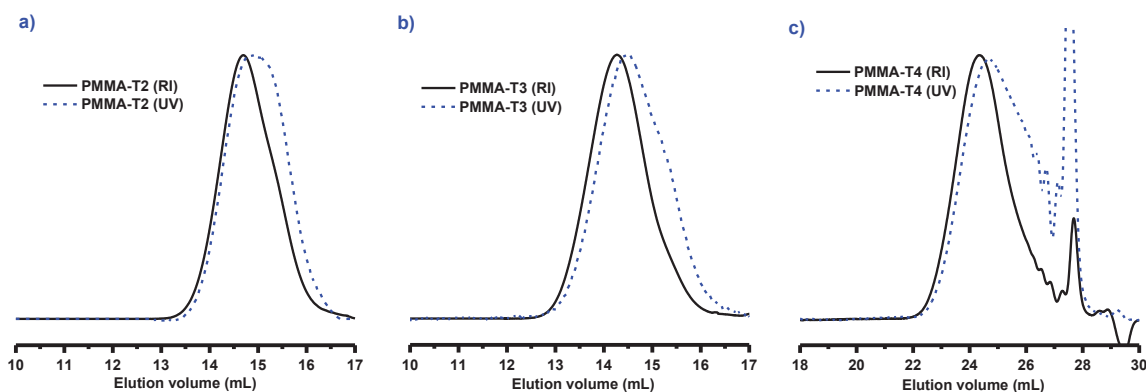
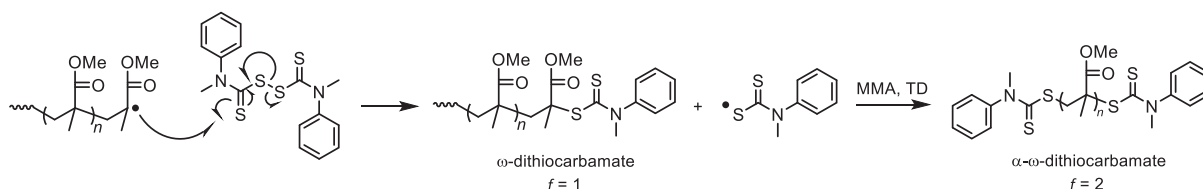


Figure 9. SEC-THF traces of PMMA-T2 (a), PMMA-T3 (b) and PMMA-T4 (c). The plain line is the refractive index (RI), the dotted line is the UV absorbance at 300 nm.

III.2.1. Chain-end analysis

Upon PMMA \cdot addition, TD undergoes fragmentation that liberates a ω -dithiocarbamate PMMA ($f = 1$) and a radical species that could, in principle, re-initiate the polymerization of MMA (Scheme 5). A PMMA chain both initiated and terminated by a fragment from TD would then be a α - ω -dithiocarbamate ($f = 2$, telechelic). This would have a major impact (although not devoid of interest) on subsequent block copolymerization with ethylene as triblock copolymers would then be formed.



Scheme 5. Possible formation of α - ω -dithiocarbamate PMMA through re-initiation by a radical fragment from TD.

Functionality f was calculated with Equation 4, $^1\text{H-NMR}$ and SEC-THF analyses. The $\text{DP}_{n,\text{NMR}}$ was determined by relative integration of the aromatic protons a-c (Figure 10) of the carbamate chain-end ($\delta = 7.35\text{-}7.55$ (3H) and $\delta = 7.15\text{-}7.25$ ppm (2H)) and of the methoxy protons f (Figure 10) of the PMMA main chain ($\delta = 3.50\text{-}3.65$ ppm). The stability of the chain-end was assessed with PMMA-T1 (entry 21 of Table 4), which was precipitated twice in methanol and no apparent loss of functionality is observed. This is in stark contrast with a xanthate-functionalized PMMA that was synthesized during our collaboration with M. Destarac, which features a pronounced loss of chain-end fidelity upon handling: a diminution of f by a factor of 2 was observed after the second precipitation step (by re-dissolution in acetonitrile and precipitation in methanol).

$$f = \frac{DP_{n,SEC}}{DP_{n,NMR}} = \frac{\frac{1}{5} \left[\left(\int_{7.35}^{7.55} C_6H_5 \right) + \left(\int_{7.15}^{7.25} C_6H_5 \right) \right]}{\frac{1}{3} \left[\int_{3.50}^{3.65} OCH_3 \right]} * DP_{n,SEC}$$

Equation 4. Determination of the functionality of PMMA-T, with $DP_{n,SEC}$ = degree of polymerization obtained from $M_{n,SEC}$.

An exemplary 1H -NMR spectrum with integral values for PMMA-T3 is given in **Figure 11a**. The complete removal of unreacted TD and the presence of at least one dithiocarbamate chain-end is confirmed by the split of the aromatic protons of TD ($\delta = 7.45$ - 7.65 ppm, **Figure 11b**) and the absence of the protons *k*.

Figure 10. 1H -NMR spectra of PMMA-T3 after isolation (a) and TD (b). (†) NMR residual solvent chloroform.

The *f* value calculated with 1H -NMR and SEC-THF is an average value and does not discriminate between ω -dithiocarbamate and α - ω -dithiocarbamate PMMA that could result from both initiation and termination of PMMA chains by radical fragments coming from TD. Accordingly, a functionality value of *f* = 0.91 (entry 22 in **Table 4**) does not necessarily mean that 91% of the chains bear one dithiocarbamate chain-end. The functionality value was therefore ascertained by matrix assisted laser desorption ionization-time of flight mass spectrometry (MALDI-TOF MS) analysis. An exemplary MALDI-TOF MS spectrum of PMMA-T2 is presented in **Figure 11**. The main species detected corresponds to a PMMA chain featuring a double bond at the ω chain-end (Tc). The intensity of this population could be consistent with its formation during the polymerization by disproportionation^[32] and the corresponding unsaturated species is also observed (Td). However, 1H -NMR does not show vinylic protons between 5 and 6 ppm while the aromatic protons from the dithiocarbamate moiety are undoubtedly assigned (**Figure 12**).

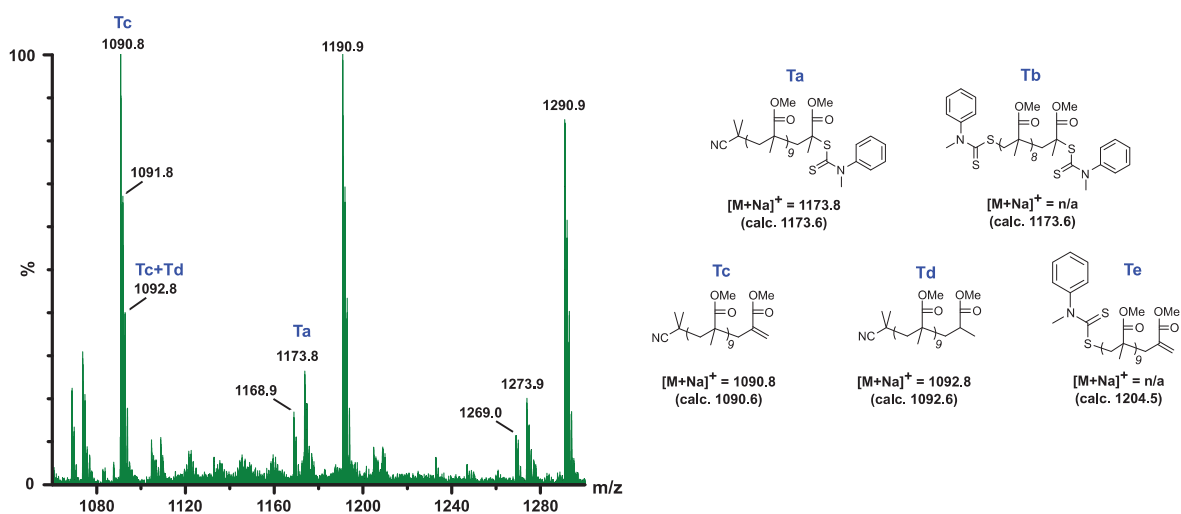


Figure 11. MALDI-TOF MS spectrum of PMMA-T2. Matrix: dithranol; cationizing agent: sodium iodide. The peak at $m/z = 1168.9$ corresponds to the $[M+H]^+$ adduct equivalent of Ta.

As a consequence, Tc and Td correspond to the expected monofunctionalized PMMA chains carrying a dithiocarbamate ω chain-end that underwent degradation in the spectrometer during ionization. Indeed, a small quantity of PMMA still bearing the ω -dithiocarbamate chain-end (Ta) is detected as well. MALDI-TOF MS shows no sign of telechelic PMMA, either before ω chain-end loss due to ionization (Tb) or after chain-end loss (Te). The combination of MALDI-TOF and $^1\text{H-NMR}$ confirms that only monofunctionalized PMMA was obtained.

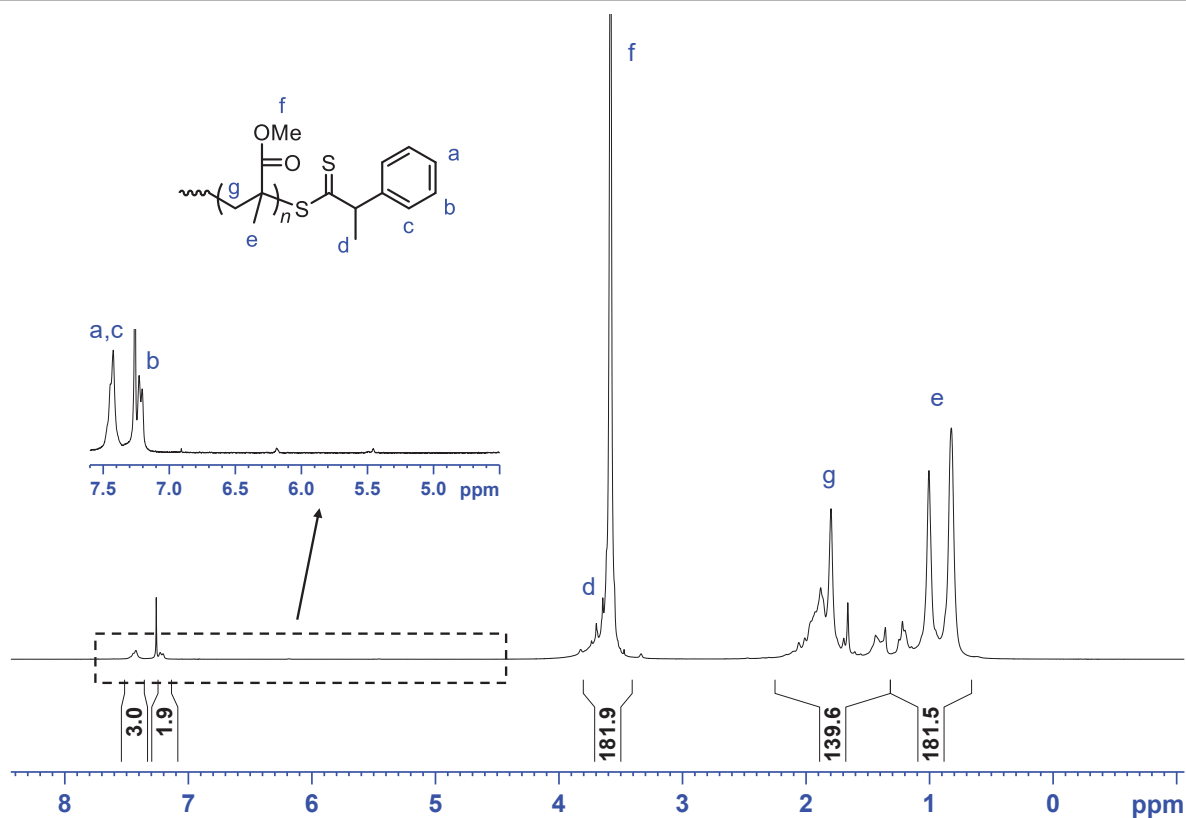


Figure 12. $^1\text{H-NMR}$ spectrum and corresponding integral values of PMMA-T2.

III.2.2. Chain-extension with vinyl acetate

The livingness of the PMMA macro-CTAs was ascertained by chain extension with vinyl acetate. PMMA-T3 (0.12 mmol) was dissolved in a mixture of ethyl acetate (2 mL) and vinyl acetate (34.8 mmol), and AIBN (0.04 mmol) was used as initiator. The polymerization was performed at 70 °C over 6 hours and samples were withdrawn at different times for $^1\text{H-NMR}$ and SEC analyses. The SEC-THF traces and the evolution of M_n and \mathcal{D} values, determined by both $^1\text{H-NMR}$ and SEC are presented in **Figure 13**.

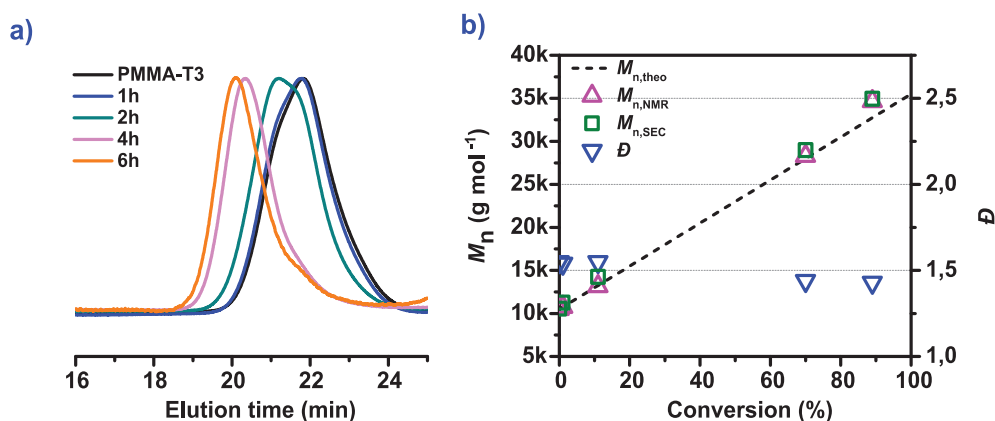


Figure 13. SEC-THF traces of the chain extension of PMMA-T3 with VAc (a) and evolution of the corresponding $M_{n,NMR}$ (Δ , determined by integration of PVAc $-(CH_2-CH(OAc))-$ signal relative to $-(CH_2-C(CH_3)(C(O)OCH_3))-$ signal), $M_{n,SEC}$ (\square , calibration PMMA standards) and \bar{D} (∇) values of PMMA-*b*-PVAc made with PMMA-T3 at 70 °C (b). The dotted line corresponds to the theoretical M_n values calculated for $f = 1$.

A clean shift of the MMD towards higher values is observed (Figure 13a) and the M_n values determined by both ¹H-NMR (integration of PVAc $-(CH_2-CH(OAc))-$ signal relative to $-(CH_2-C(CH_3)(C(O)OCH_3))-$ signal) and SEC-THF are remarkably close to theoretical values while \bar{D} values decrease from 1.55 to 1.43 as the polymerization proceeds (Figure 13b). The linear increase of M_n values with conversion of VAc and their good agreement with the theoretical values (calculated for $f = 1$) confirm that the vast majority of PMMA-T3 bears one dithiocarbamate chain-end. The minor tailing observed at elution time = 22 minutes after 6 hours of polymerization is attributed to a small fraction of non-functionalized PMMA. The growth of the PVAc block thus proceeds in a controlled fashion. The same is expected upon chain extension with ethylene instead of VAc.

III.3. Chain extension of PMMA-T with ethylene

The PMMA macro-CTAs previously synthesized were then used for chain-extension with ethylene at 80 bar and 80 °C. The experimental conditions are summarized in Table 5. As PMMA-T2 and PMMA-T3 have a relatively high molar mass (5 600 and 8 900 g mol⁻¹, respectively), their quantities used for chain-extension were adjusted for solubility and practical reasons. Keeping a constant [macro-CTA]:[AIBN] ratio of 3, this means that the AIBN quantity for PMMA-T2 and T3 was reduced down to 10 mg. 25 mg of AIBN was used for PMMA-T4.

Table 5. Block copolymerizations of ethylene with PMMA-T2, PMMA-T3 and PMMA-T4 at 80 °C and 80 bar.

Entry	macro-CTA	Time (h)	Yield of PE (g)	$M_{n,theo}^a$ PE block (g mol ⁻¹)	$M_{n,theo}^b$ diblock (g mol ⁻¹)	$M_{n,NMR}^c$ PE block (g mol ⁻¹)
25	PMMA-T2	0.5	0.13	700	6 300	-
26*	PMMA-T2	1	0.85	4 750	10 400	-
27	PMMA-T2	2	0.58	3 250	8 850	3 500
28	PMMA-T2	3	0.90	4 800	10 400	3 200
29	PMMA-T2	4	1.16	6 250	11 850	4 500
30	PMMA-T2	6	1.45	7 800	13 400	4 300
31	PMMA-T3	1	0.38	2 000	10 900	3 100 / 2 450
32	PMMA-T3	2	0.69	3 600	12 500	3 700 / 3 800
33	PMMA-T3	3	0.98	5 050	13 950	1 700 / 3 900
34	PMMA-T3	4	1.19	6 200	15 100	2 100 / 8 900
35**	PMMA-T4	2	0.55	1 150	2 730	1 400
36**	PMMA-T4	3	1.12	2 400	3 980	1 800
37**	PMMA-T4	4	1.44	2 800	4 380	1 500
38**	PMMA-T4	5	2.04	4 300	5 880	1 800
39	FRP	4	1.03	-	-	-
40**	FRP	4	1.79	-	-	-

Block copolymerization conditions: T = 80 °C, P = 80 bar, DMC: 50 mL, AIBN: 10 mg, [macro-CTA]:[AIBN] = 3:1 ; *: Polymerization performed at 110 °C due to temperature probe error; **: AIBN: 25 mg;

^a: Determined from yield of PE: $M_n = \text{Yield of PE (g)} / n_{\text{macro-CTA (mol)}}$;

^b: Determined from yield of PE and $M_{n,SEC}$ of PMMA block : $M_n = \text{Yield of PE (g)} / n_{\text{macro-CTA (mol)}} + M_{n,macro-CTA}$ (g mol⁻¹) with $M_{n,macro-CTA}$ determined by SEC-THF with conventional PMMA calibration.

^c: Determined by ¹H-NMR in TCE/C₆D₆ (2:1 v:v) at 90 °C with equation 1

For entries 31-34, $M_{n,NMR}$ values for the PE block were determined twice using two different samples from the polymeric material for each polymerization time

Using the same AIBN quantity (10 mg) the polymerization with **PMMA-T2/3** proceeds substantially faster than when **PMMA-6** was used (~1.5 times faster) and does not plateau after 4 hours of polymerization. It also proceeds slightly faster than the FRP of ethylene using 10 mg of AIBN, which is in stark contrast with the polymerization rate obtained for ethylene homopolymerization using CTA **3** (identical Z-group) in Chapter II (for which the polymerization rate was reduced by a factor of ~1.5 at 80 °C and 200 bar compared to FRP).

The plot of the RI traces versus the elution time of all attempted block copolymerizations are presented in **Figure 14**. A clean shift of the MMDs towards higher values, regardless of the macro-CTA (PMMA-T2/T3/T4) is clearly visible. The superposition of the HT-SEC traces with that of a PE obtained by FRP under the same conditions (orange dotted line in **Figure 14**) clearly shows that the new MMDs obtained do not correspond to PE homopolymer, hinting at successful block copolymerization.

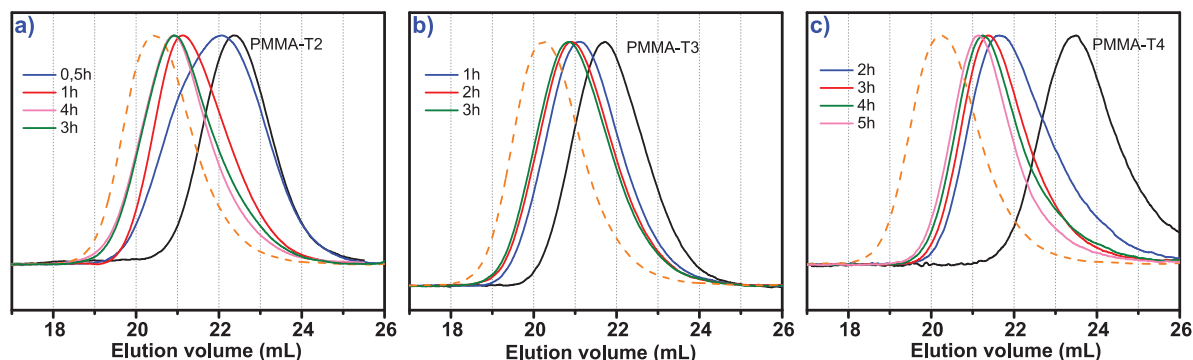


Figure 14. HT-SEC traces of the of the chain extension of PMMA-T2 (a), PMMA-T3 (b) and PMMA-T4 (c) with ethylene at 80 bar. The orange dotted line corresponds to a PE obtained by FRP at 80 bar.

An exemplary $^1\text{H-NMR}$ spectrum for a PMMA-*b*-PE copolymer obtained with PMMA-T4 after 5 hours of block copolymerization (entry 38 of Table 5) is presented in **Figure 15**. The presence of the characteristic protons **d** and **e** of the PE- $\text{CH}_2\text{-CH}_2\text{-SC(hS)Z}$ indicates that ethylene units have been inserted between the PMMA block and the thiocarbonylthio chain-end. The quasi-total consumption of the PMMA macro-CTA is confirmed by the almost complete disappearance of the protons **f'** (PMMA- SC(S)N(Me)Ph) and the appearance of the protons **f** (PE- SC(S)N(Me)Ph).

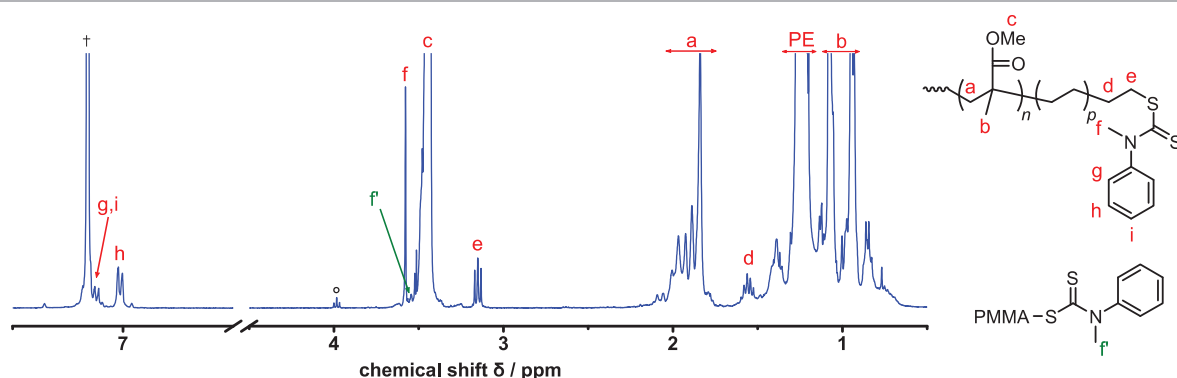


Figure 15. $^1\text{H-NMR}$ spectrum of PMMA-*b*-PE after 5 hours of block copolymerization of ethylene with PMMA-T4 (entry 38 of Table 5).

Surprisingly, the molar mass of the PE block determined by $^1\text{H-NMR}$ remains constant for all **PMMA-T** series ($\sim 4\,000\text{ g mol}^{-1}$ for PMMA-T2 (entries 25-30 of Table 5), $\sim 3\,000\text{ g mol}^{-1}$ for PMMA-T3 (entries 31-34) and $\sim 1\,500\text{ g mol}^{-1}$ for PMMA-T4 (entries 35-38)). This was not observed for PMMA-*b*-PE copolymers from **PMMA-6** (for which the molar mass of the block increased with the yield), but for experiments with **PMMA-6**, the PMMA segment has a substantially higher M_n value ($\sim 8\,000\text{ g mol}^{-1}$) than the PE segments ($\sim 3\,000\text{ g mol}^{-1}$) compared to when **PMMA-T** is used ($M_{n,\text{theo}}$ of PE up to $8\,000\text{ g mol}^{-1}$). For the PMMA-T3 series, the polymeric material recovered after solvent removal was grounded and reduced to a fine powder. Two different samples of this powder were then analyzed by $^1\text{H-NMR}$ and different results were obtained for three out of the four polymers. The large disparity in molar mass between the two samples from entry 34 of Table 5 is illustrated by their respective $^1\text{H-NMR}$ spectra in **Figure 16**.

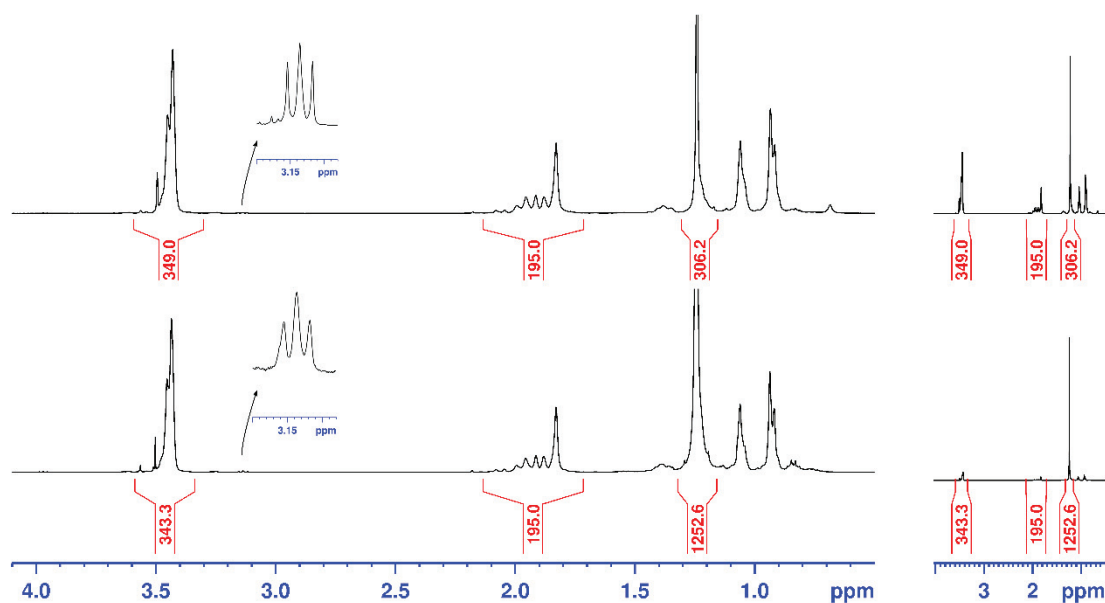


Figure 16. Overlay of two $^1\text{H-NMR}$ spectra of the same PMMA-*b*-PE obtained with PMMA-T3 after 4 hours of block copolymerization with ethylene (entry 34, Table 4).

In this context, a control $^1\text{H-NMR}$ experiment was carried out: a NMR tube was prepared in which a mixture of PE and PMMA homopolymers (50/50 wt%, $M_{n,PE} = 1\,700\text{ g mol}^{-1}$, $M_{n,PMMA} = 1\,600\text{ g mol}^{-1}$) was dispersed. The mixture was then analyzed by $^1\text{H-NMR}$ at high temperature and the relative integration of the PMMA and PE resonances ($\delta = 3.50\text{ ppm}$ and $\delta = 1.25\text{ ppm}$) gives a PE content of 13 wt% in the tube, as opposed to the 50 wt% effectively present in the tube. This illustrates how PMMA is “artificially” more detected *via* $^1\text{H-NMR}$ compared to PE.

Considering only the yields of PE, the integral value of the PE region ($\delta = 1.25\text{ ppm}$) should, at the very least, increase for each polymerization time, which is not the case here. This can be attributed to two factors: (i) a decantation of the polymer in TCE/ C_6D_6 was visually observed, even after manual homogenization at $90\text{ }^\circ\text{C}$, resulting in an accumulation outside the analysis window. (ii) the formation of aggregates. These aggregates were observed with the light scattering detectors of the HT-SEC (right-angle light scattering (RALS) and left-angle light scattering (MALS), **Figure 17**.

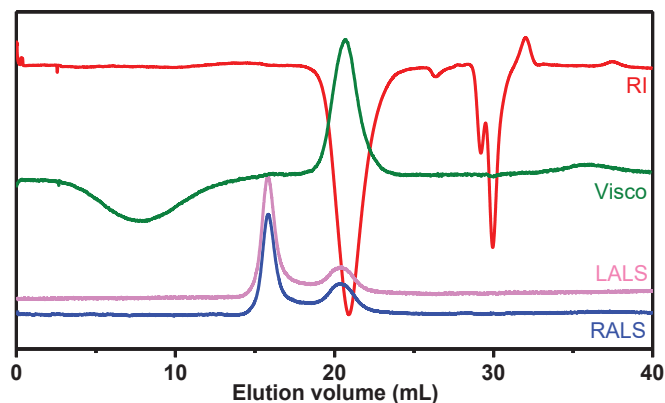


Figure 17. Exemplary HT-SEC traces of PMMA-*b*-PE (from entry 29 in Table 5). RI: refractive index, Visco: viscometer, LALS: left-angle light scattering, RALS: right-angle light scattering.

The peaks at elution volume = 21 minutes (refractive index (RI) and viscometer) correspond to the copolymer. The LALS and RALS detectors show the presence of a second population at elution volume = 16 minutes. This elution volume would correspond to a polymer with a molar mass of several millions of grams per mole, which is not attainable under the reaction conditions used for the chain-extension. This second population gives almost no RI and no viscometer signal, characteristic of aggregates and well-known in SEC and HPLC, especially for proteins.^[33,34] The quantity of aggregates observed *via* HT-SEC is minimal (proportional to the RI signal intensity), but it is conceivable that the number of aggregates is substantially higher in ¹H-NMR, performed at a lower temperature than HT-SEC (90 °C vs. 150 °C). As mentioned above, the solubility of PMMA and PE are very different and, as seen at room temperature, aggregation/self-assembly of the resulting PMMA-*b*-PE may also occur in the NMR solvent, albeit to a lesser extent at high temperature.

¹H-NMR thus failed to deliver consistent M_n values for the diblock copolymers while HT-SEC faces the same issue with the presence of the polar block and neither calibrations available gave consistent results. The shift of MMDs toward higher values as the conversion of ethylene increases (**Figure 14**) as well as the presence of the characteristic protons PE-**CH₂-CH₂**-SC(S)Z in the final polymeric materials (**Figure 15**) are nevertheless proof of the successful block copolymerizations.

Finally, DSC analyses were performed on all PMMA-*b*-PE copolymers obtained from PMMA-T macro-CTAs and did not reveal any peculiar behavior. The crystallization temperatures of the PE segment were systematically in the range $100 < T_c < 105$ °C and the fusion in the range $109 < T_f < 113$ °C. The effect of the block copolymerization on the glass transition temperature of the PMMA segment ($T_g \sim 90 - 110$ °C, depending on the molar mass) could not be studied by regular DSC analyses as this thermal event occurred at the same temperatures of the fusion/crystallization of the PE segment.

III.4. Self-assembly of PMMA-*b*-PE

At the end of any copolymerization experiment, the final mixture had systematically the appearance of a thick homogeneous milky dispersion that grew thicker as the ethylene polymerization time increased with no visible particle chunks. This contrasts with the appearance of PE homopolymer dispersions obtained after polymerization in DMC, which can be either a curd-like dispersion at low PE yield or a solid agglomeration of particles at high yield (**Figure 18**).

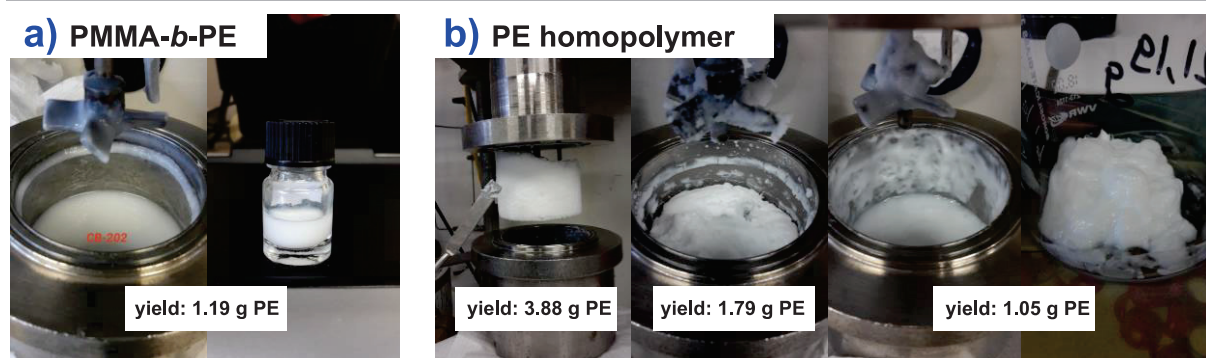


Figure 18. Physical appearances of a PMMA-*b*-PE dispersion after block copolymerization (a) and of PE homopolymers in DMC after conventional radical polymerization in DMC (b).

This already suggests not only the successful formation of the targeted block copolymers but also their ability to self-assemble during their synthesis as suggested earlier on. The self-assembly properties of PMMA-*b*-PE obtained from PMMA-T2 during polymerization in DMC were thus investigated.

An aliquot of the dispersion in DMC obtained directly after polymerization (corresponding to entry 29 in Table 5) was retained for DLS (**Figure 19**) and TEM (**Figure 20**) analyses.

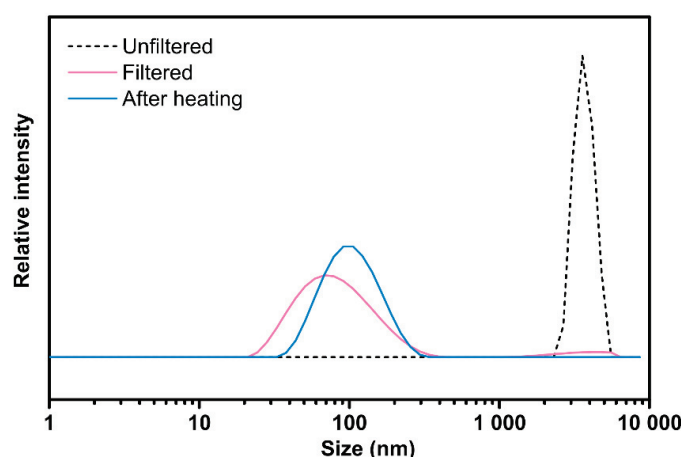


Figure 19. DLS analysis of a dispersion of PMMA-*b*-PE (from entry 29 in Table 5) in DMC after block copolymerization .

DLS on the turbid dispersion (after dilution in DMC) gave inconclusive results (out of software calibration, $Z_{avg} > 6\,000$ nm, $PdI = 1.0$). This is most likely due to the presence of aggregates or non-spherical objects (dashed line in **Figure 19**). After filtration (Nylon 0.45 μm), DLS shows a

unimodal population with $Z_{\text{avg}} = 70$ nm, PDI = 0.3. After gentle heating to 120°C in DMC (until solution is completely translucent), the unfiltered clear dispersion was analyzed again by DLS after cooling and features a unimodal population with $Z_{\text{avg}} = 94$ nm, PDI = 0.17, hinting that aggregates were disassembled by the heat treatment.

TEM analysis was performed on the turbid unfiltered dispersion and after heating to observe the particles formed during polymerization (**Figure 20 a-c**).

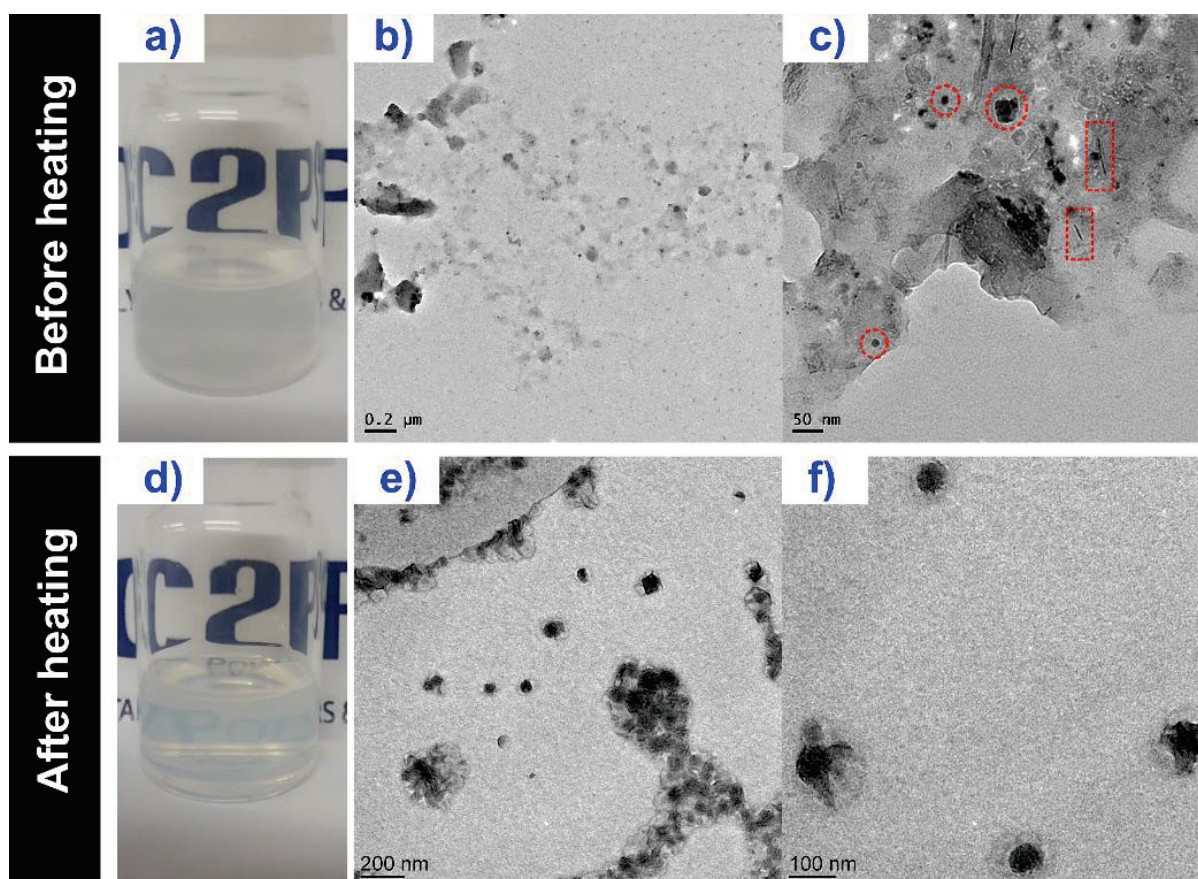


Figure 20. Digital and TEM images of a dispersion of PMMA-*b*-PE (from entry 29 in Table 5) in DMC after block copolymerization.

The unfiltered dispersion (**Figure 20a**) appears to be mostly aggregates, but small (< 100 nm) sphere-like objects (○) and rods (□) can be seen (**Figure 20b, c**). After heating, the dispersion is more translucent (**Figure 20d**) and the particles are sphere-like objects (~100 nm) that appear to each contain several crystalline lamellas (**Figure 20e, f**). The morphologies obtained appear to differ from what was seen using PMMA-6 (fiber-like particle morphology) as mostly aggregates are observed. This can arise from the differences in molar masses of the PMMA segment (8 000 g mol⁻¹ for **PMMA-6** compared to 5 600 g mol⁻¹ for PMMA-T2) and of the PE segments (2 200 g mol⁻¹ and 7 800 g mol⁻¹, respectively). Noteworthy, dispersions obtained from ethylene polymerization with **PMMA-6** or **PMMA-T** all had similar visual appearances. The re-dispersion in DMC is not expected to have affected the particle morphology, but this was not proven.

IV. Conclusion

Following the results of chapter II and the efficiency of dithiocarbamate CTAs to control ethylene polymerization, it was attempted in this chapter to synthesize PMMA chains functionalized by a dithiocarbamate chain-end to obtain the targeted PMMA-*b*-PE copolymers.

Two strategies were adopted to obtain the desired PMMA macro-CTAs:

- Use of a switchable dithiocarbamate to synthesize the PMMA and PE blocks by RAFT polymerization.
- Use of a dithiuram disulfide to obtain the PMMA block by conventional free radical polymerization and irreversible transfer, and subsequent addition of the PE block by RAFT polymerization.

PMMA-6, obtained *via* the switchable *N*-methyl-*N*-(4-pyridinyl) dithiocarbamate, afforded the desired PMMA-*b*-PE copolymers but featured a particularly pronounced slow consumption of the macro-CTA resulting in a mixture of the starting **PMMA-6** and well-defined PMMA-*b*-PE copolymers. In this context, this system could be improved by using a switchable *N*-aryl-*N*-(4-pyridinyl) dithiocarbamate (**8**, **Figure 21**), which has already proved to be effective at controlling both LAM and MAM polymerization.^[1] As a brief anticipation of Chapter V, it was indeed belatedly found that dithiocarbamates with two aromatic rings on the nitrogen (*N,N*-diphenyl dithiocarbamates with exemplary structures in **Figure 21**) were consumed instantaneously during ethylene polymerization.

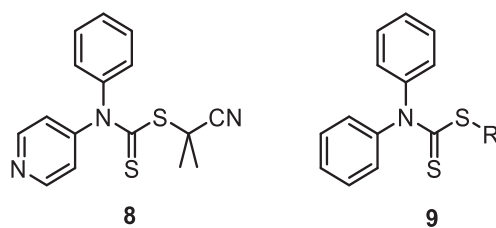


Figure 21. Exemplary structures of dithiocarbamates bearing two aromatic rings on the nitrogen of the Z-group.

PMMA-T of different molar masses were obtained using a *N,N'*-dimethyl-*N,N'*-diphenyl thiuram disulfide *via* conventional radical polymerization and irreversible transfer. The synthesis of such α -dithiocarbamate PMMAs has never been described in the literature and a full characterization of the chain-ends was carried out. These **PMMA-T** macro-CTAs exhibited a functionality close to 1 and were used for chain extension in the presence of ethylene at 80 bar to afford well-defined PMMA-*b*-PE copolymers. **PMMA-T** did not feature a slow consumption during chain extension with ethylene, which is in contrast to **PMMA-6**.

The determination of the molar masses of the block copolymers could not be reliably achieved by $^1\text{H-NMR}$ for PMMA-*b*-PE copolymers obtained with PMMA-T, which is attributed to aggregation and self-assembly properties of the resulting polar-apolar block copolymers. Assembly properties were indeed hinted at by HT-SEC and confirmed by TEM analyses with the observation of worm-like particle morphologies. It is probable that self-assembly occurred during polymerization (PISA) or during cooling and crystallization of the PE block (crystallization-driven self-assembly, CDSA). More systematic studies varying the molar masses of the PMMA block (obtained by either RAFT or radical polymerization + DT) and/or that of the PE block could probably allow us to distinguish between a PISA or CDSA process, or a combination of both.

These results represent the first examples of the synthesis of PMMA-*b*-PE copolymers by RDRP of MMA and ethylene. These block copolymers can find potential application as compatibilizer in epoxy resins and polymer blends.^[35,36]

Part of the work carried out with TD and PMMA-T has been published:

Polym. Chem., **2019**, 10, 6630-6640

V. Experimental section

Materials and methods

The comprehensive list of materials and analytical methods used for this work are presented at the end of this manuscript.

Synthesis of PMMA-6 with CTA 6-H⁺

To a cold (0°C) solution of CTA 6 (1.3 g, 1 eq.) in MeCN (8 mL) was added TfOH (0.73 g, 0.95 eq.) followed by MMA (16 mL, 30 eq.) and AIBN (0.25 g, 0.3 eq.). The solution was degassed by three freeze-vacuum-thaw cycles, filled with argon and immersed into an oil bath at 70°C. Samples were removed at different time intervals for ¹H-NMR and SEC-THF analyses. After 20 hours, the solution was cooled down in an ice bath and DIPEA (0.9 mL, 1 eq.) was added. Chloroform (20 mL) was added and the volatiles were removed *in vacuo*. The residue was dissolved in chloroform (20 mL) and precipitated in cold methanol (1 200 mL). The polymer was recovered by filtration, washed with methanol and dried *in vacuo* until constant weight. ¹H NMR (CDCl₃) δ (ppm) 8.73 (m, 2H); 7.23 (m, 2H) 3.58 (broad s, 240H); 2.25-1.55 (m, 150H); 1.30-0.70 (m, 260H).

Synthesis of *N,N'*-dimethyl-*N,N'*-diphenyl thiuram disulfide (TD)

To a cold (-20 °C) solution of *N*-methylaniline (12 g – 0.111 mol) in dry THF (50 mL) was added *n*-butyl lithium (47 mL – 0.117 mol) over 20 minutes under argon. A white precipitate appeared upon addition. The suspension was allowed to stir for 1 hour at that temperature and cooled down to -20 °C before the dropwise addition of CS₂ (10 mL – 0.167 mol). The resultant bright orange solution was allowed to stir at room temperature overnight. The reaction mixture was cooled to 0°C and an iodine solution (14 g I₂ dissolved in 250 mL 10% aqueous KI solution) was added dropwise. More water (200 mL) was added and THF was removed *in vacuo* to afford a thick suspension. The solid was isolated by filtration, washed with water, methanol and heptane until colorless filtrate. The crude product was recrystallized from DCM/MeOH to afford TD as a tan colored crystalline powder that was dried *in vacuo* until stable weight (15.71 g, 78% yield). ¹H NMR (CDCl₃) δ (ppm) 3.82 (s, 6H, 2x N-CH₃); 7.45 (m, 10H, 2x ArH). LC-MS (M+H)⁺ m/z = 365.0269 (365.0267 theo.).

General procedure for the synthesis of PMMA-T

MMA, TD, AIBN and MeCN (70 mL) were introduced in a Schlenk flask to the desired quantities (MMA/TD/AIBN ratios of 100/1/1, 50/1/1 or 25/1/1 with TD: 1.09 g and AIBN: 0.49 g). The flask was degassed by three freeze-vacuum-thaw cycles, sealed under argon and immersed in an oil bath at 80°C for 6 hours. The conversion after 6 hours was determined by ¹H-NMR and the polymerization was stopped by rapid cooling in an ice bath. The volatiles were removed in vacuo, the residue was dissolved in the minimum amount of acetonitrile and the resulting viscous oil was filtered to remove unreacted TD. The polymer was then recovered by precipitation in cold methanol (500 mL) and dried *in vacuo* to afford the desired PMMA-T. Exemplary ¹H-NMR (CDCl₃) for PMMA-T4: δ (ppm) 7.45 (m, 3H); 7.24 (m, 2H) 3.58 (broad s, 45H); 2.25-1.55 (m, 28H); 1.30-0.70 (m, 45H).

Typical block copolymerization procedure

With vinyl acetate

PMMA-T (0.12 mmol), AIBN (0.04 mmol) and VAc (34.8 mmol) were dissolved in ethyl acetate (1 mL). The mixture was transferred in a Schlenk tube equipped with a septum, degassed by three freeze-vacuum-thaw cycles and filled with argon. The flask was immersed in an oil bath at the desired temperature (70 °C) and samples withdrawn from the polymerization mixture at different times for ¹H NMR and SEC-THF analyses.

With ethylene

The employed autoclave reactor (160 mL) was equipped with a mechanical stirring apparatus, a thermometer, and a pressure sensor. In a typical polymerization procedure, a degassed solution of AIBN (10 – 25 mg, 1 eq.) and a PMMA macro-CTA (3 eq.) in DMC (50 mL) was added to the reactor preheated to 80 °C under argon atmosphere with a mechanical stirring of 600 rpm. Immediately after the injection port was closed, ethylene gas was fed into the reactor until the targeted pressure of 80 bar was reached. If necessary, additional ethylene gas was introduced to keep a constant pressure during the polymerization. After a predetermined period of time, the stirring was slowed down and the reactor was cooled with iced water. When the temperature inside the reactor dropped below 25 °C, the remaining pressure was carefully released. The content of the reactor was collected with toluene, and evaporation of the solvent gave the polymeric product.

VI. References

- [1] G. Moad, D. Keddie, C. Guerrero-Sanchez, E. Rizzardo, S. H. Thang, *Macromol. Symp.* **2015**, *350*, 34–42.
- [2] S. Harrisson, X. Liu, J.-N. Ollagnier, O. Coutelier, J.-D. Marty, M. Destarac, *Polymers*. **2014**, *6*, 1437–1488.
- [3] S. Yamago, *J. Polym. Sci. Part A Polym. Chem.* **2006**, *44*, 1–12.
- [4] B. Ray, M. Kotani, S. Yamago, *Macromolecules* **2006**, *39*, 5259–5265.
- [5] M. Benaglia, J. Chiefari, Y. K. Chong, G. Moad, E. Rizzardo, S. H. Thang, *J. Am. Chem. Soc.* **2009**, *131*, 6914–6915.
- [6] G. Moad, M. Benaglia, M. Chen, J. Chiefari, Y. K. Chong, D. J. Keddie, E. Rizzardo, S. H. Thang, *ACS Symp. Ser.* **2011**, *1066*, 81–102.
- [7] D. J. Keddie, C. Guerrero-Sanchez, G. Moad, E. Rizzardo, S. H. Thang, *Macromolecules* **2011**, *44*, 6738–6745.
- [8] M. Destarac, D. Matioszek, X. Vila, J. Ruchmann-Sternchuss, S. Z. Zard, *ACS Symp. Ser.* **2018**, *1284*, 291–305.
- [9] T. Otsu, K. Nayatani, I. Muto, M. Imai, *J. Chem. Soc.* **1958**, *61*, 142–148.
- [10] T. Otsu, K. Nayatani, *Die Makromol. Chemie* **1958**, *27*, 149–156.
- [11] M. Niwa, T. Matsumoto, H. Izumi, *J. Macromol. Sci. Part A - Chem.* **1987**, *24*, 567–585.
- [12] S. A. Haque, G. Clouet, *Macromol. Chem. Phys.* **1994**, *195*, 315–327.
- [13] M. Niwa, Y. Sako, M. Shimizu, *J. Macromol. Sci. Part A - Chem.* **1987**, *24*, 1315–1332.
- [14] S. A. Haque, *J. Macromol. Sci. Part A* **1994**, *31*, 827–833.
- [15] J. Catala, *Radical Polymerisation Method Performed in the Presence of Disulphide Compounds. WO 03/020773 A2*, **2003**.
- [16] C. Zhang, L. Li, H. Cong, S. Zheng, *J. Polym. Sci. Part A Polym. Chem.* **2014**, *52*, 952–962.
- [17] C. Dommanget, F. D’Agosto, V. Monteil, *Angew. Chem. Int. Ed.* **2014**, *53*, 6683–6686.
- [18] A. Wolpers, C. Bergerbit, B. Ebeling, F. D’Agosto, V. Monteil, *Angew. Chem. Int. Ed.* **2019**, *58*, 14295.
- [19] J. Brandrup, E. H. Immergut, E. A. Grulk, *Polymer Handbook*, **1999**.
- [20] D. J. Keddie, G. Moad, E. Rizzardo, S. H. Thang, *Macromolecules* **2012**, *45*, 5321–5342.
- [21] G. Moad, C. Barner-Kowollik, *Handbook of RAFT Polymerization. C. The Mechanism and Kinetics of the RAFT Process: Overview, Rates, Stabilities, Side Reactions, Product Spectrum and Outstanding Challenges*, **2008**.
- [22] R. Hoogenboom, C. R. Becer, C. Guerrero-Sanchez, S. Hoepfner, U. S. Schubert, *Aust. J. Chem.* **2010**, *63*, 1173.
- [23] Y. Mai, A. Eisenberg, *Chem. Soc. Rev.* **2012**, *41*, 5969–5985.
- [24] D. E. Discher, A. Eisenberg, *Science*. **2002**, *967*, 967–973.
- [25] F. D’Agosto, J. Rieger, M. Lansalot, *Angew. Chem. Int. Ed.* **2019**, *Accepted Article*, DOI doi:10.1002/anie.201911758.
- [26] A. M. Oliver, J. Gwyther, C. E. Boott, S. Davis, S. Pearce, I. Manners, *J. Am. Chem. Soc.* **2018**, *140*, 18104–18114.
- [27] C. Zhang, L. Li, H. Cong, S. Zheng, *J. Polym. Sci. Part A Polym. Chem.* **2014**, *52*, 952–962.
- [28] F. R. Mayo, *J. Am. Chem. Soc.* **1943**, *65*, 2324–2329.
- [29] G. Moad, D. H. Solomon, in *Chem. Radic. Polym. (Second Ed.* (Eds.: G. Moad, D.H. Solomon), Elsevier Science Ltd, Amsterdam, **2005**, pp. 279–331.
- [30] T. P. Davis, *Handbook of Radical Polymerization*, John Wiley & Sons, Inc. **2013**.
- [31] T. Otsu, A. Matsumoto, *Microencapsul. Microgels Iniferters. Adv. Polym. Sci.* **1999**, *136*, 75–137.
- [32] Y. Nakamura, S. Yamago, *Macromolecules* **2015**, *48*, 6450–6456.
- [33] E. Folta-Stogniew, *Methods Mol. Biol.* **2006**, *328*, 97–112.
- [34] M. P. Tarazona, E. Saiz, *J. Biochem. Biophys. Methods* **2003**, *56*, 95–116.
- [35] S. Ritzenthaler, F. Court, E. Girard-Reydet, L. Leibler, J. P. Pascault, *Macromolecules* **2003**, *36*, 118–126.
- [36] M. Hernandez, B. Sixou, J. Duchet, H. Sautereau, *Polymer*. **2007**, *48*, 4075–4086.

Chapter V

Synthesis of block copolymers based on a poly(ethylene oxide) macro-CTA

I. Introduction.....	194
I.1. RAFT-mediated emulsion polymerization	194
I.2. Emulsion polymerization of ethylene	195
I.3. Amphiphilic block copolymers with ethylene.....	196
II. Synthesis of PEO-<i>b</i>-PE copolymers in DMC.....	197
II.1. Polymerization of ethylene in the presence of PEO macro-CTAs.....	198
II.2. Chain-ends analysis	199
II.3. Self-assembly properties of PEO- <i>b</i> -PE	202
III. Synthesis of PEO-<i>b</i>-PE copolymers in water	205
III.1. Polymerization under RAFT conditions	205
III.1.1. Ethylene polymerization in water in presence of PEO macro-CTAs.....	205
III.1.2. Synthesis of PEO- <i>b</i> -EVA copolymers	207
III.2. Polymerization using lower amounts of macro-CTA	210
III.2.1. Synthesis of PEO- <i>b</i> -PE copolymers with PEO-NN	210
III.2.2. Synthesis of PEO- <i>b</i> -PE copolymers with PEO-N.....	211
IV. Conclusion	215
V. Experimental section	217
VI. References	220

I. Introduction

The ultimate goal of this chapter is to investigate the synthesis of PEO-*b*-PE copolymers by polymerization-induced self-assembly (PISA) in water using a water-soluble PEO macro-CTA. The concepts of PISA and of RAFT-mediated emulsion polymerization will be briefly presented, as well as specific works on ethylene radical polymerization in water. The feasibility of PEO-*b*-PE copolymer synthesis by the selected route will be primarily assessed by RAFT polymerization in DMC, and then DMC will be replaced by water as polymerization solvent. The change of solvent is not without importance because DMC is known to activate ethylene polymerization. On the other hand, water does not induce any transfer to solvent and the polymerization can be performed at 200 bar as the ethylene/water mixture does not become supercritical under such polymerization conditions.

I.1. RAFT-mediated emulsion polymerization

The application of RAFT polymerization to aqueous systems (*i.e.* emulsion polymerization) is not trivial. Unforeseen difficulties, such as loss of control during polymerization and poor colloidal stability have been faced when switching from bulk/solution polymerization.^[1-5] These issues were attributed to the intrinsic mechanism of emulsion polymerization and to the nature of the CTAs, and were circumvented through the use of hydrosoluble macro-CTAs, replacing molecular CTAs.^[6] The chain-extension of a hydrophilic macro-CTAs with a hydrophobic vinyl monomer leads to the formation of an amphiphilic block copolymer. As the hydrophobic block grows, the polymer becomes insoluble and can self-assemble into various morphologies. The resulting core-shell particles are stabilized by the hydrophilic corona, without the need for surfactant. This process is known as PISA.^[7-9] More generally, a PISA process is expected to happen in the case of a solvophilic living macro-CTA, chain-extended with a solvophobic monomer (**Figure 1**) and does not necessarily imply the use of water as polymerization medium.^[10] While RAFT is commonly associated with PISA,^[9-13] other RDRP techniques (ATRP,^[14] NMP,^[15,16] TERP,^[17,18] ITP^[19]) are also applicable.

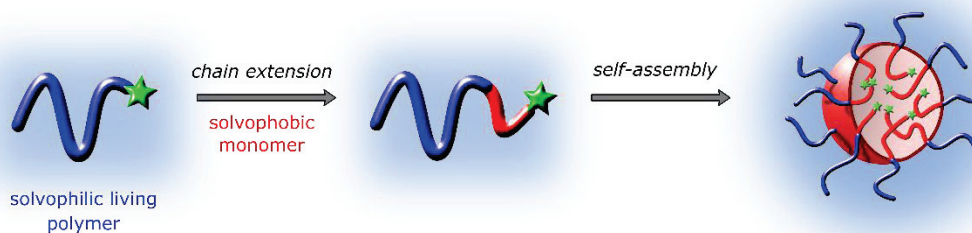


Figure 1. Schematic representation of the polymerization-induced self-assembly with a solvophilic living macro-CTA chain-extended with a solvophobic monomer.

Different particle morphologies, such as spheres, worms (rods/cylinders) or vesicles can be obtained by PISA, by varying the nature and ratio of the solvophobic/solvophilic segments, the solids content and the polymerization conditions. The hydrophilic macro-CTA is usually synthesized by RAFT from polar water-soluble monomers (e.g. (meth)acrylic acid,^[20,21] acrylamides^[22]) in organic solvent, purified and eventually used for chain-extension. It is also possible to perform the block copolymerization in an all-water, one-pot process.^[13,23,24] Alternatively, PEO macro-CTAs can be synthesized by post modification of preformed PEO chains.^[25] PEO being made by an anionic process, this method ensures a quasi-monodisperse macro-CTA. The molar mass of the PEO chains (from 1 000 to 5 000 g mol⁻¹) is known to affect both the particle sizes and the polymerization rate.^[26] Depending on the nature of the chain-end, PEO has been successfully used as macro-CTA for both LAMS (xanthate chain-end with VAc^[27,28]) and MAMs (dithiocarbonate and trithiocarbonate chain-ends with styrene^[29] and vinylidene chloride/methyl acrylate,^[30] respectively).

1.2. Emulsion polymerization of ethylene

In our group, Grau *et al.*^[31] and Billuart *et al.*^[32] investigated the free radical emulsion polymerization of ethylene (FREPE) under mild conditions ($P < 250$ bar, $T < 90$ °C). They found that stable PE latexes (particle size ~ 100 nm) could be obtained with either cationic (2,2-azobis(2-amidinopropane) dihydrochloride (AIBA)) or anionic (ammonium persulfate (APS)) initiators. The colloidal stability is explained by the presence of the charged initiator at the polymer chain-end. The addition of ionic surfactants (cetyltrimethylammonium bromide (CTAB) with AIBA and sodium dodecyl sulfate (SDS) with APS) led to higher polymerization yields (i.e. higher solids content) and smaller particles (size down to $\sim 20 - 40$ nm). PE obtained from FREPE has a high molar mass (up to 10^5 g mol⁻¹) but HT-SEC analysis often shows multimodal or exceptionally broad MMDs. In both cases, FREPE carried out without surfactant afforded spherical particles (~ 100 nm), whereas the addition of surfactant above the critical micellar concentration (CMC) affords smaller ellipsoidal particles ($\sim 20 - 40$ nm). Small and wide angle X-ray scattering (SAXS/WAXS) analyses by our group suggested that the crystallization occurs during cooling of the polymerization mixture and not during the polymerization, explaining the formation of such small particles.^[33] Emulsion polymerization of ethylene is not an ordinary one: the introduction of ethylene as a supercritical gas means that no liquid monomer droplet is present in the polymerization medium, differing in that regard to more conventional emulsion polymerization processes.

To the best of our knowledge, the RAFT emulsion polymerization of ethylene has never been attempted.

I.3. Amphiphilic block copolymers with ethylene

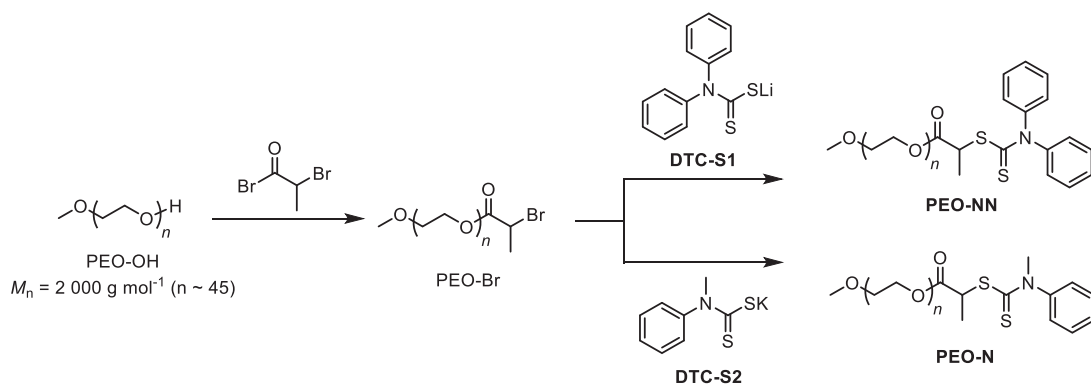
Amphiphilic PE-*b*-PEO copolymers are commercially available and find applications as compatibilizer in epoxy resins^[34] or in porous membranes.^[35] These block copolymers are synthesized by successive anionic polymerization of butadiene and ethylene oxide followed by hydrogenation of the polybutadiene block. These materials are also attainable by coordination-insertion polymerization of ethylene, post-modification and anionic ring-opening polymerization of ethylene oxide or click chemistry.^[36-38] The assembly properties of these block copolymers have been investigated in only one instance.^[36] The authors found that spherical particles could be obtained, with a diameter decreasing from ~ 55 nm down to ~ 20 nm with decreasing PE content and increasing PEO block molar mass.

In the literature, examples of RAFT mediated emulsion polymerization with a PEO macro-CTA systematically include xanthates, dithiocarbonates or trithiocarbonates chain-ends.^[28-30] To the best of our knowledge, there exists no example involving a dithiocarbamate chain-end. Based on the results obtained during this work, a dithiocarbamate functionalized PEO was preferred as macro-CTA. The use of *O*-alkyl xanthate results in side-fragmentation whereas the synthesis of PEO with an *O*-aryl xanthate is too tedious to be efficiently implemented.

*In this chapter, dithiocarbamate functionalized PEO macro-CTAs will be used for the first time for the formation of PEO-*b*-PE block copolymers, and the synthesis will be attempted both in organic solvent and in water. The growth of a PE block onto a pre-formed PEO block by RDRP has never been published. The synthesis of block copolymers in water with one insoluble semicrystalline block is also a real challenge.*

II. Synthesis of PEO-*b*-PE copolymers in DMC

A commercial PEO-OH ($M_n = 2\,000\text{ g mol}^{-1}$, $\mathcal{D} < 1.05$) was bought from Aldrich and functionalized by dithiocarbamate salts (**DTC-S1** and **DTC-S2**, **Scheme 1**) by a protocol adapted from the synthesis of PEO-xanthate^[39] to achieve **PEO-NN** ($Z=NPh_2$) and **PEO-N** ($Z=N(Ph)Me$), respectively. The synthesis of a dithiocarbamate salt followed by the addition of the bromo-functionalized PEO (**PEO-Br**, **Scheme 1**) without isolation of the salt was found to only yield a PEO macro-CTA with a poor chain-end fidelity, along with the presence of impurities. To circumvent this issue, the dithiocarbamate salts were isolated beforehand. This is easily achieved with **DTC-S2**, that can be synthesized in water by a protocol adapted from the literature^[40] and isolated by simple lyophilization. On the other hand, the synthesis of **DTC-S1** necessitates harsher conditions (*n*-BuLi, dry THF) and the salt has to be isolated under an inert atmosphere.^[41] The synthetic protocols for **PEO-N** and **PEO-NN** are fully described in the experimental part at the end of this chapter. **PEO-N** and **PEO-NN** have been fully characterized by ¹H-NMR (see **Experimental section**).



Scheme 1. Simplified synthetic route to PEO-N and PEO-NN from commercial PEO-OH.

Noteworthy, PEO-N has been designed as a direct application of CTA **3** (dithiocarbamate with $Z = N(Ph)Me$) of Chapter II. PE homopolymer obtained when this CTA was used to mediate ethylene homopolymerization featured the cleanest ¹H-NMR spectrum of all dithiocarbamates. As a brief anticipation of the following part, a remarkably slow consumption of this PEO macro-CTA was observed during block copolymerization with ethylene. It was only at a later stage during this work that full conversion of the dithiocarbamate CTA was found to be systematically achieved when $Z=NPh_2$. Consequently, PEO-NN and PEO-N were investigated almost a year apart, but the results will be presented together for direct comparison and for the sake of clarity.

II.1. Polymerization of ethylene in the presence of PEO macro-CTAs

The chain-extension of **PEO-N** and **PEO-NN** with ethylene was performed at 80 °C, 80 bar and using 50 and 25 mg of AIBN, respectively. The difference in the quantity of **PEO-N** and **PEO-NN** used is due to the lesser amount of **PEO-NN** isolated with sufficient purity, for the reasons stated above. In both cases, the [macro-CTA]:[AIBN] ratio is 3:1. The results of the polymerizations are presented in **Table 1**.

Table 1. Polymerization of ethylene in the presence PEO-N and PEO-NN at 80 °C and 80 bar.

Entry	macro-CTA	AIBN (mg)	Time (h)	Yield of PE (g)	$M_{n,theo}^a$ PE block (g mol ⁻¹)	$M_{n,NMR}^b$ PE block (g mol ⁻¹)	Conv. ^b of macro-CTA (%)
1	PEO-N	50	1	0.15	160	850	37
2	PEO-N	50	3	0.82	890	1 500	76
3	PEO-N	50	4	1.20	1 250	1 750	86
4	PEO-N	50	5	1.83	2 000	1 800	89
5	PEO-N	50	6	1.99	2 180	2 700	92
6	PEO-NN	25	2	0.30	650	900	100
7	PEO-NN	25	4	0.58	1 250	1 450	100
8	PEO-NN	25	6	0.82	1 850	1 800	100
9	PEO-NN	25	8	1.26	2 600	2 500	100

Polymerization conditions: T = 80°C, P = 80 bar, DMC: 50 mL, PEO-N: 2.0 g (18.3 mmol L⁻¹), PEO-NN: 1.1 g (9.1 mmol L⁻¹). ^a:

Calculated from yield;

^b: Determined by ¹H-NMR in TCE/C₆D₆ according to equation 1

Unsurprisingly and consistently with what was observed in Chapter II, both macro-CTAs have a substantial rate retardation effect compared to the FRP of ethylene using the same initiator amount (**Figure 2**). The polymerization proceeds ca. 3 times slower than in the absence of macro-CTA.

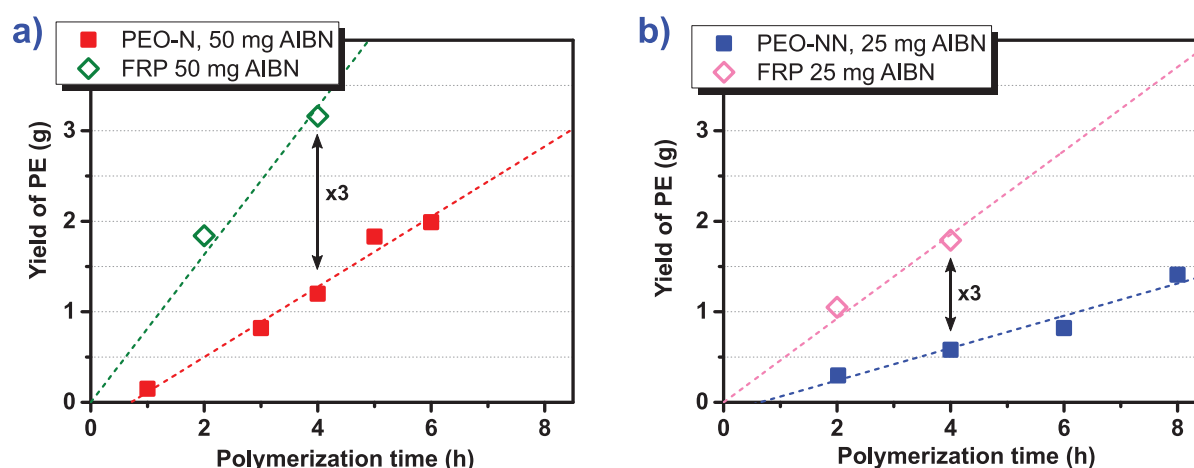


Figure 2. Kinetics of the polymerization of ethylene in the presence of PEO-N (a) and PEO-NN (b). The kinetics of the corresponding FRP of ethylene are also plotted for comparison. The dotted lines correspond to the linear fits. See table 1 for experimental details.

The HT-SEC traces of the chain-extensions of **PEO-N** and **PEO-NN** are presented in **Figure 3**. When PEO-N (**Figure 3a**) is used, the molar masses shift indeed towards higher values. However,

a high-intensity shoulder is detected at elution time = 22.8 minutes, corresponding to the starting macro-CTA. The shoulder is still detected even at polymerization time = 6 hours, indicating a particularly slow consumption of **PEO-N**. This behavior mirrors what was observed in Chapter IV with the chain-extension of **PMMA-6** with ethylene. On the other hand, when **PEO-NN** is used, the chain-extension proceeds smoothly with a clean shift of molar masses towards higher values (**Figure 3b**). No shoulder is detected, indicating a fast and quantitative consumption of **PEO-NN**. The MMDs become undoubtedly narrower as the polymerization proceeds, characteristic of an efficient transfer. The MMDs evolution when **PEO-N** is used is even more remarkable considering that when a PMMA macro-CTA with the same Z-group is used (Chapter IV), this behavior is not observed, suggesting a strong influence of the nature of the macro R-group. Molar masses and dispersity values could not confidently be determined by HT-SEC for the reasons previously stated in this manuscript.

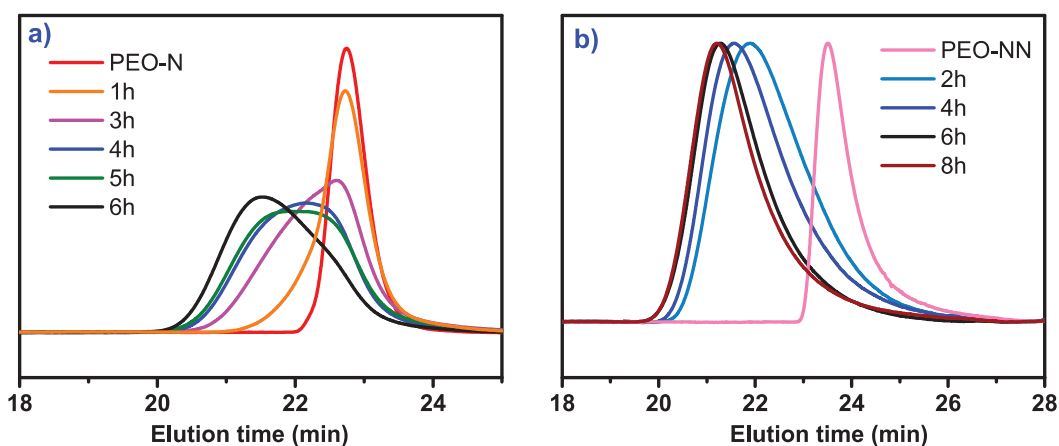


Figure 3. HT-SEC traces of the polymers resulting from ethylene polymerization in the presence of **PEO-N** (a) and **PEO-NN** (b) at 80 °C and 80 bar.

II.2. Chain-ends analysis

An overlay of the $^1\text{H-NMR}$ spectra of all **PEO-*b*-PE** copolymers obtained with **PEO-N** is presented in **Figure 4**. The slow consumption of **PEO-N**, by relative integration of the characteristic **PEO-C(O)CH(CH₃)SC(S)Z** (proton **c**, $\delta = 4.75$ ppm) proton for the **PEO** macro-CTA with respect to its counterpart after chain-extension **PEO-C(O)CH(CH₃)-PE-SC(S)Z** (**c'**, $\delta = 2.33$ ppm), is evidenced. Indeed, the intensity of the signals from protons **c** and **d** gradually decreases during polymerization, whereas the intensity of the protons **c'**, **d'** and **e**, characteristic of the macro-CTA chain-extended with ethylene, increases. As it was the case for ethylene homopolymerization with CTA **3** (see Chapter II), the baseline between 2.4 and 3.0 ppm is remarkably clean, proof of the absence of parasitic side reactions when $\text{Z}=\text{N}(\text{Ph})\text{Me}$.

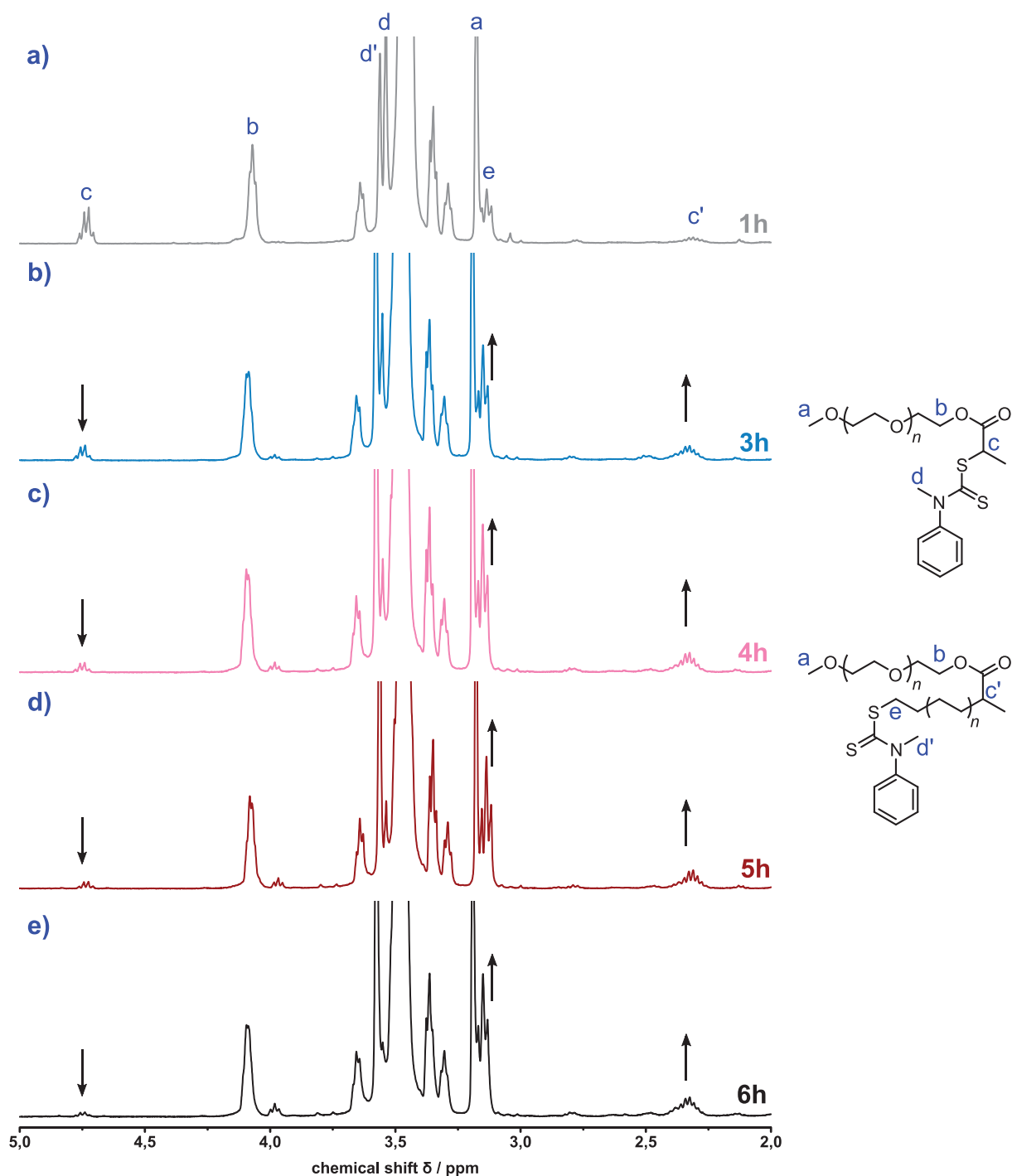


Figure 4. $^1\text{H-NMR}$ spectra of the polymers obtained after ethylene polymerization in the presence PEO-N for different polymerization times: a) 1 hour; b) 3 hours; c) 4 hours; d) 5 hours; e) 6 hours at $80\text{ }^\circ\text{C}$ and 80 bar.

This is not the case for **PEO-NN**, which features a complete consumption at any polymerization time, as expected from the HT-SEC traces. An exemplary $^1\text{H-NMR}$ spectrum of a PEO-*b*-PE obtained with **PEO-NN** after 4 hours of polymerization is given in **Figure 5**, along with the spectrum of the starting macro-CTA. Albeit full consumption of the macro-CTA and clean chain-extension observed by HT-SEC, all PEO-*b*-PE obtained from PEO-NN exhibit a triplet at $\delta = 2.39\text{ ppm}$ (labelled with * in Figure 5). This triplet most likely stems from the formation of the thioether species

previously identified (**SP2**, Chapter **II**, **Scheme 3**), indicating potential cross-termination side reactions. The expected better stabilization of the radical intermediate with **PEO-NN** might be responsible for this phenomenon, prolonging the lifetime of the intermediate radical so that cross-termination can happen. However, the intensity of this triplet is very small (integrates for 0.28 when the integral value of protons a + e is fixed at 5 in Figure 5) and those side reactions, do not seem to affect the course of the polymerization to a large extent.

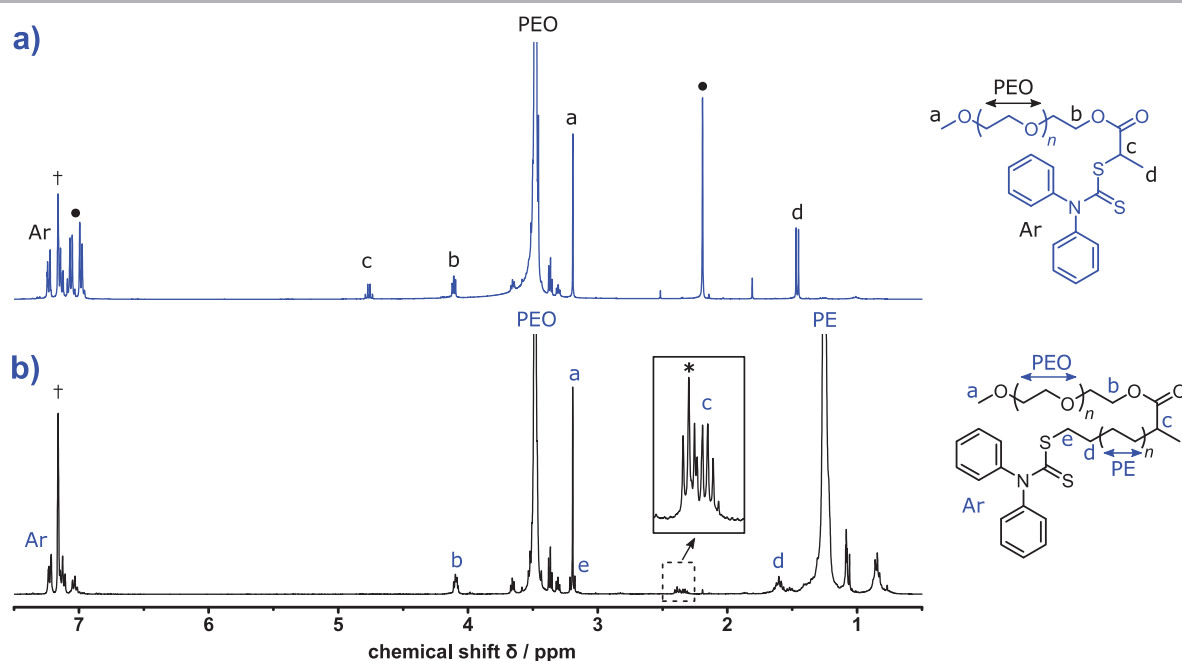


Figure 5. ¹H-NMR spectra of PEO-NN (a) and after 4 hours of block copolymerization with ethylene (b), corresponding to entry 7 of Table 1. (†) NMR residual solvent benzene, (•) toluene.

The integrations of the PEO region ($\delta = 3.48$ ppm) and of the PE region ($\delta = 1.25$ ppm) give access to the average molar mass of the PE block according to **Equation 1** (corrected with the conversion in the case of PEO-N), which are presented in **Table 1**.

$$M_{n,NMR} = M_{n,PEO} + \frac{DP_n(PEO) * \int_{1.10}^{1.50} (CH_2CH_2)_p}{\int_{3.25}^{3.85} (CH_2CH_2O)_n} * MW(C_2H_4)$$

Equation 1. Calculation the molar masses of the block copolymers determined by ¹H-NMR, with $DP_n(PEO) = 45$.

The average molar masses of the diblock copolymers increase linearly with the yield of PE regardless of the structure of the macro-CTA (**Figure 6**). For **PEO-N**, the M_n values are substantially higher than the theoretical ones for the lower yields, which is a direct consequence of a low chain transfer constant, traduced by the slow consumption of **PEO-N**. The molar mass of the diblock copolymer tends to get closer to the expected as the yield goes up (**Figure 6a**), hinting again at a low C_{tr} value.^[42] The molar masses calculated for the chain-extension with PEO-NN are

remarkably close to the theoretical line (**Figure 6b**), consistent with a higher C_{tr} and thus an instantaneous consumption of the macro-CTA.

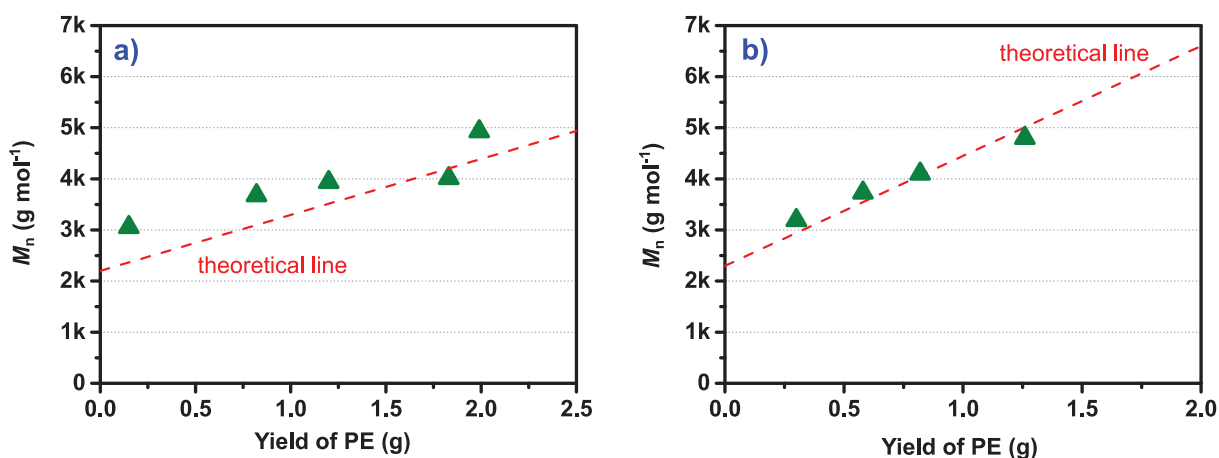


Figure 6. Plot of the molar masses determined by ¹H-NMR of PEO-*b*-PE copolymers obtained with PEO-N (a) and PEO-NN (b) macro-CTAs.

II.3. Self-assembly properties of PEO-*b*-PE

The content of the reactor after ethylene polymerization in the presence of **PEO-N** or **PEO-NN** was systematically a milky white dispersion. These dispersions were stable (up to a few days) and easily re-dispersible by manual shaking, with viscosities increasing with PE yield. As for PMMA-*b*-PE copolymers, this motivated us to investigate the particle morphology by transmission electron microscopy (TEM). It is indeed anticipated that a PISA process is occurring, or alternatively a polymerization-induced crystallization-driven self-assembly (PI-CDSA), as recently termed by Manners *et al.* for block copolymers with a crystalline cores.^[43]



Figure 7. Visual appearance of a dispersion in DMC obtained directly after polymerization of ethylene in the presence of PEO-NN corresponding to the entry 7 of Table 1.

An aliquot of the dispersion in DMC was set aside directly at the end of the polymerization, diluted with DMC and deposited on a TEM grid. Exemplary TEM pictures of the dispersions obtained after 4 hours and 8 hours of block copolymerization of **PEO-NN** with ethylene (entries 7 and 9 of Table 1) are presented in **Figure 8**. PEO-*b*-PE samples from **PEO-NN** were preferred for TEM analyses because of the absence of unreacted macro-CTA. In both cases, worms are observed,

which tend to agglomerate. The worm lengths are shorter after 4 hours (~ 100-200 nm) of block copolymerization than after 8 hours (~ 200-500 nm).

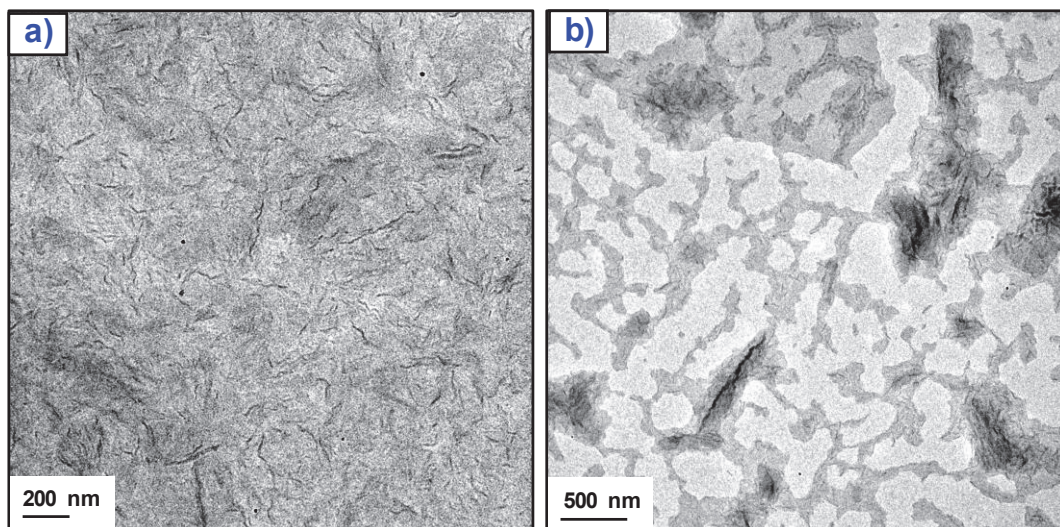


Figure 8. TEM images of PEO-*b*-PE dispersions in DMC obtained after 4 (a) and 8 (c) hours of polymerization of ethylene in the presence of PEO-NN in DMC.

Cryo-TEM in water was used as an alternative to TEM analyses in DMC in an attempt to avoid the formation of aggregates which may occur when DMC evaporates. As cryo-TEM observations are not technically possible on DMC dispersions, the samples obtained after polymerization in DMC were dried and re-dispersed in water (evaporation of solvent at room temperature under the fumehood then at 60 °C and under high vacuum). This treatment should in principle not affect the particle morphologies as the melting temperature of the PE block ($T_f \sim 110$ °C) is not reached. Exemplary cryo-TEM pictures of the dispersions in water of the PEO-*b*-PE after 4 and 8 hours of block copolymerization of PEO-NN with ethylene (entries 7 and 9 of Table 1) are presented in **Figure 9**. The same worm-like morphologies are observed in water. The length of the worms appears to be similar compared to what was observed in DMC: ~ 100-200 nm after 4 hours of polymerization (**Figure 9a**) and > 200 nm after 8 hours (**Figure 9b**). These worms tend to arrange parallel to each other, a behavior already seen for fibers with crystallizable core-forming blocks by Manners and coworkers.^[43]

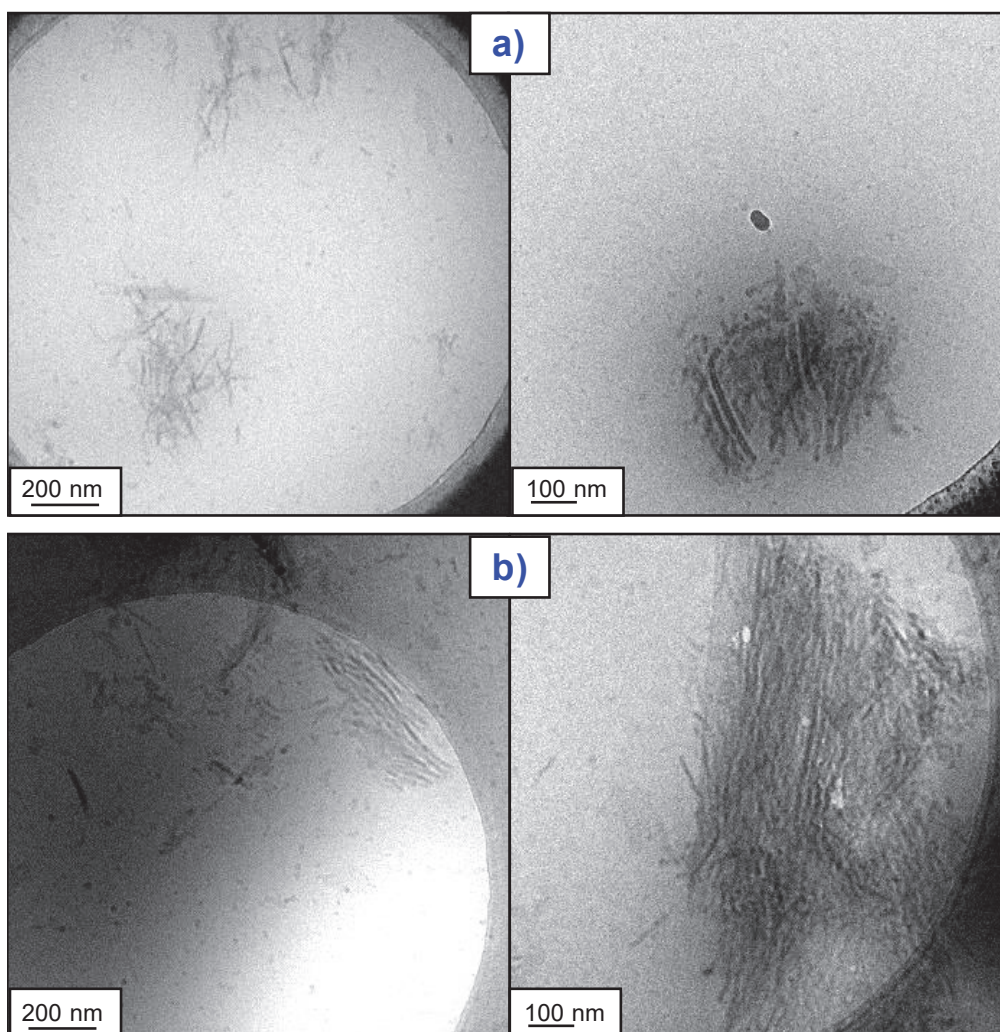


Figure 9. Cryo-TEM images of PEO-*b*-PE dispersions in water obtained after 4 (a) and 8 (b) hours of polymerization of ethylene in the presence of PEO-NN in DMC.

*Chain-extensions of PEO macro-CTAs in DMC with ethylene afforded the desired block copolymers at 80 °C and 80 bar. The slow consumption of PEO-N ($Z=N(\text{Ph})\text{Me}$) was evidenced by HT-SEC and ^1H -NMR analyses, attributed to low chain-transfer constant. The system using PEO-NN ($Z=N\text{Ph}_2$) featured instantaneous consumption in DMC and well-defined PEO-*b*-PE copolymers were obtained. In short, PEO-NN appears to be more efficient to obtained block copolymers than PEO-N.*

III. Synthesis of PEO-*b*-PE copolymers in water

The successful synthesis of PEO-*b*-PE in DMC and the observation of worm-like morphologies *via* TEM and cryo-TEM analyses strongly motivated us to transpose the polymerization from an organic to an aqueous medium. As aforementioned, the use of water as polymerization solvent can potentially have several advantages, such as compartmentalization of radicals, low transfer ability to solvent and the possibility to perform the copolymerization at 200 bar because the ethylene/water mixture is not supercritical at that pressure. The direct block copolymerization using the water-soluble **PEO-N** and **PEO-NN** macro-CTAs appeared as the logical next step in this work.

In the following, two different conditions will be used: RAFT conditions with the aim of controlling the growth of the PE block (i.e. [macro-CTA]:[initiator] ratio = 3:1); and using a lower amount of macro-CTA (i.e. ratio < 3:1) targeting the synthesis of stable surfactant-free PE particles without trying to control the molar mass of PE.

III.1. Polymerization under RAFT conditions

III.1.1. Ethylene polymerization in water in presence of PEO macro-CTAs

PEO-N and **PEO-NN** were both investigated to mediate ethylene polymerization in water. The cationic initiator AIBA was used as it is structurally close to AIBN and is known to provide the highest yields of PE when used without surfactants.^[31] Typical experiments were performed at a temperature of either 70 or 80 °C, a pressure of 200 bar with 50 mL of water and 80 mg of AIBA. As a replication of the conditions used for block copolymerization in DMC, the [macro-CTA]:[AIBA] ratio was set to 3:1. **Table 2** gathers the results of these block copolymerizations, as well as those of a control experiment performed in the absence of macro-CTA.

Table 2. Polymerization of ethylene in the presence of PEO-N and PEO-NN in water under RAFT conditions.

Entry	T (°C)	macro-CTA	Time (h)	Yield of PE ^a (g)	SC (%)	Z _{av} ^b (nm)	PdI ^b
10	70	-	4	2.94	6	162	0.02
11	80	PEO-NN	20	0	-	-	-
12	80	PEO-N	4	0	-	-	-
13	80	PEO-N	20	0	-	-	-
14	70	PEO-N	20	0	-	-	-

Polymerization conditions: P = 200 bar ; AIBA: 80 mg; macro-CTA: 2 g; H₂O: 50 mL; [macro-CTA]:[AIBA] = 3:1. ^a: Determined by gravimetry. ^b: Determined by DLS; SC: solid content

The surfactant-free free radical emulsion polymerization of ethylene at 70 °C affords a stable latex after four hours of polymerization (entry 10) with reasonable PE yield and solids content (SC, 6 %). The addition of PEO macro-CTAs has a dramatic effect on the polymerization as no PE

is produced even after 20 hours of polymerization and increased temperature (80 °C), regardless of the nature of the Z-group. This is in stark contrast with the results obtained when the polymerization is performed in DMC.

In RAFT-mediated PISA emulsion polymerization, the main nucleation mechanism expected to happen is by self-assembly, providing that fast and efficient transfer is taking place. The system may however suffer from unwanted homogeneous nucleation if the transfer is slow, leading to the formation of solvophobic homopolymer (**Figure 10**). This typically happens when the radical initiator rapidly reacts with the solvophobic monomer and the resulting oligomers precipitate before reacting with the solvophilic macro-CTA.^[23]

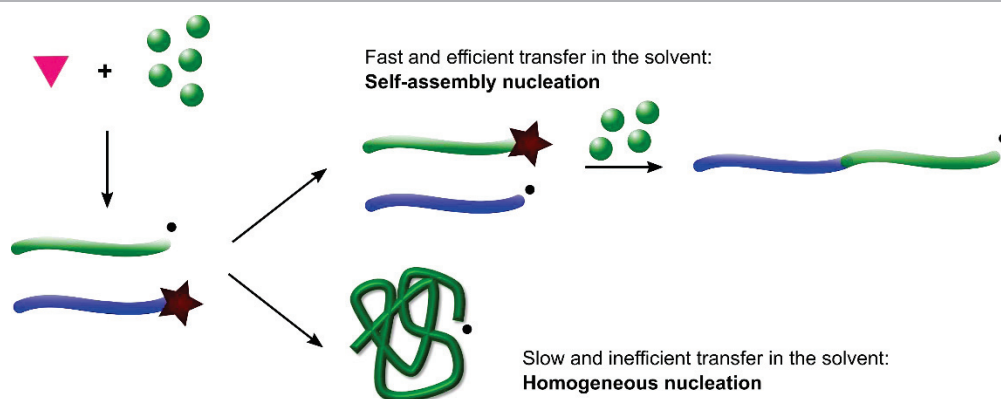


Figure 10. Schematic representation of the expected self-assembly nucleation versus the non-expected homogeneous nucleation in RAFT-mediated emulsion polymerization in presence of a water-soluble macro-CTA and a water soluble radical initiator (▼). Adapted with permission from ^[23]. Copyright 2012 American Chemical Society.

As no PE homopolymer is formed under the presently used conditions, such competitive mechanism to PISA can be ruled out. It is known from the block copolymerizations in DMC that the macro-radical PEO• is able to re-initiate ethylene polymerization. Hence, inefficient re-initiation can also be ruled out. ¹H-NMR and SEC-THF analyses were performed on the residue obtained after polymerization. SEC-THF shows that the residue from the entry 11 in **Table 2** is mostly composed of a population of PEO with a lower molar mass than the starting PEO-NN, superimposable to the original unfunctionalized commercial PEO-OH. A second population is detected at a molar mass about twice the value of the main population, which is likely to correspond to recombination products (**Figure 11a**). The corresponding UV absorbance traces of the starting PEO-NN and of the residue of entry 11 are presented in **Figure 11b**. The residue features a negligible absorbance at 300 nm (maximum of the C=S double bond of PEO-NN), for similar concentration of the sample analyzed (~ 5 mg mL⁻¹). This indicates that the dithiocarbamate functionality was partially lost during the attempted polymerization and that some recombination probably occurred, hinting that the release of PEO• did indeed occur at some point during the reaction. Thus, it is likely that the PEO• were either too short-lived to re-initiate

ethylene or that ethylene monomers were simply not available in the environment of that generated PEO•. ¹H-NMR analysis was inconclusive towards the exact nature of the residue as it was not purified (aromatic protons were still detected). However, no signal corresponding to the PEO-C(O)CH(CH₃)SC(S)Z proton ($\delta = 4.75$ ppm) was detected, confirming chain-end degradation and loss of the dithiocarbamate chain-end. Similar results were obtained with **PEO-N**.

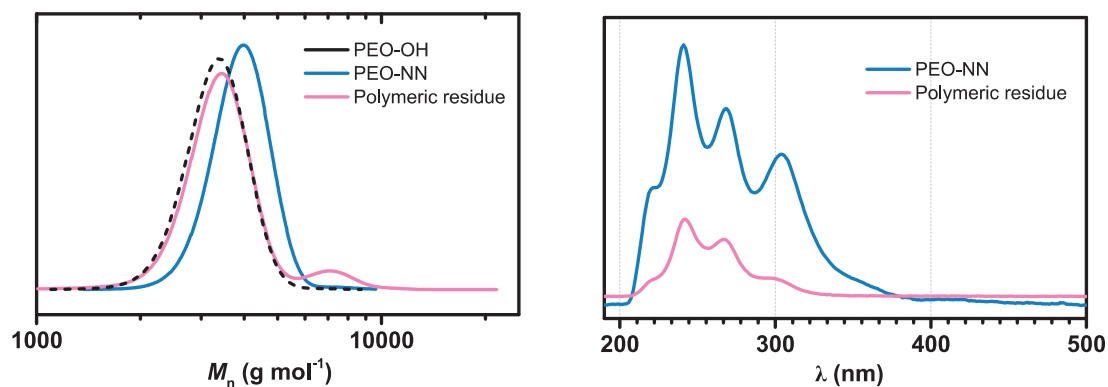


Figure 11. SEC-THF traces of PEO-OH, PEO-NN and of the residue obtained after 20 hours of polymerization in the presence of PEO-NN in water (a) and corresponding UV absorbance spectra (b).

These results give clues as to what might happen. The macro-CTAs lose their dithiocarbamate chain-ends during the 20 hours of polymerization. This could happen either by hydrolysis or upon radical addition (from the radical initiator). PEO macro-CTAs and molecular dithiocarbamates have not been reported to undergo rapid hydrolysis in water under polymerization conditions.^[27,44] However, the effect of the pressure of ethylene and the use of dithiocarbamate functionalized PEOs have not been specifically studied. To gain further insight into the system, the polymerization of VAc and with a mixture of VAc and ethylene was attempted in the presence of these macro-CTAs. Indeed, VAc is far more soluble in water (43 g L⁻¹ at 50 °C^[45]) than ethylene (~ 0.77 g L⁻¹ at 200 bar and 80 °C^[46]) and its presence should favor polymerization and the formation of block copolymers with a PEO macro-CTA. The similar reactivity ratios between ethylene and VAc (see Chapter I) should also act in favor of the formation of PEO-*b*-EVA copolymers.

III.1.2. Synthesis of PEO-*b*-EVA copolymers

The polymerization of VAc on the presence of **PEO-N** and of VAc and ethylene in the presence of **PEO-NN** with increasing ethylene pressure (0, 35 and 100 bar) was thus attempted under RAFT conditions at 70 °C. The AIBA and PEO quantities were reduced for these experiments (19 and 470 mg respectively) and the PEO quantity was fixed to be equal to 10 wt% of the VAc quantity. A final solid content of 10 % is targeted for 100 % conversion of VAc without ethylene pressure.

Table 3. Polymerization of VAc in the presence of PEO-N and PEO-NN and of a mixture of VAc/ethylene in the presence of PEO-NN at different ethylene pressures in water.

Entry	Pressure (bar)	Conv. ^c (%)	Yield of polymer (g)	SC (%)	M_n^d (g mol ⁻¹)	\bar{D}^e	Z_{av}^f (nm)	PdI ^f
15 ^a	0	48	2.26	6	10 200	1.75	295	0.16
16 ^b	0	73	3.43	8	15 100	2.24	165	0.10
17 ^b	35	-	0.59	2	5 300	1.40	54	0.65
18 ^b	100	-	0	-	3 400	1.09	-	-

Polymerizations carried out in autoclave. T = 70 °C; VAc: 4.7 g; PEO: 470 mg; AIBA: 19 mg; H₂O: 47 mL; [macro-CTA]:[AIBA] = 3:1. Time of polymerization: 4 hours. ^a: macro-CTA: PEO-N, ^b: macro-CTA: PEO-NN, ^c: Conversion of VAc determined by gravimetry. ^d: Determined by SEC-THF, PS equivalents. ^e: Determined by DLS

Polymerizations carried out in absence of ethylene pressure with **PEO-N** and **PEO-NN** (entries 15 and 16 respectively) afford stable white latexes, slightly viscous. The conversion reached with **PEO-N** is slightly lower (48 %) than with **PEO-NN** (73 %), which explains the lower molar mass achieved with the former ($M_n = 10\,200\text{ g mol}^{-1}$, $M_{n,theo} = 12\,700\text{ g mol}^{-1}$) compared to the latter ($M_n = 15\,100\text{ g mol}^{-1}$, $M_{n,theo} = 19\,100\text{ g mol}^{-1}$). The MMDs obtained after block copolymerization with both macro-CTAs feature a tailing for low molar masses, which can arise from incomplete consumption of the macro-CTAs or unwanted termination (**Figure 12**). Particle sizes differ for the two systems (295 nm with **PEO-N** and 165 nm with **PEO-NN**), but this likely stems from the difference in conversions.

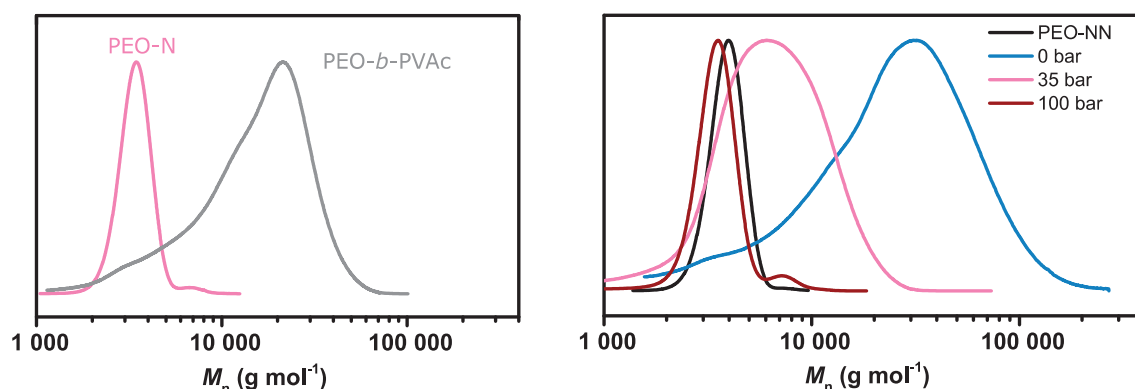


Figure 12. Molar mass distributions of PEO-*b*-PVAc obtained with PEO-N (a) and PEO-*b*-EVA/PEO-*b*-PVAc obtained with PEO-NN (b) obtained at different ethylene pressures.

Ethylene pressure was then added to the system using **PEO-NN**. The addition of ethylene, even at a pressure as low as 35 bar (entry 17), has a dramatic effect on the yield of polymer, which decreases from 3.4 g to 0.6 g. But still, a stable translucent latex was obtained with however broad particle size distribution (PdI = 0.65). At 100 bar, the polymer yield is null, indicating a complete inhibition of the polymerization by ethylene, at least over the considered polymerization time (4 hours). SEC-THF analyses (**Figure 12**) show that the highest molar mass and broadest MMD are obtained when no ethylene is added into the reactor (*i.e.* PEO-*b*-PVAc, $\bar{D} = 2.24$, compared to $\bar{D} = 1.40$ in the presence of ethylene). At 35 bar, the molar mass is greatly reduced, but clean block copolymerization cannot be ascertained as the MMD is broad and overlaps with that of the starting

macro-CTA. At 100 bar, no polymerization occurred and the SEC-THF trace is similar to what was obtained with 200 bar of ethylene and without VAc (entry 12 of **Table 2** and **Figure 11a**). This indicates possible chain-end degradation (without re-initiation and polymerization, further corroborated by the absence of UV absorbance at 300 nm), or, alternatively that the EVA produced is too ethylene-rich and did not go through the filter before SEC analysis. This second assumption can however be ruled out as no resistance was encountered during filtration, indicating the absence of insoluble parts (*i.e.* ethylene-rich EVA). This is further corroborated by $^1\text{H-NMR}$ analysis of the residue after polymerization that shows negligible presence of VAc and ethylene repeating units (**Figure 13**).

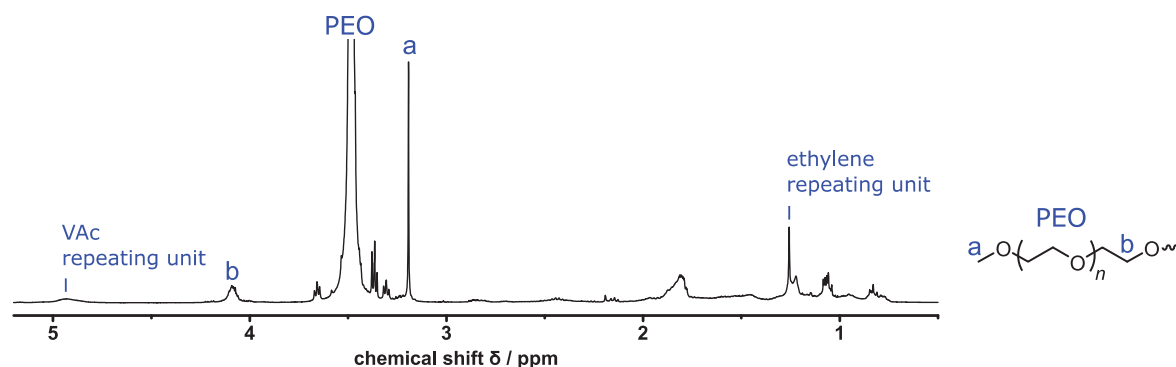


Figure 13. $^1\text{H-NMR}$ spectrum of the residue obtained after polymerization of VAc and ethylene in the presence of PEO-NN at 100 bar of ethylene pressure.

In short, the addition of ethylene at a pressure higher than 35 bar completely inhibits the polymerization and chain-end degradation of the macro-CTA occurs, although the reason behind this phenomenon eludes us. The presence of VAc in the polymerization medium appears to be of little aid (even considering the favorable reactivity ratios between ethylene and VAc, as seen in Chapter I). It is possible that the inhibition period is longer than 4 hours but experiments performed over 8 hours have yielded the same results (data not shown).

To try to overcome this inhibition, polymerization with $[\text{macro-CTA}]:[\text{AIBA}]$ ratios lower than 3 were attempted, by reducing the initial amount of macro-CTA, which can result in the loss of control over polymerization if the amount of CTA is too low compared to the amount of initiator.

III.2. Polymerization using lower amounts of macro-CTA

The absence of polymerization with a [macro-CTA]:[AIBA] ratio of 3:1 might stem from pronounced rate retardation or complete inhibition. This ratio was thus lowered to overcome rate retardation. Different ratios were used: 0.06:1, 0.6:1 and 1:1. Apart from this parameter, the polymerization conditions were similar to the experiments using the standard 3:1 ratio in part II.1: AIBA: 96 mg, H₂O: 50 mL, P = 200 bar and T = 70 °C. Several parameters were found to have a critical influence on both the polymer yield and the particle sizes: nature of the macro-CTA (**PEO-N** vs **PEO-NN**); [macro-CTA]:[AIBA] ratio; ethylene pressure; time of polymerization; stirring speed; temperature; presence or absence of VAc. By lack of time, all these parameters could not be comprehensively investigated and only a succinct study was conducted, of which the principle results will be presented. The following parameters were investigated: nature and quantity of the macro-CTA.

III.2.1. Synthesis of PEO-*b*-PE copolymers with PEO-NN

PEO-NN was used to mediate ethylene polymerization at 200 bar and 70 °C with varying [macro-CTA]:[AIBA] ratio: 0.06, 0.6 and 1. The results of the polymerizations are presented in **Table 4**.

Table 4. Emulsion polymerization of ethylene at 200 bar in the presence of increasing amounts of PEO-NN.

Entry	[macro-CTA]:[AIBA] ratio	Time (h)	Yield of PE ^a (g)	SC (%)	Z _{av} ^b (nm)	PdI ^b
19	-	1	0.80	1.6	102	0.02
20 (10)	-	4	2.94	6	162	0.02
21	-	20	4.82	10	218	0.05
22	0.06	4	2.50	5	118	0.14
23	0.6	4	0	-	-	-
24	1	20	0	-	-	-

Polymerization conditions: T = 70 °C, P = 200 bar, AIBA: 96 mg, H₂O: 50 mL. Ratio 0.06: PEO: 47 mg, AIBA: 96 mg; ratio 0.6: PEO: 470 mg, AIBA: 96 mg, ratio 1: PEO: 650 mg, AIBA: 80 mg. ^a: Determined by gravimetry. ^b: Determined by DLS.

The polymerization in the absence of macro-CTA (entries 19-21) yields stable latexes with increasing solid content (up to 10 %). The particle sizes increase with the yield of PE (from 102 to 218 nm) and remain monodisperse (PdI ≤ 0.05). In the presence of macro-CTA, polymerization only occurs with the lowest quantity of **PEO-NN** (ratio 0.06, entry 22 of **Table 5**), leading to the formation of a stable latex, using in the end less than 2 wt% of PEO with respect to PE. Compared to a reference experiment carried out without **PEO-NN** (entry 20), the yield is slightly impacted (solid content down from 6 to 5%) and the particle size is reduced (from 160 to 120 nm). This last result indicates that the PEO chains may be involved in particle stabilization. Cryo-TEM analysis reveals that the obtained particles are almost spherical, monodisperse, with a size in good agreement with the one determined by DLS. In addition, they appear to contain several PE

crystalline lamellae (**Figure 14**). However, when the **PEO-NN** quantity is increased (entries 23 and 24), a complete inhibition is observed and no polymerization is taking place anymore, even after 20 hours (entry 24).

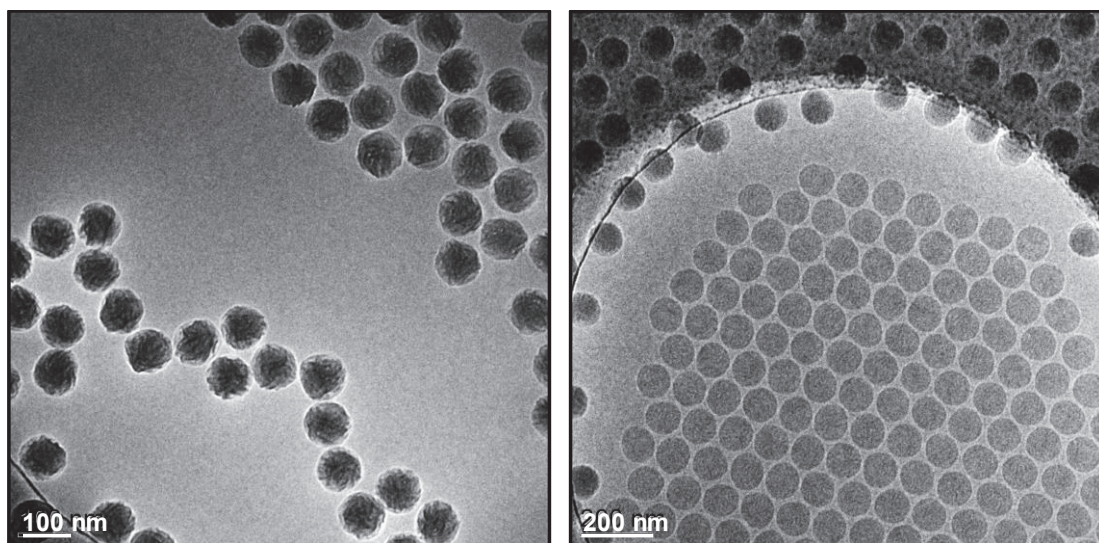


Figure 14. Cryo-TEM pictures of the latex obtained after 4 hours of polymerization with a [PEO-NN]:[AIBA] ratio of 0.06 (entry 22 of Table 5).

III.2.2. Synthesis of PEO-*b*-PE copolymers with PEO-N

PEO-N was also investigated to mediate ethylene polymerization at 200 bar and 70 °C with varying [macro-CTA]:[AIBA] ratios: 0.06, 0.6 and 1. The results of the polymerizations are presented in **Table 5**.

Table 5. Emulsion polymerization of ethylene at 200 bar in the presence of increasing amounts of PEO-N.

Entry	[macro-CTA]:[AIBA] ratio	Time (h)	Yield of PE ^a (g)	SC (%)	Z _{av} ^b (nm)	PdI ^b
19	-	1	0.80	1.6	102	0.02
20 (10)	-	4	2.94	6	162	0.02
21	-	20	4.82	10	218	0.05
25	0.06	4	2.56	5	125	0.06
26	0.6	4	0.88	3	348	0.59
27	1	20	0.70	2.5	58	0.61

Polymerization conditions: T = 70 °C, P = 200 bar, AIBA: 96 mg, H₂O: 50 mL. Ratio 0.06: PEO: 47 mg, AIBA: 96 mg; ratio 0.6: PEO: 470 mg, AIBA: 96 mg, ratio 1: PEO: 650 mg, AIBA: 80 mg. ^a: Determined by gravimetry. ^b: Determined by DLS.

Unlike **PEO-NN**, **PEO-N** does not completely inhibit the polymerization as PE is produced for all ratios (entries 25-27). For the lowest ratio (0.06, entry 25), the PE yield, the particle size and PdI are very similar to those obtained for the latex synthesized with **PEO-NN** (entry 22, Table 4). The particle size observed by cryo-TEM (**Figure 16**) is also in good agreement with the Z_{av} value. PE yield and particle size values are again slightly lower than the reference experiment carried

out without macro-CTA (entry 20 and 25), indicating an influence of the macro-CTA for the stabilization of the particles.

As the amount of **PEO-N** is increased, the yield of PE is reduced (entries 26 and 27, 0.88 and 0.70 g yield respectively). This is in stark contrast with the results obtained with **PEO-NN** that feature a complete inhibition of the polymerization at those ratios, but again in contrast to the behavior observed in DMC, in which **PEO-NN** was more efficient for the synthesis of PEO-*b*-PE copolymers. The apparent increase of particle size with a ratio of 0.6 ($Z_{av} = 345$ nm) then decrease with a ratio of 1 ($Z_{av} = 58$ nm) are to be taken with care as multimodal distributions are detected by DLS. Indeed, large particles are known to produce more light scattering than the smaller ones. Hence, a negligible number of large particles will have a greater scattering intensity than a large number of small particles. This is confirmed by the superimposition of the intensity distributions and number distributions of the particle size (**Figure 15**). The main particle size distribution for a ratio of 0.6 is thus centered at 17 nm (**Figure 15a**), and at 13 nm for a ratio of 1 (**Figure 15b**). Taking into consideration only the most numerous particle population, particle sizes appear to drastically decrease as the quantity of PEO increases (**Figure 15c**).

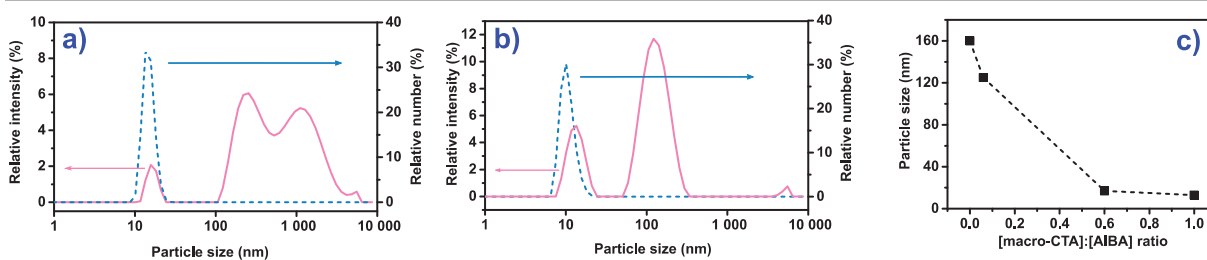


Figure 15. Particle size distributions of the latexes obtained for the 0.6 (a) and 1 (b) [macro-CTA]:[AIBA] ratios and evolution of particle sizes *versus* [macro-CTA]:[AIBA] ratio (c).

Cryo-TEM analyses (**Figure 16**) reveal that particle morphology changes from spherical (~ 100 nm, ratio 0.06, **Figure 16a**) to ellipsoids ($\sim 17 - 13$ nm, ratios 0.6 and 1, **Figure 16b, c**). The spheres appear to contain several PE crystalline lamellae, whereas the ellipsoids are composed each of a single lamella. For the 0.6 ratio, vesicle morphologies (> 200 nm) are observed in addition to the olives, indicating a probable change in particle morphologies as the DP_n of the PE block increases. Noteworthy, the macro-CTA quantity used (470 mg) is sufficient to consider that only block copolymers are formed and that particle stabilization is assured by the PEO chains. Interestingly, the ellipsoidal particles closely resemble those obtained by Billuart *et al.*^[31,32] using APS and SDS as anionic surfactant. A PE latex obtained after 1 hour of polymerization without **PEO-N** (entry 19) with a similar solid content to what is obtained for the 0.6 and 1 ratios (entries 26 and 27) has particle sizes of ~ 100 nm, which is quite larger than the observed ellipsoids. This confirms that the PE particles are efficiently stabilized by the PEO chains without the use of conventional surfactants. It is also worth mentioning that these morphologies contrast with the ones observed with PEO-*b*-PE copolymers obtained in DMC and re-dispersed in water (**Figure 8**).

Noteworthy, the particle morphologies observed might stem from either a PISA process, or a CD-PISA process. It was indeed shown by Brunel *et al.* that the crystallization of the PE segment in emulsion polymerization occurs in all likelihood during cooling.^[33]

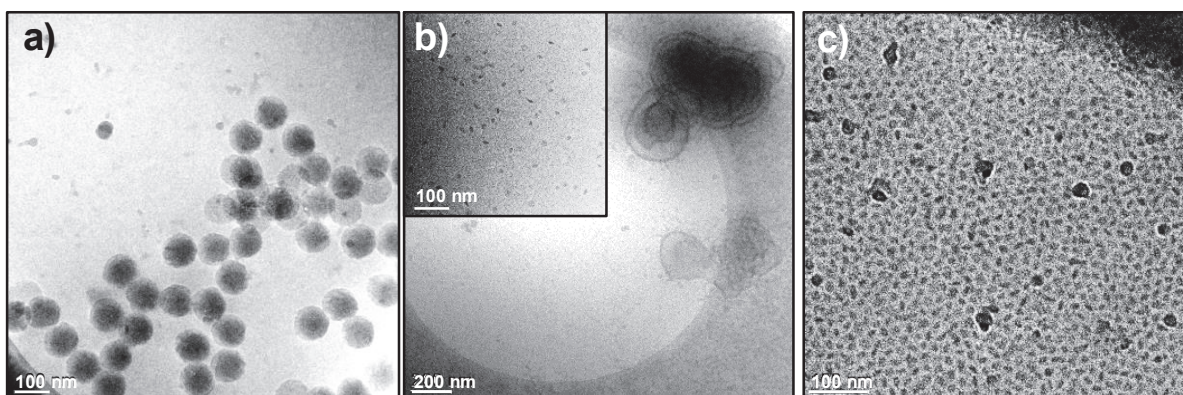


Figure 16. Cryo-TEM pictures of the latexes obtained after block copolymerizations of ethylene with PEO-NN at different ratios: 0.06 (a), 0.6 (b), 1 (c). Darker spots in (c) are ice deposits.

HT-SEC analyses of the dried latexes obtained after polymerization are presented in **Figure 17**. The MMD of a PE obtained by FREPE (entry 20 of Table 5, black trace) is bimodal with two maxima at elution time = 18.5 and 21 minutes, consistently with what was observed in the works of Grau^[31] and Billuart.^[32] As the ratio of [PEO]:[AIBA] increases, the MMDs gradually shift towards lower M_n values. HT-SEC traces from ratios of 0.6 (grey) and 1 (pink) show a second MMD at elution time = 24 minutes, corresponding to unreacted PEO macro-CTA. Nevertheless, the main distribution for the ratios of 0.6 and 1 (elution time ~ 22 minutes) has a significant lower molar mass than that of PE homopolymer obtained under similar conditions, indication a control of the molar masses by **PEO-N**.

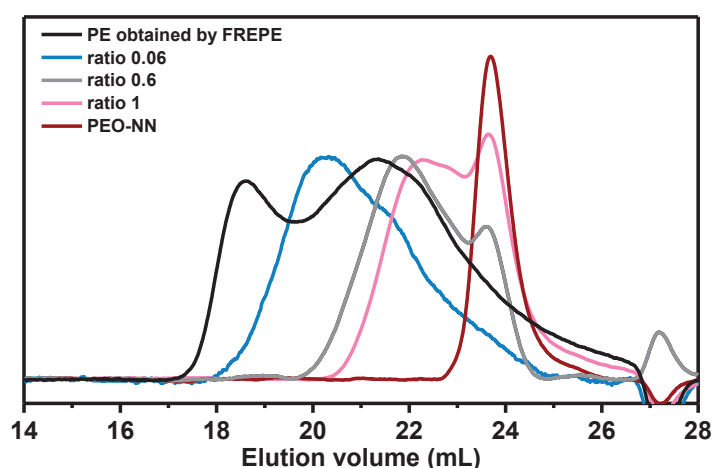


Figure 17. HT-SEC traces of PEO-*b*-PE obtained with PEO-N at different ratios (entries 25-27 of Table 6), of a PE homopolymer obtained by FREPE in the absence of PEO-N and of the starting PEO-N.

¹H-NMR analysis confirms the absence of unreacted **PEO-N** (without the dithiocarbamate chain-end) in the final latex and the presence of the characteristic methylene protons of PE α to

the dithiocarbamate moiety ($\delta = 3.15$ ppm, **Figure 18**). When fixing the integral value of the **a** protons at 3, protons **d** integrate for 1.1, indicating a chain-end fidelity of about 55 %, hinting that about 50 % of the PEO chains have reacted, the rest most likely underwent chain-end degradation. The presence of the characteristic proton PEO-C(O)**CH**(CH₃)-PE-SC(S)Z ($\delta = 2.33$ ppm) is also detected. The baseline between 2 and 3 ppm is however less clean than upon block copolymerization in DMC, which is likely to be the consequence of the chain-end degradation.

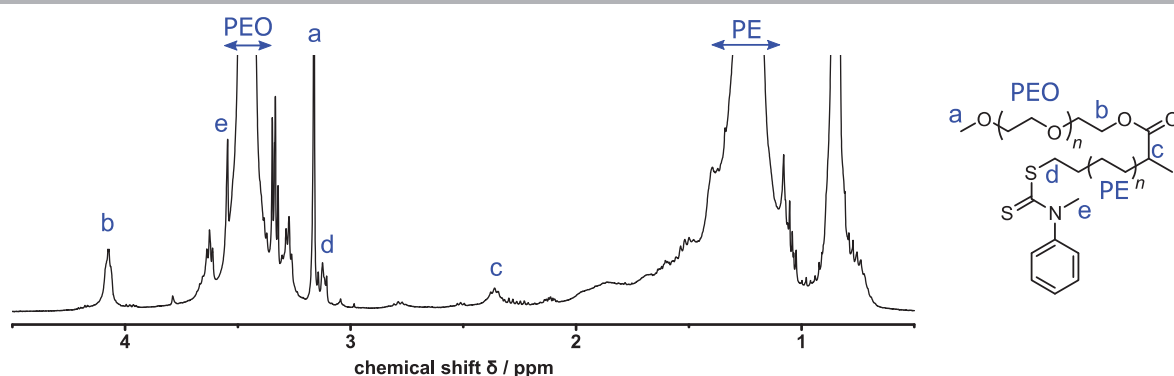


Figure 18. ¹H-NMR spectrum of the polymeric material obtained after ethylene polymerization in the presence PEO-N after 20 hours in water (entry 27 of Table 1).

*Chain-extensions of PEO macro-CTAs in water with ethylene proved to be challenging, compared to when it is performed in DMC. A complete inhibition of ethylene polymerization was observed under RAFT conditions ([macro-CTA]:[AIBA] ratio = 3) and polymerization only occurred at lower ratios. The inhibition was found to be stronger with **PEO-NN** than with **PEO-N**. In summary, the results are as follow: keeping a constant PEO quantity: the yield of polymer diminishes as the ethylene pressure is increased; keeping a constant ethylene pressure, the yield of polymer diminishes as the PEO quantity is increased. Ellipsoidal particles (~ 15 nm) were eventually obtained with **PEO-N**.*

IV. Conclusion

Dithiocarbamate functionalized PEO macro-CTAs were used to mediate the RAFT polymerization of ethylene in DMC and in water. The nature of the polymerization medium as well as the substituents on the nitrogen of the dithiocarbamate chain-end were found to strongly affect the performances of the systems.

In DMC, **PEO-N** was found to be slowly consumed during chain-extension, resulting in bimodal HT-SEC traces and broad MMDs. On the contrary, **PEO-NN** was instantaneously consumed upon chain-extension in DMC and narrow, unimodal MMDs characteristic of well-defined PEO-*b*-PE copolymers were obtained. ¹H-NMR analyses confirmed the slow consumption of the **PEO-N** macro-CTA and side-products were not detected. Conversely, despite a fast consumption of the macro-CTA, block copolymerization with **PEO-NN** generates a dithioether species, identified by the characteristic triplet at $\delta = 2.39$ ppm, indicating potential cross-termination. TEM and cryo-TEM analyses revealed that those block copolymers self-assemble into worms in DMC and in water, with a polymerization time – worm length dependence.

Block copolymerization of **PEO-N** and **PEO-NN** with ethylene was then attempted in water and no polymerization occurred under RAFT conditions ([macro-CTA]:[AIBA] ratio = 3) with either CTAs. Experiments conducted in the presence of VAc revealed a detrimental effect of the addition of ethylene in the polymerization medium traduced by a complete inhibition of the polymerization above 35 bar of ethylene pressure. Ethylene polymerization only occurred with lower [macro-CTA]:[AIBA] ratios and a strong influence of the nature of the chain-end was identified. Using **PEO-NN**, polymerization could only be achieved with a ratio of 0.06 and spherical particles were obtained. A complete inhibition of the polymerization was observed for ratios of 0.6 and 1. On the other hand, ethylene polymerization occurred in the presence of **PEO-N** with ratios of 0.06, 0.6 and 1. Different particle morphologies were obtained, ranging from spheres (~100 nm, 0.06 ratio), to ellipsoidal particles (< 20 nm, 0.6 and 1 ratios).

From these results, two modes of particle stabilization in water can be deduced, depending on the ratio between AIBA and the macro-CTA

- Ratio 0.06; the amount of PEO is too low (47 mg) compared to the quantity of PE produced (~ 2.5 g) to be solely responsible for particle stabilization. The mode of stabilization of the particles is similar to that of surfactant-free polymerization and a mixture of copolymer and PE homopolymer is obtained. The spherical particles closely resemble those stabilized by a fragment resulting from AIBA decomposition alone (albeit with a smaller average diameter).

- Ratios 0.6 and 1; the amount of PEO (470 and 600 mg) is sufficient to contemplate particle stabilization by the formation of PEO-*b*-PE copolymers. The anisotropic olive-like particles greatly differ from the system using only AIBA, but closely resemble what was obtained by Billuart *et al.* using CTAB at three times the critical micellar concentration.

In this chapter, the synthesis of amphiphilic block copolymers containing a PE block in water was attempted. This preliminary work allows the synthesis of surfactant-free PE particles using PEO macro-CTA as reactive stabilizer. This system can potentially be greatly improved by playing on the nature of the macro-CTA and on the nature of the chain-ends, providing that the observed chain-end degradation can be avoided.

V. Experimental section

Materials and methods

The comprehensive list of materials and analytical methods used for this work are presented at the end of this manuscript.

Synthesis of PEO precursor PEO-Br

PEO-OH (40.0 g, 1 eq.) was dissolved in DCM (100 mL). Et₃N (5.5 g, 2.7 eq.) was added and the clear colorless solution was cooled down to 0 °C. 2-bromopropionyl bromide (9.9 g, 2.3 eq.) was added dropwise while the temperature was maintained at 0 °C. A white precipitate appeared upon addition and the dispersion was stirred overnight at room temperature. The solid was removed by filtration, more DCM was added (200 mL) and the clear yellow solution was washed with a saturated NH₄Cl aqueous solution (2 x 50 mL), a saturated NaHCO₃ aqueous solution (2 x 50 mL), water (2 x 50 mL) and brine (2x 50 mL). The organic phase was dried over MgSO₄ and the solvent was removed *in vacuo*. The residue was dissolved in the minimum amount of DCM and crashed in diethyl ether (1 L). The white powder was recovered by filtration and washed with more diethyl ether followed by heptane. The product was dried *in vacuo* until constant weight to afford PEO-Br as a white powder. ¹H NMR (CDCl₃) δ (ppm) 4.37 (q, 1H); 4.29 (t, 2H); 3.61 (s, 180H); 3.38 (s, 3H); 1.79 (d, 3H).

Synthesis of PEO-N

Potassium hydroxide (2.6 g, 1 eq.) was dissolved in water (50 mL). After complete dissolution, methyl aniline (5.1 g, 1 eq.) and CS₂ (3.6 g, 1 eq.) were added and the biphasic mixture was stirred at room temperature overnight. The resulting monophasic yellow solution was extracted with diethyl ether (2 x 10 mL) and the yellow aqueous solution was lyophilized (-102 °C, 0.015 mbar). A portion of the resulting yellow powder (4.4 g, 3 eq. compared to PEO-Br) was added portion wise over 15 minutes to a solution of PEO-Br (20 g, 1 eq.) in DCM (150 mL) and the resulting yellow dispersion was stirred overnight at room temperature. The solid was removed by filtration, more DCM (200 mL) was added and the clear yellow solution was washed with a saturated NH₄Cl aqueous solution (2 x 50 mL), a saturated NaHCO₃ aqueous solution (2 x 50 mL), water (2 x 50 mL) and brine (2x 50 mL). The organic phase was dried over MgSO₄ and the solvent was removed *in vacuo*. The residue was dissolved in the minimum amount of DCM and crashed in diethyl ether (1 L). The white powder was recovered by filtration and washed with more diethyl ether followed by heptane. The product was dried *in vacuo* until constant weight to afford PEO-N

as a white powder. ^1H NMR (CDCl_3) δ (ppm) 7.44 (m, 3H); 7.26 (m, 2H); 4.64 (q, 1H); 4.26 (t, 2H); 3.73 (s, 3H); 3.61 (s, 180H); 3.38 (s, 3H); 1.48 (d, 3H).

Synthesis of PEO-NN

Each step of this synthesis was done under controlled atmosphere (Argon) unless otherwise stated. A dimethyl lithium solution was prepared by adding *n*-BuLi (10 mL, 1.1 eq.) in a solution of DMSO (3.5 mL, 2.2 eq.) in THF (150 mL) at 0 °C. The resulting thick white suspension was stirred for 30 minutes at 0 °C and transferred *via* cannula into a solution of diphenyl amine (3.8 g, 1 eq.) in THF (40 mL). The resulting suspension was stirred for another 30 minutes at 0 °C, CS_2 (8.5 g, 5 eq.) was added dropwise at 0 °C, and a pale yellow color appeared. The reaction mixture was stirred overnight at room temperature, upon which a brown color appeared. The volatiles were removed in *vacuo*, dry diethyl ether was added (200 mL) and the solid was recovered by filtration using a sintered-glass filter stick. The cake was washed with more dry diethyl ether and dried under vacuum. The integrity of the product was suspended into dry dichloromethane and a solution of PEO-Br (24 g, 0.5 eq) in dry DCM (50 mL) was slowly added at 0 °C. The brownish solid particles disappeared to afford a dark red solution which was stirred overnight at room temperature, upon which a white precipitate appeared. The solid was removed by filtration under air and the dark red solution was washed with a saturated NH_4Cl aqueous solution (2 x 50 mL), a saturated NaHCO_3 aqueous solution (2 x 50 mL), water (2 x 50 mL) and brine (2 x 50 mL). The organic phase was dried over MgSO_4 and the solvent was removed in *vacuo*. The dark red oil was suspended in ethanol (100 mL) and a precipitate appeared, which was removed by passing through a Nylon 0.22 μm filter. The oil was concentrated again in *vacuo*. The final dark red oil was crashed in diethyl ether (1 L). The pale brown powder was recovered by filtration and washed with more diethyl ether followed by heptane. The product was dried in *vacuo* until constant weight to afford PEO-NN as tan colored powder. ^1H NMR (CDCl_3) δ (ppm) 7.40 (m, 10H); 4.69 (q, 1H); 4.29 (t, 2H); 3.61 (s, 180H); 3.38 (s, 3H); 1.54 (d, 3H).

Typical block copolymerization procedure in DMC

The employed autoclave reactor (160 mL) was equipped with a mechanical stirring apparatus, a thermometer, and a pressure sensor. In a typical polymerization procedure, a degassed solution of AIBN (10 - 25 mg, 1 eq.) and a PEO macro-CTA (3 eq.) in DMC (50 mL) was added to the reactor preheated to 80 °C under argon atmosphere with a mechanical stirring of 600 rpm. Immediately after the injection port was closed, ethylene gas was fed into the reactor until the targeted pressure of 80 bar was reached (instantaneous). If necessary, additional ethylene gas was

introduced to keep a constant pressure during the polymerization. After a predetermined period of time, the stirring was slowed down and the reactor was cooled with iced water. When the temperature inside the reactor dropped below 25 °C, the remaining pressure was carefully released. The content of the reactor was collected with toluene, and evaporation of the solvent gave the polymeric product.

Typical block copolymerization procedure in water

The employed autoclave reactor (160 mL) was equipped with a mechanical stirring apparatus, a thermometer, and a pressure sensor. In a typical polymerization procedure, a degassed solution of AIBA (1 eq.) and a PEO macro-CTA (0.06 - 3 eq.) in water (50 mL) was added to the reactor preheated to 80 °C under argon atmosphere with a mechanical stirring of 600 rpm. VAc (4.7 g) was added to the solution for the synthesis of PEO-*b*-PVAc and PEO-*b*-EVA copolymers. Immediately after the injection port was closed, ethylene gas was fed into the reactor until the targeted pressure of 200 bar was reached. This step took about 4 min. If necessary, additional ethylene gas was introduced to keep a constant pressure during the polymerization. After a predetermined period of time, the stirring was slowed down and the reactor was cooled with iced water. When the temperature inside the reactor dropped below 25 °C, the remaining pressure was carefully released. The content of the reactor was collected and stored as a dispersion. The solids content was determined by gravimetry on a small aliquot (~ 5 mL) and analyses were performed on the dried product.

VI. References

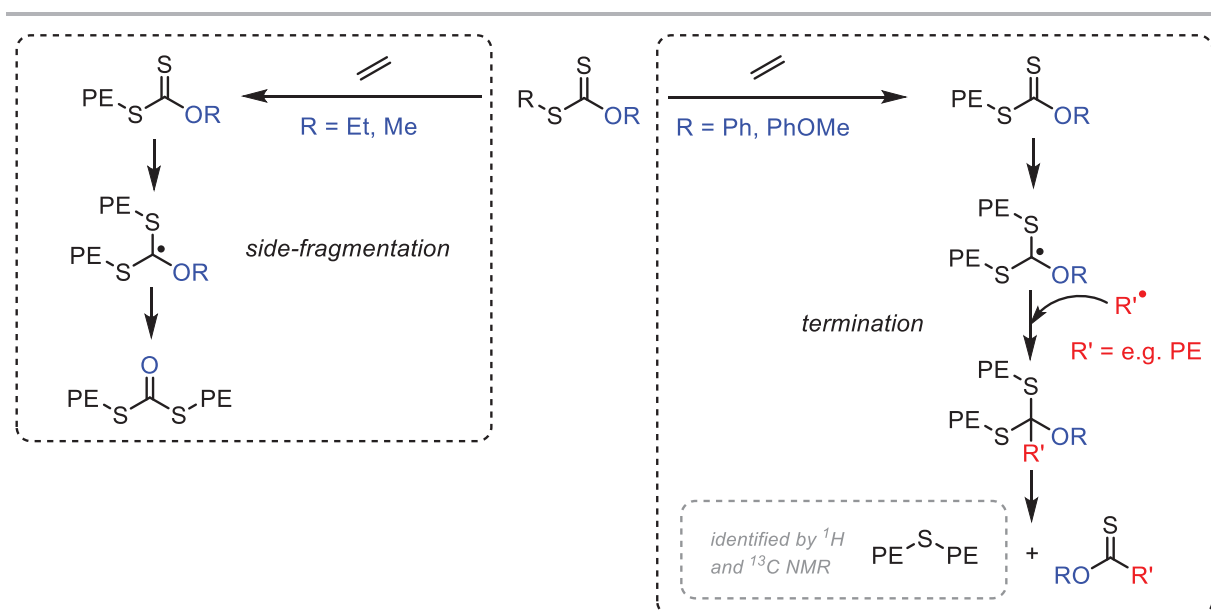
- [1] J. B. McLeary, B. Klumperman, *Soft Matter* **2006**, *2*, 45–53.
- [2] M. F. Cunningham, *Prog. Polym. Sci.* **2008**, *33*, 365–398.
- [3] P. B. Zetterlund, Y. Kagawa, M. Okubo, *Chem. Rev.* **2008**, *108*, 3747–3794.
- [4] M. Save, Y. Guillaneuf, R. G. Gilbert, *Aust. J. Chem.* **2006**, *59*, 693–711.
- [5] P. B. Zetterlund, S. C. Thickett, S. Perrier, E. Bourgeat-Lami, M. Lansalot, *Chem. Rev.* **2015**, *115*, 9745–9800.
- [6] C. J. Ferguson, R. J. Hughes, B. T. T. Pham, B. S. Hawkett, R. G. Gilbert, A. K. Serelis, C. H. Such, *Macromolecules* **2002**, *35*, 9243–9245.
- [7] D. Le, D. Keller, G. Delaittre, *Macromol. Rapid Commun.* **2019**, *40*, 1–21.
- [8] M. Lansalot, J. Rieger, F. D’Agosto, in *Macromol. Self-Assembly* (Eds.: L. Billon, O. Borisov), John Wiley & Sons, Inc., **2016**, pp. 33–82.
- [9] F. D’Agosto, J. Rieger, M. Lansalot, *Angew. Chem. Int. Ed.* **2019**, *Accepted Article*, DOI doi:10.1002/anie.201911758.
- [10] M. J. Derry, L. A. Fielding, S. P. Armes, *Prog. Polym. Sci.* **2016**, *52*, 1–18.
- [11] N. J. Warren, S. P. Armes, *J. Am. Chem. Soc.* **2014**, *136*, 10174–10185.
- [12] S. L. Canning, G. N. Smith, S. P. Armes, *Macromolecules* **2016**, *49*, 1985–2001.
- [13] J. Zhou, H. Yao, J. Ma, *Polym. Chem.* **2018**, *9*, 2532–2561.
- [14] G. Wang, M. Schmitt, Z. Wang, B. Lee, X. Pan, L. Fu, J. Yan, S. Li, G. Xie, M. R. Bockstaller, et al., *Macromolecules* **2016**, *49*, 8605–8615.
- [15] G. Delaittre, J. Nicolas, C. Lefay, M. Save, B. Charleux, *Chem. Commun.* **2005**, *1*, 614–616.
- [16] E. Groison, S. Brusseau, F. D’Agosto, S. Magnet, R. Inoubli, L. Couvreur, B. Charleux, *ACS Macro Lett.* **2012**, *1*, 47–51.
- [17] M. Okubo, Y. Sugihara, Y. Kitayama, Y. Kagawa, H. Minami, *Macromolecules* **2009**, *42*, 1979–1984.
- [18] Y. Kitayama, H. Moribe, K. Kishida, M. Okubo, *Polym. Chem.* **2012**, *3*, 1555–1559.
- [19] J. Tonnar, P. Lacroix-Desmazes, *Soft Matter* **2008**, *4*, 1255–1260.
- [20] S. Boissé, J. Rieger, K. Belal, A. Di-Cicco, P. Beaunier, M. H. Li, B. Charleux, *Chem. Commun.* **2010**, *46*, 1950–1952.
- [21] I. Chaduc, M. Lansalot, F. D’Agosto, B. Charleux, *Macromolecules* **2012**, *45*, 1241–1247.
- [22] J. Rieger, W. Zhang, F. Stoffelbach, B. Charleux, *Macromolecules* **2010**, *43*, 6302–6310.
- [23] B. Charleux, G. Delaittre, J. Rieger, F. D’Agosto, *Macromolecules* **2012**, *45*, 6753–6765.
- [24] I. Chaduc, W. Zhang, J. Rieger, M. Lansalot, F. D’Agosto, B. Charleux, *Macromol. Rapid Commun.* **2011**, *32*, 1270–1276.
- [25] J. Rieger, F. Stoffelbach, C. Bui, D. Alaimo, C. Jérôme, B. Charleux, *Macromolecules* **2008**, *41*, 4065–4068.
- [26] J. Rieger, G. Osterwinter, C. Bui, F. Stoffelbach, B. Charleux, *Macromolecules* **2009**, *42*, 5518–5525.
- [27] S. Binauld, L. Delafresnaye, B. Charleux, F. D’Agosto, M. Lansalot, *Macromolecules* **2014**, *47*, 3461–3472.
- [28] L. Etchenausia, A. Khoukh, E. Deniau Lejeune, M. Save, *Polym. Chem.* **2017**, *8*, 2244–2256.
- [29] T. Le Bris, A. Martins dos Santos, C. Graillat, F. D’Agosto, M. Lansalot, *Macromolecules* **2009**, *42*, 946–956.
- [30] E. Velasquez, J. Rieger, F. Stoffelbach, B. Charleux, F. D’Agosto, M. Lansalot, P. E. Dufils, J. Vinas, *Polymer* **2013**, *54*, 6547–6554.
- [31] E. Grau, P. Y. Dugas, J. P. Broyer, C. Boisson, R. Spitz, V. Monteil, *Angew. Chemie - Int. Ed.* **2010**, *49*, 6810–6812.
- [32] G. Billuart, E. Bourgeat-Lami, M. Lansalot, V. Monteil, *Macromolecules* **2014**, *47*, 6591–6600.
- [33] F. Brunel, G. Billuart, P. Y. Dugas, M. Lansalot, E. Bourgeat-Lami, V. Monteil, *Macromolecules* **2017**, *50*, 9742–9749.
- [34] J. Puig, I. A. Zucchi, M. Ceolin, W. F. Schroeder, R. J. J. Williams, *RSC Adv.* **2016**, *6*, 34903–34912.
- [35] M. Zhang, C. F. Zhang, Z. K. Yao, J. L. Shi, B. K. Zhu, Y. Y. Xu, *Chinese J. Polym. Sci.* **2010**, *28*, 337–346.
- [36] T. Li, W. J. Wang, R. Liu, W. H. Liang, G. F. Zhao, Z. Y. Li, Q. Wu, F. M. Zhu, *Macromolecules* **2009**, *42*, 3804–3810.
- [37] Y. Zhang, H. Li, J. Y. Dong, Y. Hu, *Polym. Chem.* **2014**, *5*, 105–115.
- [38] Y. Lu, Y. Hu, Z. M. Wang, E. Manias, T. C. Chung, *J. Polym. Sci. Part A Polym. Chem.* **2002**, *40*, 3416–3425.
- [39] G. Pound, J. B. Mcleary, R. F. M. Lange, B. Klumperman, **2007**, 8861–8871.
- [40] D. C. Onwudiwe, P. A. Ajibade, *Int. J. Mol. Sci.* **2011**, *12*, 1964–1978.
- [41] P. Padungros, A. Wei, *Synth. Commun.* **2014**, *44*, 2336–2343.
- [42] D. J. Keddie, G. Moad, E. Rizzardo, S. H. Thang, *Macromolecules* **2012**, *45*, 5321–5342.

- [43] A. M. Oliver, J. Gwyther, C. E. Boott, S. Davis, S. Pearce, I. Manners, *J. Am. Chem. Soc.* **2018**, *140*, 18104–18114.
- [44] D. J. Keddie, C. Guerrero-Sanchez, G. Moad, E. Rizzardo, S. H. Thang, *Macromolecules* **2011**, *44*, 6738–6745.
- [45] A. M. Van Herk, *Chemistry and Technology of Emulsion Polymerisation*, Blackwell Publishing **2005**.
- [46] J. E. Davis, J. J. Mcketta, *J. Chem. Eng. Data* **1960**, *5*, 374–375.

General conclusion

The work conducted in this thesis revolved around two major challenges in the field of polyolefins, the most industrially produced polymers: the control of the synthesis of block copolymers and the introduction of polar functions. Reversible addition-fragmentation chain transfer (RAFT) polymerization was chosen as the preferred reversible-deactivation radical polymerization (RDRP) technique. Building upon the expertise of the C2P2 group in RAFT and ethylene radical polymerization, the synthesis of polyethylene (PE) by RAFT polymerization using different chain transfer agents (CTAs) was attempted. Targets in term of polar vinyl monomers included less-activated monomers (vinyl acetate, VAc) and more activated ones (methyl methacrylate, MMA). While the RAFT polymerization of ethylene and synthesis of PVAc-*b*-PE and PMMA-*b*-PE copolymers originally took place in organic solvent (dimethyl carbonate, DMC), a variant of the synthetic process was performed in water through the use of poly(ethylene oxide) (PEO) as water soluble macro-CTA to attain amphiphilic block copolymers *via* polymerization-induced self-assembly (PISA).

RAFT ethylene homopolymerization mediated by aromatic xanthates and aromatic dithiocarbamates was first investigated. The use of xanthates with Z = OPh and Z = OPhOMe revealed the absence of side-fragmentation, identified previously by our group with Z = OEt and Z = OMe. A substantial rate retardation was however observed, accompanied by the emergence of new side products attributed to cross-termination reactions occurring at the intermediate radical (**Scheme 1**).



Scheme 1. Schematic representation of side-fragmentation and suggested cross-termination reaction products observed with *O*-alkyl xanthates and *O*-aryl xanthates, respectively.

Despite the occurrence of the suggested termination mechanism happening at the intermediate radical and gradual loss of chain-end fidelity, the control over molar masses could be maintained up to 3 000 g mol⁻¹ and unprecedented low dispersity values were obtained for the

shortest polymerization times ($\mathcal{D} < 1.3$). An unexpected loss of control with the emergence of conventional radical polymerization, consequence of the xanthate chain-ends being inaccessible (but still present, as confirmed by $^1\text{H-NMR}$) was found to occur at 200 bar of ethylene pressure for $M_n > 1\,000\text{ g mol}^{-1}$. This was attributed to a segregation of the polymer chains in the supercritical ethylene/DMC mixture, observed with a reactor equipped with a sapphire window. This issue was circumvented by performing the polymerization below the phase transition of the ethylene/DMC mixture, namely 80 bar, and control could be maintained throughout the entire polymerization. Aromatic dithiocarbamates ($Z = \text{N(Ph)Me}$, $Z = \text{N(Pyr)Me}$) offered better control over ethylene polymerization with chain-end fidelity close to 100 %. These CTAs however suffered from slow consumption, *a priori* a consequence of low chain transfer constant. Evidence of cross-termination, traduced by the identification of traces of a thioether species PE-S-PE by ^1H and $^{13}\text{C-NMR}$ was found when $Z = \text{N(Pyr)Me}$, whereas remarkably good control was obtained when $Z = \text{N(Ph)Me}$.

Based on these results, suitable CTAs were selected for the synthesis of target block copolymers. A compromise was found to be needed to achieve satisfactory control over both the polar and apolar blocks. For example, this resulted in the choice of a xanthate CTA for the synthesis of PVAc-*b*-PE copolymers. Indeed, while a better control over ethylene polymerization was obtained with dithiocarbamates, the control over VAc was not satisfactory.

Despite pronounced loss of chain-end fidelity, a phenoxymethoxy xanthate ($Z = \text{OPhOMe}$) was found to be best suited for the control of both VAc and ethylene. PVAc macro-CTAs were thus synthesized with this xanthate and chain-extended with ethylene in DMC to achieve, for the first time, well-defined PVAc-*b*-PE copolymers. The difficulty of characterization of polar-apolar block copolymers by high temperature size exclusion chromatography (HT-SEC), mandatory for polyolefins, was evidenced with these copolymers, and the determination of molar masses and dispersity values could not be achieved with this technique. $^1\text{H-NMR}$ was used to determine molar mass values for both blocks and revealed the linear increase of the molar masses of the formed block copolymer upon consumption of ethylene as expected for a pseudo-living process.

To target PMMA-*b*-PE block copolymers, PMMA carrying a dithiocarbamate chain end was envisioned according to two strategies. In the first one, a switchable dithiocarbamate ($Z = \text{N(Pyr)Me}$) was used to mediate the RAFT polymerization of MMA in the presence of a strong acid. Deprotonation of the chain-end enabled the synthesis of PMMA carrying a dithiocarbamate chain-end able to mediate RAFT ethylene polymerization. Both HT-SEC and $^1\text{H-NMR}$ analyses revealed a particularly pronounced slow consumption of the PMMA macro-CTA, which was observed to a much lesser extent with the molecular version of the CTA ($R = \text{C}(\text{CH}_3)_2\text{CN}$ instead of $R = \text{PMMA}$). Unreacted PMMA macro-CTA could be separated from the final mixture by trituration in an alcoholic solution and filtration, revealing that well-defined PMMA-*b*-PE copolymers formed. An

alternative strategy to obtain a PMMA carrying a dithiocarbamate chain-end was attempted in collaboration with Pr. Mathias Destarac and Dr. Simon Harrisson at Université Toulouse III (IMRCP group). A dithiuram disulfide was used as irreversible CTA to mediate the polymerization of MMA. Dithiocarbamate functionalized PMMA macro-CTAs of different molar masses were thus obtained and used for chain-extension with ethylene. Characterization issues were encountered and evidences of aggregation of the block copolymers were found by HT-SEC. Molar masses were found to plateau by $^1\text{H-NMR}$, reaching a different value for each series of block. The value reached depended on the molar mass of the starting PMMA macro-CTA used. This was also attributed to this aggregation phenomenon. Besides, as evidenced by transmission electron microscopy (TEM), PMMA-*b*-PE copolymers in DMC form a stable white dispersion that was analyzed by electronic microscopy. Particles adopting worm-like morphologies were observed in dispersion samples dried from DMC. Considering the solvent quality of DMC for PE and PMMA segments, this strongly suggests that the growth of the PE segment leads to a self-assembly of the forming block copolymers according to a polymerization-induced self-assembly (PISA) process. The favored worm morphology could be due to the crystallinity of PE segment via a crystallization driven self-assembly (CDSA) process. This crystallinity is either exacerbated by the growth of PE segments or when cooling the polymerization medium at the end of the polymerization.

A last study involved the use of a dithiocarbamate functionalized PEO macro-CTA ($Z = \text{N(Ph)Me}$) to obtain amphiphilic block copolymers in water. A preliminary study conducted in DMC revealed that such a PEO macro-CTA was particularly slowly consumed during block copolymerization, leading to higher than expected molar masses for the PE segment and bimodal HT-SEC traces. This slow consumption could be avoided by using another dithiocarbamate with $Z = \text{N(Ph)}_2$, instantaneously consumed during block copolymerization with ethylene, leading to narrow unimodal HT-SEC traces and experimental molar masses matching theoretical ones. Worm-like morphologies were again observed by TEM analyses in DMC and cryo-TEM analyses of the re-dispersed block copolymers in water, with worm length increasing with the molar mass of the PE segment. The above mentioned PISA and CDSA processes are again probably at play although further studies are required to show the underpinning mechanism of this block copolymer assembly. The transposition of the system and self-assembly process to aqueous medium was appealing considering the water solubility of the PEO moiety. It however resulted in the complete inhibition of ethylene polymerization. Polymerization only occurred with low [macro-CTA]:[initiator] ratios (0.06, 0.6 and 1) $Z = \text{N(Ph)Me}$. The inhibition was more severe with $Z = \text{N(Ph)}_2$ and ethylene polymerization only occurred with a 0.06 ratio. Different particle morphologies were observed with $Z = \text{N(Ph)Me}$: spheres (ratio 0.06), vesicles (ratio 0.6) and ellipsoids (ratios 0.6 and 1). This represents the first known examples of a PISA process for ethylene in organic or aqueous media.

In short, polar-apolar olefin block copolymers were successively obtained by RAFT polymerization. Aromatic xanthates and dithiocarbamates were used to obtain PVAc-*b*-PE and PMMA-*b*-PE copolymers by sequential monomer addition. A PEO was equipped with a dithiocarbamate chain-end and well defined PEO-*b*-PE were obtained in DMC. These systems can however still be improved: xanthate-mediated ethylene RAFT polymerization suffers from substantial loss of chain-end fidelity; dithiocarbamate-mediated ethylene RAFT polymerization suffers from slow consumption of the CTA, particularly when using macro-CTAs. The systems also feature substantially reduced polymerization rate, except in the case of PMMA macro-CTAs with $Z = N(\text{Ph})\text{Me}$. Improvements can still be made towards a better control over ethylene RAFT polymerization, as evidenced by recent results with dithiocarbamates with $Z = N(\text{Ph})_2$. Some disadvantages evidenced during this work could be circumvented by further optimizing the polymerization conditions (e.g. structure of the RAFT agents). However, some disadvantages are inherent to RAFT polymerization (side-fragmentation and cross-termination, slow consumption of the macro-CTA, inhibition in water) and would be difficult to avoid with this process. Alternative RDRP techniques involving less stable radical intermediates (TERP) or no intermediate at all (ITP) are alluring and worth investigating. In this context, ITP of ethylene is currently being investigated in our group. Keeping in mind the advantages and disadvantages of the different existing RDRP techniques, it is probable that none of them is optimal to obtain PE-*b*-PX copolymers and compromises between control, monomer scope and applications have to be found.

As mentioned in the first chapter of this manuscript, PE-*b*-PX copolymers have potentially interesting material properties. In this context, the properties of the PMMA-*b*-PE copolymers synthesized during this work are being investigated as compatibilizing agents in epoxy resins and PMMA blends. This work is performed through a collaboration with the IMP INSA Lyon group.

Materials and methods

Experimental procedure for the work presented in this manuscript are described separately at the end of their relevant chapter. In the following, the materials used during the presented work are listed and the common analyses techniques are presented.

Materials

Ethylene (99.95 %, Air liquide), 2,2'-azobis(2-methylpropionitrile) (AIBN, 98 %, Aldrich), 2,2'-azobis(2-methylpropionamide) dihydrochloride (AIBA, 97 %, Aldrich), phenol (≥ 99 %, Aldrich), 4-methoxyphenol (99 %, Aldrich), dimethyl sulfoxide (DMSO, Fisher), N,N-diisopropylethylamine (DIPEA, ≥ 99 %, Aldrich), carbon disulfide (CS₂, anhydrous ≥ 99 %, Aldrich), methyl bromoacetate (97 %, Aldrich), acetonitrile (HPLC grade, Fisher), trifluoromethanesulfonic acid (TfOH, 99%, Acros Organics), *N*-methyl aniline (98%, TCI), *n*-butyl lithium (2.5M in hexanes, Aldrich), iodine (99%, Acros Organics), potassium iodide (98%, Acros Organics), polyethylene glycol methyl ether (PEO-OH, 2 000 g mol⁻¹, Aldrich), dichloromethane (DCM, ACS reagent, Aldrich), triethylamine (Et₃N, ≥ 99 %, Aldrich), 2-bromopropionyl bromide (97 %, Aldrich), potassium hydroxide (99.98%, Acros Organics) and diphenyl amine (99%, Aldrich) were used as received. Dimethyl carbonate (DMC, 99%, Aldrich) was stored on molecular sieves (3 Å) and kept under Argon. Tetrahydrofuran (THF, HPLC grade, Fisher) was distilled on CaH₂ prior to use. Vinyl acetate (VAc, 99%, Acros Organics) was distilled, stored on molecular sieves (3 Å) and kept under Argon. Methyl methacrylate (MMA, 99%, Acros Organics) was purified by passing through a basic alumina column. Tetrachloroethylene (ACS reagent, Aldrich) was purified by passing through silica.

Methods

Nuclear magnetic resonance (NMR)

¹H (400 MHz) and ¹³C NMR (100 MHz) spectra were measured in solution using either a D₆-benzene/tetrachloroethylene mixture (1:2 by volume) at 90 °C, or CDCl₃ at room temperature, and are reported in ppm with the residual solvent peak ($\delta = 7.16$ ppm for deuterated benzene; $\delta = 7.26$ ppm for deuterated chloroform) as internal standard on a Bruker Avance II 400 Ascend spectrometer.

Size exclusion chromatography in THF (SEC-THF)

Size-exclusion chromatography (SEC) analyses were performed using a Viscotek system (Malvern Instruments) including a four-capillary differential viscometer, a differential refractive index detector (RI) and a UV detector. THF was used as the mobile phase at a flow rate of 1 mL

min⁻¹ at 35 °C. All samples were injected at a concentration of 3-6 mg mL⁻¹ after filtration through a 0.45 µm PTFE membrane. The separation was carried out on three Polymer Standard Service columns (SDVB, 5 µm, 300 x 7.5 mm) and a guard column. Calibrations were performed with narrow polystyrene or narrow poly(methyl methacrylate) standards (Polymer Standards Service).

High temperature size exclusion chromatography (HT-SEC)

Size-exclusion chromatography (SEC) analyses were performed using a Viscotek system (Malvern Instruments) equipped with three columns (PLgel Olexis 300 mm × 7 mm from Agilent Technologies) and a refractive index (RI) detector. Sample volumes of 200 µL with concentrations between 3 and 8 mg mL⁻¹ were eluted in 1,2,4-trichlorobenzene (TCB) using a flow rate of either 0.7 or 1.0 mL min⁻¹ at 150 °C. The mobile phase was stabilized with 2,6-di-tert-butyl-4-methylphenol (200 mg L⁻¹). The polymer samples were dissolved in TCB at 150 °C for 5 min before the start of the analysis. The molar-mass distributions for PE homopolymer samples were calculated by means of a conventional calibration curve on the basis of linear polyethylene standards (Polymer Standards Service).

Differential scanning calorimetry (DSC)

DSC analyses were performed on a Mettler Toledo DSC 1. Measurements were carried by two successive heating and cooling cycles (20 K min⁻¹ for the first cycle and 5 K min⁻¹ for the second cycle) with temperatures ranging either from - 60 to + 160 °C for PVAc containing samples or + 25 to + 160 °C. Crystallization, melting and glass transition temperatures were recorded on the second cycle.

Dynamic light scattering (DLS)

Hydrodynamic particle diameters (Z_{avg} , nm) were measured using a Malvern Zetasizer Nano ZS. A 633 nm wavelength laser beam was sent to a highly diluted sample and the scattered signal intensity was measured at a 173° angle at 25 °C.

Transmission electron microscopy (TEM)

TEM analyses were performed on a Philips CM120 transmission electron microscope. Samples with a 0.5% solid content were prepared in water or in DMC and a drop of the dispersion was deposited on a carbon-coated copper grid left to dry at room temperature for a few minutes and the excess was removed with a filter paper. The grids were then left to dry for several hours. The analyses were performed at 120 kV.

Cryogenic transmission electron microscopy (cryo-TEM)

Cryo-TEM analyses were performed on a Philips CM120 transmission electron microscope. Samples with a 0.5% solid content were prepared in water and a drop was deposited on a

Quantifoil R2/1 copper grid with 100 holey carbon support film. The grid was then plunged into liquid ethane. The analyses were performed at 120 kV and the grid was maintained cold throughout the analysis by liquid nitrogen.

Matrix-assisted laser desorption and ionization - time of flight (MALDI-TOF)

MALDI-TOF MS measurements were performed on an applied Biosystems Voyager System 4243. The polymer sample and the dithranol matrix were dissolved in THF and premixed in a 1:3 volume ratio.

Abstract

The synthesis of polar-apolar olefin block copolymers, combining a semi-crystalline polyethylene (PE) block and a polar block (poly(vinyl acetate) (PVAc), poly(methyl methacrylate) (PMMA), poly(ethylene oxide) (PEO)) was investigated by RAFT polymerization. A preliminary study on ethylene homopolymerization revealed parasite cross-termination reactions happening at the intermediate radical, resulting in the loss of chain-end fidelity when using aromatic xanthates as chain transfer agents (CTA) under relative mild conditions ($T = 70 - 80\text{ }^{\circ}\text{C}$, $P = 200\text{ bar}$). The extent of cross-termination was greatly reduced with aromatic dithiocarbamates, and for the first time, PE chains with a high livingness were obtained. These first results were used to equip polar macromolecular CTAs (PVAc, PMMA, PEO), with selected aromatic xanthates and dithiocarbamates, that were further used for block copolymerization with ethylene in a low-transferring organic solvent (dimethyl carbonate, DMC). A critical influence of the ethylene pressure was evidenced as block polymerization at 200 bar could not be achieved due to solubility issues in the resulting supercritical DMC/ethylene mixture. This was circumvented by performing the block copolymerization below the supercritical point of the mixture ($P < 100\text{ bar}$) and well-defined PVAc-*b*-PE, PMMA-*b*-PE and PEO-*b*-PE copolymers were eventually obtained. The block copolymers were found to feature self-assembly properties and worm-like morphologies were observed for PMMA-*b*-PE and PEO-*b*-PE synthesized in DMC, hinting at a plausible polymerization-induced self-assembly (PISA) mechanism. The successful switch from DMC to water for the synthesis of PEO-*b*-PE copolymers enabled the observation of various particle morphologies: spheres, vesicles and ellipsoidal particles, depending on the initial macro-CTA:initiator molar ratio.

Keywords

Polyethylene – RAFT – block copolymers – PISA – poly(vinyl acetate) – poly(methyl methacrylate) – poly(ethylene oxide)

Titre

Polymérisation RAFT de l'éthylène pour la synthèse de copolymères à blocs polaires-apolaires.

Résumé

La synthèse de copolymères à blocs, comprenant un bloc semi-cristallin de polyéthylène (PE) apolaire et un bloc polaire (poly(acétate de vinyle) (PVAc), poly(méthacrylate de méthyle (PMMA), poly(oxide d'éthylène) (PEO)) a été étudiée par polymérisation RAFT. L'étude préliminaire de l'homopolymérisation de l'éthylène en conditions relativement douces ($T = 70 - 80\text{ }^{\circ}\text{C}$, $P = 200\text{ bar}$) a révélé que l'utilisation d'agents de transfert de chaîne (ATC) de type xanthates aromatiques conduit à une perte de fonctionnalité des extrémités de chaînes au cours de la polymérisation, conséquence directe de réactions de terminaison se produisant sur le radical intermédiaire. L'utilisation de dithiocarbamates aromatiques a permis de s'affranchir de ce mécanisme parasite et pour la première fois des chaînes de PE présentant une fonctionnalité de bout de chaîne proche de 100%. Des ATCs macromoléculaires polaires, obtenus avec les agents de transfert de chaînes identifiés au cours de l'étude préliminaire, ont ensuite été utilisés pour la synthèse de copolymères à blocs dans le carbonate de diméthyle (DMC), un solvant organique peu transférant. Le rôle clé de la thermodynamique du milieu de polymérisation (mélange DMC/éthylène supercritique à 200 bar) a alors été mis en évidence. En effet, les macro-ATCs sont insolubles dans un tel milieu, ce qui a conduit à la formation d'un mélange d'homopolymères. La diminution de la pression de polymérisation ($P < 100\text{ bar}$) a toutefois permis d'éviter ce phénomène et les copolymères PVAc-*b*-PE, PMMA-*b*-PE et PEO-*b*-PE attendus ont été obtenus. Des propriétés d'auto-assemblage ont été mises en évidence et des morphologies de type fibre ont été obtenues pour les copolymères PMMA-*b*-PE et PEO-*b*-PE synthétisés dans le DMC, permettant d'envisager un mécanisme de type auto-assemblage induit par la polymérisation (PISA). Le passage en milieu aqueux en utilisant le macro-ATC hydrosoluble PEO a permis l'observation de morphologies de type sphériques, vésicules ou encore ellipsoïdes selon le rapport molaire macro-ATC/amorceur utilisé.

Mots-clés

Polyéthylène – RAFT – copolymères à blocs – PISA – acétate de vinyle – méthacrylate de méthyle – poly(oxyle d'éthylène)

Laboratoire C2P2 – Equipe LCPP
CNRS, Université Lyon 1, Université de Lyon
CPE Lyon, Bâtiment F, BP 2077
43, Bd. du 11 Novembre 1918
69616 Villeurbanne Cedex

